

Fundamental Limitations on Communication over a Quantum Network

Junjing Xing,¹ Tianfeng Feng,² Zhaobing Fan,^{1,*} Haitao Ma,^{3,†}
Kishor Bharti,^{4,‡} Dax Enshan Koh,^{4,§} and Yunlong Xiao^{4,¶}

¹College of Intelligent Systems Science and Engineering, Harbin Engineering University,
Harbin, Heilongjiang 150001, People's Republic of China

²State Key Laboratory of Optoelectronic Materials and Technologies and School of Physics,
Sun Yat-sen University, Guangzhou, Guangdong 510275, People's Republic of China

³College of Mathematics Science, Harbin Engineering University,
Harbin, Heilongjiang 150001, People's Republic of China

⁴Institute of High Performance Computing (IHPC), Agency for Science,
Technology and Research (A*STAR), 1 Fusionopolis Way,
#16-16 Conneris, Singapore 138632, Republic of Singapore
(Dated: June 9, 2023)

Entanglement, a fundamental feature of quantum mechanics, has long been recognized as a valuable resource in enabling secure communications and surpassing classical limits. However, previous research has primarily concentrated on static entangled states generated at a single point in time, overlooking the crucial role of the quantum dynamics responsible for creating such states. Here, we propose a framework for investigating entanglement across multiple time points, termed temporal entanglement, and demonstrate that the performance of a quantum network in transmitting information is inherently dependent on its temporal entanglement. Through case studies, we showcase the capabilities of our framework in enhancing conventional quantum teleportation and achieving exponential performance growth in the protocol of quantum repeaters. Additionally, our framework effectively doubles the communication distance in certain noise models. Our results address the longstanding question surrounding temporal entanglement within non-Markovian processes and its impact on quantum communication, thereby pushing the frontiers of quantum information science.

Introduction—The advent of modern network technology has catalyzed a monumental transformation in our daily lives, reshaping the way we communicate and access information. From instant messaging to social media platforms, networks have revolutionized our interactions with one another, enabling real-time connectivity across the globe. The impact of networks on our daily lives is undeniable, and it continues to shape the way we work, learn, and play in an ever-evolving digital landscape. Notwithstanding these remarkable achievements, our current communication infrastructure is built on classical information processing techniques that are constrained by physical limitations. In stark contrast, global quantum network (Fig. 1) [1–4] holds the promise of an unprecedented leap forward in communication capabilities and security by capitalizing on a unique resource of quantum mechanics – quantum entanglement [5].

Despite considerable progress in investigating entanglement and its effectiveness in quantum communication, most studies have predominantly focused on a static view of entanglement at specific time points. However, the intrinsic nature of quantum systems defies fixation to any particular moment, embracing an unceasing odyssey of incessant evolution. In quantum information science, the evolution of quantum systems finds

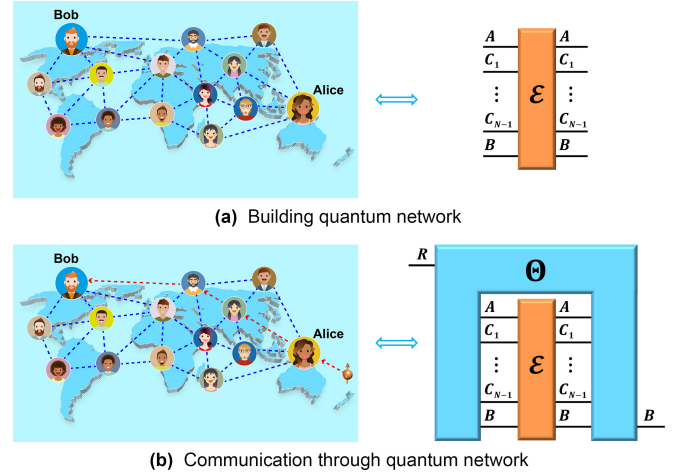


FIG. 1. **Quantum Network:** a schematic diagram of single-round quantum network communication. The physical quantum network connects the sender Alice (A), the receiver Bob (B), and third-party agents (C_k with $k = 1, \dots, N-1$), and is created using a multi-input and multi-output quantum channel \mathcal{E} (a), highlighted in orange. System R encodes the quantum information, while the blue superchannel Θ represents its subsequent transmission within the network (b).

its expression through the framework of quantum channels [6–8], encompassing diverse processes such as the operations of polarization beam splitters, wave plates, and single photon detectors in photonic systems. Mirroring the dynamic evolution inherent in quantum systems, quantum channels also undergo temporal transfor-

* fanzhaobing@hrbeu.edu.cn

† hmamath@hrbeu.edu.cn

‡ kishor.bharti1@gmail.com

§ dax_koh@ihpc.a-star.edu.sg

¶ mathxiao123@gmail.com

mations that shape their behavior over time [9–11]. To encapsulate their evolution, quantum superchannels [12] emerges as a powerful tool. While a quantum channel can be regarded as a single quantum process, a quantum superchannel incorporates a sequential combination of two processes: pre-processing and post-processing procedures, with the integration of quantum memory serving as a connecting bridge. This formulation empowers us to explore the fundamental nature of quantum dynamics spanning multiple time points, where quantum channels are interconnected through the orchestration of quantum memory. These quantum dynamics underpin a myriad of protocols, including quantum causal inference [13–15], quantum-enhanced agents [16–19], quantum network communication [20–28], distributed quantum computing [29–31], and non-Markovian open systems [32–34]. Hence, there is a pressing need for a more comprehensive understanding of entanglement across multiple temporal instances and its impact on quantum communications.

Guided by this dynamic perspective, we embark on an illuminating journey into quantum teleportation [35–39], where the remarkable efficiency in surpassing classical communication limitations stems from the entangling bipartite channel shared between the sender and receiver. Real-world quantum communication is susceptible to environmental factors that degrade its performance. Free space encounters atmospheric thinness and turbulence [40–45], while fiber channels face temperature fluctuations, Kerr non-linearity, and reference frame disparities [46–49]. In response to these issues, conventional strategies focus on post-processing through maximizing local operations and classical communication (LOCC) [50]. Yet, the general manipulation of quantum channels encompasses both pre-processing and post-processing. This prompts fundamental questions: Which approach, pre-processing or post-processing, demonstrates superior efficacy in unlocking the communication capabilities of noisy bipartite channels? Can superchannel-assisted protocols outperform conventional scenarios without incurring additional resource costs? Additionally, what is the ultimate performance limit achievable by leveraging superchannels? Similar inquiries apply to quantum repeaters [51]. Looking ahead to general quantum networks, wherein multiple rounds of communication occur among the sender, receiver, and intermediate agents, an intriguing query surfaces: What is the optimal performance for transmitting quantum information? This model assumes profound significance in the domains of distributed and cloud-based quantum computing [52–55]. Nevertheless, the answer to this crucial question remains elusive.

Results— This work answers a diverse array of questions, converging upon a central theme: the intricate interplay of quantum dynamics across multiple temporal instances and their impact on the performance of quantum communication. Our investigation unveils the driving force behind these dynamics – temporal entanglement, the evolution of entanglement over time. Through

this lens, we make a series of interesting discoveries: (i) For quantum teleportation, we showcase the supremacy of pre-processing techniques over all post-processing approaches under specific noise models. This emphatically highlights the indispensable role of pre-processing in enhancing quantum communication vis-à-vis conventional protocols. (ii) For quantum repeaters, we uncover the astonishing ability of pre-processing techniques to effectively double the communication distance in select scenarios. Moreover, under specific noise models, the power of pre-processing becomes even more remarkable, resulting in exponential performance growth as the number of connection nodes increases. (iii) For general quantum networks, we formulate their performance limit in terms of temporal entanglement, resolving a long-standing open question since the inception of quantum information science. Our results not only establish a fundamental limitation for quantum network communication, igniting a captivating path for the future development of quantum communication technology, but also introduce a practical and experimentally viable approach to enhance existing quantum communication technologies through pre-processing techniques.

Temporal Entanglement— Quantum entanglement – the emergence of non-local correlations among multiple systems – marks a definitive departure from classical physics [5]. This holistic property of compound systems has unlocked avenues for quantum cryptography [56–58], communication [59–64], and computing [65–69]. Although investigations of entanglement have grown significantly in recent years, most studies focus on entanglement within a single quantum process, including static entanglement of states [70–74] and dynamical entanglement of channels [75–79]. While such works have yielded valuable insights, a comprehensive understanding of the dynamics of molecules and biochemical systems [80], distributed and cloud-based quantum computing, as well as quantum network communication, demands a theory of temporal entanglement that can describe non-local correlations associated with non-Markovian quantum processes across various time points.

Investigating temporal entanglement encoded in non-Markovian processes is a challenge, with far-reaching implications for quantum information processing, computation, and metrology [81–83]. Concurrently, the rapid development of quantum resource theory as a powerful tool for understanding and manipulating diverse quantum phenomena has opened up new avenues for tackling this challenge [84–88]. Here, riding the waves of quantum resource theories, we explore the nature and properties of temporal entanglement in quantum systems. The object of research is a non-Markovian process \mathcal{E} [89–93] comprising k multipartite quantum channels \mathcal{E}_i ($1 \leq i \leq k$) that are interconnected via quantum memory, i.e., $\mathcal{E} := \mathcal{E}_k \circ \dots \circ \mathcal{E}_1$ (colored orange in Fig. 2).

Free manipulation of \mathcal{E} is a variable concept that depends on the restrictions imposed in a physical laboratory. For example, LOCC, which involves communication

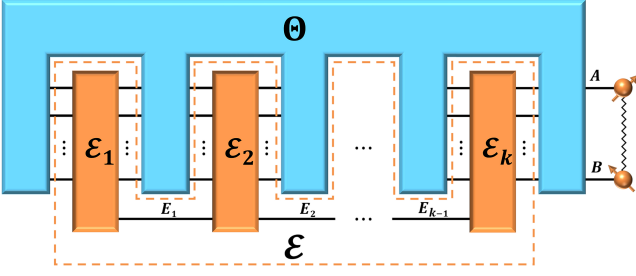


FIG. 2. **Process of distilling static entanglement from a non-Markovian process:** For a non-Markovian quantum process \mathcal{E} (depicted in orange) consisting of k multipartite quantum channels, namely $\mathcal{E} := \mathcal{E}_k \circ \dots \circ \mathcal{E}_1$, a free manipulation Θ (shown in blue) can be applied to transform it into a static state shared between systems A and B . The fidelity $\text{Tr}[\Theta(\mathcal{E}) \cdot \phi_d^+]$ quantifies the similarity between the output state $\Theta(\mathcal{E})$ and a d -dimensional maximally entangled state ϕ_d^+ . By maximizing over all possible free manipulations, we obtain the d -fidelity of \mathcal{S} distillation $F_{\max}^{d,\mathcal{S}}(\mathcal{E}) := \max_{\Theta \in \mathcal{S}\text{-free}} \text{Tr}[\Theta(\mathcal{E}) \cdot \phi_d^+]$. It represents an upper bound on the amount of static entanglement that can be obtained from \mathcal{E} through \mathcal{S} -free manipulation.

between parties and is considered free in theoretical investigations of entanglement theory, may not be feasible in practical experiments due to the impractically large number of communication rounds it may require, coupled with the exponentially growing amount of communication bits in each round. In such cases, experimentalists may choose to use a modified set of free operations denoted as $\text{LOCC}_1(\text{poly}(d))$. This approach involves local operations and one-way classical communication, with the communication complexity polynomially dependent on the dimension ($d := d_R$) of the message system R , followed by a coarse-graining of quantum instruments [94]. By employing these operations, the operational complexity is reduced, making the experiment more feasible in real-world scenarios. Returning to the transformation of a non-Markovian process, we define a manipulation Θ (colored blue in Fig. 2) as being \mathcal{S} -free if it can be expressed as a sequence of quantum channels, with each channel belonging to the set \mathcal{S} . As technology continues to progress, it opens up new possibilities for performing increasingly complex and powerful operations, expanding the feasible set of manipulations. To ensure that the operations performed by \mathcal{S} are at least as powerful as those achievable in laboratories, it is essential to assume that $\text{LOCC}_1(\text{poly}(d)) \subset \mathcal{S}$. We remark that while *convexity* and *closedness* are desirable mathematical properties of free manipulations, we do not require them in our analysis as they are not necessary and cannot be justified a priori.

Our goal is to evaluate the temporal entanglement encoded in a non-Markovian process \mathcal{E} , and explore its relevance in quantum network communication. To accomplish this, we introduce the d -fidelity of \mathcal{S} distillation, denoted as $F_{\max}^{d,\mathcal{S}}(\mathcal{E})$, which quantifies the maximum amount

of static entanglement that can be extracted and distributed among designated parties through \mathcal{S} -free manipulations (Fig. 2). We further demonstrate that this quantity plays a crucial role in determining the performance of quantum network communication. By emphasizing the broadest form of non-Markovian processes, our exploration of temporal entanglement naturally encompasses previous studies [95–101], assimilating them as specific instances. A more detailed resource-theoretic framework is presented in [102, Sec. II].

Quantum Teleportation— Teleportation is a fundamental process in quantum information science that allows the secure transfer of quantum information between distant parties without physically transmitting the information carrier [103]. It involves four essential components: First, the message to be transmitted is encoded in a quantum state ψ on system R ; Second, a pre-processing step prepares two ancillary qubits in the state $|0\rangle$ for both the sender Alice and the receiver Bob; Third, an entangling gate that creates a quantum correlation between the sender and receiver; Finally, a post-processing step Θ_0^{post} involves standard Bell measurements on the sender’s system followed by a local unitary operation on the receiver’s system. Fig. 3(a) visualizes the physical implementation of standard quantum teleportation.

Achieving perfect information transmission requires the creation of a maximally entangled state between the sender and receiver. While this can be accomplished theoretically, practical implementations are challenged by the presence of noise and decoherence, which can significantly impact the reliability and accuracy of the communication. Before analyzing a general noisy model, let us examine a specific scenario in which local noise follows the gate that creates maximally entangled state. We denote the resulting bipartite channel shared between Alice and Bob as $\mathcal{E}(p, q)$ (Fig. 3(b)), with p and q representing the noise parameters acting on the sender’s and receiver’s systems, respectively. To fully exploit the capabilities of noisy entangling gate $\mathcal{E}(p, q)$ and optimize the performance of teleportation, the conventional approach [50] involves maximizing over all possible LOCC post-processing protocols where the implementation of the noisy entangling gate is followed by a LOCC operation shared between the sender Alice and the receiver Bob (Fig. 3(c)). This approach encompasses Θ_0^{post} as a specific case, thus enabling a more robust and efficient implementation of quantum teleportation. It is natural to wonder whether the conventional approach can achieve optimal performance given a noisy entangling gate?

Our analysis indicates that there is still room for improvement in the performance of noisy quantum teleportation protocols, and that new strategies can be developed to achieve better results. The temporal entanglement shared between Alice and Bob, which is carried by the bipartite channel $\mathcal{E}(p, q)$, is the *bona fide* quantum resource in teleportation. To fully exploit the capabilities of noisy entangling gates, we consider the most general way of manipulating quantum channels, namely,

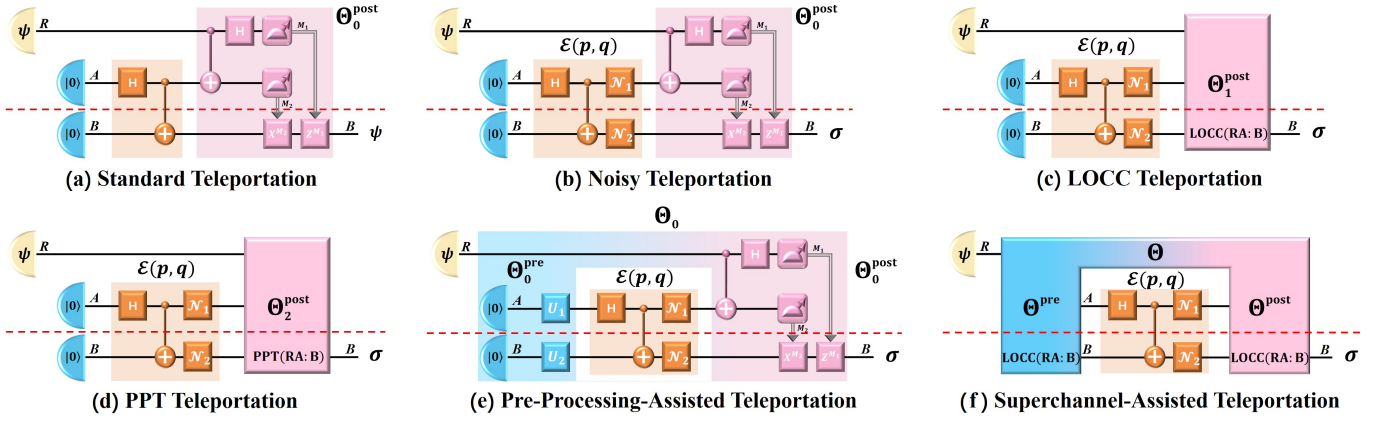


FIG. 3. **Teleportation protocols:** (a) standard teleportation, where the quantum information ψ_R is transmitted from sender Alice to receiver Bob. Alice has access to systems RA , while Bob has access to system B . The protocol employs a standardized LOCC operation Θ_0^{post} , which is graphically represented by the pink box in the diagram. (b) noisy teleportation, where the entangling gates are followed by channels $\mathcal{N}_1(p)$ and $\mathcal{N}_2(q)$, resulting in a noisy entangling gate $\mathcal{E}(p, q)$. (c) LOCC teleportation, which maximizes all possible LOCC operations after applying the noisy entangling gate $\mathcal{E}(p, q)$. (d) PPT teleportation, where the set of allowable operations following the application of the noisy entangling gate $\mathcal{E}(p, q)$ has been extended to include all PPT channels. (e) pre-processing-assisted teleportation, where a special pre-processing protocol $\Theta_0^{\text{pre}} := \mathcal{U}_1(|0\rangle\langle 0|)_A \otimes \mathcal{U}_2(|0\rangle\langle 0|)_B$ has been considered, followed by the noisy entangling gate $\mathcal{E}(p, q)$ and standardized LOCC operation Θ_0^{post} . (f) superchannel-assisted teleportation, in which a LOCC superchannel Θ has transformed the entangling gate $\mathcal{E}(p, q)$ into a teleportation channel $\Theta(\mathcal{E}(p, q))_{R \rightarrow B}$. We remark that protocol f does not require any additional resources compared to protocol c, as the extra pre-processing involved in protocol f falls under the umbrella of LOCC operations, which are considered free. These diagrams distinguish between systems belonging to Alice, which are located above the dashed red line, and those belonging to Bob, which are situated below the dashed line.

by using quantum superchannels. This concept involves pre-processing and post-processing operations connected through a quantum memory. In the conventional approach to quantum teleportation, the maximization over all possible LOCC post-processing operations is typically performed. However, it is important to recognize that this approach neglects the potential benefits of maximizing all LOCC for pre-processing as well. By incorporating LOCC superchannel-assisted teleportation protocols (Fig. 3(f)), we can achieve a better performance of quantum teleportation in the presence of noise, without requiring additional resources.

While it is evident that the teleportation performance of the superchannel-assisted protocols in Fig. 3(f) outperforms that of the conventional approach in Fig. 3(c), comparing the two can be challenging as both require the maximization over the set of LOCC operations, whose mathematical structure is difficult to characterize. Nevertheless, we propose a new pre-processing-assisted teleportation protocol that incorporates local unitaries as a pre-processing step, followed by the standard post-processing step Θ_0^{post} (Fig. 3(e)); this protocol serves as a lower bound for the performance of superchannel-assisted protocol (Fig. 3(f)). At the same time, we propose a positive-partial-transpose (PPT) teleportation protocol that optimizes the post-processing step over all possible completely-PPT-preserving operations (Fig. 3(d)); this protocol functions as an upper bound for the performance of conventional protocol (Fig. 3(c)). We find noisy en-

tangling gates that the protocol in Fig. 3(e) outperforms Fig. 3(d), providing a clear distinction between the protocols shown in Fig. 3(f) and Fig. 3(c). In particular, we conducted a numerical experiment where system A underwent an amplitude damping channel with a noise parameter $p = 0.23$, and system B experienced a depolarizing channel with a noise parameter $q = 0.91$. To assess the impact of pre-processing on the performance under different parameter regimes, we present the results of a comprehensive analysis in Fig. 4(a). Upon maximizing over all parameters of pre-processing, we present a comparison between protocols of Fig. 3(e) and Fig. 3(d) in Fig. 4(b). Our results unequivocally demonstrate that, in this case, the performance of PPT teleportation, despite employing entangling operations, is inferior to pre-processing-assisted teleportation that relies solely on pre-processing operations. Finally, we present the improvement ratio for various noise models and parameters in Fig. 4(c), highlighting the efficacy of pre-processing-assisted teleportation.

In actual experiments, the magnitude of ambient noise frequencies is often considerably lower compared to the frequency of photon distribution. This particular characteristic allows for efficient learning of these noises within a defined time interval. As a result, the implementation of pre-processing techniques becomes not only theoretically viable but also practically feasible. While the findings presented here provide valuable insights into several noisy models, it is important to note that Fig. 4 repre-

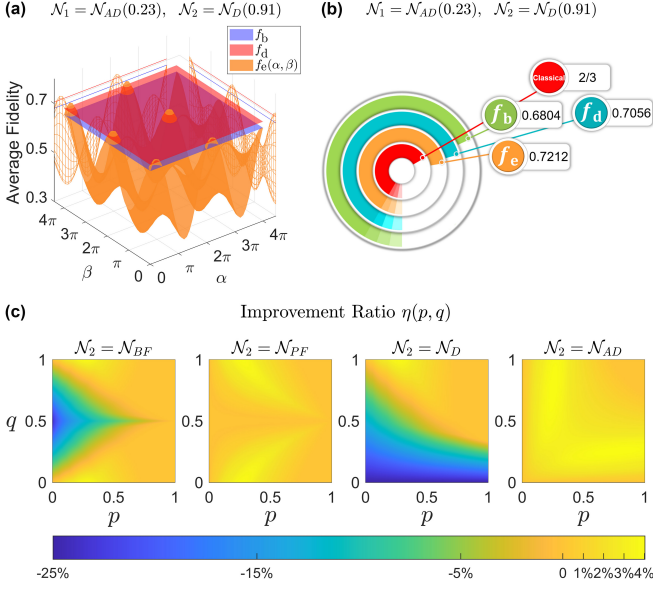


FIG. 4. Performance comparison of different teleportation protocols: In order to evaluate the effectiveness of a quantum channel \mathcal{E} in transmitting quantum information, we employ the average fidelity, $f(\mathcal{E}) := \int d\psi \text{Tr}[\psi \cdot \mathcal{E}(\psi)]$, where the integral is taken over the Haar measure. We consider the noise channels shown in Fig. 3 with $\mathcal{N}_1 = \mathcal{N}_{AD}(p = 0.23)$ and $\mathcal{N}_2 = \mathcal{N}_D(q = 0.91)$ being amplitude damping and depolarizing channels. The pre-processing, given by $U_1(\alpha) := R_y(\alpha)$ and $U_2(\beta) := R_y(\beta)$, are rotations along the y -axis with angles α and β . The performances of protocols b, c, d, e, and f are denoted as f_b , f_c , f_d , $f_e(\alpha, \beta)$, and f_f , satisfying $f_b \leq f_c \leq f_d$ and $f_e(\alpha, \beta) \leq f_f$. Figure (a) demonstrates a performance comparison between f_b , f_d , and $f_e(\alpha, \beta)$. We maximize the performance of protocol e by optimizing over all R_y gates in the pre-processing step, resulting in $f_e := \max_{\alpha, \beta} f_e(\alpha, \beta)$ with $f_e(\alpha, \beta) \leq f_e \leq f_f$. Figure (b) displays the advantage of performance f_e over f_b , f_d , and the classical limit. Figure (c) illustrates the improvement ratio $\eta(p, q) := (f_e - f_d)/f_d$ for various noisy models, where we set $\mathcal{N}_1 = \mathcal{N}_{AD}$ and choose \mathcal{N}_2 from bit flip \mathcal{N}_{BF} , phase flip \mathcal{N}_{PF} , depolarizing \mathcal{N}_D , and amplitude damping \mathcal{N}_{AD} channels.

sents only a small fraction of the potential models that can be explored. As such, we urge interested readers to consult [102, Sec. III] for a thorough account of our numerical experiments and additional theoretical results that may further inform future investigations.

The characterization of the ultimate capabilities of a bipartite channel $\mathcal{E}(p, q)$ in the context of quantum teleportation under all possible S -free superchannels is a fundamental question in quantum information theory. While previous discussions have focused on specific choices of free operations, a comprehensive understanding of the fundamental limitation remains elusive. Our framework of quantum network communication, which accounts for non-Markovian processes and encompasses channels as special cases, will address this problem and provide a unified approach to investigating the role of temporal entanglement in quantum communication.

Quantum Repeater– Quantum communication, despite its numerous advantages over classical communication, encounters a fundamental obstacle when transmitting information over long distances [104]: the likelihood of errors increases as the length of the channel connecting the parties grows. This is especially true when using photonic quantum communication over optical fibers, as both photon absorption and depolarization tend to increase exponentially with the length of the fiber. As a result, longer quantum communications experience significant signal quality degradation, leading to increased error rates and reduced efficiency and reliability. A promising approach to overcome this challenge involves the incorporation of quantum repeaters [51]. These repeaters can be built with auxiliary particles at intermediate connection points, enabling the transmission of quantum information over longer distances [105–126]. By distributing entangled pairs of particles, quantum repeaters can help to maintain the integrity of the transmitted information and ensure that the communication remains reliable, efficient, and secure, even over long distances.

Entanglement swapping [127–129] is a critical technical tool that enables quantum repeaters by creating a new, entangled pair between remote locations. This process bypasses the need for direct transmission, and entangling gates are valuable resources within this setup. The construction of a quantum repeater can be seen as a multipartite quantum channel shared between sender, receiver, and intermediate connection points. Since entanglement swapping is a post-processing step, a free superchannel should be the most general approach to manipulating the multipartite quantum channel that underlies quantum repeaters. Motivated by this, we investigate the potential of pre-processing-assisted quantum repeater protocols and their ability to enhance the performance of quantum communication. The behavior of superchannel-assisted repeaters remains a topic for investigation in our forthcoming framework for quantum networks.

In the conventional protocol of quantum repeaters, a communication channel between two distant nodes A and B is divided into N segments, and N pairs of qubits are created, with each pair being shared between a connection point and a node (Fig. 5(a)). Let us now demonstrate the benefits of using pre-processing – that is, how pre-processing applied prior to multipartite quantum channel that creates quantum repeaters can enhance their performance. Our research focuses on the use of noisy singlets, as illustrated in Fig. 5(b). We compare the performance of a conventional quantum repeater, where entanglement swapping is performed directly on the noisy singlets, to that of a pre-processing-assisted quantum repeater, where pre-processing is applied before entangling gate that creates quantum repeater. The only difference between the noisy singlets in Fig. 5(b) is the presence of pre-processing. The pre-processing assisted protocol outperforms the conventional approach, as it maximizes over all possible pre-processings, while the conventional approach is simply obtained by setting the local unitary

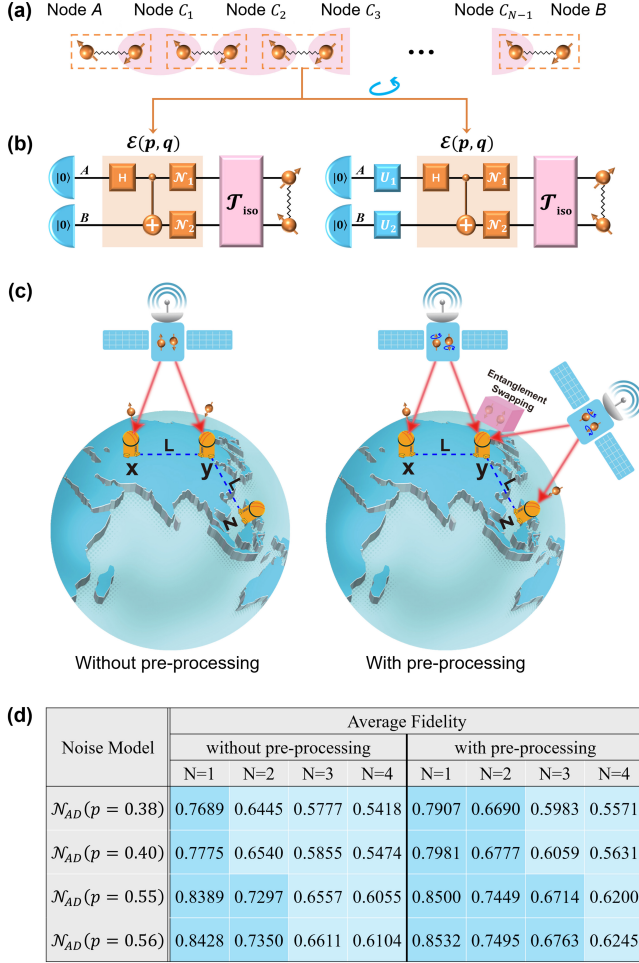


FIG. 5. **Enhancing quantum repeaters:** Figure (a) illustrates a quantum repeater schematic where distant nodes A and B are divided into N segments. N pairs of qubits are created and shared between nodes. Each intermediate node undergoes entanglement swapping. Figure (b) depicts the creation of noise singlet shared between nodes. We use the same model, i.e., $\mathcal{E}(p, q)$, discussed previously in teleportation (Fig. 3), followed by isotropic twirling $\mathcal{T}_{\text{iso}}(\cdot) := \int dU U \otimes \bar{U}(\cdot) U^\dagger \otimes U^T$ [130]. Figure (c) shows how communication distance can be doubled using pre-processing techniques. Assuming a satellite distributes a noise singlet, with \mathcal{N}_1 as the amplitude damping channel with $p = 0.38$ and \mathcal{N}_2 as the noiseless channel, to ground stations labeled x and y , separated by a distance L . While information transmission from x to an additional ground station z located at the same distance L from y via entanglement swapping cannot exceed the classical limit, as $0.6445 < 2/3$, pre-processing can be used to surpass the limit without additional resource consumption. Figure (d) analyzes the fidelity of a state obtained through N copies of noise singlet under entanglement swapping, and compare their performance with and without pre-processing. The amplitude damping channel \mathcal{N}_1 has a noisy parameter chosen from $\{0.38, 0.40, 0.55, 0.56\}$, while the identity channel $\mathcal{N}_2 = \text{id}$ represents noiseless evolution. The average fidelity is indicated by blue shading, with dark blue representing performance that exceeds the classical limit of $2/3$, and light blue indicating cases where the performance falls below this limit.

in pre-processing to the identity. To evaluate the effectiveness, we computed the improvement ratio $\zeta(p, q)$, which represents the percentage increase in performance attained through the use of pre-processing (see [102, Sec. IVA] for a formal definition). By connecting N adjacent pairs through entanglement swapping, we can generate a new pair with fidelity $1/4 + 3((4F_1 - 1)/3)^N / 4$ with F_1 being the entanglement fidelity of noisy singlet shown in the left subfigure of Fig. 5(b). Assuming that the maximization over pre-processing has been taken into account, the entanglement fidelity of the resulting state can be expressed as $1/4 + 3(1 + \zeta(p, q))^N ((4F_1 - 1)/3)^N / 4$, displaying an exponential growth, compared with the one without pre-processing, as the number of N increases.

Next, we will transition to conducting numerical experiments to further investigate this topic. Specifically, we examine the case with a single noisy gate: \mathcal{N}_1 is the amplitude damping channel with noisy parameter $p = 0.38$, while at the same time \mathcal{N}_2 is the noiseless channel. Assume that such a state can be used to teleport quantum information with length L . Our results demonstrate that without pre-processing, only one copy of such a state can beat the classical limit $2/3$, resulting in a communication distance of L . However, with pre-processing, even the connection of two copies, with a communication distance of $2L$, can outperform the classical bound of communication. Fig. 5(c) portrays a schematic diagram of the doubling of communication distance, which highlights the significant potential of pre-processing techniques for global quantum communication. We also observe a similar doubling effect in the case of $p = 0.4$, where the use of pre-processing techniques doubles the communication distance in transmitting quantum information. However, the data in the last two rows of Fig. 5(d) reveals that doubling the communication distance is not always feasible. Nevertheless, the pre-processing techniques enable the extension of connective copies of states in the quantum network of Fig. 5(a) from 2 to 3 for different noise parameters. A more comprehensive analysis has been included in [102, Sec. IVA].

Quantum Network– The development of a reliable quantum network capable of transmitting information over long distances is an indispensable step towards the advancement of quantum communication and computation. The quantum repeater has emerged as a promising approach for achieving this goal. However, the assumption of identical Bell measurements on independent and identically distributed (i.i.d.) quantum states in each round, which is commonly used in this approach, cannot be justified a priori despite its analytical convenience. In reality, fluctuations in error rates can occur due to variations in nodes or environmental factors, necessitating the introduction of an adaptive communication protocol that can dynamically adjust its behavior in response to such changes. The presence of imperfect devices and transmission channels further exacerbates this problem, highlighting the need for continuous monitoring and adjustment of the network to ensure reliable and

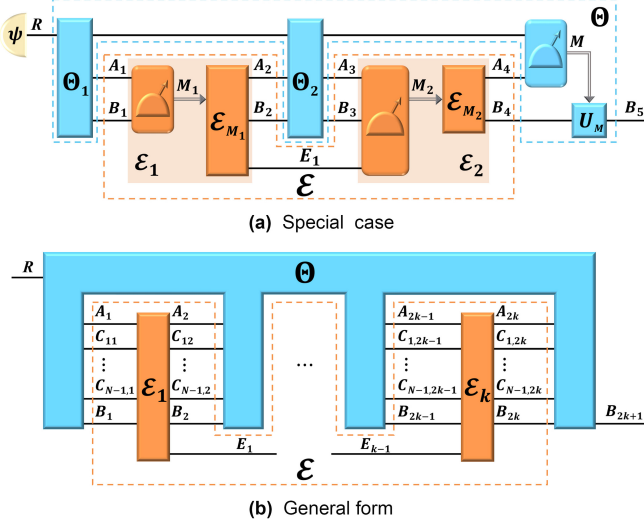


FIG. 6. **Adaptive quantum communication protocols:** Figure (a) shows an example of adaptive quantum communication protocol. The protocol uses multipartite operations \mathcal{E}_1 and \mathcal{E}_2 implemented via a positive operator-valued measure (POVM) and a retrieving quantum channel. Figure (b) presents the general adaptive quantum communication protocol \mathcal{E} in orange, which can be converted into a communication channel between the message and the receiver's system using free manipulation Θ in blue.

efficient quantum communication. In classical wireless communication, adaptive communication protocols [131–133] have proven effective in optimizing communication parameters to account for variations in network conditions. Extending this approach to the quantum realm, we propose a framework called *adaptive quantum communication protocols*. The framework comprises multiple rounds of quantum communications, connected by quantum memory, which enables the optimization of communication parameters based on the current state of the network. This allows for the adaptation of communication parameters to changing conditions, ensuring that communication remains reliable and efficient even in the presence of noise and other environmental factors.

Single-round quantum network communications serve as fundamental building blocks within adaptive quantum communication protocols. Such a network, as depicted in Fig. 1(a), is constructed using a multipartite quantum channel \mathcal{E} , responsible for generating and maintaining entanglement among the sender Alice, the receiver Bob, and any intermediary agents involved. Notably, both quantum teleportation and repeaters can be regarded as specific instances of this general description. To fully unfold the potential of \mathcal{E} , it is essential to employ a \mathcal{S} -free manipulation Θ , as illustrated in Fig. 1(b). The term “free” in this context refers to the experimental accessibility of manipulating \mathcal{E} in a laboratory setting, enabling the creation of a communication channel $\Theta(\mathcal{E})$ between sender Alice and receiver Bob.

For a protocol to be truly adaptive, it should incor-

porate multiple rounds of quantum network communications linked by memory. Fig. 6(a) provides a concrete example of adaptive quantum communication protocol, which helps to develop a more intuitive understanding. This protocol involves two resourceful bipartite operations, denoted as \mathcal{E}_1 and \mathcal{E}_2 , each comprising a learning machine implemented through a joint POVM on multiple systems, and a retrieving device realized using a quantum channel. The communication between these operations is dynamically adjusted based on changing conditions of the channel, thanks to the use of a memory-assisted quantum feedback control scheme. This dynamic adjustment allows the protocol to respond to variations in network conditions, such as the presence of intermediate nodes between sender and receiver. While this special scheme does not account for intermediate nodes, the inclusion of such nodes can greatly enhance the long-distance quantum communication capabilities of the protocol.

An adaptive quantum communication protocol is formulated by composing finite rounds of multipartite quantum channels, denoted by \mathcal{E}_1 through \mathcal{E}_k , resulting in the overall non-Markovian process $\mathcal{E} := \mathcal{E}_k \circ \dots \circ \mathcal{E}_1$. This shared resource, \mathcal{E} , is used by Alice, Bob, and intermediaries over multiple time points. To ensure secure communication, they apply a \mathcal{S} -free manipulation Θ , resulting in channel $\Theta(\mathcal{E})$ between the message and receiver systems, as illustrated in Fig. 6(b). The d -fidelity of \mathcal{S} distillation can be used to quantify the temporal entanglement associated with an adaptive quantum communication protocol. At the same time, the communication performance of the resulting channel $\Theta(\mathcal{E})$ can be characterized by the optimization $f_{\max}(\mathcal{E}) := \max_{\Theta \in \mathcal{S}\text{-free}} f(\Theta(\mathcal{E}))$, where f is the average fidelity. The following theorem shows that the performance is entirely determined by the amount of temporal entanglement that can be generated and utilized by the adaptive quantum communication protocol.

Theorem. *An adaptive quantum communication protocol \mathcal{E} can be converted into a communication channel $\Theta(\mathcal{E})$, shared between the message and receiver systems (Fig. 6(b)). This transformation utilizes a \mathcal{S} -free manipulation Θ , involving a series of quantum channels, each belonging to the set \mathcal{S} , wherein \mathcal{S} encompasses $\text{LOCC}_1(\text{poly}(d))$ as a subset. The optimal performance f_{\max} , as measured by the average fidelity, under all possible \mathcal{S} -free manipulations is given by*

$$f_{\max}(\mathcal{E}) = \frac{dF_{\max}^{d,\mathcal{S}}(\mathcal{E}) + 1}{d + 1}, \quad (1)$$

where $F_{\max}^{d,\mathcal{S}}(\mathcal{E})$ stands for the d -fidelity of \mathcal{S} distillation of \mathcal{E} (Fig. 2), and d corresponds to the dimension of the message system.

When \mathcal{E} adopts the specific form of $\mathcal{E}(p, q)$, Eq. 1 delineates the fundamental limits of teleportation considered in Fig. 3. In the context of repeaters, where nodes are interconnected by implementing $\mathcal{E}_1 \otimes \dots \otimes \mathcal{E}_N$, the optimal performance thereof is governed by $F_{\max}^{d,\mathcal{S}}(\mathcal{E}_1 \otimes \dots \otimes \mathcal{E}_N)$.

If \mathcal{E} is regarded as a bipartite state subject to LOCC, our theorem encompasses and extends the earlier seminal findings presented in Ref. [50].

The generality of our theorem arises from two aspects. Firstly, unlike many existing models, our model does not rely on any specific assumptions or structures about the protocol, making it applicable to a wide range of communication scenarios, including those with different numbers of communication rounds or spatial correlations shared between quantum systems. The only constraint is the principle of causality [134–136], which ensures that information cannot be transmitted from the future to the past. This allows our theorem to be readily adapted to arbitrary quantum causal networks. Secondly, our approach does not assume any specific manipulations of the adaptive quantum communication protocols or make any assumptions about their mathematical properties. This lack of constraints enables our theorem to provide a more comprehensive and flexible framework for understanding and analyzing adaptive quantum communication protocols under different quantum resource theories.

Discussion— In this work, we demonstrate that the performance of a quantum communication protocol is solely determined by its temporal entanglement. Therefore, the effectiveness of communication is contingent upon the manipulation of temporal entanglement. In quantum teleportation, the temporal entanglement is carried by a bipartite channel between two time points, and its manipulation is characterized by a superchannel. Building upon this consideration, we propose a novel superchannel-assisted teleportation protocol. Our numerical experiments show that even a subprotocol with pre-processing can surpass the conventional approach. In contrast to catalyst-assisted protocols [137–145], our method stands out by eliminating the need for ancillary systems, resulting in a more streamlined and practical approach for experimental implementation. In quantum repeaters, temporal entanglement is carried by tensors of bipartite channels shared between connection points, and their manipulation is also characterized by the framework of superchannels. Theoretical investigation has further shown that the pre-processing techniques can lead to an exponential growth in performance with respect to the number of connection points, offering a promising approach to achieving high-fidelity quantum communication over long distances. In addition, numerical exper-

iments have demonstrated the advantages conferred by doubling the communication distance within specific scenarios, providing further evidence for the effectiveness of pre-processing techniques in quantum repeaters.

Adaptive quantum communication protocols are a key component in the construction of general quantum networks, which enable the iterative exchange of quantum information between parties. Among these protocols, quantum memory plays a critical role in facilitating communication, allowing for the storage and retrieval of quantum states that can be accessed and manipulated by the parties involved. The performance of these protocols in transmitting quantum information is determined by the temporal entanglement of the network. Understanding the relationship between quantum network communication and temporal entanglement can help improve the performance of non-Markovian communication protocols in practice. Specifically, more temporal entanglement leads to better performance in communication.

The need for further investigation is apparent, and it begs the question: how can we calculate the optimal performance of an adaptive quantum communication protocol? This problem depends on two factors: the set of free operations that are allowed in a given physical laboratory, and how optimization can be performed under these free operations [146–150]. Solving such questions requires a more detailed discussion, which we leave for future works. Finally, it is essential to note that, advances in quantum communication protocols have implications beyond quantum information processing. For example, quantum networks can improve the accuracy and resolution of clocks and sensors [151–155], secure communication, and enable new forms of distributed and cloud-based computing. Therefore, further research in this area is critical for advancing both fundamental science and technology.

ACKNOWLEDGMENTS

We would like to thank Varun Narasimhachar, Davit Aghamalyan, Rahul Arvind, and Mile Gu for fruitful discussions. This research is supported by the National Research Foundation, Singapore and A*STAR under its Quantum Engineering Programme (NRF2021-QEP2-02-P03), and by A*STAR under its Central Research Funds.

-
- [1] H. J. Kimble, The quantum internet, *Nature* **453**, 1023 (2008).
 - [2] S. Pirandola and S. L. Braunstein, Physics: Unite to build a quantum internet, *Nature* **532**, 169 (2016).
 - [3] C. Simon, Towards a global quantum network, *Nature Photonics* **11**, 678 (2017).
 - [4] S. Wehner, D. Elkouss, and R. Hanson, Quantum internet: A vision for the road ahead, *Science* **362**, eaam9288 (2018),

- <https://www.science.org/doi/pdf/10.1126/science.aam9288>.
- [5] R. Horodecki, P. Horodecki, M. Horodecki, and K. Horodecki, Quantum entanglement, *Rev. Mod. Phys.* **81**, 865 (2009).
- [6] M. A. Nielsen and I. L. Chuang, *Quantum Computation and Quantum Information: 10th Anniversary Edition* (Cambridge University Press, 2010).
- [7] M. M. Wilde, *Quantum Information Theory* (Cambridge University Press, 2013).

- [8] J. Watrous, *The Theory of Quantum Information* (Cambridge University Press, 2018).
- [9] G. Chiribella, G. M. D'Ariano, and P. Perinotti, Theoretical framework for quantum networks, *Phys. Rev. A* **80**, 022339 (2009).
- [10] G. Chiribella, G. M. D'Ariano, and P. Perinotti, Quantum circuit architecture, *Phys. Rev. Lett.* **101**, 060401 (2008).
- [11] G. Chiribella, G. M. D'Ariano, and P. Perinotti, Informational derivation of quantum theory, *Phys. Rev. A* **84**, 012311 (2011).
- [12] G. Chiribella, G. M. D'Ariano, and P. Perinotti, Transforming quantum operations: Quantum supermaps, *EPL (Europhysics Letters)* **83**, 30004 (2008).
- [13] K. Ried, M. Agnew, L. Vermeyden, D. Janzing, R. W. Spekkens, and K. J. Resch, A quantum advantage for inferring causal structure, *Nature Physics* **11**, 414 (2015).
- [14] J.-P. W. MacLean, K. Ried, R. W. Spekkens, and K. J. Resch, Quantum-coherent mixtures of causal relations, *Nature Communications* **8**, 15149 (2017).
- [15] Y. Xiao, Y. Yang, X. Wang, Q. Liu, and M. Gu, Quantum uncertainty principles for measurements with interventions (2023), arXiv:2305.07914 [quant-ph].
- [16] M. Gu, K. Wiesner, E. Rieper, and V. Vedral, Quantum mechanics can reduce the complexity of classical models, *Nature Communications* **3**, 762 (2012).
- [17] J. Thompson, A. J. P. Garner, V. Vedral, and M. Gu, Using quantum theory to simplify input-output processes, *npj Quantum Information* **3**, 6 (2017).
- [18] T. J. Elliott, M. Gu, A. J. P. Garner, and J. Thompson, Quantum adaptive agents with efficient long-term memories, *Phys. Rev. X* **12**, 011007 (2022).
- [19] K.-D. Wu, C. Yang, R.-D. He, M. Gu, G.-Y. Xiang, C.-F. Li, G.-C. Guo, and T. J. Elliott, Implementing quantum dimensionality reduction for non-markovian stochastic simulation, *Nature Communications* **14**, 2624 (2023).
- [20] M. Pant, H. Krovi, D. Towsley, L. Tassioulas, L. Jiang, P. Basu, D. Englund, and S. Guha, Routing entanglement in the quantum internet, *npj Quantum Information* **5**, 25 (2019).
- [21] R. Valivarthi, S. I. Davis, C. Peña, S. Xie, N. Lauk, L. Narváez, J. P. Allmaras, A. D. Beyer, Y. Gim, M. Hussein, G. Iskander, H. L. Kim, B. Korzh, A. Mueller, M. Rominsky, M. Shaw, D. Tang, E. E. Wollman, C. Simon, P. Spentzouris, D. Oblak, N. Sinclair, and M. Spiropulu, Teleportation systems toward a quantum internet, *PRX Quantum* **1**, 020317 (2020).
- [22] D. Awschalom, K. K. Berggren, H. Bernien, S. Bhav, L. D. Carr, P. Davids, S. E. Economou, D. Englund, A. Faraon, M. Fejer, S. Guha, M. V. Gustafsson, E. Hu, L. Jiang, J. Kim, B. Korzh, P. Kumar, P. G. Kwiat, M. Lončar, M. D. Lukin, D. A. Miller, C. Monroe, S. W. Nam, P. Narang, J. S. Orcutt, M. G. Raymer, A. H. Safavi-Naeini, M. Spiropulu, K. Srinivasan, S. Sun, J. Vučković, E. Waks, R. Walsworth, A. M. Weiner, and Z. Zhang, Development of quantum interconnects (quics) for next-generation information technologies, *PRX Quantum* **2**, 017002 (2021).
- [23] S. L. N. Hermans, M. Pompili, H. K. C. Beukers, S. Baier, J. Borregaard, and R. Hanson, Qubit teleportation between non-neighbouring nodes in a quantum network, *Nature* **605**, 663 (2022).
- [24] S. F. Bush, W. A. Challener, and G. Manentelet, A perspective on industrial quantum networks, *AVS Quantum Science* **3**, 030501 (2021), <https://doi.org/10.1116/5.0051881>.
- [25] W. J. Munro, N. L. Piparo, J. Dias, M. Hanks, and K. Nemoto, Designing tomorrow's quantum internet, *AVS Quantum Science* **4**, 020503 (2022), <https://doi.org/10.1116/5.0092069>.
- [26] A. Forbes, Progress in quantum networks, *AVS Quantum Science* **4**, 030401 (2022), <https://doi.org/10.1116/5.0118569>.
- [27] K. Fang, J. Zhao, X. Li, Y. Li, and R. Duan, Quantum network: from theory to practice (2022), arXiv:2212.01226 [quant-ph].
- [28] K. Azuma, S. E. Economou, D. Elkouss, P. Hilaire, L. Jiang, H.-K. Lo, and I. Tzitrin, Quantum repeaters: From quantum networks to the quantum internet (2022), arXiv:2212.10820 [quant-ph].
- [29] R. Van Meter and S. J. Devitt, The path to scalable distributed quantum computing, *Computer* **49**, 31 (2016).
- [30] M. Caleffi, A. S. Cacciapuoti, and G. Bianchi, Quantum internet: From communication to distributed computing!, in *Proceedings of the 5th ACM International Conference on Nanoscale Computing and Communication, NANOCOM '18* (Association for Computing Machinery, New York, NY, USA, 2018).
- [31] A. S. Cacciapuoti, M. Caleffi, F. Tafuri, F. S. Cataliotti, S. Gherardini, and G. Bianchi, Quantum internet: Networking challenges in distributed quantum computing, *IEEE Network* **34**, 137 (2020).
- [32] F. A. Pollock, C. Rodríguez-Rosario, T. Frauenheim, M. Paternostro, and K. Modi, Non-Markovian quantum processes: Complete framework and efficient characterization, *Phys. Rev. A* **97**, 012127 (2018).
- [33] P. Taranto, F. A. Pollock, S. Milz, M. Tomamichel, and K. Modi, Quantum markov order, *Phys. Rev. Lett.* **122**, 140401 (2019).
- [34] S. Milz and K. Modi, Quantum stochastic processes and quantum non-markovian phenomena, *PRX Quantum* **2**, 030201 (2021).
- [35] C. H. Bennett and S. J. Wiesner, Communication via one- and two-particle operators on einstein-podolsky-rosen states, *Phys. Rev. Lett.* **69**, 2881 (1992).
- [36] C. H. Bennett, G. Brassard, C. Crépeau, R. Jozsa, A. Peres, and W. K. Wootters, Teleporting an unknown quantum state via dual classical and Einstein-podolsky-rosen channels, *Phys. Rev. Lett.* **70**, 1895 (1993).
- [37] C. H. Bennett, D. P. DiVincenzo, J. A. Smolin, and W. K. Wootters, Mixed-state entanglement and quantum error correction, *Phys. Rev. A* **54**, 3824 (1996).
- [38] D. Bouwmeester, J.-W. Pan, K. Mattle, M. Eibl, H. Weinfurter, and A. Zeilinger, Experimental quantum teleportation, *Nature* **390**, 575 (1997).
- [39] D. Boschi, S. Branca, F. De Martini, L. Hardy, and S. Popescu, Experimental realization of teleporting an unknown pure quantum state via dual classical and einstein-podolsky-rosen channels, *Phys. Rev. Lett.* **80**, 1121 (1998).
- [40] J.-G. Ren, P. Xu, H.-L. Yong, L. Zhang, S.-K. Liao, J. Yin, W.-Y. Liu, W.-Q. Cai, M. Yang, L. Li, K.-X. Yang, X. Han, Y.-Q. Yao, J. Li, H.-Y. Wu, S. Wan, L. Liu, D.-Q. Liu, Y.-W. Kuang, Z.-P. He, P. Shang, C. Guo, R.-H. Zheng, K. Tian, Z.-C. Zhu, N.-L. Liu, C.-Y. Lu, R. Shu, Y.-A. Chen, C.-Z. Peng, J.-Y. Wang, and

- J.-W. Pan, Ground-to-satellite quantum teleportation, *Nature* **549**, 70 (2017).
- [41] E. Diamanti, Quantum signals could soon span the globe, *Nature* **549**, 41 (2017).
- [42] X.-X. Xia, Q.-C. Sun, Q. Zhang, and J.-W. Pan, Long distance quantum teleportation, *Quantum Science and Technology* **3**, 014012 (2017).
- [43] H. Dai, Q. Shen, C.-Z. Wang, S.-L. Li, W.-Y. Liu, W.-Q. Cai, S.-K. Liao, J.-G. Ren, J. Yin, Y.-A. Chen, Q. Zhang, F. Xu, C.-Z. Peng, and J.-W. Pan, Towards satellite-based quantum-secure time transfer, *Nature Physics* **16**, 848 (2020).
- [44] B. Li, Y. Cao, Y.-H. Li, W.-Q. Cai, W.-Y. Liu, J.-G. Ren, S.-K. Liao, H.-N. Wu, S.-L. Li, L. Li, N.-L. Liu, C.-Y. Lu, J. Yin, Y.-A. Chen, C.-Z. Peng, and J.-W. Pan, Quantum state transfer over 1200 km assisted by prior distributed entanglement, *Phys. Rev. Lett.* **128**, 170501 (2022).
- [45] C.-Y. Lu, Y. Cao, C.-Z. Peng, and J.-W. Pan, Micius quantum experiments in space, *Rev. Mod. Phys.* **94**, 035001 (2022).
- [46] I. Marcikic, H. de Riedmatten, W. Tittel, H. Zbinden, and N. Gisin, Long-distance teleportation of qubits at telecommunication wavelengths, *Nature* **421**, 509 (2003).
- [47] O. Landry, J. A. W. van Houwelingen, A. Beveratos, H. Zbinden, and N. Gisin, Quantum teleportation over the swisscom telecommunication network, *J. Opt. Soc. Am. B* **24**, 398 (2007).
- [48] R. Valivarthi, M. I. G. Puigibert, Q. Zhou, G. H. Aguilar, V. B. Verma, F. Marsili, M. D. Shaw, S. W. Nam, D. Oblak, and W. Tittel, Quantum teleportation across a metropolitan fibre network, *Nature Photonics* **10**, 676 (2016).
- [49] F. Grosshans, Teleportation becomes streetwise, *Nature Photonics* **10**, 623 (2016).
- [50] M. Horodecki, P. Horodecki, and R. Horodecki, General teleportation channel, singlet fraction, and quasidistillation, *Phys. Rev. A* **60**, 1888 (1999).
- [51] H.-J. Briegel, W. Dür, J. I. Cirac, and P. Zoller, Quantum repeaters: The role of imperfect local operations in quantum communication, *Phys. Rev. Lett.* **81**, 5932 (1998).
- [52] S. J. Devitt, Performing quantum computing experiments in the cloud, *Phys. Rev. A* **94**, 032329 (2016).
- [53] H.-Y. Ku, N. Lambert, F.-J. Chan, C. Emary, Y.-N. Chen, and F. Nori, Experimental test of non-macrorealistic cat states in the cloud, *npj Quantum Information* **6**, 98 (2020).
- [54] Z.-P. Yang, H.-Y. Ku, A. Baishya, Y.-R. Zhang, A. F. Kockum, Y.-N. Chen, F.-L. Li, J.-S. Tsai, and F. Nori, Deterministic one-way logic gates on a cloud quantum computer, *Phys. Rev. A* **105**, 042610 (2022).
- [55] Y. Ma, E. Kashefi, M. Arapinis, K. Chakraborty, and M. Kaplan, Qenclave - a practical solution for secure quantum cloud computing, *npj Quantum Information* **8**, 128 (2022).
- [56] A. K. Ekert, Quantum cryptography based on bell's theorem, *Phys. Rev. Lett.* **67**, 661 (1991).
- [57] A. K. Ekert, Quantum cryptography and Bell's theorem, in *Quantum Measurements in Optics*, edited by P. Tombesi and D. F. Walls (Springer US, Boston, MA, 1992) pp. 413–418.
- [58] D. Deutsch, A. Ekert, R. Jozsa, C. Macchiavello, S. Popescu, and A. Sanpera, Quantum privacy amplification and the security of quantum cryptography over noisy channels, *Phys. Rev. Lett.* **77**, 2818 (1996).
- [59] Z. Zhao, Y.-A. Chen, A.-N. Zhang, T. Yang, H. J. Briegel, and J.-W. Pan, Experimental demonstration of five-photon entanglement and open-destination teleportation, *Nature* **430**, 54 (2004).
- [60] X.-M. Jin, J.-G. Ren, B. Yang, Z.-H. Yi, F. Zhou, X.-F. Xu, S.-K. Wang, D. Yang, Y.-F. Hu, S. Jiang, T. Yang, H. Yin, K. Chen, C.-Z. Peng, and J.-W. Pan, Experimental free-space quantum teleportation, *Nature Photonics* **4**, 376 (2010).
- [61] X.-S. Ma, T. Herbst, T. Scheidl, D. Wang, S. Kropatschek, W. Naylor, B. Wittmann, A. Mech, J. Kofler, E. Anisimova, V. Makarov, T. Jennewein, R. Ursin, and A. Zeilinger, Quantum teleportation over 143 kilometres using active feed-forward, *Nature* **489**, 269 (2012).
- [62] S. Takeda, T. Mizuta, M. Fuwa, P. van Loock, and A. Furusawa, Deterministic quantum teleportation of photonic quantum bits by a hybrid technique, *Nature* **500**, 315 (2013).
- [63] S. Pirandola, J. Eisert, C. Weedbrook, A. Furusawa, and S. L. Braunstein, Advances in quantum teleportation, *Nature Photonics* **9**, 641 (2015).
- [64] Q.-C. Sun, Y.-L. Mao, S.-J. Chen, W. Zhang, Y.-F. Jiang, Y.-B. Zhang, W.-J. Zhang, S. Miki, T. Yamashita, H. Terai, X. Jiang, T.-Y. Chen, L.-X. You, X.-F. Chen, Z. Wang, J.-Y. Fan, Q. Zhang, and J.-W. Pan, Quantum teleportation with independent sources and prior entanglement distribution over a network, *Nature Photonics* **10**, 671 (2016).
- [65] R. Raussendorf and H. J. Briegel, A one-way quantum computer, *Phys. Rev. Lett.* **86**, 5188 (2001).
- [66] R. Raussendorf and H. J. Briegel, Computational model underlying the one-way quantum computer, *Quantum Info. Comput.* **2**, 443–486 (2002).
- [67] R. Raussendorf, D. E. Browne, and H. J. Briegel, Measurement-based quantum computation on cluster states, *Phys. Rev. A* **68**, 022312 (2003).
- [68] H. J. Briegel, D. E. Browne, W. Dür, R. Raussendorf, and M. Van den Nest, Measurement-based quantum computation, *Nature Physics* **5**, 19 (2009).
- [69] J. D. Biamonte, M. E. S. Morales, and D. E. Koh, Entanglement scaling in quantum advantage benchmarks, *Phys. Rev. A* **101**, 012349 (2020).
- [70] C. H. Bennett, G. Brassard, S. Popescu, B. Schumacher, J. A. Smolin, and W. K. Wootters, Purification of noisy entanglement and faithful teleportation via noisy channels, *Phys. Rev. Lett.* **76**, 722 (1996).
- [71] F. Buscemi and N. Datta, Distilling entanglement from arbitrary resources, *Journal of Mathematical Physics* **51**, 10.1063/1.3483717 (2010), 102201, https://pubs.aip.org/aip/jmp/article-pdf/doi/10.1063/1.3483717/15605799/102201_1_online.pdf.
- [72] F. Buscemi and N. Datta, Entanglement cost in practical scenarios, *Phys. Rev. Lett.* **106**, 130503 (2011).
- [73] F. Buscemi and N. Datta, General theory of environment-assisted entanglement distillation, *IEEE Transactions on Information Theory* **59**, 1940 (2013).
- [74] X. Wang and R. Duan, Irreversibility of asymptotic entanglement manipulation under quantum operations completely preserving positivity of partial transpose,

- Phys. Rev. Lett. **119**, 180506 (2017).
- [75] M. Berta, F. G. S. L. Brandão, M. Christandl, and S. Wehner, Entanglement cost of quantum channels, *IEEE Transactions on Information Theory* **59**, 6779 (2013).
 - [76] X. Wang and M. M. Wilde, Cost of quantum entanglement simplified, *Phys. Rev. Lett.* **125**, 040502 (2020).
 - [77] X. Wang and M. M. Wilde, Exact entanglement cost of quantum states and channels under positive-partial-transpose-preserving operations, *Phys. Rev. A* **107**, 012429 (2023).
 - [78] G. Gour and C. M. Scandolo, Dynamical entanglement, *Phys. Rev. Lett.* **125**, 180505 (2020).
 - [79] G. Gour and C. M. Scandolo, Entanglement of a bipartite channel, *Phys. Rev. A* **103**, 062422 (2021).
 - [80] N. Lambert, Y.-N. Chen, Y.-C. Cheng, C.-M. Li, G.-Y. Chen, and F. Nori, Quantum biology, *Nature Physics* **9**, 10 (2013).
 - [81] Y. Yang, Memory effects in quantum metrology, *Phys. Rev. Lett.* **123**, 110501 (2019).
 - [82] A. Altherr and Y. Yang, Quantum metrology for non-markovian processes, *Phys. Rev. Lett.* **127**, 060501 (2021).
 - [83] Q. Liu, Z. Hu, H. Yuan, and Y. Yang, Optimal strategies of quantum metrology with a strict hierarchy, *Phys. Rev. Lett.* **130**, 070803 (2023).
 - [84] B. Coecke, T. Fritz, and R. W. Spekkens, A mathematical theory of resources, *Information and Computation* **250**, 59 (2016), quantum Physics and Logic.
 - [85] E. Chitambar and G. Gour, Quantum resource theories, *Rev. Mod. Phys.* **91**, 025001 (2019).
 - [86] G. Gour, Comparison of quantum channels by superchannels, *IEEE Transactions on Information Theory* **65**, 5880 (2019).
 - [87] B. Regula and R. Takagi, Fundamental limitations on distillation of quantum channel resources, *Nature Communications* **12**, 4411 (2021).
 - [88] B. Regula and R. Takagi, One-shot manipulation of dynamical quantum resources, *Phys. Rev. Lett.* **127**, 060402 (2021).
 - [89] L. Mazzola, C. A. Rodríguez-Rosario, K. Modi, and M. Paternostro, Dynamical role of system-environment correlations in non-markovian dynamics, *Phys. Rev. A* **86**, 010102 (2012).
 - [90] M. Ringbauer, C. J. Wood, K. Modi, A. Gilchrist, A. G. White, and A. Fedrizzi, Characterizing quantum dynamics with initial system-environment correlations, *Phys. Rev. Lett.* **114**, 090402 (2015).
 - [91] F. A. Pollock, C. Rodríguez-Rosario, T. Frauenheim, M. Paternostro, and K. Modi, Operational markov condition for quantum processes, *Phys. Rev. Lett.* **120**, 040405 (2018).
 - [92] L. Li, M. J. Hall, and H. M. Wiseman, Concepts of quantum non-markovianity: A hierarchy, *Physics Reports* **759**, 1 (2018).
 - [93] G. A. L. White, C. D. Hill, F. A. Pollock, L. C. L. Hollenberg, and K. Modi, Demonstration of non-markovian process characterisation and control on a quantum processor, *Nature Communications* **11**, 6301 (2020).
 - [94] E. Chitambar, D. Leung, L. Mančinska, M. Ozols, and A. Winter, Everything you always wanted to know about locc (but were afraid to ask), *Communications in Mathematical Physics* **328**, 303 (2014).
 - [95] C. Brukner, S. Taylor, S. Cheung, and V. Vedral, Quantum entanglement in time (2004), arXiv:quant-ph/0402127 [quant-ph].
 - [96] S. Milz, F. A. Pollock, T. P. Le, G. Chiribella, and K. Modi, Entanglement, non-markovianity, and causal non-separability, *New Journal of Physics* **20**, 033033 (2018).
 - [97] F. Costa, M. Ringbauer, M. E. Goggin, A. G. White, and A. Fedrizzi, Unifying framework for spatial and temporal quantum correlations, *Phys. Rev. A* **98**, 012328 (2018).
 - [98] M. Zych, F. Costa, I. Pikovski, and Č. Brukner, Bell's theorem for temporal order, *Nature Communications* **10**, 3772 (2019).
 - [99] S. Milz, D. Jurkschat, F. A. Pollock, and K. Modi, Delayed-choice causal order and nonclassical correlations, *Phys. Rev. Res.* **3**, 023028 (2021).
 - [100] S. Milz, C. Spee, Z.-P. Xu, F. A. Pollock, K. Modi, and O. Gühne, Genuine multipartite entanglement in time, *SciPost Phys.* **10**, 141 (2021).
 - [101] G. Giudice, G. Giudici, M. Sonner, J. Thoenness, A. Leroise, D. A. Abanin, and L. Piroli, Temporal entanglement, quasiparticles, and the role of interactions, *Phys. Rev. Lett.* **128**, 220401 (2022).
 - [102] See Supplemental Material for comprehensive details, including full proofs, mathematical elucidation of our results, additional theoretical findings, the resource-theoretic framework of temporal entanglement, insightful applications of our framework in quantum communication protocols, and corresponding numerical experiments, as well as Refs. [156–203].
 - [103] I. Georgescu, 25 years of experimental quantum teleportation, *Nature Reviews Physics* **4**, 695 (2022).
 - [104] W. Tittel, J. Brendel, H. Zbinden, and N. Gisin, Violation of bell inequalities by photons more than 10 km apart, *Phys. Rev. Lett.* **81**, 3563 (1998).
 - [105] L. M. Duan, M. D. Lukin, J. I. Cirac, and P. Zoller, Long-distance quantum communication with atomic ensembles and linear optics, *Nature* **414**, 413 (2001).
 - [106] Z.-S. Yuan, Y.-A. Chen, B. Zhao, S. Chen, J. Schmiedmayer, and J.-W. Pan, Experimental demonstration of a bdcz quantum repeater node, *Nature* **454**, 1098 (2008).
 - [107] L. Jiang, J. M. Taylor, K. Nemoto, W. J. Munro, R. Van Meter, and M. D. Lukin, Quantum repeater with encoding, *Phys. Rev. A* **79**, 032325 (2009).
 - [108] A. G. Fowler, D. S. Wang, C. D. Hill, T. D. Ladd, R. Van Meter, and L. C. L. Hollenberg, Surface code quantum communication, *Phys. Rev. Lett.* **104**, 180503 (2010).
 - [109] N. Sangouard, C. Simon, H. de Riedmatten, and N. Gisin, Quantum repeaters based on atomic ensembles and linear optics, *Rev. Mod. Phys.* **83**, 33 (2011).
 - [110] W. J. Munro, A. M. Stephens, S. J. Devitt, K. A. Harrison, and K. Nemoto, Quantum communication without the necessity of quantum memories, *Nature Photonics* **6**, 777 (2012).
 - [111] S. Muralidharan, J. Kim, N. Lütkenhaus, M. D. Lukin, and L. Jiang, Ultrafast and fault-tolerant quantum communication across long distances, *Phys. Rev. Lett.* **112**, 250501 (2014).
 - [112] W. J. Munro, K. Azuma, K. Tamaki, and K. Nemoto, Inside quantum repeaters, *IEEE Journal of Selected Topics in Quantum Electronics* **21**, 78 (2015).

- [113] K. Azuma, K. Tamaki, and H.-K. Lo, All-photonic quantum repeaters, *Nature Communications* **6**, 6787 (2015).
- [114] F. Ewert, M. Bergmann, and P. van Loock, Ultrafast long-distance quantum communication with static linear optics, *Phys. Rev. Lett.* **117**, 210501 (2016).
- [115] S. Pirandola, R. Laurenza, C. Ottaviani, and L. Banchi, Fundamental limits of repeaterless quantum communications, *Nature Communications* **8**, 15043 (2017).
- [116] M. Zwerger, A. Pirker, V. Dunjko, H. J. Briegel, and W. Dür, Long-range big quantum-data transmission, *Phys. Rev. Lett.* **120**, 030503 (2018).
- [117] M. K. Bhaskar, R. Riedinger, B. Machielse, D. S. Levonian, C. T. Nguyen, E. N. Knall, H. Park, D. Englund, M. Lončar, D. D. Sukachev, and M. D. Lukin, Experimental demonstration of memory-enhanced quantum communication, *Nature* **580**, 60 (2020).
- [118] J. Borregaard, H. Pichler, T. Schröder, M. D. Lukin, P. Lodahl, and A. S. Sørensen, One-way quantum repeater based on near-deterministic photon-emitter interfaces, *Phys. Rev. X* **10**, 021071 (2020).
- [119] J. Wallnöfer, A. A. Melnikov, W. Dür, and H. J. Briegel, Machine learning for long-distance quantum communication, *PRX Quantum* **1**, 010301 (2020).
- [120] Y.-F. Pu, S. Zhang, Y.-K. Wu, N. Jiang, W. Chang, C. Li, and L.-M. Duan, Experimental demonstration of memory-enhanced scaling for entanglement connection of quantum repeater segments, *Nature Photonics* **15**, 374 (2021).
- [121] C. Liorni, H. Kampermann, and D. Bruß, Quantum repeaters in space, *New Journal of Physics* **23**, 053021 (2021).
- [122] F. Rozpędek, K. Noh, Q. Xu, S. Guha, and L. Jiang, Quantum repeaters based on concatenated bosonic and discrete-variable quantum codes, *npj Quantum Information* **7**, 102 (2021).
- [123] K. Sharman, F. Kimiaee Asadi, S. C. Wein, and C. Simon, Quantum repeaters based on individual electron spins and nuclear-spin-ensemble memories in quantum dots, *Quantum* **5**, 570 (2021).
- [124] M. F. Askarani, A. Das, J. H. Davidson, G. C. Amaral, N. Sinclair, J. A. Slater, S. Marzban, C. W. Thiel, R. L. Cone, D. Oblak, and W. Tittel, Long-lived solid-state optical memory for high-rate quantum repeaters, *Phys. Rev. Lett.* **127**, 220502 (2021).
- [125] H. Wang, M. E. Trusheim, L. Kim, H. Raniwala, and D. R. Englund, Field programmable spin arrays for scalable quantum repeaters, *Nature Communications* **14**, 704 (2023).
- [126] K. Ito, T. Kondo, K. Mannami, K. Niizeki, D. Yoshida, K. Minaguchi, M. Zheng, X. Xie, F.-L. Hong, and T. Horikiri, Frequency-multiplexed storage and distribution of narrowband telecom photon pairs over a 10-km fiber link with long-term system stability, *Phys. Rev. Appl.* **19**, 024070 (2023).
- [127] M. Żukowski, A. Zeilinger, M. A. Horne, and A. K. Ekert, “event-ready-detectors” Bell experiment via entanglement swapping, *Phys. Rev. Lett.* **71**, 4287 (1993).
- [128] A. Zeilinger, M. A. Horne, H. Weinfurter, and M. Żukowski, Three-particle entanglements from two entangled pairs, *Phys. Rev. Lett.* **78**, 3031 (1997).
- [129] J.-W. Pan, D. Bouwmeester, H. Weinfurter, and A. Zeilinger, Experimental entanglement swapping: Entangling photons that never interacted, *Phys. Rev. Lett.* **80**, 3891 (1998).
- [130] M. Horodecki and P. Horodecki, Reduction criterion of separability and limits for a class of distillation protocols, *Phys. Rev. A* **59**, 4206 (1999).
- [131] W. R. Heinzelman, J. Kulik, and H. Balakrishnan, Adaptive protocols for information dissemination in wireless sensor networks, in *Proceedings of the 5th Annual ACM/IEEE International Conference on Mobile Computing and Networking*, MobiCom ’99 (Association for Computing Machinery, New York, NY, USA, 1999) p. 174–185.
- [132] A. Dunkels, F. Österlind, and Z. He, An adaptive communication architecture for wireless sensor networks, in *Proceedings of the 5th International Conference on Embedded Networked Sensor Systems*, SenSys ’07 (Association for Computing Machinery, New York, NY, USA, 2007) p. 335–349.
- [133] P. Padhy, R. K. Dash, K. Martinez, and N. R. Jennings, A utility-based adaptive sensing and multihop communication protocol for wireless sensor networks, *ACM Trans. Sen. Netw.* **6**, 10.1145/1754414.1754423 (2010).
- [134] C. Simon, V. Bužek, and N. Gisin, No-signaling condition and quantum dynamics, *Phys. Rev. Lett.* **87**, 170405 (2001).
- [135] A. Peres and D. R. Terno, Quantum information and relativity theory, *Rev. Mod. Phys.* **76**, 93 (2004).
- [136] P. Horodecki and R. Ramanathan, The relativistic causality versus no-signaling paradigm for multi-party correlations, *Nature Communications* **10**, 1701 (2019).
- [137] D. Jonathan and M. B. Plenio, Entanglement-assisted local manipulation of pure quantum states, *Phys. Rev. Lett.* **83**, 3566 (1999).
- [138] R. Duan, Y. Feng, X. Li, and M. Ying, Multiple-copy entanglement transformation and entanglement catalysis, *Phys. Rev. A* **71**, 042319 (2005).
- [139] F. Ding, X. Hu, and H. Fan, Amplifying asymmetry with correlating catalysts, *Phys. Rev. A* **103**, 022403 (2021).
- [140] P. Lipka-Bartosik and P. Skrzypczyk, All states are universal catalysts in quantum thermodynamics, *Phys. Rev. X* **11**, 011061 (2021).
- [141] N. Shiraishi and T. Sagawa, Quantum thermodynamics of correlated-catalytic state conversion at small scale, *Phys. Rev. Lett.* **126**, 150502 (2021).
- [142] P. Lipka-Bartosik and P. Skrzypczyk, Catalytic quantum teleportation, *Phys. Rev. Lett.* **127**, 080502 (2021).
- [143] T. V. Kondra, C. Datta, and A. Streltsov, Catalytic transformations of pure entangled states, *Phys. Rev. Lett.* **127**, 150503 (2021).
- [144] R. Takagi and N. Shiraishi, Correlation in catalysts enables arbitrary manipulation of quantum coherence, *Phys. Rev. Lett.* **128**, 240501 (2022).
- [145] R. Rubboli and M. Tomamichel, Fundamental limits on correlated catalytic state transformations, *Phys. Rev. Lett.* **129**, 120506 (2022).
- [146] E. Kaur, S. Das, M. M. Wilde, and A. Winter, Extendibility limits the performance of quantum processors, *Phys. Rev. Lett.* **123**, 070502 (2019).
- [147] E. Kaur, S. Das, M. M. Wilde, and A. Winter, Resource theory of unextendibility and nonasymptotic quantum capacity, *Phys. Rev. A* **104**, 022401 (2021).
- [148] M. Berta, F. Borderi, O. Fawzi, and V. B. Scholz, Semidefinite programming hierarchies for constrained bilinear optimization, *Mathematical Programming* **194**,

- 781 (2022).
- [149] T. Holdsworth, V. Singh, and M. M. Wilde, Quantifying the performance of approximate teleportation and quantum error correction via symmetric 2-ppt-extendible channels, *Phys. Rev. A* **107**, 012428 (2023).
 - [150] A. U. Siddiqui and M. M. Wilde, The swap imposter: Bidirectional quantum teleportation and its performance, *AVS Quantum Science* **5**, 011407 (2023), <https://doi.org/10.1116/5.0135467>.
 - [151] P. Kómár, E. M. Kessler, M. Bishof, L. Jiang, A. S. Sørensen, J. Ye, and M. D. Lukin, A quantum network of clocks, *Nature Physics* **10**, 582 (2014).
 - [152] X. Liu, J. Hu, Z.-F. Li, X. Li, P.-Y. Li, P.-J. Liang, Z.-Q. Zhou, C.-F. Li, and G.-C. Guo, Heralded entanglement distribution between two absorptive quantum memories, *Nature* **594**, 41 (2021).
 - [153] L.-Z. Liu, Y.-Z. Zhang, Z.-D. Li, R. Zhang, X.-F. Yin, Y.-Y. Fei, L. Li, N.-L. Liu, F. Xu, Y.-A. Chen, and J.-W. Pan, Distributed quantum phase estimation with entangled photons, *Nature Photonics* **15**, 137 (2021).
 - [154] K. Beloy, M. I. Bodine, T. Bothwell, S. M. Brewer, S. L. Bromley, J.-S. Chen, J.-D. Deschênes, S. A. Diddams, R. J. Fasano, T. M. Fortier, Y. S. Hassan, D. B. Hume, D. Kedar, C. J. Kennedy, I. Khader, A. Koepke, D. R. Leibrandt, H. Leopardi, A. D. Ludlow, W. F. McGrew, W. R. Milner, N. R. Newbury, D. Nicolodi, E. Oelker, T. E. Parker, J. M. Robinson, S. Romisch, S. A. Schäfer, J. A. Sherman, L. C. Sinclair, L. Sonderhouse, W. C. Swann, J. Yao, J. Ye, X. Zhang, and B. A. C. O. N. B. Collaboration*, Frequency ratio measurements at 18-digit accuracy using an optical clock network, *Nature* **591**, 564 (2021).
 - [155] B. K. Malia, Y. Wu, J. Martínez-Rincón, and M. A. Kasevich, Distributed quantum sensing with mode-entangled spin-squeezed atomic states, *Nature* **612**, 661 (2022).
 - [156] A. Jamiołkowski, Linear transformations which preserve trace and positive semidefiniteness of operators, *Reports on Mathematical Physics* **3**, 275 (1972).
 - [157] M.-D. Choi, Completely positive linear maps on complex matrices, *Linear Algebra and its Applications* **10**, 285 (1975).
 - [158] F. Verstraete, V. Murg, and J. Cirac, Matrix product states, projected entangled pair states, and variational renormalization group methods for quantum spin systems, *Advances in Physics* **57**, 143 (2008), <https://doi.org/10.1080/14789940801912366>.
 - [159] R. Orús, A practical introduction to tensor networks: Matrix product states and projected entangled pair states, *Annals of Physics* **349**, 117 (2014).
 - [160] J. C. Bridgeman and C. T. Chubb, Hand-waving and interpretive dance: an introductory course on tensor networks, *Journal of Physics A: Mathematical and Theoretical* **50**, 223001 (2017).
 - [161] J. I. Cirac, D. Pérez-García, N. Schuch, and F. Verstraete, Matrix product states and projected entangled pair states: Concepts, symmetries, theorems, *Rev. Mod. Phys.* **93**, 045003 (2021).
 - [162] B. Coecke and R. Duncan, Interacting quantum observables, in *Automata, Languages and Programming*, edited by L. Aceto, I. Damgård, L. A. Goldberg, M. M. Halldórsson, A. Ingólfssdóttir, and I. Walukiewicz (Springer Berlin Heidelberg, Berlin, Heidelberg, 2008) pp. 298–310.
 - [163] B. Coecke and R. Duncan, Interacting quantum observables: categorical algebra and diagrammatics, *New Journal of Physics* **13**, 043016 (2011).
 - [164] B. Coecke and A. Kissinger, *Picturing Quantum Processes: A First Course in Quantum Theory and Diagrammatic Reasoning* (Cambridge University Press, 2017).
 - [165] J. van de Wetering, ZX-calculus for the working quantum computer scientist, *arXiv preprint arXiv:2012.13966* (2020).
 - [166] B. Coecke, Basic ZX-calculus for students and professionals, *arXiv preprint arXiv:2303.03163* (2023).
 - [167] G. Chiribella and D. Ebler, Optimal quantum networks and one-shot entropies, *New Journal of Physics* **18**, 093053 (2016).
 - [168] A. Uhlmann, The “transition probability” in the state space of a $*$ -algebra, *Reports on Mathematical Physics* **9**, 273 (1976).
 - [169] R. Jozsa, Fidelity for mixed quantum states, *Journal of Modern Optics* **41**, 2315 (1994), <https://doi.org/10.1080/09500349414552171>.
 - [170] E. Rains, A semidefinite program for distillable entanglement, *IEEE Transactions on Information Theory* **47**, 2921 (2001).
 - [171] M. R. Geller and Z. Zhou, Efficient error models for fault-tolerant architectures and the pauli twirling approximation, *Phys. Rev. A* **88**, 012314 (2013).
 - [172] Z. Cai and S. C. Benjamin, Constructing smaller pauli twirling sets for arbitrary error channels, *Scientific reports* **9**, 11281 (2019).
 - [173] M. A. Nielsen, A simple formula for the average gate fidelity of a quantum dynamical operation, *Physics Letters A* **303**, 249 (2002).
 - [174] D. Leung and W. Matthews, On the power of ppt-preserving and non-signalling codes, *IEEE Transactions on Information Theory* **61**, 4486 (2015).
 - [175] S. Popescu and D. Rohrlich, Causality and nonlocality as axioms for quantum mechanics, in *Causality and Locality in Modern Physics*, edited by G. Hunter, S. Jeffers, and J.-P. Vigiér (Springer Netherlands, Dordrecht, 1998) pp. 383–389.
 - [176] D. Beckman, D. Gottesman, M. A. Nielsen, and J. Preskill, Causal and localizable quantum operations, *Phys. Rev. A* **64**, 052309 (2001).
 - [177] T. Eggeling, D. Schlingemann, and R. F. Werner, Semicausal operations are semilocalizable, *Europhysics Letters* **57**, 782 (2002).
 - [178] M. Piani, M. Horodecki, P. Horodecki, and R. Horodecki, Properties of quantum nonsignaling boxes, *Phys. Rev. A* **74**, 012305 (2006).
 - [179] M. Piani and J. Watrous, All entangled states are useful for channel discrimination, *Phys. Rev. Lett.* **102**, 250501 (2009).
 - [180] M. Piani, M. Cianciaruso, T. R. Bromley, C. Napoli, N. Johnston, and G. Adesso, Robustness of asymmetry and coherence of quantum states, *Phys. Rev. A* **93**, 042107 (2016).
 - [181] C. Napoli, T. R. Bromley, M. Cianciaruso, M. Piani, N. Johnston, and G. Adesso, Robustness of coherence: An operational and observable measure of quantum coherence, *Phys. Rev. Lett.* **116**, 150502 (2016).
 - [182] W. Zheng, Z. Ma, H. Wang, S.-M. Fei, and X. Peng, Experimental demonstration of observability and operability of robustness of coherence, *Phys. Rev. Lett.* **120**,

- 230504 (2018).
- [183] R. Takagi, B. Regula, K. Bu, Z.-W. Liu, and G. Adesso, Operational advantage of quantum resources in sub-channel discrimination, *Phys. Rev. Lett.* **122**, 140402 (2019).
 - [184] A. F. Ducuara and P. Skrzypczyk, Operational interpretation of weight-based resource quantifiers in convex quantum resource theories, *Phys. Rev. Lett.* **125**, 110401 (2020).
 - [185] R. Uola, T. Bullock, T. Kraft, J.-P. Pellonpää, and N. Brunner, All quantum resources provide an advantage in exclusion tasks, *Phys. Rev. Lett.* **125**, 110402 (2020).
 - [186] A. Streltsov, G. Adesso, and M. B. Plenio, Colloquium: Quantum coherence as a resource, *Rev. Mod. Phys.* **89**, 041003 (2017).
 - [187] S. Mac Lane, *Categories for the working mathematician*, Vol. 5 (Springer Science & Business Media, 2013).
 - [188] D. Sauerwein, N. R. Wallach, G. Gour, and B. Kraus, Transformations among pure multipartite entangled states via local operations are almost never possible, *Phys. Rev. X* **8**, 031020 (2018).
 - [189] M. Grassl, M. Rötteler, and T. Beth, Computing local invariants of quantum-bit systems, *Phys. Rev. A* **58**, 1833 (1998).
 - [190] B. Kraus, Local unitary equivalence of multipartite pure states, *Phys. Rev. Lett.* **104**, 020504 (2010).
 - [191] B. Kraus, Local unitary equivalence and entanglement of multipartite pure states, *Phys. Rev. A* **82**, 032121 (2010).
 - [192] V. Gheorghiu and R. B. Griffiths, Separable operations on pure states, *Phys. Rev. A* **78**, 020304 (2008).
 - [193] E. Chitambar and R. Duan, Nonlocal entanglement transformations achievable by separable operations, *Phys. Rev. Lett.* **103**, 110502 (2009).
 - [194] F. G. S. L. Brandão and M. B. Plenio, Entanglement theory and the second law of thermodynamics, *Nature Physics* **4**, 873 (2008).
 - [195] F. G. S. L. Brandão and M. B. Plenio, A generalization of quantum stein's lemma, *Communications in Mathematical Physics* **295**, 791 (2010).
 - [196] M. Berta, F. G. S. L. Brandão, G. Gour, L. Lami, M. B. Plenio, B. Regula, and M. Tomamichel, On a gap in the proof of the generalised quantum stein's lemma and its consequences for the reversibility of quantum resources (2022), arXiv:2205.02813 [quant-ph].
 - [197] L. Lami and B. Regula, No second law of entanglement manipulation after all, *Nature Physics* **19**, 184 (2023).
 - [198] E. M. Rains, Bound on distillable entanglement, *Phys. Rev. A* **60**, 179 (1999).
 - [199] E. M. Rains, Erratum: Bound on distillable entanglement [phys. rev. a 60, 179 (1999)], *Phys. Rev. A* **63**, 019902 (2000).
 - [200] K. Audenaert, M. B. Plenio, and J. Eisert, Entanglement cost under positive-partial-transpose-preserving operations, *Phys. Rev. Lett.* **90**, 027901 (2003).
 - [201] L. Vandenberghe and S. Boyd, Semidefinite programming, *SIAM Review* **38**, 49 (1996), <https://doi.org/10.1137/1038003>.
 - [202] S. Boyd and L. Vandenberghe, *Convex Optimization* (Cambridge University Press, 2004).
 - [203] R. F. Werner, Quantum states with Einstein-Podolsky-Rosen correlations admitting a hidden-variable model, *Phys. Rev. A* **40**, 4277 (1989).

Fundamental Limitations on Communication over a Quantum Network

Supplemental Material

Junjing Xing,¹ Tianfeng Feng,² Zhaobing Fan,^{1,*} Haitao Ma,^{3,†}
Kishor Bharti,^{4,‡} Dax Enshan Koh,^{4,§} and Yunlong Xiao^{4,¶}

¹*College of Intelligent Systems Science and Engineering, Harbin Engineering University,
Harbin, Heilongjiang 150001, People's Republic of China*

²*State Key Laboratory of Optoelectronic Materials and Technologies and School of Physics,
Sun Yat-sen University, Guangzhou, Guangdong 510275, People's Republic of China*

³*College of Mathematics Science, Harbin Engineering University,
Harbin, Heilongjiang 150001, People's Republic of China*

⁴*Institute of High Performance Computing (IHPC), Agency for Science,
Technology and Research (A*STAR), 1 Fusionopolis Way,
#16-16 Conneris, Singapore 138632, Republic of Singapore*

(Dated: June 9, 2023)

Quantum communication is a rapidly advancing and highly promising field that has the potential to revolutionize information transmission by providing unprecedented levels of security and efficiency. In this work, we explore the intrinsic relationship between the entanglement of quantum dynamics and the performance of quantum communication, from quantum teleportation and quantum repeaters to general quantum networks. To ensure a comprehensive and rigorous treatment of the topic, we provide this supplemental material that offers a detailed examination and rigorous proof of the results presented in the main text. This supplementary material is designed to be explicit and self-contained, with a focus on providing a thorough understanding of the underlying principles and mechanisms that drive quantum communication. Importantly, the supplementary material provides an extensive array of supplementary data, encompassing not only the results expounded upon in the main text but also other pertinent information essential for a comprehensive understanding of the communication over a quantum network.

CONTENTS

I. Quantum Dynamics	2
A. Quantum Channels: From Choi-Jamiołkowski Isomorphism to Link Product	2
B. How to Quantify a Quantum Channel: Twist It	4
C. Quantum Superchannels: Pre-Processing, Post-Processing, and Non-Signalling	9
D. Quantum Circuit Fragments: Framework of Non-Markovian Dynamics	12
II. Temporal Entanglement	14
A. Entangled Circuit Fragments: Quantum Correlations across Space and Time	14
B. Fidelity of Circuit Fragment Distillation: Quantifying Temporal Entanglement	17
III. Quantum Communications	18
A. Quantum Teleportation: A Channel-Theoretic Perspective	18
B. Fidelity Benchmarking: The Role of Temporal Entanglement	24
C. Numerical Experiments: Dancing with Data	32
IV. Quantum Network	36
A. Quantum Repeater: Towards a Global Quantum Communication Network	36
B. All-In-One Communication Framework: That's all you need	53
References	58

* fanzhaobing@hrbeu.edu.cn

† hmamath@hrbeu.edu.cn

‡ kishor.bharti1@gmail.com

§ dax_koh@ihpc.a-star.edu.sg

¶ mathxiao123@gmail.com

I. QUANTUM DYNAMICS

In this section, we lay the foundation for the results presented in this work by introducing our notations and investigating the physical properties of a quantum channel through its Choi-Jamiołkowski operator (refer to Def. I.1). We also formulate the sequential composition of channels using the link product (refer to Def. I.2) in Subsec. I A. After a bit of these concepts, we delve into two important quantifiers of a quantum channel: the average fidelity (refer to Def. I.3) and the entanglement fidelity (refer to Def. I.4). By employing the link product in Lem. I.12 of Subsec. I B, we establish their intrinsic connection. In addition, we discuss the most general way of manipulating a quantum channel – quantum superchannel via the language of non-signalling maps (refer to Def. I.13) in Subsec. I C. Finally, we address the broadest framework of non-Markovian quantum processes, which we refer to as quantum circuit fragments in Subsec. I D. Our aim in this section is to provide a clear and concise understanding of the concepts and terminologies that will be used throughout the rest of the work.

A. Quantum Channels: From Choi-Jamiołkowski Isomorphism to Link Product

Just as Lego bricks can be assembled and connected in countless ways to construct various objects, including castles, machinery, vehicles, Millennium Falcon, and even robots, quantum channels are the fundamental building blocks of the circuit model for quantum computing and information processing. These channels play a critical role in numerous aspects of quantum theory, including the preparation of quantum states, implementation of quantum measurements, handling of noise from system-environment interactions, and execution of quantum gates in a circuit. Essentially, the concept of quantum channels is integral to the whole field of quantum theory, acting as a foundational tool that enables scientists to push the boundaries of what is possible in the realm of quantum information processing and beyond. In this subsection, we will briefly review the theory of quantum channels, which forms the backbone of this work. The main mathematical toolkit employed here is known as Choi-Jamiołkowski (CJ) isomorphism [1, 2] in literature. While we provide an overview of the concept and the corresponding mathematical framework, readers seeking a more in-depth understanding can refer to Refs. [3–5] and the cited references therein, which offer comprehensive insights into the topic.

Generally speaking, a linear map $\mathcal{E}_{A \rightarrow B}$ from linear operators to linear operators is called a quantum channel if it satisfies the following conditions:

- **Complete Positivity (CP);**
- **Trace Preservation (TP).**

Here, complete positivity means that by applying $\mathcal{E}_{A \rightarrow B}$ to part of a quantum state $\rho_{A'A}$, the resultant state is still positive semidefinite, namely $\text{id}_{A'} \otimes \mathcal{E}_{A \rightarrow B}(\rho_{A'A}) \geq 0$. Meanwhile, as indicated by the name, the trace-preserving property guarantees that $\text{Tr}[\mathcal{E}(\rho)] = \text{Tr}[\rho]$ for all ρ . A powerful tool for investigating the mathematical properties of quantum channels is the so-called Choi-Jamiołkowski (CJ) isomorphism. Formally, it is defined as

Definition I.1: Choi-Jamiołkowski Isomorphism [1, 2]

Given a quantum channel $\mathcal{E}_{A \rightarrow B}$, there is an isomorphism between map $\mathcal{E}_{A \rightarrow B}$ and matrix $J_{AB}^{\mathcal{E}}$ (known as the Choi-Jamiołkowski operator of channel $\mathcal{E}_{A \rightarrow B}$). Mathematically, $J_{AB}^{\mathcal{E}}$ is defined as

$$J_{AB}^{\mathcal{E}} := \text{id}_A \otimes \mathcal{E}_{A' \rightarrow B}(\Gamma_{AA'}), \quad (1)$$

where $\Gamma_{AA'} := |\Gamma\rangle\langle\Gamma|_{AA'}$, and $|\Gamma\rangle_{AA'} := \sum_i |ii\rangle_{AA'}$ stands for the unnormalized maximally entangled state (UMES) with A' being a replica of system A , and $\{|i\rangle\}$ being an orthonormal basis on A . For maximally entangled state (MES) $\phi_{AA'}^+$, we define the Choi-Jamiołkowski state of channel $\mathcal{E}_{A \rightarrow B}$ as

$$\rho_{AB}^{\mathcal{E}} := \text{id}_A \otimes \mathcal{E}_{A' \rightarrow B}(\phi_{AA'}^+), \quad (2)$$

where $\phi_{AA'}^+ := |\phi^+\rangle\langle\phi^+|_{AA'}$, and $|\phi^+\rangle_{AA'} := (1/\sqrt{d_A}) \sum_i |ii\rangle_{AA'}$ with d_A being the dimension of system A . It is now straightforward to check that $\rho_{AB}^{\mathcal{E}} = J_{AB}^{\mathcal{E}}/d_A$.

See Fig. 1 for an illustration of Eq. 1 and Eq. 2.

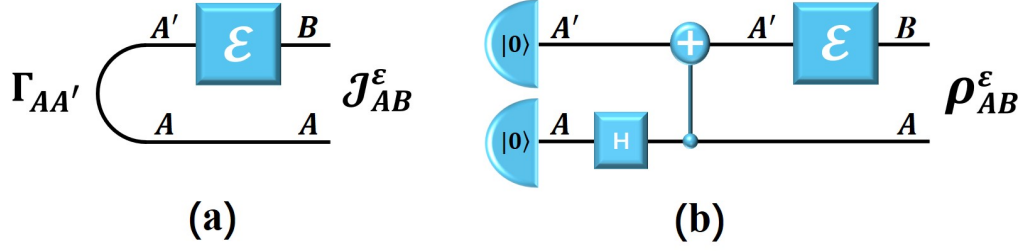


FIG. 1. (color online) Generations of the Choi-Jamiołkowski operator $J_{AB}^{\mathcal{E}}$ (see Eq. 1) and state $\rho_{AB}^{\mathcal{E}}$ (see Eq. 2). In (a), $\Gamma_{AA'}$ stands for $|\Gamma\rangle\langle\Gamma|_{AA'}$ with $|\Gamma\rangle_{AA'} := \sum_i |ii\rangle_{AA'}$. When the unnormalized operator Γ has been replaced by the maximally entangled state ϕ^+ , we obtain the Choi-Jamiołkowski state $\rho_{AB}^{\mathcal{E}}$, shown in (b).

Remark I.1. In the fields of quantum information, computing, and condensed matter physics, conventional diagrammatic techniques, such as tensor networks [6–9] and ZX-calculus [10–14], are widely used. Although our graphical representation bears similarity to these existing techniques, there exists a key difference in our approach. Specifically, in the conventional techniques, a cup symbol (i.e., \cup) represents a vector $|\Gamma\rangle$, whereas in our work, it represents the unnormalized maximally entangled state Γ . Similarly, in the conventional approach, a cap symbol (i.e., \cap) represents the effect $\langle\Gamma|$. However, in our approach, the cup acting on an operator M represents the trace of $\Gamma \cdot M$, denoted as $\text{Tr}[\Gamma \cdot M]$. Finally, we note that the yanking equations, which relate the graphical notations in ZX-calculus, also hold in our graphical language.

Remark I.2. The Choi-Jamiołkowski operator for quantum effects can be defined by substituting the quantum channel in Eq. 1 with a completely positive and trace non-increasing map (CPTNI). This mathematical tool is crucial in understanding the impact of quantum measurement and probabilistic protocols in quantum information processing.

Equipped with Choi-Jamiołkowski isomorphism, we can now translate the properties of completely positive and trace-preserving into the language of Choi-Jamiołkowski operators. More precisely, a linear map $\mathcal{E}_{A \rightarrow B}$ is completely positive if and only if its Choi-Jamiołkowski operator $J_{AB}^{\mathcal{E}}$ is positive semidefinite, i.e., $J_{AB}^{\mathcal{E}} \geq 0$. Furthermore, such a map is trace-preserving if and only if $J_{AB}^{\mathcal{E}}$ satisfies $\text{Tr}_B[J_{AB}^{\mathcal{E}}] = \mathbb{1}_A$. To conclude, given a linear operator $J_{AB}^{\mathcal{E}}$, it represents a quantum channel from system A to system B if both $J_{AB}^{\mathcal{E}} \geq 0$ and $\text{Tr}_B[J_{AB}^{\mathcal{E}}] = \mathbb{1}_A$ are satisfied.

A natural question that arises is how to determine the Choi-Jamiołkowski operator of the sequential composition of two quantum channels, such as $\mathcal{E}_{A \rightarrow B}$ and $\mathcal{F}_{B \rightarrow C}$, denoted by $(\mathcal{F} \circ \mathcal{E})_{A \rightarrow C}$, in terms of $J_{AB}^{\mathcal{E}}$ and $J_{BC}^{\mathcal{F}}$. To tackle this question, we can utilize a useful tool called the *link product* \star . This product allows us to efficiently compute the Choi-Jamiołkowski operator of the composite channel and is a powerful technique for analyzing the properties of quantum channels.

Definition I.2: Link Product [15–17]

Given two Hermitian operators M and N with X being the intersection of the systems on which M and N act, their link product, denoted by $M \star N$, is defined as

$$M \star N := \text{Tr}_X[M^{\mathbf{T}_X} \cdot N], \quad (3)$$

indicating that the link between M and N , namely system X , has been “swallowed” by the product \star . Here Tr_X and \mathbf{T}_X represent the partial trace and partial transpose over the common system X respectively, and the identity operator $\mathbb{1}$ has been ignored.

With the help of the link product \star , we can now address the question posed earlier regarding the Choi-Jamiołkowski operator of the composite channel $(\mathcal{F} \circ \mathcal{E})_{A \rightarrow C}$ in terms of $J_{AB}^{\mathcal{E}}$ and $J_{BC}^{\mathcal{F}}$. In this context, system B serves as the link between $J_{AB}^{\mathcal{E}}$ and $J_{BC}^{\mathcal{F}}$, and we can obtain the resultant Choi-Jamiołkowski operator $J_{AC}^{\mathcal{E} \circ \mathcal{F}}$ as follows

$$J_{AC}^{\mathcal{F} \circ \mathcal{E}} = J_{AB}^{\mathcal{E}} \star J_{BC}^{\mathcal{F}} = \text{Tr}_B[(J_{AB}^{\mathcal{E}})^{\mathbf{T}_B} \otimes \mathbb{1}_C] \cdot (\mathbb{1}_A \otimes J_{BC}^{\mathcal{F}}). \quad (4)$$

A graphical visualization of link product appeared in Eq. 4 is demonstrated in Fig. 2, where the equivalence between Fig. 2(a) and Fig. 2(b) is obtained by using the yanking equation [10–13]; that is

$$\text{Tr}_B[(J_{AB}^{\mathcal{E}})^{\mathbf{T}_B} \otimes \mathbb{1}_C] \cdot (\mathbb{1}_A \otimes J_{BC}^{\mathcal{F}}) = \text{Tr}_{BB''}[(J_{AB''}^{\mathcal{E}} \otimes J_{BC}^{\mathcal{F}}) \cdot (\mathbb{1}_A \otimes \Gamma_{B''B} \otimes \mathbb{1}_C)]. \quad (5)$$

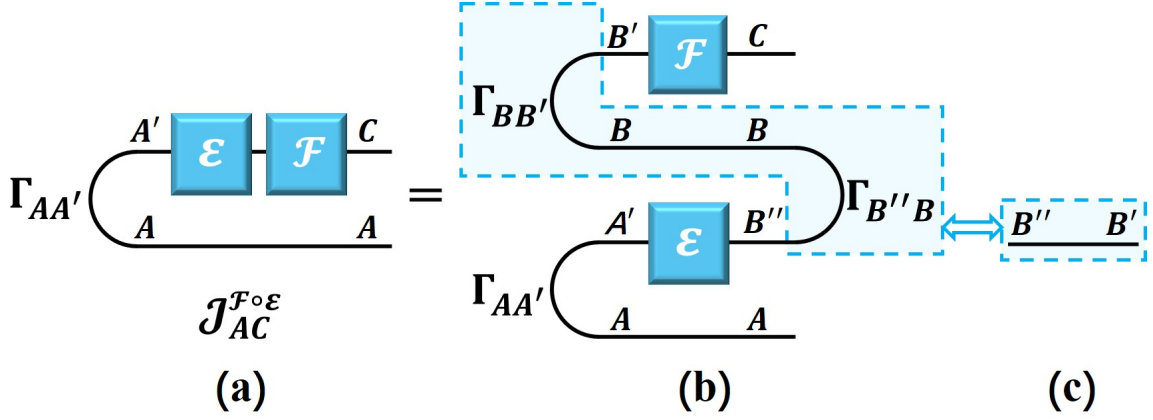


FIG. 2. (Color online) Physical realization (up to a scalar) of the Choi-Jamiołkowski operator $J_{AC}^{\mathcal{F} \circ \mathcal{E}}$ (see Eq. 4 for detail). Here the cup (i.e. \cup) stands for the preparation of $\Gamma_{AA'}$, and the cap (i.e. \cap) represents the effect of measuring the operator with respect to $\langle \Gamma |$. In particular, (a) illustrates the Choi-Jamiołkowski operator of channel $\mathcal{F} \circ \mathcal{E}$. In (b), we re-derive the Choi-Jamiołkowski operator $J^{\mathcal{F} \circ \mathcal{E}}$ by using the yanking equation, which states that the snake line shown in blue dashed box of (b) is equal to the line drawn in blue dashed box of (c).

The definition of the link product (e.g., Eq. 4) involves the partial transpose \mathbf{T}_B , which is not completely positive and may seem unphysical. However, our Eq. 5 and Fig. 2 demonstrate that the partial transpose can be obtained by implementing Bell state measurements (up to a scalar factor). This highlights the fact that seemingly unphysical operations like \mathbf{T}_B can have practical interpretation in quantum information processing.

Let us discuss two specific scenarios to illustrate the usefulness of the link product \star (see Def. I.2): First, the link product helps us to demonstrate the action of quantum channel in terms of its Choi-Jamiołkowski operator. More precisely, given a quantum state ρ acting on system A , the quantum channel $\mathcal{E}_{A \rightarrow B}$ will transform it into

$$\mathcal{E}(\rho) = \rho \star J_{AB}^{\mathcal{E}}, \quad (6)$$

where $J_{AB}^{\mathcal{E}}$ is the Choi-Jamiołkowski operator of channel \mathcal{E} ; Second, the *Born rule* can be rewritten as a link product. In particular, denote by p_x the probability distribution obtained by measuring ρ with respect to $0 \leq M_x \leq 1$, then we have

$$p_x = \rho \star M_x^{\mathbf{T}}. \quad (7)$$

Here $M_x^{\mathbf{T}}$ stands for the Choi-Jamiołkowski operator of effect M_x (see Remark I.2).

Remark I.3. The link product \star is commutative under SWAP [18]. Take operators M_{AB} and N_{BC} for instance, we have

$$M_{AB} \star N_{BC} = \text{SWAP}_{A \leftrightarrow C}(N_{BC} \star M_{AB}). \quad (8)$$

Once the order of operations is determined, we can disregard the need for the SWAP operation and treat the resulting link product as a commutative operation. However, it is important to note that without the inclusion of the SWAP operation, the property of commutativity no longer holds. For convenience of presentation, in this work, we will fix the order of systems to make the link product commutative. Let's take Eq. 4 for example, when the lexicographical order is considered, we have

$$J_{AC}^{\mathcal{F} \circ \mathcal{E}} = J_{AB}^{\mathcal{E}} \star J_{BC}^{\mathcal{F}} = J_{BC}^{\mathcal{F}} \star J_{AB}^{\mathcal{E}}. \quad (9)$$

Similarly, Eqs. 6 and 7 can be rewritten as $\mathcal{E}(\rho) = J_{AB}^{\mathcal{E}} \star \rho$ and $p_x = M_x^{\mathbf{T}} \star \rho$ respectively. Furthermore, it is worth noting that in addition to commutativity, the link product \star is also associative. This property allows for the grouping of multiple Choi-Jamiołkowski operators without changing the outcome of their product and is a useful feature in the analysis of complex network structures.

B. How to Quantify a Quantum Channel: Twist It

While there is a variety of ways to quantify quantum channels, good channel quantifiers must have operational interpretations in some quantum information processing or quantum computation tasks. In this subsection, we

review two such channel quantifiers, namely the average fidelity f and the entanglement fidelity F . Specifically, the average fidelity $f(\mathcal{E})$ characterizes the performance of a quantum channel \mathcal{E} in transmitting quantum information, and meanwhile the entanglement fidelity $F(\mathcal{E})$ measures how \mathcal{E} preserves the quantum correlations between distant parties. Despite the obvious differences in mathematical expression and physical interpretation, the average fidelity and the entanglement fidelity enjoy a one-to-one correspondence, which was originally proved by M. Horodecki, P. Horodecki, and R. Horodecki in Ref. [19]. Here we provide an alternative proof of the one-to-one correspondence between average fidelity and entanglement fidelity, showing a different perspective on these channel quantifiers. Our mathematical toolkit includes the link product (see Def. I.2) and twirling.

Let us start with the first channel quantifier: the average fidelity. For an input state ψ_A acting on system A , the quantum channel $\mathcal{E}_{A \rightarrow B}$ will transform it into the state $\mathcal{E}(\psi)$, and we can use the *Uhlmann fidelity* F_U [20, 21] to measure the similarity between the input and output states of channel $\mathcal{E}_{A \rightarrow B}$, i.e.,

$$F_U(\psi, \mathcal{E}(\psi)) = \langle \psi | \mathcal{E}(\psi) | \psi \rangle = \text{Tr}[\psi \cdot \mathcal{E}(\psi)]. \quad (10)$$

In this work, we have adopted the notational convention that $\psi := |\psi\rangle\langle\psi|$. Now the consideration of similarity between the input and output states over all possible ψ leads to the average fidelity $f(\mathcal{E})$.

Definition I.3: Average Fidelity

The average fidelity $f(\mathcal{E}_{A \rightarrow B})$ of a quantum channel $\mathcal{E}_{A \rightarrow B}$ is defined by

$$f(\mathcal{E}_{A \rightarrow B}) := \int d\psi F_U(\psi_B, \mathcal{E}_{A \rightarrow B}(\psi_A)) = \int d\psi \text{Tr}[\psi_B \cdot \mathcal{E}_{A \rightarrow B}(\psi_A)], \quad (11)$$

where the integral is over the *Haar measure*, satisfying $\int d\psi = 1$. Notation F_U stands for the Uhlmann fidelity.

The second channel quantifier considered in this work is the so-called entanglement fidelity. Applying the quantum channel $\mathcal{E}_{A' \rightarrow B}$ to part of the maximally entangled state $\phi_{AA'}^+$ leads to the output state $\text{id}_A \otimes \mathcal{E}_{A' \rightarrow B}(\phi_{AA'}^+)$, whose difference with the maximally entangled state implies the entanglement fidelity $F(\mathcal{E})$.

Definition I.4: Entanglement Fidelity

The entanglement fidelity $F(\mathcal{E}_{A \rightarrow B})$ of a quantum channel $\mathcal{E}_{A \rightarrow B}$ is defined by

$$F(\mathcal{E}_{A \rightarrow B}) := F_U(\phi_{AB}^+, \mathcal{E}_{A' \rightarrow B}(\phi_{AA'}^+)) = \text{Tr}[\phi_{AB}^+ \cdot (\text{id}_A \otimes \mathcal{E}_{A' \rightarrow B}(\phi_{AA'}^+))], \quad (12)$$

where F_U stands for the Uhlmann fidelity, with ϕ^+ being the maximally entangled state.

Remark I.4. Since the systems of quantum channels are usually clear from the context, the notations of average fidelity $f(\mathcal{E}_{A \rightarrow B})$ (see Eq. 11) and entanglement fidelity $F(\mathcal{E}_{A \rightarrow B})$ (see Eq. 12) will be abbreviated to $f(\mathcal{E})$ and $F(\mathcal{E})$ respectively, and the maximally entangled state will be shortened to ϕ^+ . Sometimes we will also ignore the identity channel id . Adopting these conventions, the cumbersome expressions can be simplified. For example, Eqs. 11 and 12 can be rewritten as $f(\mathcal{E}) = \int d\psi \text{Tr}[\psi \cdot \mathcal{E}(\psi)]$ and $F(\mathcal{E}) = \text{Tr}[\phi^+ \cdot \mathcal{E}(\phi^+)]$ respectively.

Symmetry is a fundamental concept in nature and is of great importance in quantum information processing and computing. Twirling is a powerful technique in quantum information theory that enables the analysis of quantum systems by exploiting their symmetries. Specifically, twirling transforms a quantum state in a symmetric manner, preserving its properties under certain operations. This technique has numerous applications in quantum information theory, such as the analysis of entanglement [22], quantum error correction [23, 24], and communication protocols [19]. In this context, we can explore the symmetry of quantum dynamics by applying different types of twirling. One such type is channel twirling, denoted by \mathcal{T}_{ch} .

Definition I.5: Channel Twirling

Given a quantum channel \mathcal{E} , the channel twirling of \mathcal{E} is defined by

$$\mathcal{T}_{\text{ch}}(\mathcal{E}) := \int dU \mathcal{U}^\dagger \circ \mathcal{E} \circ \mathcal{U}, \quad (13)$$

where the integral is over the *Haar measure*, with $\mathcal{U}(\rho) := U \rho U^\dagger$ and $\mathcal{U}^\dagger(\rho) := U^\dagger \rho U$. Notation \circ stands for the composition of channels, and † represents the *Hermitian adjoint* of operators.

It is worth mentioning that both the average fidelity $f(\mathcal{E})$ (see Def. I.3) and entanglement fidelity $F(\mathcal{E})$ (see Def. I.4) are invariant under channel twirling \mathcal{T}_{ch} . To make our work self-contained, we will provide the formal statements about these properties, including their proofs.

Lemma I.6: Invariance of Average Fidelity under Channel Twirling

The average fidelity $f(\mathcal{E})$ (see Eq. 11) of a quantum channel \mathcal{E} is invariant under channel twirling \mathcal{T}_{ch} (see Eq. 13); that is

$$f(\mathcal{T}_{\text{ch}}(\mathcal{E})) = f(\mathcal{E}). \quad (14)$$

Proof. According to Def. I.3 and Def. I.5, we have

$$f(\mathcal{T}_{\text{ch}}(\mathcal{E})) = \int d\psi \text{Tr}[\psi \cdot \mathcal{T}_{\text{ch}}(\mathcal{E})(\psi)] \quad (15)$$

$$= \int d\psi \int dU \text{Tr}[\psi \cdot \mathcal{U}^\dagger \circ \mathcal{E} \circ \mathcal{U}(\psi)] \quad (16)$$

$$= \int d\psi \int dU \text{Tr}[\mathcal{U}(\psi) \cdot \mathcal{E}(\mathcal{U}(\psi))] \quad (17)$$

$$= \int dU f(\mathcal{E}) \quad (18)$$

$$= f(\mathcal{E}), \quad (19)$$

which completes the proof. \square

Lemma I.7: Invariance of Entanglement Fidelity under Channel Twirling

The entanglement fidelity $F(\mathcal{E})$ (see Eq. 12) of a quantum channel \mathcal{E} is invariant under channel twirling \mathcal{T}_{ch} (see Eq. 13); that is

$$F(\mathcal{T}_{\text{ch}}(\mathcal{E})) = F(\mathcal{E}). \quad (20)$$

Proof. Note that $\bar{U} \otimes U |\phi^+\rangle = |\phi^+\rangle$, where \bar{U} stands for the complex conjugate of U . Hence, we obtain

$$F(\mathcal{T}_{\text{ch}}(\mathcal{E})) = \text{Tr}[\phi^+ \cdot \mathcal{T}_{\text{ch}}(\mathcal{E})(\phi^+)] \quad (21)$$

$$= \text{Tr}[\phi^+ \cdot (\mathcal{U}^\dagger \circ \mathcal{E} \circ \mathcal{U})(\phi^+)] \quad (22)$$

$$= \text{Tr}[(\mathbb{1} \otimes U \phi^+ \mathbb{1} \otimes U^\dagger) \cdot (U^\mathbf{T} \otimes \mathbb{1} \mathcal{E}(\phi^+) \bar{U} \otimes \mathbb{1})] \quad (23)$$

$$= \text{Tr}[(\bar{U} \otimes U \phi^+ U^\mathbf{T} \otimes U^\dagger) \cdot \mathcal{E}(\phi^+)] \quad (24)$$

$$= \text{Tr}[\phi^+ \cdot \mathcal{E}(\phi^+)] \quad (25)$$

$$= F(\mathcal{E}), \quad (26)$$

which completes the proof of the lemma. \square

Another type of twirling is the isotropic twirling \mathcal{T}_{iso} [25], which was originally introduced by M. Horodecki and P. Horodecki in formulating the reduction criterion of separability.

Definition I.8: Isotropic Twirling

Given a bipartite state ρ , the isotropic twirling of ρ is defined by

$$\mathcal{T}_{\text{iso}}(\rho) := \int dU U \otimes \bar{U} \rho U^\dagger \otimes U^\mathbf{T}, \quad (27)$$

where the integral is over the *Haar measure*.

Remark I.5. Despite their differences in expressions, channel twirling \mathcal{T}_{ch} (see Eq. 13) and isotropic twirling \mathcal{T}_{iso} (see Eq. 27) are closely related with each other. In particular, the Choi-Jamiołkowski operator $J^{\mathcal{T}_{\text{ch}}(\mathcal{E})}$ of channel $\mathcal{T}_{\text{ch}}(\mathcal{E})$ is equal to $\mathcal{T}_{\text{iso}}(J^\mathcal{E})$, obtained by implementing the isotropic twirling \mathcal{T}_{iso} to the Choi-Jamiołkowski operator of channel \mathcal{E} . A graphic proof of above statement, i.e., $J^{\mathcal{T}_{\text{ch}}(\mathcal{E})} = \mathcal{T}_{\text{iso}}(J^\mathcal{E})$, is given in Fig. 3.

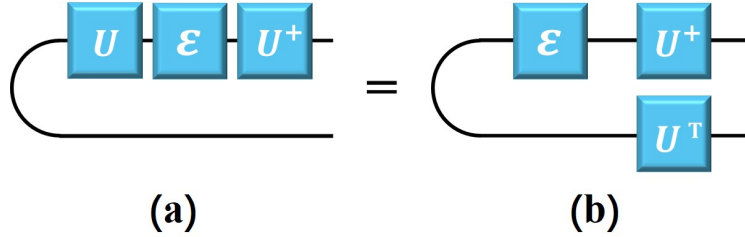


FIG. 3. (Color online) Equivalence between the Choi-Jamiołkowski operators of $J^{U^\dagger \circ \mathcal{E} \circ U}$ in (a) and $U^\mathbf{T} \otimes U^\dagger J^\mathcal{E} \bar{U} \otimes U$ in (b), which leads to the equation $J^{\mathcal{T}_{\text{ch}}(\mathcal{E})} = \mathcal{T}_{\text{iso}}(J^\mathcal{E})$ as required.

The isotropic twirling \mathcal{T}_{iso} is indeed a quantum channel, and thus its Choi-Jamiołkowski operator $J^{\mathcal{T}_{\text{iso}}}$ completely characterizes the mathematical properties of \mathcal{T}_{iso} . For more related results, we refer the interested readers to the work of E. M. Rains [22], which also contains the prototype of link product (see Def. I.2).

Lemma I.9: Choi-Jamiołkowski Operator of Isotropic Twirling [22]

Assume the isotropic twirling \mathcal{T}_{iso} is a map from systems $A_1 \otimes B_1$ to $A_2 \otimes B_2$, with $d := \dim A_1 = \dim A_2 = \dim B_1 = \dim B_2$, then its Choi-Jamiołkowski operator is given by

$$J_{A_1 B_1 A_2 B_2}^{\mathcal{T}_{\text{iso}}} = \phi_{A_1 B_1}^+ \otimes \phi_{A_2 B_2}^+ + \frac{1}{d^2 - 1} (\mathbb{1}_{A_1 B_1} - \phi_{A_1 B_1}^+) \otimes (\mathbb{1}_{A_2 B_2} - \phi_{A_2 B_2}^+), \quad (28)$$

where ϕ^+ is the maximally entangled state. By using the conventional abbreviations $A := A_1 A_2$, $B := B_1 B_2$, $\mathbf{1} := A_1 B_1$, and $\mathbf{2} := A_2 B_2$, Eq. 28 can be simplified to $J_{AB}^{\mathcal{T}_{\text{iso}}} = \phi_1^+ \otimes \phi_2^+ + (\mathbb{1}_1 - \phi_1^+) \otimes (\mathbb{1}_2 - \phi_2^+) / (d^2 - 1)$.

We now wish to show that the output state of isotropic twirling $\mathcal{T}_{\text{iso}} : \mathbf{1} \rightarrow \mathbf{2}$ is always a noisy singlet, i.e. in the form of $p\phi_2^+ + (1-p)\mathbb{1}_2/d^2$. To do so, let us consider the link product between a given state ρ_1 acting on system $\mathbf{1}$ and the Choi-Jamiołkowski operator of \mathcal{T}_{iso} . Written out explicitly, we have

$$\mathcal{T}_{\text{iso}}(\rho_1) = J_{AB}^{\mathcal{T}_{\text{iso}}} \star \rho_1 \quad (29)$$

$$= \left(\phi_1^+ \otimes \phi_2^+ + \frac{1}{d^2 - 1} (\mathbb{1}_1 - \phi_1^+) \otimes (\mathbb{1}_2 - \phi_2^+) \right) \star \rho_1 \quad (30)$$

$$= \text{Tr}[\phi_1^+ \cdot \rho_1] \phi_2^+ + \frac{(1 - \text{Tr}[\phi_1^+ \cdot \rho_1])}{d^2 - 1} (\mathbb{1}_2 - \phi_2^+) \quad (31)$$

$$= \frac{\text{Tr}[\phi_1^+ \cdot \rho_1] d^2 - 1}{d^2 - 1} \phi_2^+ + \frac{(1 - \text{Tr}[\phi_1^+ \cdot \rho_1]) d^2}{d^2 - 1} \frac{\mathbb{1}_2}{d^2}, \quad (32)$$

implying that

Theorem I.10: Noisy Singlet

Assume the isotropic twirling \mathcal{T}_{iso} is a map from systems $A_1 \otimes B_1$ to $A_2 \otimes B_2$ (i.e., $A_1 B_1 \rightarrow A_2 B_2$), with $d := \dim A_1 = \dim A_2 = \dim B_1 = \dim B_2$, and ρ_1 being an input state acting on system $A_1 \otimes B_1$, then the output state under \mathcal{T}_{iso} is a noisy singlet, i.e.,

$$p\phi_2^+ + (1-p)\frac{\mathbb{1}_2}{d^2}, \quad (33)$$

with the parameter p being characterized by

$$p = \frac{\text{Tr}[\phi_1^+ \cdot \rho_1]d^2 - 1}{d^2 - 1}. \quad (34)$$

Here we have adopted the notational conventions that $1 := A_1 B_1$, and $2 := A_2 B_2$.

Let us turn our attention to the output channel of channel twirling $\mathcal{T}_{\text{ch}} : A_2 \rightarrow A_1, B_1 \rightarrow B_2$. For any input channel $\mathcal{E} : A_1 \rightarrow B_1$, the Choi-Jamiołkowski operator of output channel $\mathcal{T}_{\text{ch}}(\mathcal{E})$ is then given by

$$J_2^{\mathcal{T}_{\text{ch}}(\mathcal{E})} = \mathcal{T}_{\text{iso}}(J_1^{\mathcal{E}}) \quad (35)$$

$$= \left(\phi_1^+ \otimes \phi_2^+ + \frac{1}{d^2 - 1}(\mathbb{1}_1 - \phi_1^+) \otimes (\mathbb{1}_2 - \phi_2^+) \right) \star J_1^{\mathcal{E}} \quad (36)$$

$$= \text{Tr}[\phi_1^+ \cdot J_1^{\mathcal{E}}]\phi_2^+ + \frac{(d - \text{Tr}[\phi_1^+ \cdot J_1^{\mathcal{E}}])}{d^2 - 1}(\mathbb{1}_2 - \phi_2^+) \quad (37)$$

$$= \frac{\text{Tr}[\phi_1^+ \cdot J_1^{\mathcal{E}}]d^2 - d}{d(d^2 - 1)}\Gamma_2 + \frac{(d - \text{Tr}[\phi_1^+ \cdot J_1^{\mathcal{E}}])d}{d^2 - 1}\frac{\mathbb{1}_2}{d}, \quad (38)$$

where the first equality (i.e., Eq. 35) has been investigated in Remark. I.5, the second equality (i.e., Eq. 36) is a result of Lem. I.9, and the third equality (i.e., Eq. 37) follows from the property of trace-preservation; namely,

$$\mathbb{1}_1 \star J_1^{\mathcal{E}} = \text{Tr}_{A_1}[\mathbb{1}_{A_1}] = d. \quad (39)$$

Thanks to the Choi-Jamiołkowski isomorphism, we know that Γ_2 represents the Choi-Jamiołkowski operator of the noiseless quantum channel $\text{id}_{A_2 \rightarrow B_2}$. Meanwhile, $\mathbb{1}_2/d$ is the Choi-Jamiołkowski operator of the replacement channel $\mathbb{1}_{B_2}/d \otimes \text{Tr}_{A_2}$. Written in full, that is

$$\mathcal{T}_{\text{ch}}(\mathcal{E}) = \left(\frac{\text{Tr}[\phi_1^+ \cdot J_1^{\mathcal{E}}]d^2 - d}{d(d^2 - 1)} \right) \text{id}_{A_2 \rightarrow B_2} + \left(\frac{(d - \text{Tr}[\phi_1^+ \cdot J_1^{\mathcal{E}}])d}{d^2 - 1} \right) \frac{\mathbb{1}_{B_2}}{d} \otimes \text{Tr}_{A_2}. \quad (40)$$

To conclude, we have the following theorem for channel twirling $J^{\mathcal{T}_{\text{ch}}}$.

Theorem I.11: Depolarizing Channel

Given a channel $\mathcal{E} : A_1 \rightarrow B_1$, the channel twirling $\mathcal{T}_{\text{ch}} : A_2 \rightarrow A_1, B_1 \rightarrow B_2$ will transform it into a depolarizing channel, i.e.,

$$\mathcal{T}_{\text{ch}}(\mathcal{E}) = p \text{id}_{A_2 \rightarrow B_2} + (1-p) \frac{\mathbb{1}_{B_2}}{d} \otimes \text{Tr}_{A_2}, \quad (41)$$

where the parameter p is given by

$$p = \frac{\text{Tr}[\phi_1^+ \cdot J_1^{\mathcal{E}}]d^2 - d}{d(d^2 - 1)}, \quad (42)$$

with $d := \dim A_1 = \dim A_2 = \dim B_1 = \dim B_2$.

Before the end of this subsection, let us return to the average fidelity $f(\mathcal{E})$ (see Def. I.3) and the entanglement fidelity $F(\mathcal{E})$ (see Def. I.4). In Ref. [19], M. Horodecki, P. Horodecki, and R. Horodecki find the essential connection between $f(\mathcal{E})$ and $F(\mathcal{E})$, in particular that

Lemma I.12: Connection between Average Fidelity and Entanglement Fidelity [19]

Given a quantum channel $\mathcal{E} : A \rightarrow B$, its average fidelity $f(\mathcal{E})$ (see Def. I.3) and entanglement fidelity $F(\mathcal{E})$ (see Def. I.4) satisfy the following equation,

$$f(\mathcal{E}) = \frac{dF(\mathcal{E}) + 1}{d + 1}, \quad (43)$$

with $d := \dim A = \dim B$.

Remark I.6. *There are several ways to prove Lem. I.12. The original proof was given by M. Horodecki, P. Horodecki, and R. Horodecki in Ref. [19], which had later been simplified by M. A. Nielsen in Ref. [26]. Here we will provide an alternative proof based on the Choi-Jamiołkowski operator of isotropic twirling \mathcal{T}_{iso} (see Lem. I.9) and the link product \star (see Def. I.2). In particular, our method relies heavily on Thm. I.11 presented in this subsection, whose proof is completed by using the Choi-Jamiołkowski operator of isotropic twirling and the link product. Hence, we conclude that our proof of Lem. I.12 is based on $J^{\mathcal{T}_{iso}}$ and \star . Besides its fundamental importance in understanding channel quantifiers, Lem. I.12 is also a key to characterizing general quantum teleportation [19].*

Proof. To prove this claim, we start with the input state ψ and consider the corresponding output under quantum channel $\mathcal{T}_{ch}(\mathcal{E})$. Thanks to Eq. 41 of Thm. I.11, we immediately obtain

$$\mathcal{T}_{ch}(\mathcal{E})(\psi) = p\psi + (1-p)\frac{\mathbb{1}}{d}, \quad (44)$$

with p given by Eq. 42. Thus, by using Lem. I.6, we see that

$$f(\mathcal{E}) = f(\mathcal{T}_{ch}(\mathcal{E})) = p + \frac{1-p}{d} = \frac{p(d-1) + 1}{d}. \quad (45)$$

On the other hand, the entanglement fidelity $F(\mathcal{E})$ of channel \mathcal{E} is equal to $\text{Tr}[\phi_1^+ \cdot J_1^{\mathcal{E}}]/d$, implying that

$$p = \frac{F(\mathcal{E})d^2 - 1}{d^2 - 1}. \quad (46)$$

Combining Eq. 45 with Eq. 46 leads to Eq. 43, as desired. \square

C. Quantum Superchannels: Pre-Processing, Post-Processing, and Non-Signalling

Exploring quantum channels primarily involves manipulating them in specific contexts. For instance, when dealing with a noisy quantum channel, determining its capacity to transmit information through the use of encoder and decoder leads to the development of quantum information theory – a rapidly evolving and dynamic field that seeks to unleash the extraordinary capabilities of quantum mechanics in revolutionizing information processing. Mathematically, the sender's encoder and the receiver's decoder can be represented as a bipartite quantum operation known as a *superchannel* [27]. This concept encapsulates the most general way of manipulating a quantum channel, including the channel twirling \mathcal{T}_{ch} (see Def. I.5) discussed in Subsec. IB. Quantum superchannels also constitute a fundamental tool for understanding dynamical resources and the associated resource measures [28–30]. In this subsection, we provide a rigorous introduction to the basic concepts of quantum superchannels and investigate their properties using the powerful Choi-Jamiołkowski isomorphism (see Def. I.1).

A quantum superchannel is formed by combining two quantum channels, which can be implemented in sequence and connected through a quantum memory in accordance with the principle of causality in the theory of relativity [31–33]. This causal structure is formally known as *non-signalling* (NS) between the parties involved in quantum coding protocols. A comprehensive review of non-signalling codes is beyond the scope of this discussion. Interested readers are referred to Ref. [34] and the references therein for a more detailed introduction. In the context of causal boxes, the causality property of quantum superchannels is referred to as *semicausality* [35–37]. The use of the Choi-Jamiołkowski isomorphism has proven to be a powerful tool in analyzing the properties of semicausal maps and their relation to *semilocalizability*, as discussed in previous works [38]. Now let us start with the definition of non-signalling.

Definition I.13: Non-Signalling

A bipartite channel $\Theta_{A_1 B_1 \rightarrow A_2 B_2}$ is non-signalling from $B := B_1 B_2$ to $A := A_1 A_2$, denoted as $B \nrightarrow A$, if

$$\text{Tr}_{B_2} \circ \Theta_{A_1 B_1 \rightarrow A_2 B_2} = \text{Tr}_{B_1} \otimes \mathcal{E}_{A_1 \rightarrow A_2}, \quad (47)$$

holds for some quantum channel $\mathcal{E}_{A_1 \rightarrow A_2}$. Similarly, a bipartite channel $\Theta_{A_1 B_1 \rightarrow A_2 B_2}$ is non-signalling (NS) from $A \rightarrow B$, denoted as $A \nrightarrow B$, if

$$\text{Tr}_{A_2} \circ \Theta_{A_1 B_1 \rightarrow A_2 B_2} = \text{Tr}_{A_1} \otimes \mathcal{F}_{B_1 \rightarrow B_2}, \quad (48)$$

holds for some quantum channel $\mathcal{F}_{B_1 \rightarrow B_2}$. A map Θ is non-signalling if it is both $A \nrightarrow B$ and $B \nrightarrow A$.

Physically, non-signalling from B to A means that no action on system B can cause any detectable effect on system A . A visualization of non-signalling bipartite channels is provided in Fig. 4.

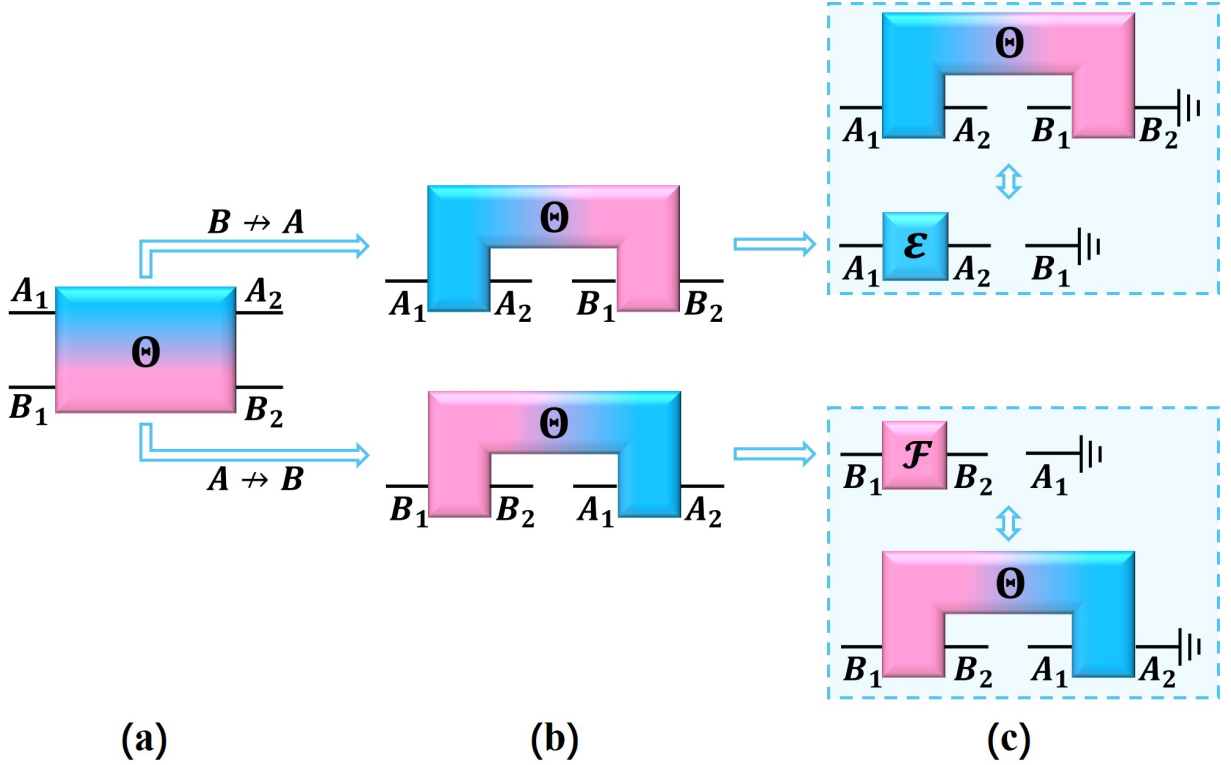


FIG. 4. (Color online) Demonstration of non-signalling bipartite channel Θ . A general bipartite quantum channel $\Theta_{A_1 B_1 \rightarrow A_2 B_2}$ is depicted in (a), where systems A_1 and A_2 belongs to Alice, systems B_1 and B_2 belongs to Bob. If the bipartite channel Θ is non-signalling from B to A , i.e., Bob's action cannot affect Alice, we arrive at the top of (b). In other words, tracing out system B_2 will lead to the form of $\mathcal{E}_{A_1 \rightarrow A_2} \otimes \text{Tr}_{B_1}$ (see Eq. 47) for some quantum channel \mathcal{E} on Alice's side, shown in the top box of (c). On the other hand, if the bipartite channel Θ is non-signalling from A to B , i.e. Alice's behavior won't influence Bob, the bipartite channel Θ can be transformed into the form illustrated in the bottom of (b). In this case, discarding system A_2 will imply the decomposition of bipartite operation between Alice and Bob; that is $\text{Tr}_{A_1} \otimes \mathcal{F}_{B_1 \rightarrow B_2}$ (see Eq. 48) with \mathcal{F} being a quantum acting on Bob's side, painted in the bottom box of (c).

Given a quantum channel $\mathcal{E}_{A_2 \rightarrow B_1}$, the general quantum supermap $\Theta_{A_1 B_1 \rightarrow A_2 B_2}$ that maps $\mathcal{E}_{A_2 \rightarrow B_1}$ to a channel $\Theta(\mathcal{E})_{A_1 \rightarrow B_2}$, called superchannel, satisfies the following conditions [27]:

- **Completely Positivity (CP);**
- **Trace Preservation (TP);**
- **Non-Signalling (NS) from B to A .**

Similar to the construction of Choi-Jamiołkowski operator for a quantum channel (see Def. I.1 and Fig. 1), we can introduce the Choi-Jamiołkowski operator for superchannels. In particular, the Choi-Jamiołkowski operator for superchannel $\Theta_{A_1 B_1 \rightarrow A_2 B_2}$ is defined as

$$J_{A_1 B_1 A_2 B_2}^\Theta := \text{id}_{A_1} \otimes \Theta_{A'_1 B'_1 \rightarrow A_2 B_2} \otimes \text{id}_{B_1} (\Gamma_{A_1 A'_1} \otimes \Gamma_{B_1 B'_1}), \quad (49)$$

where $\Gamma_{A_1 A'_1}$ and $\Gamma_{B_1 B'_1}$ are unnormalized maximally entangled states acting on systems $A_1 A'_1$ and $B_1 B'_1$ respectively. An illustration of Eq. 49 is given in Fig. 5(a), including the corresponding quantum circuit realization (see Fig. 5(b)).

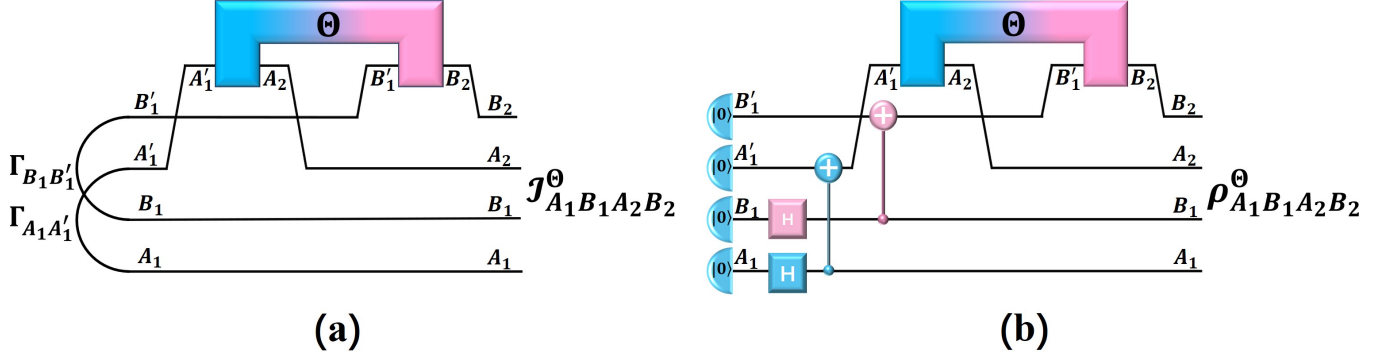


FIG. 5. (Color online) Pictorial representation of the Choi-Jamiołkowski operator $J_{A_1 B_1 A_2 B_2}^\Theta$ (see Eq. 49) for superchannel $\Theta_{A_1 B_1 \rightarrow A_2 B_2}$ that is non-signalling from B to A (a), and circuit realization of normalized Choi-Jamiołkowski state $\rho_{A_1 B_1 A_2 B_2}^\Theta$ (b). Here $\rho_{A_1 B_1 A_2 B_2}^\Theta = J_{A_1 B_1 A_2 B_2}^\Theta / d_{A_1} d_{B_1}$.

Using the language of Choi-Jamiołkowski isomorphism, we say that a quantum supermap $\Theta_{A_1 B_1 \rightarrow A_2 B_2}$ is completely positive if and only if its Choi-Jamiołkowski operator $J_{A_1 B_1 A_2 B_2}^\Theta$ is positive semidefinite, namely $J_{A_1 B_1 A_2 B_2}^\Theta \geq 0$. It is said to be trace-preserving if and only if $\text{Tr}_{B_1 B_2} J_{A_1 B_1 A_2 B_2}^\Theta = \mathbb{1}_{A_1 A_2}$. Finally, such a supermap is non-signalling from B to A if and only if its Choi-Jamiołkowski operator $J_{A_1 B_1 A_2 B_2}^\Theta$ satisfies

$$\text{Tr}_{B_2} [J_{A_1 B_1 A_2 B_2}^\Theta] = J_{A_1 A_2}^\mathcal{E} \otimes \mathbb{1}_{B_1}, \quad (50)$$

where $J_{A_1 A_2}^\mathcal{E}$ stands for the Choi-Jamiołkowski operator of some quantum channel \mathcal{E} from A_1 to A_2 .

Equivalently, a superchannel $\Theta_{A_1 B_1 \rightarrow A_2 B_2}$ can also be viewed as the sequential composition of two quantum channels; that is

$$\Theta_{A_1 B_1 \rightarrow A_2 B_2} = \Theta_{B_1 E \rightarrow B_2}^{\text{post}} \circ \Theta_{A_1 \rightarrow A_2 E}^{\text{pre}}, \quad (51)$$

where E is a memory system between Θ^{pre} and Θ^{post} (see Fig. 6). Here, quantum channels Θ^{pre} and Θ^{post} are

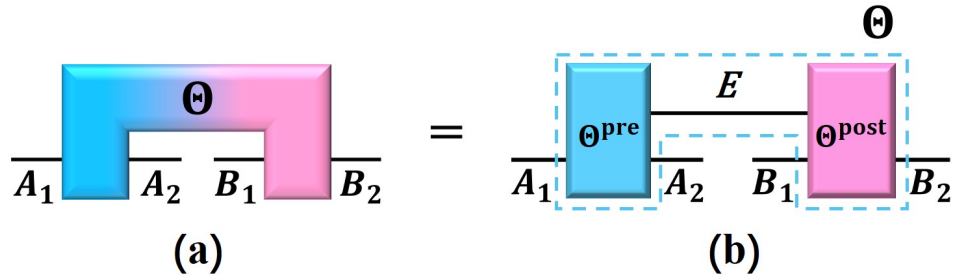


FIG. 6. (Color online) Decomposition of superchannel $\Theta_{A_1 B_1 \rightarrow A_2 B_2}$ (see Eq. 51). In other words, superchannel Θ (a) can be realized by preparing a pre-processing $\Theta_{A_1 \rightarrow A_2 E}^{\text{pre}}$ and a post-processing $\Theta_{B_1 E \rightarrow B_2}^{\text{post}}$, which are connected by a hidden memory system E (b).

known as the pre-processing and post-processing of Θ respectively. Denote their Choi-Jamiołkowski operators as J^{pre}

and J^{post} , then it is straightforward to write down the Choi-Jamiołkowski operator of superchannel Θ by using link product \star (see Def. I.2), i.e.,

$$J_{A_1 B_1 A_2 B_2}^\Theta = J_{A_1 A_2}^{\text{pre}} \star J_{B_1 B_2}^{\text{post}}. \quad (52)$$

For any quantum channel $\mathcal{E}_{A_2 \rightarrow B_1}$, the Choi-Jamiołkowski operator of resultant channel $\Theta(\mathcal{E})_{A_1 \rightarrow B_2}$ under $\Theta_{A_1 B_1 \rightarrow A_2 B_2}$ is characterized by

$$J_{A_1 B_2}^{\Theta(\mathcal{E})} = J_{A_1 B_1 A_2 B_2}^\Theta \star J_{A_2 B_1}^\mathcal{E} = \text{Tr}_{A_2 B_1} [J_{A_1 B_1 A_2 B_2}^\Theta \cdot ((J_{A_2 B_1}^\mathcal{E})^\text{T} \otimes \mathbb{1}_{A_1 B_2})]. \quad (53)$$

Then, for an input state ρ_{A_1} , the output state of channel $\Theta(\mathcal{E})_{A_1 \rightarrow B_2}$ reads

$$\Theta(\mathcal{E})_{A_1 \rightarrow B_2}(\rho_{A_1}) = J_{A_1 B_2}^{\Theta(\mathcal{E})} \star \rho_{A_1} = J_{A_1 B_1 A_2 B_2}^\Theta \star J_{A_2 B_1}^\mathcal{E} \star \rho_{A_1} = \text{Tr}_{A_2 B_1} [J_{A_1 B_1 A_2 B_2}^\Theta \cdot (\rho_{A_1}^\text{T} \otimes (J_{A_2 B_1}^\mathcal{E})^\text{T} \otimes \mathbb{1}_{B_2})]. \quad (54)$$

The formula presented above is well-defined due to the commutativity and associativity properties of the link product \star , as noted in Remark I.3.

D. Quantum Circuit Fragments: Framework of Non-Markovian Dynamics

Quantum channels are a central concept in quantum mechanics, characterizing the time-evolution of quantum systems between two different time points (see Fig. 1). The most general way of manipulating quantum channels is through the use of quantum superchannels, which describe the non-Markovian dynamics of four time points (see Fig. 5). These superchannels capture the complex interplay between system and memory, allowing for a more comprehensive understanding of quantum dynamics. A notable example is the superchannel $\Theta_{A_1 B_1 \rightarrow A_2 B_2}$, shown in Fig. 6(b). This superchannel captures the system-memory dynamics from A_1 to A_2 and from B_1 to B_2 , via the composition of two channels, i.e., $\Theta_{A_1 \rightarrow A_2 E}^{\text{pre}}$ and $\Theta_{B_1 E \rightarrow B_2}^{\text{post}}$. The study of non-Markovian quantum processes that involve multiple time points is critical for various fields, such as distributed quantum computing [39–41], cloud-based quantum computing [42–45], quantum network communication [46–58], quantum-enhanced agents [59–62], quantum metrology [63–65], open quantum systems [66–68], quantum clocks and sensors [69–73]. Furthermore, it has significant implications for emerging areas such as quantum biology [74], making it a topic of utmost importance. Generally, non-Markovian quantum processes offer a window into the interplay between system and environment, allowing us to explore the rich landscape of quantum phenomena that arise from it. In this subsection, we introduce the concept of *quantum circuit fragment* as a general framework for understanding these processes. The corresponding Choi-Jamiołkowski operator, which characterizes the quantum circuit fragment, is known as the *quantum comb*, and has been extensively investigated in literature [15–17].

Consider the collection of all quantum circuit fragments consisting of k sequential quantum channels, denoted as \mathfrak{F}_k . It then follows that for any given point-to-point quantum channel \mathcal{E} , we have

$$\mathcal{E} \in \mathfrak{F}_1. \quad (55)$$

Here, the set \mathfrak{F}_1 represents the exact set of all quantum channels, encompassing the full range of physical operations that can be used to manipulate quantum states. Notably, both the set of quantum states, denoted by $\mathfrak{S}_{\text{State}}$, and the set of positive operator-valued measures (POVMs), denoted by $\mathfrak{S}_{\text{POVM}}$, are subsets of \mathfrak{F}_1 [4]. Writing everything out explicitly, we have

$$\mathfrak{S}_{\text{State}} \cup \mathfrak{S}_{\text{POVM}} \subset \mathfrak{F}_1 = \mathfrak{S}_{\text{Channel}}, \quad (56)$$

where $\mathfrak{S}_{\text{Channel}}$ stands for the collection of all quantum channels. The set \mathfrak{F}_2 , on the other hand, refers to the collection of all quantum superchannels. In the context of quantum causal inference [75–77], the set of causal maps under investigation is denoted as $\mathfrak{S}_{\text{CMap}}$. By examining the relationship between these two sets, it becomes evident that $\mathfrak{S}_{\text{CMap}}$ is naturally embedded within \mathfrak{F}_2 , as all causal maps can be realized as special cases of superchannels.

$$\mathfrak{S}_{\text{CMap}} \subset \mathfrak{F}_2 = \mathfrak{S}_{\text{Channel}}. \quad (57)$$

Here $\mathfrak{S}_{\text{Channel}}$ is the set of all quantum superchannels. Let us now turn our attention to the case of a general set \mathfrak{F}_k , which comprises elements that consist of k sequential quantum channels. Consider a sequence of quantum channels $\mathcal{E}_1, \mathcal{E}_2, \dots, \mathcal{E}_k$ that belongs to \mathfrak{F}_1 and possesses the following defining characteristics:

$$\mathcal{E}_1 : \mathcal{H}_0 \rightarrow \mathcal{H}_1 E_1, \quad (58)$$

$$\mathcal{E}_i : \mathcal{H}_{2i-2} E_{i-1} \rightarrow \mathcal{H}_{2i-1} E_i, \quad 2 \leq i \leq k-1 \quad (59)$$

$$\mathcal{E}_k : \mathcal{H}_{2k-2} E_{k-1} \rightarrow \mathcal{H}_{2k-1}. \quad (60)$$

In this context, it is important to note that intermediate channels typically have both an environment input system and an environment output system. In contrast, the first channel in the sequence generally lacks an environment input system, while the final channel lacks an environment output system. In our analysis of quantum circuits, we adopt the term “quantum circuit fragment” [77] to refer to the overall dynamics of the circuit, which is composed of a sequence of k quantum channels. In full, a quantum circuit fragment can be expressed as the composite of k quantum channels, denoted as

$$\mathcal{E} := \mathcal{E}_k \circ \mathcal{E}_{k-1} \circ \cdots \circ \mathcal{E}_2 \circ \mathcal{E}_1. \quad (61)$$

Quantum circuit fragment (see Eq. 61) offers us the most general way of demonstrating quantum dynamics of non-Markovian processes [78–82], including the time evolution of quantum systems under environment coupling and designing and operating quantum devices in quantum computing. The corresponding Choi-Jamiołkowski operator is called quantum comb [15–17]. See Fig. 7 for an illustration of the dynamics of quantum circuit fragment \mathcal{E} introduced in Eq. 61 and its Choi-Jamiołkowski state $\rho^\mathcal{E}$. Denote the Choi-Jamiołkowski operator of channel \mathcal{E}_i ($1 \leq i \leq k$) as

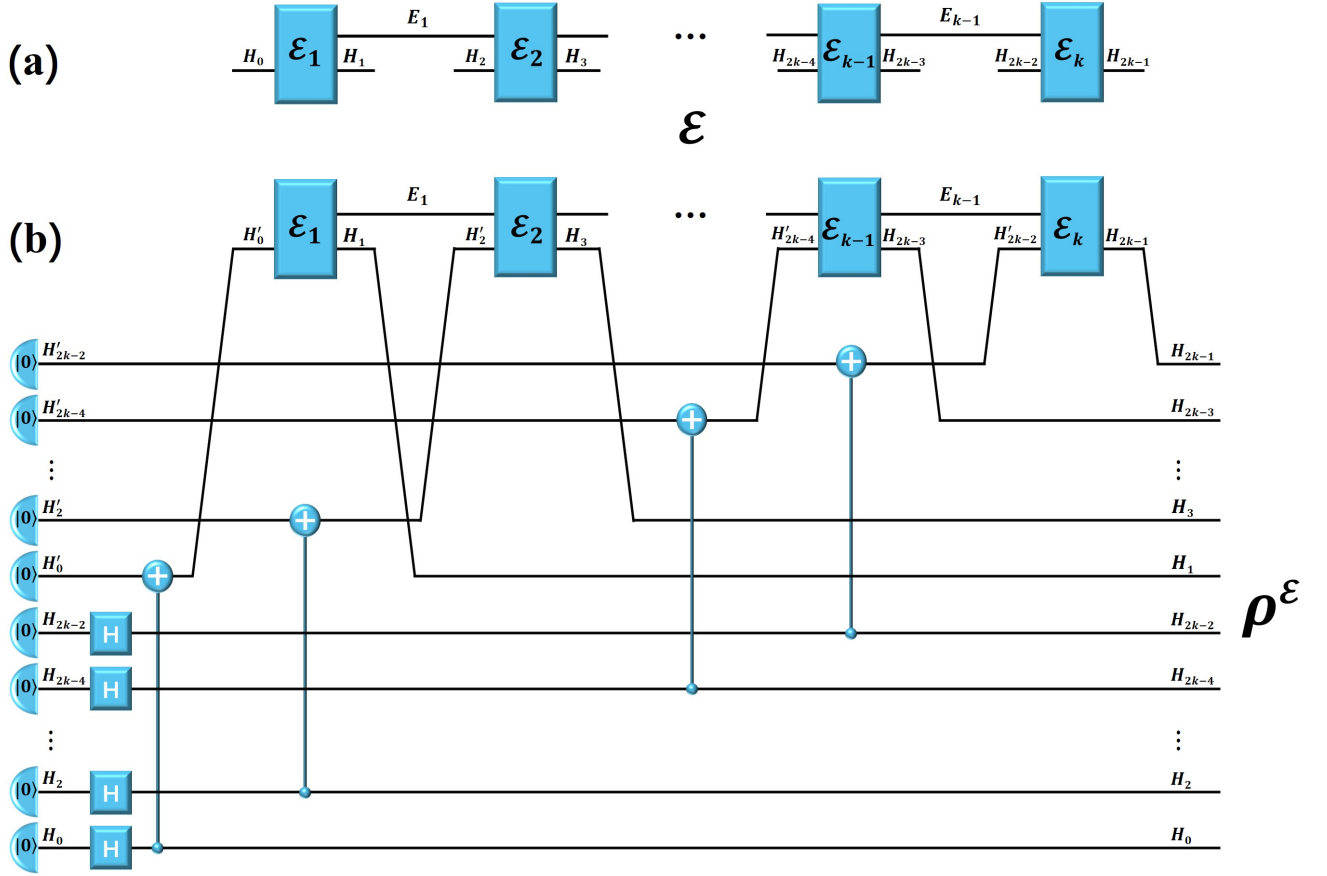


FIG. 7. (Color online) The quantum circuit fragment \mathcal{E} (a) and the implementation of its Choi-Jamiołkowski state $\rho^\mathcal{E}$ (b). Here \mathcal{E} is constituted of k sequential quantum channels $\mathcal{E}_1, \mathcal{E}_2, \dots, \mathcal{E}_k$ (see Eq. 61).

$J^{\mathcal{E}_i}$, then the quantum comb $J^\mathcal{E}$ can be re-expressed as the link product between channels, namely

$$J^\mathcal{E} = J^{\mathcal{E}_1} \star J^{\mathcal{E}_2} \star \cdots \star J^{\mathcal{E}_{k-1}} \star J^{\mathcal{E}_k}. \quad (62)$$

The process of measuring a quantum circuit fragment is referred to as an *interactive measurement*, which is an essential tool for witnessing non-Markovianity and inferring causality. While the topic of interactive measurements is complex and important, a full discussion of this topic is beyond the scope of this work. We therefore leave the exploration of interactive measurements to future research endeavors [77]. Nevertheless, it is worth noting that interactive measurements represent a promising avenue for advancing our understanding of quantum systems over multiple time points. By leveraging the principles of interactive measurement, we can gain valuable insights into the behavior of quantum systems and develop new approaches to solving complex problems in various fields.

II. TEMPORAL ENTANGLEMENT

In this section, we present a comprehensive framework of temporal entanglement from a quantum resource theoretical perspective, extending the entanglement theory from states and channels to the most general form of quantum circuit fragments (refer to Subsec. ID). In Subsec. IIA, we demonstrate the framework of quantum resource theory and examine various options for free morphism in the context of temporal entanglement. Additionally, we introduce the fidelity of quantum circuit fragments (refer to Def. II.3) concerning various free morphisms in Subsec. IIB. It is essential to develop this framework to investigate the concepts of quantum teleportation, quantum repeaters, and communication in quantum networks thoroughly. The connection between temporal entanglement and quantum network communication lies at the heart of our research, and we will unravel this relationship in greater detail in the following sections.

A. Entangled Circuit Fragments: Quantum Correlations across Space and Time

Quantum entanglement is one of the most remarkable and puzzling features of quantum mechanics, where two or more particles become intrinsically connected in such a way that the state of one particle instantaneously affects the state of the other, even when they are separated by significant distances. This extraordinary phenomenon has emerged as a key resource in various fields [83], ranging from communication [84–89], cryptography [90–92], to computation [93–97]. The study of entangled states, which represent a form of quantum entanglement at a given moment, has become a major focus of research since its inception, owing to their indispensable role in understanding the fundamentals of quantum mechanics and their potential for advancing a wide range of quantum technologies. As such, entangled states have been the subject of numerous research articles in the literature. In the realm of physical systems, change is the only constant. As famously stated by Chuck Palahniuk in *Fight Club*, “nothing is static, everything is evolving”. Recent progress has extended the theory of entanglement [98–102] to encompass quantum channels [103–107], enabling a comprehensive investigation into the intricate entanglement of dynamical processes. Both point-to-point and bipartite channels have been explored, offering a multifaceted approach to understanding quantum dynamics. Notably, there is no fundamental difference between quantum states and quantum channels, as both are elements of \mathfrak{F}_1 , i.e., quantum circuit fragments with a single process. Despite these advancements, the generic entanglement theory of quantum dynamics over multiple time points [108–114], represented by the quantum circuit fragment \mathfrak{F}_k (see Subsec. ID), is still absent. Deeper insights into the intricate interactions of quantum systems, particularly as they evolve over time, hold immense potential to illuminate fundamental theoretical concepts and practical applications. The continued expansion of our understanding of quantum dynamics over multiple time points will undoubtedly shape the future of quantum computing and technology. In order to tackle this issue, our attention is directed towards examining temporal entanglement - that is, the entanglement of general quantum circuit fragments - in this subsection. Through our analysis, we aim to develop a quantum resource theory that aligns with our findings, obtained through a meticulous analysis.

Quantum resource theory is a vibrant and rapidly developing field at the forefront of modern quantum theories. At its core, the theory focuses on free states or channels, which can be prepared or manipulated without the need for any additional resources [115, 116]. On the contrary, the use of resources can provide quantum advantages in a wide range of tasks, including channel (or phase) discrimination [117–121] and exclusion [122, 123]. Entangled states [83] and coherent states [124] are among the most important and widely studied quantum resources in quantum resource theory. They represent distinct types of resources that can be used to perform a variety of tasks with advantages that cannot be achieved using classical resources alone. For example, entangled states can be used to perform tasks such as quantum teleportation, superdense coding, and quantum cryptography, while coherent states can be used in applications such as quantum metrology and quantum computing. In order to streamline the nomenclature of quantum resource theories and clarify the distinction between the subject of study and its manipulation, we adopt the language of category theory [125]. Specifically, we refer to the subject of study as *free objects* and the corresponding physical manipulation of these objects as *free morphisms* in this work. For instance, in the conventional resource theory of entanglement, the SWAP operation serves as a morphism. On the other hand, in the investigation of dynamical entanglement, the SWAP becomes an object. In summary, a quantum resource theory \mathcal{R} is a framework that allows researchers to study the properties and behaviors of quantum resources in a rigorous and systematic way. It is constituted of three fundamental components that are essential to its functioning:

- **Set of Free Objects $\text{ob}(\mathcal{R})$:** These are quantum circuit fragments that can be prepared or manipulated without the need for any additional resources. The free objects are the starting point for understanding the properties of more complex quantum systems over multiple time points, such as entangled or coherent non-Markovian quantum processes;

- **Set of Free Morphisms $\text{hom}(\mathcal{R})$:** These are the physical transformations that can be applied to the free objects without creating new resources. Free morphisms play a crucial role in the manipulation and transformation of quantum resources, and they provide a framework for understanding the ways in which quantum circuit fragments can be transformed and manipulated;
- **Golden Rule $\Theta(\text{ob}(\mathcal{R})) \subset \text{ob}(\mathcal{R}), \forall \Theta \in \text{hom}(\mathcal{R})$:** This is a fundamental principle that guides the manipulation and transformation of quantum resources. It states that in any given quantum resource theory, the set of free objects should be closed under the action of the free morphisms.

A prominent example is the study of conventional resource theory of entanglement for quantum states, where $\text{ob}(\mathcal{R})$ is the set of all separable states. Meanwhile, set $\text{hom}(\mathcal{R})$ is the collection of all local operations and classical communication (LOCC). The use of free morphisms has been instrumental in establishing the resource theory of entanglement of quantum states. By considering the action of free morphisms, it is possible to generate all separable states using local operations and classical communication. This means that the entire resource theory of entanglement can be built upon the framework of free morphisms. In practical laboratory settings, there are physical limitations on the types of operations that can be performed, and as a result, the set of LOCC can be divided into different classes [126]:

- **Local Operations (LO):** quantum operations that can be performed on individual subsystems of a composite quantum system. These operations can be performed independently by each party without any communication between them [127]. A typical example is the local unitary (LU) operations [128–130], which form a special class of local operations, namely $\text{LU} \subset \text{LO}$, that involve applying a unitary transformation to one or more subsystems of a composite quantum system. These operations are commonly used in the context of entangled quantum states to manipulate the entanglement between subsystems;
- **$\text{LOCC}_1(\text{poly}(d))$:** local quantum operations and one-way classical communication with respect to a fixed party, followed by a coarse-graining map. Here, the communication complexity is polynomially dependent on an integral parameter d . This parameter d represents a measure of the dimensionality or complexity of the quantum system under consideration, such as the dimension of the message system. By incorporating the concept of $\text{LOCC}_1(\text{poly}(d))$, the communication complexity is effectively reduced, making it more feasible to implement in real-world scenarios.
- **LOCC_1 :** local quantum operations and one-way classical communication with respect to a fixed party, followed by a coarse-graining map. LOCC_1 is a specific subclass of LOCC operations that has been extensively studied in the field of quantum information theory. It has been shown to be strictly less powerful than the set of all LOCC operations, which means that there are entangled states that cannot be transformed into one another using LOCC_1 operations but can be transformed using more general LOCC operations;
- **LOCC_k :** quantum channels that are LOCC-linked – obtaining by implementing LOCC_1 and coarse-graining maps – to a element of LOCC_{k-1} , where $k \geq 2$. LOCC_k operations are a generalization of LOCC_1 and provide a way to perform more complex entanglement manipulation tasks. However, as k increases, the set of LOCC_k operations becomes more powerful and less well-understood;
- **$\text{LOCC}_{\mathbb{N}}$:** a element of LOCC_k for some $k \in \mathbb{N}$;
- **LOCC:** quantum channel \mathcal{E} is a LOCC channel if there exists a sequence of quantum channels $\{\mathcal{E}_1, \mathcal{E}_2, \dots\}$ satisfying (i) each of them belongs to the set $\text{LOCC}_{\mathbb{N}}$, (ii) \mathcal{E}_k is LOCC-linked to \mathcal{E}_{k-1} , and (iii) \mathcal{E}'_k , obtained by implementing coarse-graining maps on \mathcal{E}_k , converges to \mathcal{E} . LOCC operations are important in quantum information theory because they are considered to be the most basic and physically realistic class of operations that can be performed on entangled quantum systems. They are also used as a benchmark for the study of several important tasks, such as entanglement distillation, entanglement cost, and quantum teleportation;
- **$\overline{\text{LOCC}_{\mathbb{N}}}$:** topological closure of $\text{LOCC}_{\mathbb{N}}$.

The formal definitions of coarse-graining maps, LOCC-link, and convergence of channels can be found in Ref. [126], which is a comprehensive reference on LOCC. These concepts are important for studying the behavior of entangled quantum systems under local operations and classical communication. In addition to these concepts, there are many other related operations in entanglement theory that are of interest to researchers. These include:

- **Separable Operations (SEP):** quantum channels that can be expressed using a product form of *Kraus operators*. It is noteworthy that when considering two bipartite pure quantum states, the existence of a separable operation capable of transforming one into the other implies the existence of a LOCC operation that can achieve the same result. Specifically, Gheorghiu and Griffiths have demonstrated that any transformation of

a pure state using separable operations satisfies the same necessary and sufficient conditions as an LOCC transformation [131]. It should be noted, however, that this equivalence does not hold for mixed states, as illustrated by Chitambar and Duan in Ref. [132]. In fact, every LOCC operation can be expressed in terms of a Kraus operator-sum representation, using product Kraus operators only. However, the converse is not necessarily true;

- **Separability Preserving Operations (SEPP):** quantum channels that preserve the separability of states. To further elaborate, SEPP is a set of operations that are non-entangling, meaning they do not create any entanglement from separable states. The study of SEPP, especially its approximate versions, is important in the context of entanglement manipulation, as it provides a framework for the reversible manipulation of entanglement. A deeper exploration of approximate SEPP can be found in various literature references, including Ref. [133–136], which discuss the generalization of quantum Stein’s lemma and the second law of entanglement manipulation. These references provide detailed explanations and mathematical formulations of the properties and applications of SEPP, and can be a valuable resource for those interested in studying this topic;
- **Positive-Partial-Transpose Preserving Operations (PPT):** quantum channels that completely preserve the positivity of the partial transpose of states. More precisely, any quantum state that has a positive partial transpose will remain positive under a PPT operation. This property distinguishes PPT operations from other types of quantum operations, such as LOCC operations, because they can create bound entangled states that cannot be created using only LOCC operations. One of the key advantages of using PPT operations over LOCC operations is that PPT operations are generally easier to characterize. This is because the set of PPT operations is a convex set that can be described by using semidefinite programming (SDP) techniques [137–139], whereas the set of LOCC operations is a non-convex set that is much harder to handle.

The models under consideration follow a hierarchical structure, with each model being more general and encompassing than the previous one. This hierarchy allows for a systematic study of the different models and their relationships to one another in entanglement theory. Specifically, the models considered in this work can be organized in the following hierarchy, starting from the most restrictive:

$$\text{LO} \subsetneq \text{LOCC}_1(\text{poly}(d)) \subset \text{LOCC}_1 \subsetneq \text{LOCC}_k \subsetneq \text{LOCC}_{k+1} \subsetneq \text{LOCC}_{\mathbb{N}} \subsetneq \text{LOCC} \subsetneq \overline{\text{LOCC}_{\mathbb{N}}} \subsetneq \text{SEP} \subsetneq \text{SEPP} \subsetneq \text{PPT}, \quad (63)$$

for any $k > 1$.

Remark II.1. While $\text{LOCC}_1(\text{poly}(d))$ is clearly a subset of LOCC_1 , encompassing operations with a narrower range of communication complexities, it is still unclear whether this inclusion is strict. This ambiguity arises from the possibility that there are scenarios where $\text{LOCC}_1(\text{poly}(d))$ and LOCC_1 result in the same set of achievable transformations. To gain a comprehensive understanding of the relationship between $\text{LOCC}_1(\text{poly}(d))$ and LOCC_1 , more thorough examination and in-depth analysis are required.

We will now expand the scope of these definitions to encompass quantum circuit fragments – the carrier of temporal entanglement. The first new and important concept is called the \mathcal{S} -simulable quantum circuit fragment.

Definition II.1: \mathcal{S} -Simulable Quantum Circuit Fragment

A quantum circuit fragment $\mathcal{E} \in \mathfrak{F}_k$ can be referred to as a \mathcal{S} -simulable quantum circuit fragment if it can be decomposed into a series of quantum channels $\{\mathcal{E}_1, \mathcal{E}_2, \dots, \mathcal{E}_k\}$, where each $\mathcal{E}_i \in \mathcal{S}$. The set \mathcal{S} is chosen from $\{\text{LO}, \text{LOCC}_1(\text{poly}(d)), \text{LOCC}_k, \text{LOCC}_{\mathbb{N}}, \text{LOCC}, \overline{\text{LOCC}_{\mathbb{N}}}, \text{SEP}, \text{SEPP}, \text{PPT}\}$. We denote the set of all \mathcal{S} -simulable quantum circuit fragments as $\mathfrak{F}_k(\mathcal{S})$.

Remark II.2. When examining LOCC_1 -simulable quantum circuit fragments, namely $\mathfrak{F}_k(\text{LOCC}_1)$, we impose the restriction that all of its components are LOCC_1 with respect to the same party.

Having introduced \mathcal{S} -simulable quantum circuit fragments in Def. II.1, we can now present the formal definition of an entangled circuit fragment, which captures the essence of temporal entanglement over multiple time points.

Definition II.2: Entangled Circuit Fragment

We refer to a quantum circuit fragment \mathcal{E} as an entangled circuit fragment if it does not belong to the set $\mathfrak{F}_k(\text{SEPP})$.

Remark II.3. The significance of Def. II.2 lies in its ability to extend the concept of entanglement to its most general form, which includes not just quantum states and channels but also quantum circuit fragments. In doing so, it provides a crucial framework for characterizing and understanding entanglement in the context of non-Markovian quantum processes. In particular, by introducing

$$\text{Sta}(\mathcal{S}) := \{\rho \mid \rho \in \mathfrak{F}_1(\mathcal{S}), \text{Tr}[\rho] = 1\}, \quad (64)$$

with $\mathcal{S} \in \{\text{LO}, \text{LOCC}_k, \text{LOCC}_{\mathbb{N}}, \text{LOCC}, \overline{\text{LOCC}}_{\mathbb{N}}, \text{SEP}, \text{SEPP}, \text{PPT}\}$, the collection of separable states is completely captured by

$$\text{Sta}(\text{LOCC}) = \text{Sta}(\text{SEP}) = \text{Sta}(\text{SEPP}). \quad (65)$$

If a state $\rho \notin \text{Sta}(\text{SEPP})$, it is entangled. Therefore, an entangled state can be regarded as a specific instance of an entangled quantum circuit fragment, which consists of a single quantum process.

While we trigger the investigation of entangled quantum circuit fragments, or directly temporal entanglement, our objective of this work is only to explore their connection to quantum network communication, including quantum teleportation and quantum repeater-based protocols. We will not dive into the complete framework here, but our upcoming works will present a more comprehensive understanding of temporal entanglement.

B. Fidelity of Circuit Fragment Distillation: Quantifying Temporal Entanglement

Entanglement distillation is a critical component of quantum information processing, involving the conversion of a large number of weakly entangled quantum states into a smaller number of highly entangled ones. This transformation is essential for numerous quantum communication and computation applications, as the strength of entanglement between parties constrains their operational effectiveness. In this subsection, we will delve into the topic of entanglement distillation for quantum circuit fragments, and introduce the notion of k -fidelity of \mathcal{S} distillation.

With a focus on practicality, our attention in this work is directed towards single-shot entanglement distillation of quantum circuit fragments. More precisely, we are interested in transforming a single instance of quantum circuit fragment $\mathcal{E} \in \mathfrak{F}_k$ into a state that closely approximates the maximally entangled state ϕ_d^+ through the application of operation $\Theta \in \mathfrak{F}_{k+1}(\mathcal{S})$ with $\mathcal{S} \in \{\text{LO}, \text{LOCC}_k, \text{LOCC}_{\mathbb{N}}, \text{LOCC}, \overline{\text{LOCC}}_{\mathbb{N}}, \text{SEP}, \text{SEPP}, \text{PPT}\}$; that is

Definition II.3: d -Fidelity of \mathcal{S} Distillation

The d -fidelity $F_{d,\mathcal{S}}(\mathcal{E})$ of a quantum circuit fragment $\mathcal{E} \in \mathfrak{F}_k$ under operation $\Theta \in \mathfrak{F}_{k+1}(\mathcal{S})$ is defined by

$$F_{d,\mathcal{S}}(\mathcal{E}) := \max_{\Theta \in \mathfrak{F}_{k+1}(\mathcal{S})} F_U(\Theta(\mathcal{E}), \phi_d^+) = \max_{\Theta \in \mathfrak{F}_{k+1}(\mathcal{S})} \text{Tr}[\Theta(\mathcal{E}) \cdot \phi_d^+], \quad (66)$$

where F_U stands for the Uhlmann fidelity, with ϕ_d^+ being the d -dimensional maximally entangled state.

The d -Fidelity of \mathcal{S} distillation offers a quantitative assessment of how closely the output channel – $\Theta(\mathcal{E})$ – resembles the ideal, maximally entangled state ϕ_d^+ under operations $\Theta \in \mathfrak{F}_{k+1}(\mathcal{S})$, characterizing their similarity through the overlap between $\Theta(\mathcal{E})$ and ϕ_d^+ . The functional $F_{d,\mathcal{S}}(\mathcal{E})$ is a generalization of the concept of single-shot entanglement distillation, where the goal is to generate states that are as close as possible to a maximally entangled state under LOCC from initial object, which can be a quantum state or a quantum channel. When \mathcal{E} is a quantum state and the set of allowed operations are LOCC, i.e., $\mathcal{S} = \text{LOCC}$, then $F_{d,\mathcal{S}}(\mathcal{E})$ recovers the concept of single-shot entanglement distillation under LOCC. On the other hand, when the set of operations that can be applied to state \mathcal{E} are PPT channels, namely $\mathcal{S} = \text{PPT}$, then $F_{d,\mathcal{S}}(\mathcal{E})$ gives the fidelity of d -state PPT distillation [22]. Moreover, when \mathcal{E} is a quantum channel and Θ represents a superchannel, the function $F_{d,\mathcal{S}}(\mathcal{E})$ captures the concept of single-shot entanglement distillation of dynamical entanglement [103–107].

Remark II.4. Here, $F_{d,\mathcal{S}}(\mathcal{E})$ is not an entanglement monotone as it is not faithful, i.e., $F_{d,\mathcal{S}}(\mathcal{E}) > 0$ if and only if \mathcal{E} is an entangled circuit fragment (see Def. II.2). But, it is still monotonically non-increasing under free morphism $\Xi \in \mathfrak{F}_{k+1}(\mathcal{S})$. That is, given a quantum circuit fragment \mathcal{E} , we have $F_{d,\mathcal{S}}(\mathcal{E}) \geq F_{d,\mathcal{S}}(\Xi(\mathcal{E}))$ holds for all $\Xi \in \mathfrak{F}_{k+1}(\mathcal{S})$.

This subsection introduced the basic idea of d -Fidelity of \mathcal{S} distillation $F_{d,\mathcal{S}}(\mathcal{E})$ and explored its importance in single-shot entanglement distillation. However, the comprehensive scope of temporal entanglement extends far beyond what was discussed here. This raises many questions, such as: How can we formulate the standard entanglement cost and

distillable entanglement in the asymptotic case of quantum circuit fragments under $\mathfrak{F}_k(\text{LOCC})$? Is it possible to solve the entanglement cost of a quantum circuit fragment and find a quantity that unifies both κ entanglement [104] for states and max-logarithmic negativity [106] for bipartite channels in the case of $\mathfrak{F}_k(\text{PPT})$? These questions exceed the boundaries of this work and will be presented in our upcoming works.

III. QUANTUM COMMUNICATIONS

In this section, we will provide a fresh perspective on quantum teleportation by focusing on the role of resourceful quantum channels in the protocol. Instead of simply considering the entanglement of a static state, we will examine the crucial role of the entanglement-generating channel that connects the sender and receiver. To explore the optimal performance of a bipartite channel in quantum teleportation, we will introduce a new superchannel-assisted teleportation protocol (shown in Fig. 8(f)) in Subsec. III A. In the subsequent Subsec. III B, we will dive deeper into the general mathematical framework that underlies these protocols. By doing so, we will gain a more complete understanding of the principles that govern a variety of quantum teleportation protocols (illustrated in Fig. 8) and the role of entanglement-generating channel in superchannel-assisted quantum teleportation. Finally, in Subsec. III C, we will demonstrate the superior performance of our newly proposed teleportation protocol compared to conventional methods in certain noise models. This result highlights the practical significance of our approach and its potential for real-world applications.

A. Quantum Teleportation: A Channel-Theoretic Perspective

At the heart of quantum communication is the ability to securely transfer information between parties [140]. This is crucial for a variety of applications, from quantum cryptography to quantum computing. The most widely recognized and effective method for achieving secure transfer of quantum information is through the use of quantum teleportation [141–145]. This protocol, which was first introduced by Bennett et al. in Ref. [142], enables the transfer of quantum states from one location to another, without physically transporting the particles that carry the information. Its effectiveness has been experimentally demonstrated in Refs. [144, 145]. Recently, efforts to build a global-scale quantum network have resulted in the successful ground-to-satellite teleportation over distances of up to 1,400 kilometers as reported in Ref. [146]. To facilitate a thorough exploration of related topics, we highly recommend consulting Ref. [147–151]. Theoretically, the transfer of any quantum information from Alice to Bob can be achieved perfectly through the use of a maximally entangled state shared between them (see Fig. 8(a)). However, the physical implementation of teleportation is subject to various sources of quantum noise resulting from interactions between the system and its environment (see Fig. 8(b)) [147–155]. The conventional approach to combating the noise is to replace the standard teleportation protocol (i.e., Θ_0^{post} of Fig. 8(b)) with a general LOCC protocol (i.e., Θ_1^{post} of Fig. 8(c)) [19], as Θ_0^{post} is only a special case of LOCC. The power of teleportation originates from the entangling gate (brown boxes in Fig. 8) between different parties. One might then wonder: does the conventional approach (see Fig. 8(c)) fully leverage the capabilities of the entangling gate?

Regrettably, the answer to the question posed above is negative. There is concrete evidence that the use of a superchannel-based protocol is demonstrably superior to one that relies solely on post-processing techniques. To provide a more concrete illustration, we demonstrate that there exist examples where a straightforward application of local unitary operations in the pre-processing stage (see Fig. 8(e)) can outperform any possible PPT-post-processing technique (see Fig. 8(d)), which naturally encompasses all LOCC-post-processing protocols as a subset (see Fig. 8(c)).

To provide a comprehensive explanation, we will evaluate each of the protocols depicted in Fig. 8 systematically, along with their corresponding performance.

- **Protocol a: Standard Teleportation (see Fig. 8(a)).** The mechanism of teleportation can be traced back to classical textbooks, such as Refs. [3–5]. Here, we visually demonstrate the standard teleportation through a diagram in Fig. 9.
- **Protocol b: Noisy Teleportation (see Fig. 8(b)).** In this case, the entangling gate is subject to local noise, which affects its performance. Denote by \mathcal{N}_1 and \mathcal{N}_2 the local noise affecting systems A and B , respectively. In the subsequent analysis, we will make use of the following noise models; that are

$$\mathcal{N}_1, \mathcal{N}_2 \in \{\text{Bit Flip } \mathcal{N}_{\text{BF}}, \text{Phase Flip } \mathcal{N}_{\text{PF}}, \text{Depolarizing } \mathcal{N}_{\text{D}}, \text{Amplitude Damping } \mathcal{N}_{\text{AD}}\}. \quad (67)$$

As a fundamental type of error in quantum computing and communication, the bit flip channel \mathcal{N}_{BF} can cause a qubit state to flip from 0 to 1 or from 1 to 0 with a certain probability, which is typically described by a

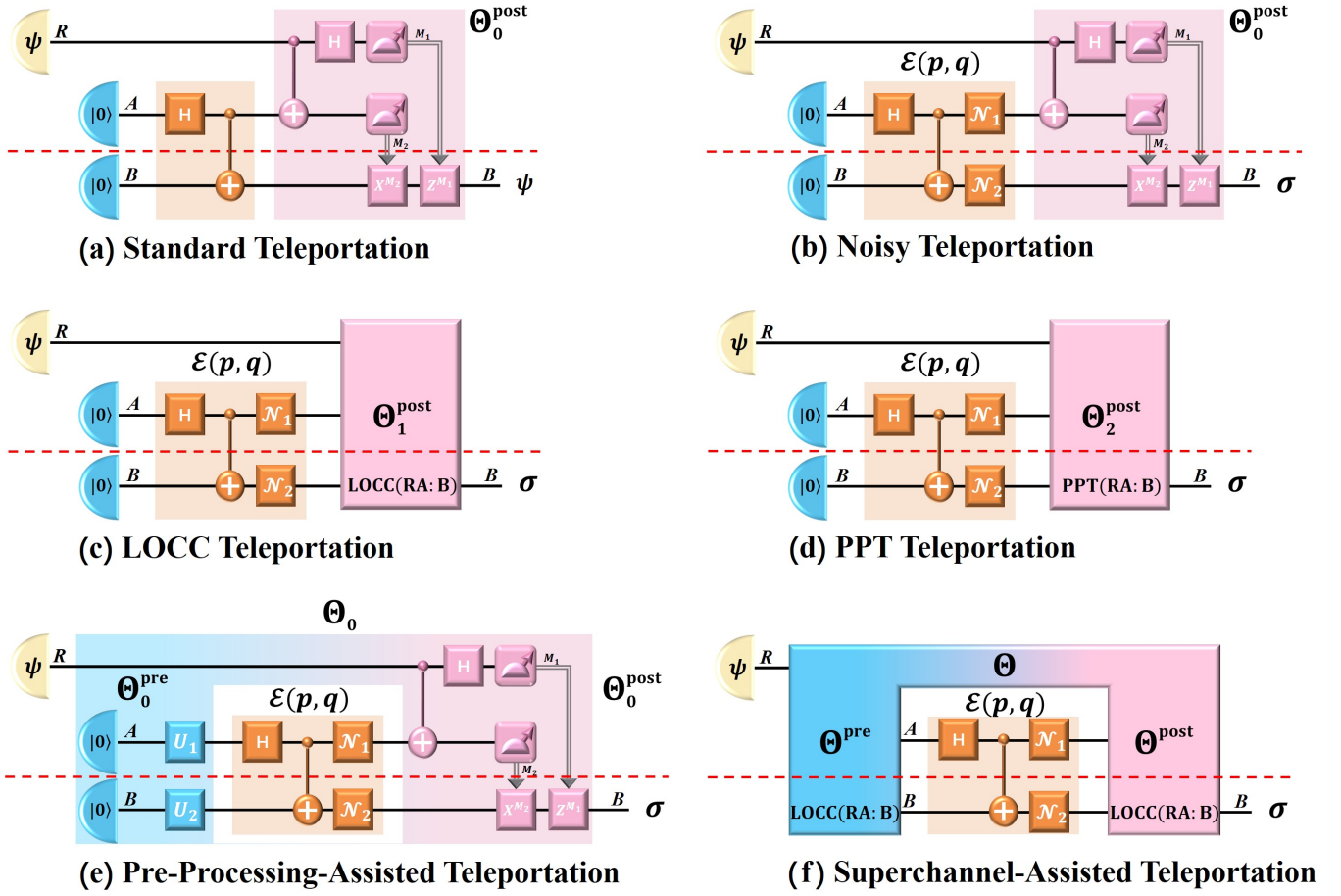


FIG. 8. (Color online) Quantum teleportation protocols: (a) standard teleportation, a fundamental process in quantum information theory where a quantum state is transmitted from one location to another. The protocol involves the sharing of a maximally entangled state between two parties, Alice and Bob, who are situated at distinct locations. The quantum information that needs to be transmitted from Alice to Bob is stored in the state ψ_R that acts on system R . Alice has access to systems RA , while Bob has access to system B . The protocol is enabled by implementing a standardized operation, which is represented by the pink box in the diagram and denoted as $\Theta_0^{\text{post}} \in \mathfrak{F}_1(\text{LOCC}(RA : B))$; (b) noisy teleportation, where the entangling gates are followed by channels $\mathcal{N}_1(p)$ and $\mathcal{N}_2(q)$ (see Eq. 68), resulting in a noisy entangling gate $\mathcal{E}(p, q)$ (see Eq. 70). Despite these noises, the transmission of quantum information ψ_R remains through Θ_0^{post} ; (c) LOCC teleportation [19]. Rather than relying on a standardized operation Θ_0^{post} executed by remote parties, a more versatile LOCC channel $\Theta_1^{\text{post}} \in \mathfrak{F}_1(\text{LOCC}(RA : B))$ has been utilized to facilitate the transmission of quantum information between the composite systems RA and B . After optimizing over all possible LOCC channels, this protocol demonstrates superior performance compared to the previous protocol (b); (d) PPT teleportation. The set of allowable operations has been expanded to include all PPT channels, which means that the LOCC channel Θ_1^{post} has been replaced by a PPT channel $\Theta_2^{\text{post}} \in \mathfrak{F}_1(\text{PPT}(RA : B))$. As a result, the performance of quantum state teleportation has been further enhanced; (e) pre-processing-assisted teleportation. When the entangling gate (represented by the brown box) is seen as a shared dynamical resource between Alice and Bob, there is no justification for limiting consideration solely to the implementation of post-processing. In this case, we consider a special pre-processing protocol $\Theta_0^{\text{pre}} := \mathcal{U}_1(|0\rangle\langle 0|)_A \otimes \mathcal{U}_2(|0\rangle\langle 0|)_B$, followed by the standard teleportation protocol Θ_0^{post} ; (f) superchannel-assisted teleportation, achieved by implementing a superchannel $\Theta \in \mathfrak{F}_2(\text{LOCC})$. Here, gate $\mathcal{E}(p, q)$ has been transformed into channel $\Theta(\mathcal{E}(p, q))_{R \rightarrow B}$. This consideration leads to superior performance compared to the case with only post-processing, i.e., protocol (c); From protocols (b) to (f), the output is represented by σ . These diagrams distinguish between systems belonging to Alice, which are located above the dashed red line, and those belonging to Bob, which are situated below the dashed line.

single parameter known as the error probability. This type of error can arise from a variety of noise sources, such as thermal fluctuations and electromagnetic interference. The phase flip channel \mathcal{N}_{PF} , which arises from fluctuations in the local magnetic field, can cause a qubit phase to flip between $|0\rangle$ and $|1\rangle$ states with a certain probability. Specifically, if the qubit is initially in the state $\alpha|0\rangle + \beta|1\rangle$, then the phase flip channel can transform this state to $\alpha|0\rangle - \beta|1\rangle$ with a certain probability. As a combination of the bit flip, phase flip, and the bit-

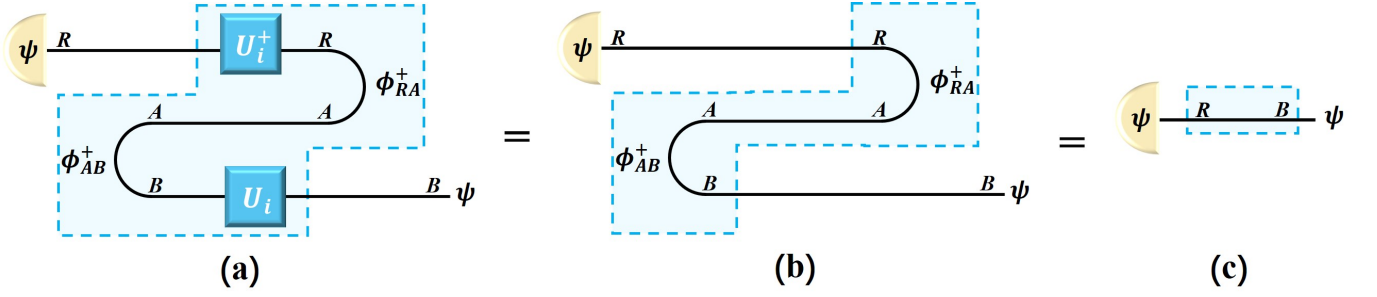


FIG. 9. (Color online) Graphical illustration of standard teleportation procedure (see Fig. 8(a)). Here, $(U_i \otimes \mathbb{1} |\phi^+\rangle)^\dagger$ stands for the standard Bell measurements with $U_0 = \mathbb{1}$, $U_1 = Z$, $U_2 = X$ and $U_3 = XZ$. Thanks to $U \otimes \mathbb{1} |\phi^+\rangle = \mathbb{1} \otimes U^T |\phi^+\rangle$, we have (a) = (b). By further using the yanking equation, we obtain the equivalence between (b) and (c). The technique employed here is akin to that illustrated in Fig. 2.

phase flip channels, the quantum depolarizing channel, denoted as \mathcal{N}_D , takes its initial state to a completely mixed state with some probability. The amplitude damping channel \mathcal{N}_{AD} is a type of noise that is commonly encountered in various physical systems, such as superconducting qubits and trapped ions. This channel causes a qubit to lose energy and transition to a lower energy state, resulting in a decay of the amplitude of its quantum state. Using the Kraus decomposition $\mathcal{N}(\cdot) = \sum_i E_i \cdot E_i^\dagger$, we can characterize these noise models in Tab. I. For more details on this topic, see Ref. [3].

Kraus Decomposition of Error Models				
Type of Error	Operator E_0	Operator E_1	Operator E_2	Operator E_3
Bit Flip Channel \mathcal{N}_{BF}	$\sqrt{p} \mathbb{1}$	$\sqrt{1-p} X$	$\mathbb{0}$	$\mathbb{0}$
Phase Flip Channel \mathcal{N}_{PF}	$\sqrt{p} \mathbb{1}$	$\sqrt{1-p} Z$	$\mathbb{0}$	$\mathbb{0}$
Quantum Depolarizing Channel \mathcal{N}_D	$\sqrt{\frac{1+3p}{4}} \mathbb{1}$	$\sqrt{\frac{1-p}{4}} X$	$\sqrt{\frac{1-p}{4}} Y$	$\sqrt{\frac{1-p}{4}} Z$
Amplitude Damping Channel \mathcal{N}_{AD}	$\begin{bmatrix} 1 & 0 \\ 0 & \sqrt{p} \end{bmatrix}$	$\begin{bmatrix} 0 & \sqrt{1-p} \\ 0 & 0 \end{bmatrix}$	$\mathbb{0}$	$\mathbb{0}$

TABLE I. Kraus decomposition of the fundamental noisy channels, including bit flip channel \mathcal{N}_{BF} , phase flip channel \mathcal{N}_{PF} , quantum depolarizing channel \mathcal{N}_D , and amplitude damping channel \mathcal{N}_{AD} . In this context, the symbols $\mathbb{1}$, X , Y , and Z represent the *Pauli operators*.

To differentiate the parameters associated with the quantum channels \mathcal{N}_1 and \mathcal{N}_2 , we denote their corresponding parameters as p and q , respectively. More precisely, we express this distinction as

$$\mathcal{N}_1 = \mathcal{N}_1(p), \quad (68)$$

$$\mathcal{N}_2 = \mathcal{N}_2(q). \quad (69)$$

These notations allow us to clearly identify the parameter associated with each channel, which is essential for analyzing and comparing their effects in noisy quantum teleportation. Having defined \mathcal{N}_1 and \mathcal{N}_2 , we can now completely characterize the entangling gate between Alice and Bob as $\mathcal{E}(p, q)$, colored brown in Fig. 8(b). Expressed mathematically, the noisy entangling gate $\mathcal{E}(p, q)$ can be represented by

$$\mathcal{E}(p, q)_{AB \rightarrow AB} := \mathcal{N}_1(p)_{A \rightarrow A} \otimes \mathcal{N}_2(q)_{B \rightarrow B} \circ \text{CNOT}_{AB \rightarrow AB} \circ \text{H}_{A \rightarrow A} \otimes \text{id}_{B \rightarrow B}. \quad (70)$$

Here, we use the symbol H to refer to the *Hadamard gate*, and CNOT to denote the controlled NOT gate (also known as the controlled-X gate). In this scenario, the resultant channel $\mathcal{F}_b(p, q)$ from system R to B takes the form of

$$\mathcal{F}_b(p, q)_{R \rightarrow B} := \Theta_{0, RAB \rightarrow B}^{\text{post}} \circ \mathcal{E}(p, q)_{AB \rightarrow AB} (|0\rangle\langle 0|_A \otimes |0\rangle\langle 0|_B). \quad (71)$$

The subscript ‘b’ in \mathcal{F} indicates that the channel from R to B is obtained using protocol b. In order to measure and evaluate the performance of protocol b, we use the metric of average fidelity f , which is defined in Def. I.3. This metric provides a quantitative measure of how accurately the teleported state $\mathcal{F}_b(p, q)(\psi)$ matches the original state ψ that was being teleported. In particular, the average fidelity f of channel $\mathcal{F}_b(p, q)$ is given by

$$f(\mathcal{F}_b(p, q)) = \int d\psi F_U(\psi, \mathcal{F}_b(p, q)(\psi)) = \int d\psi \text{Tr}[\psi \cdot (\mathcal{F}_b(p, q)(\psi))]. \quad (72)$$

To simplify notation, we can use the abbreviation f_b to refer to the performance of protocol b, i.e.,

$$f_b := f(\mathcal{F}_b(p, q)). \quad (73)$$

Using Lem. I.12, we can prove that f_b can be expressed as

$$f_b = \frac{2F(\mathcal{F}_b(p, q)) + 1}{3}. \quad (74)$$

Here, $F(\mathcal{F}_b(p, q))$ represents the entanglement fidelity (defined in Def. I.4) of the channel $\mathcal{F}_b(p, q)$.

- **Protocol c: LOCC Teleportation (see Fig. 8(c)).** It is worth noting that the standard teleportation protocol Θ_0^{post} involves performing Bell measurements and applying local unitary operations based on the measurement outcomes. Such an operation can be understood as a specific instance of a LOCC channel. Given this connection, it is reasonable to consider whether optimizing over all possible LOCC channels could potentially improve the performance of teleportation. Formally, if we replace the standardized operation Θ_0^{post} , as depicted in Fig. 8(b), with a general LOCC channel $\Theta_1^{\text{post}} \in \text{LOCC}(RA : B)$, the resultant channel $\mathcal{F}_c(\Theta_1^{\text{post}}, p, q)$ from the sender to the receiver can be expressed as

$$\mathcal{F}_c(\Theta_1^{\text{post}}, p, q)_{R \rightarrow B} := \Theta_{1, RAB \rightarrow B}^{\text{post}} \circ \mathcal{E}(p, q)_{AB \rightarrow AB}(|0\rangle\langle 0|_A \otimes |0\rangle\langle 0|_B). \quad (75)$$

While both $\mathcal{F}_b(p, q)$ (see Eq. 71) and $\mathcal{F}_c(\Theta_1^{\text{post}}, p, q)$ (see Eq. 75) are influenced by parameters p and q , $\mathcal{F}_c(\Theta_1^{\text{post}}, p, q)$ is more complex as it also takes into account the variable of LOCC channel Θ_1^{post} . The inclusion of Θ_1^{post} in $\mathcal{F}_c(\Theta_1^{\text{post}}, p, q)$ adds an extra layer of complexity that enhances the performance of teleportation. The expression for the average fidelity f (see Eq. 11) of $\mathcal{F}_c(\Theta_1^{\text{post}}, p, q)$ is

$$f(\mathcal{F}_c(\Theta_1^{\text{post}}, p, q)) = \int d\psi F_U(\psi, \mathcal{F}_c(\Theta_1^{\text{post}}, p, q)(\psi)) = \int d\psi \text{Tr}[\psi \cdot \mathcal{F}_c(\Theta_1^{\text{post}}, p, q)(\psi)]. \quad (76)$$

Now, if we maximize over all possible $\Theta_1^{\text{post}} \in \text{LOCC}(RA : B)$, we get

$$f_c := \max_{\Theta_1^{\text{post}} \in \text{LOCC}(RA : B)} f(\mathcal{F}_c(\Theta_1^{\text{post}}, p, q)). \quad (77)$$

Because Θ_0^{post} is a LOCC channel and we have optimized over all possible choices of Θ_1^{post} , the resulting fidelity of f_c is guaranteed to be greater than or equal to that of f_b , i.e.,

$$f_c \geq f_b. \quad (78)$$

The fidelity f_c represents the maximum achievable fidelity that can be obtained via conventional teleportation. However, the computation of the quantity f_c remains elusive to us in general. This difficulty lies in the fact that the mathematical representation of LOCC operations is often hard to specify.

- **Protocol d: PPT Teleportation (see Fig. 8(d)).** Expanding the class of permissible post-processing operations beyond just LOCC channels can lead to an improvement in establishing an upper bound for the fidelity f_c (see Eq. 77). We can achieve this by incorporating positive partial transpose (PPT) channels into our analysis. Specifically, we consider the use of a PPT channel $\Theta_2^{\text{post}} \in \text{PPT}(RA : B)$ for post-processing operations. In this scenario, the resulting channel $\mathcal{F}_d(\Theta_2^{\text{post}}, p, q)$ from the sender to the receiver can be fully characterized by

$$\mathcal{F}_d(\Theta_2^{\text{post}}, p, q)_{R \rightarrow B} := \Theta_{2, RAB \rightarrow B}^{\text{post}} \circ \mathcal{E}(p, q)_{AB \rightarrow AB}(|0\rangle\langle 0|_A \otimes |0\rangle\langle 0|_B). \quad (79)$$

The average fidelity f (see Eq. 11) of channel $\mathcal{F}_d(\Theta_2^{\text{post}}, p, q)$ is now given by

$$f(\mathcal{F}_d(\Theta_2^{\text{post}}, p, q)) = \int d\psi F_U(\psi, \mathcal{F}_d(\Theta_2^{\text{post}}, p, q)(\psi)) = \int d\psi \text{Tr}[\psi \cdot (\mathcal{F}_d(\Theta_2^{\text{post}}, p, q)(\psi))]. \quad (80)$$

Taking the maximum over all PPT channel Θ_2^{post} , we arrive at the following fidelity.

$$f_d := \max_{\Theta_2^{\text{post}} \in \text{PPT}(RA:B)} f(\mathcal{F}_d(\Theta_2^{\text{post}}, p, q)). \quad (81)$$

As LOCC channels represent a subset of PPT channels (as shown in Eq. 63), we can derive an inequality between the fidelities f_c and f_d as follows

$$f_d \geq f_c. \quad (82)$$

The fidelity f_d is the maximum achievable fidelity of teleportation that can be obtained through post-processing using PPT channels.

- **Protocol e: Pre-Processing-Assisted Teleportation (see Fig. 8(e)).** Traditionally, post-processing, such as Θ_0^{post} in protocols a (see Fig. 8(a)) and b (see Fig. 8(b)), Θ_1^{post} in protocol c (see Fig. 8(c)), and Θ_2^{post} in protocol d (see Fig. 8(d)), has been the primary focus for mitigating noise in teleportation protocols. However, incorporating pre-processing techniques alongside post-processing can further enhance the fidelity and reliability of teleportation. There are two primary factors that motivate the pre-processing-assisted quantum teleportation, as outlined below: (i) First, in the realm of quantum communication theory, particularly in the investigation of quantum channel capacity, reliable transmission of information requires both encoding and decoding. Pre-processing serves as a means of encoding the information, while post-processing functions as a decoding mechanism. Therefore, incorporating both pre-processing and post-processing techniques is crucial for achieving efficient and accurate quantum teleportation. (ii) Second, when viewed through the lens of quantum resource theory [116], specifically the resource theory of dynamical entanglement [103–107], the shared resource between Alice and Bob is the bipartite channel $\mathcal{E}(p, q)$ (brown boxes in Fig. 8(b)-(f)). As such, it is imperative to evaluate its maximum performance under all feasible free morphisms, namely the set of all LOCC superchannels $\mathfrak{F}_2(\text{LOCC}(RA : B))$ (for further information, please refer to Def. II.1 in Subsec. II A). Additionally, the preparation of the initial state $|0\rangle\langle 0|_A \otimes |0\rangle\langle 0|_B$ is merely a specific instance of free pre-processing. Therefore, it is not necessary to exclusively focus on this particular choice, as any free pre-processing can be employed instead. In this scenario, we examine a specific selection of free pre-processing Θ_0^{pre}

$$\Theta_0^{\text{pre}} := \mathcal{U}_1(|0\rangle\langle 0|)_A \otimes \mathcal{U}_2(|0\rangle\langle 0|)_B \quad (83)$$

and demonstrate that even with this particular choice, the resulting fidelity cannot be attained by any protocol that employs solely LOCC post-processing. In Eq. 83, \mathcal{U}_1 and \mathcal{U}_2 are local unitary gates satisfying $\mathcal{U}_i(\cdot) = U_i \cdot U_i^\dagger$ with $i \in \{1, 2\}$. It is worth noting that any unitary operator U acting on a qubit can be written in terms of a global phase shift, a rotation operator about the y -axis, and two rotation operators about the z -axis [3]. More precisely, we have

$$U = e^{i\alpha} \begin{bmatrix} e^{-i\beta/2} & 0 \\ 0 & e^{i\beta/2} \end{bmatrix} \begin{bmatrix} \cos \frac{\gamma}{2} & -\sin \frac{\gamma}{2} \\ \sin \frac{\gamma}{2} & \cos \frac{\gamma}{2} \end{bmatrix} \begin{bmatrix} e^{-i\delta/2} & 0 \\ 0 & e^{i\delta/2} \end{bmatrix}. \quad (84)$$

Here, α , β , γ , and δ are real-valued parameters. To facilitate our analysis and numerical simulations, we simplify the discussion by focusing on specific unitary operations, which has the following form:

$$U_1(\alpha) := \begin{bmatrix} \cos \frac{\alpha}{2} & -\sin \frac{\alpha}{2} \\ \sin \frac{\alpha}{2} & \cos \frac{\alpha}{2} \end{bmatrix}, \quad U_2(\beta) := \begin{bmatrix} \cos \frac{\beta}{2} & -\sin \frac{\beta}{2} \\ \sin \frac{\beta}{2} & \cos \frac{\beta}{2} \end{bmatrix}. \quad (85)$$

With the pre-processing step taken into account, the overall effect of the protocol is to establish a quantum channel, denoted by $\mathcal{F}_e(\Theta_0^{\text{pre}}(\alpha, \beta), p, q)$ or simply $\mathcal{F}_e(\alpha, \beta, p, q)$, from the sender to the receiver. This channel can be expressed as follows

$$\mathcal{F}_e(\alpha, \beta, p, q)_{R \rightarrow B} := \Theta_{0, RAB \rightarrow B}^{\text{post}} \circ \mathcal{E}(p, q)_{AB \rightarrow AB} \circ \Theta_{0, C \rightarrow AB}^{\text{pre}} \quad (86)$$

$$= \Theta_{0, RAB \rightarrow B}^{\text{post}} \circ \mathcal{E}(p, q)_{AB \rightarrow AB} \left(\left(U_1(\alpha) |0\rangle\langle 0| U_1^\dagger(\alpha) \right)_A \otimes \left(U_2(\beta) |0\rangle\langle 0| U_2^\dagger(\beta) \right)_B \right), \quad (87)$$

where the unitary operators $U_1(\alpha)$ and $U_2(\beta)$ are defined in Eq. 85. Mathematically, the average fidelity f (see Eq. 11) of the resulting channel $\mathcal{F}_e(\alpha, \beta, p, q)$ is expressed as

$$f(\mathcal{F}_e(\alpha, \beta, p, q)) = \int d\psi F_U(\psi, \mathcal{F}_e(\alpha, \beta, p, q)(\psi)) = \int d\psi \text{Tr}[\psi \cdot (\mathcal{F}_e(\alpha, \beta, p, q)(\psi))]. \quad (88)$$

By maximizing over all possible values of α and β , we arrive at the following fidelity expression.

$$f_e := \max_{\alpha, \beta} f(\mathcal{F}_e(\alpha, \beta, p, q)). \quad (89)$$

As $\mathcal{F}_e(\alpha, \beta, p, q)$ (see Eq. 86) equals $\mathcal{F}_b(p, q)$ (see Eq. 71) when $\alpha = 0$ and $\beta = 0$ (see Eq. 85), it follows that

$$f_e \geq f_b, \quad (90)$$

where f_b is defined in Eq. 73. Although protocol e has the ability to mitigate the effects of noise and improve the fidelity of teleportation, its interplay with f_c (see Eq. 77) and f_d (see Eq. 81) is currently unknown.

- **Protocol f: Superchannel-Assisted Teleportation (see Fig. 8(f)).** A quantum superchannel is the most comprehensive method for manipulating a quantum channel, allowing the transformation of a quantum channel into another quantum channel by enabling the channel to have memory and transmit information across multiple time steps. This feature makes quantum superchannels a crucial component in the development of efficient and reliable quantum communication protocols and quantum computing algorithms. To mitigate the noise that occurs in $\mathcal{E}(p, q)$, this protocol utilizes a quantum superchannel $\Theta = \Theta^{\text{post}} \circ \Theta^{\text{pre}} \in \mathfrak{F}_2(\text{LOCC}(RA : B))$. This superchannel consists of both pre-processing Θ^{pre} and post-processing Θ^{post} channels, which are both local operations and classical communication channels. Now, the output channel $\mathcal{F}_f(\Theta, p, q)$ that transmits information from R to B reads

$$\mathcal{F}_f(\Theta, p, q)_{R \rightarrow B} := \Theta(\mathcal{E}(p, q)) = \Theta^{\text{post}} \circ \mathcal{E}(p, q) \circ \Theta^{\text{pre}}. \quad (91)$$

In this case, the average fidelity f (see Eq. 11) of the output channel $\mathcal{F}_f(\Theta, p, q)$ is calculated as

$$f(\mathcal{F}_f(\Theta, p, q)) = \int d\psi F_U(\psi, \mathcal{F}_f(\Theta, p, q)(\psi)) = \int d\psi \text{Tr}[\psi \cdot (\mathcal{F}_f(\Theta, p, q)(\psi))]. \quad (92)$$

Upon maximizing over all LOCC superchannels, we obtain the following expression for fidelity.

$$f_f := \max_{\Theta \in \mathfrak{F}_2(\text{LOCC}(RA:B))} f(\mathcal{F}_f(\Theta, p, q)). \quad (93)$$

The subscript ‘f’ is used in average fidelity f to signify that the fidelity is determined using protocol f. Protocol e considers a specific LOCC superchannel $\Theta_0 := \Theta_0^{\text{post}} \circ \Theta_0^{\text{pre}}$ (see Fig. 8(e)), which is only a special case of the broader class of LOCC superchannels. The fidelity f_f is obtained by maximizing over all LOCC superchannels, and therefore captures the optimal performance of the teleportation protocol. As a result, we can establish the following relationship between f_e (see Eq. 89) and f_f (see Eq. 93).

$$f_f \geq f_e. \quad (94)$$

Additionally, it is worth mentioning that protocol c, as shown in Fig. 8(c), implements a special form of LOCC superchannel. This further illuminates the connection between the two protocols, which can be summarized as follows

$$f_f \geq f_c. \quad (95)$$

The protocol f discussed here provides the most general method for manipulating the bipartite channel shared between the sender and receiver, and effectively leverages the resources associated with the noisy entangling gate $\mathcal{E}(p, q)$. Therefore, if LOCC operations are considered to be free, the average fidelity achieved by f_f represents the highest performance achievable in practical scenarios.

To assess the relative performance of each protocol (see Fig. 8), we will compare their average fidelity (see Eq. 11). From the results presented in Eq. 78 and Eq. 82, it is evident that the fidelity of protocol d is superior to those of protocols c and b.

$$f_d \geq f_c \geq f_b. \quad (96)$$

Similarly, Eq. 90 and Eq. 94 reveal that the fidelity of protocol f is higher than that of protocols e and b.

$$f_f \geq f_e \geq f_b. \quad (97)$$

However, the relationship between the average fidelity of protocol e and those of protocols d and c remains ambiguous, and requires further examination. The inequality chains described above, i.e., Eq. 96 and Eq. 97, hold for any noisy bipartite channel $\mathcal{E}(p, q)$ (brown boxes in Fig. 8(b)-(f)), meaning that they apply to a broad range of noise models. Therefore, these bounds provide a general framework for evaluating the performance of quantum teleportation protocols in the presence of noise. Mathematically, the average fidelities associated with different protocols form a partially ordered set (poset), which can be visualized using a *Hasse diagram* such as Fig. 10. In this poset, the nodes represent different average fidelities, and there is a directed edge from node f_x to node f_y if and only if f_y is less than or equal to f_x ($x, y \in \{b, c, d, e, f\}$); that is

$$f_x \rightarrow f_y \iff f_x \geq f_y, \quad x, y \in \{b, c, d, e, f\}. \quad (98)$$

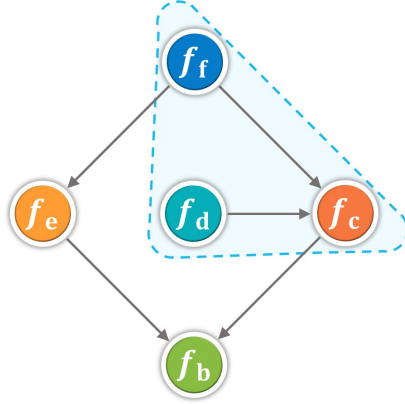


FIG. 10. (Color online) Hasse diagram for the average fidelities. Here the arrows connecting the nodes indicate the direction of the partial ordering between the quantities. Specifically, an arrow pointing from node f_x to node f_y indicates that the quantity f_x is greater than or equal to f_y , with $x, y \in \{b, c, d, e, f\}$. Computing the fidelities, as shown in the blue dashed box, involves optimizing over a set of allowable operations, making it a difficult problem to solve.

In the upcoming subsection (i.e., Subsec. III C), we will further demonstrate that there are specific noise models (in terms of $\mathcal{N}_1(p)$ and $\mathcal{N}_2(q)$) for which the fidelity of protocol e is strictly higher than that of protocol d.

$$f_e > f_d. \quad (99)$$

Building on previous analysis, we can now establish the following hierarchy in this case.

$$f_f \geq f_e > f_d \geq f_c \geq f_b. \quad (100)$$

This analysis highlights the importance of investigating the performance of quantum teleportation protocols with pre-processing, as the effectiveness of a simply LOCC pre-processing-assisted protocol like e (see Fig. 8(e)) cannot be achieved even by allowing all possible PPT post-processing operations (see Fig. 8(d)). Therefore, these results emphasize the necessity of investigating the potential benefits of superchannel techniques in the development of robust quantum communication protocols, such as the protocol f illustrated in Fig. 8(f).

B. Fidelity Benchmarking: The Role of Temporal Entanglement

To assess the quality of the teleportation protocols, we typically use the average fidelity, which measures the similarity between the input state and the teleported state. However, computing the average fidelity can be a challenging task, especially for high-dimensional states. To simplify the discussion, we can roughly categorize the fidelities considered in Subsec. III A into two types: (i) The first type corresponds to protocols with standard teleportation operation Θ_0^{post} , such as f_e (see Eq. 89) and f_b (see Eq. 73), which are determined solely by the properties of the quantum channel and the measurements; (ii) The second type, on the other hand, requires the maximization of fidelity over a

set of allowed operations or protocols, such as f_f (see Eq. 93), f_d (see Eq. 81), and f_c (see Eq. 77). This optimization allows us to find the maximum fidelity achievable using the given set of operations and protocols, and therefore provides a way to compare the performance of different quantum teleportation schemes. In this subsection, we will explore the process of calculating these fidelities and prepare ourselves for upcoming numerical experiments. Through this discussion, we will gain a deeper understanding of the mathematical underpinnings of the fidelities and develop the necessary tools to confidently analyze our experimental results.

Let's begin our discussion of teleportation protocols b and e. It is worth noting that both protocols share a common feature (see Fig. 8(b) and (e)): their post-processing step is based on the standard teleportation operation Θ_0^{post} . In other words, after the measurements are performed, the classical information is sent from the receiver to the sender, who can then apply the appropriate correction operations to reconstruct the teleported state. This use of a common post-processing operation makes it easier to compute the performance of the two protocols. To begin, let us refer to the state of the system AB before post-processing Θ_0^{post} as ρ_{AB} . It is important to understand the relationship between this state and the teleportation channel $\mathcal{F}(\rho)$ that is generated by ρ_{AB} . For a visual representation, consult the accompanying Fig. 11. Here channel $\mathcal{F}(\rho)$ is given by

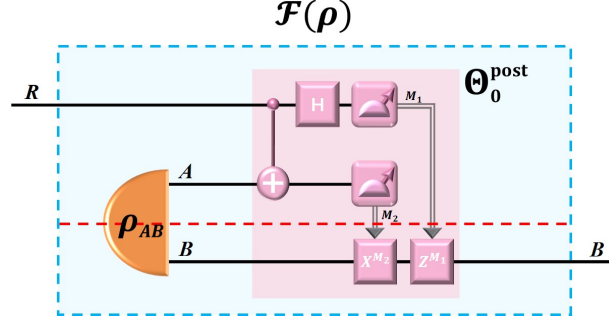


FIG. 11. (Color online) Teleportation channel $\mathcal{F}(\rho)$ (see Eq. 101), which is generated by first preparing a bipartite state ρ_{AB} and subsequently implementing a standard teleportation operation Θ_0^{post} . The resulting channel $\mathcal{F}(\rho)$ can be used to transmit quantum states over distances.

$$\mathcal{F}(\rho)_{R \rightarrow B} := \Theta_{0, RAB \rightarrow B}^{\text{post}}(\rho_{AB}). \quad (101)$$

The average fidelity of the teleportation channel $\mathcal{F}(\rho)$ is a key metric for assessing its performance in quantum teleportation. However, its calculation is notoriously challenging. The problem can be simplified by borrowing the insights from Lemma I.12, which enables us to transform the calculation of average fidelity f into the calculation of entanglement fidelity F . Although the calculation of entanglement fidelity is still a formidable task, we present a new lemma that establishes a direct connection between the entanglement fidelity of $\mathcal{F}(\rho)$ and the fidelity of the state ρ shared between the sender and receiver. Our proof is based on a novel diagrammatic approach that offers a fresh perspective on the problem and provides valuable intuition for understanding the underlying physics.

Lemma III.1: Connection between Entanglement Fidelity and Uhlmann fidelity

When a state ρ on system AB is subjected to the standard teleportation operation Θ_0^{post} , as illustrated in Fig. 11, the resulting entanglement fidelity $F(\mathcal{F}(\rho))$ of the generated channel $\mathcal{F}(\rho)$ (see Eq. 101) can be expressed as the Uhlmann fidelity $F_U(\rho, \phi^+)$ between ρ and the maximally entangled state ϕ^+ . More specifically, this is given by

$$F(\mathcal{F}(\rho)) = F_U(\rho, \phi^+) = \text{Tr}[\rho \cdot \phi^+]. \quad (102)$$

Above equation simplifies the calculation of entanglement fidelity F for the teleportation channel $\mathcal{F}(\rho)$. By providing a closed-form expression for the quantity, our equation allows for efficient and accurate evaluation of the performance of the channel, which is essential for assessing its suitability for practical applications in quantum information processing.

Proof. Our analysis is geared towards qubits for the sake of clarity and simplicity. In order to illustrate our findings, we have opted for a pictorial method. Specifically, we have depicted the entanglement fidelity $F(\mathcal{F}(\rho))$ as a diagram, as shown in Fig. 12.

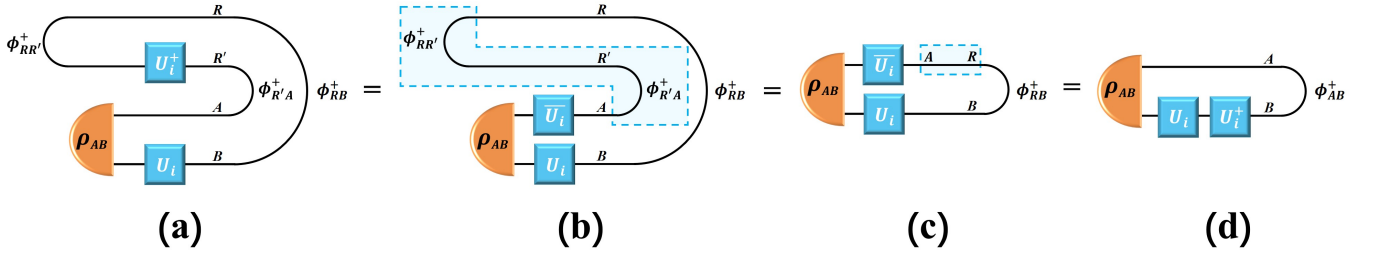


FIG. 12. (Color online) A graphical representation of the entanglement fidelity F (see Def. I.4) of channel $\mathcal{F}(\rho)$ (see Eq. 101).

Given the Bell measurement's equal probability of all outcomes at $1/4$ in this scenario, we will narrow our focus to the measurement $\mathbb{1} \otimes U_i |\phi^+\rangle$. The mathematical characteristic of the maximally entangled state permits us to equate Fig. 12(a) to Fig. 12(b) and Fig. 12(c) to Fig. 12(d). In addition, Fig. 12(b) and Fig. 12(c) are demonstrated to be identical through the application of the yanking equation. The correspondence between Fig. 12(d) and the Uhlmann fidelity $F_U(\rho, \phi^+)$ is apparent, thereby concluding the proof. \square

Remark III.1. While our proof in Lemma III.1 focuses on qubits, it should be noted that our approach is applicable beyond this specific scenario. In fact, one can substitute the Pauli operators with the Heisenberg-Weyl operators to extend our method to systems of any finite dimension. Moreover, while we present many of our results with a pictorial representation in the qubit case, it is important to emphasize that our findings hold for arbitrary finite-dimensional systems.

To analyze the properties of the quantum teleportation protocols b and e, let us denote the state of the system AB before post-processing Θ_0^{post} as

$$\rho_b := \mathcal{N}_1(p)_{A \rightarrow A} \otimes \mathcal{N}_2(q)_{B \rightarrow B} \circ \text{CNOT}_{AB \rightarrow AB} \circ H_{A \rightarrow A} \otimes \text{id}_{B \rightarrow B}(|0\rangle\langle 0|_A \otimes |0\rangle\langle 0|_B), \quad (103)$$

$$\rho_e(\alpha, \beta) := \mathcal{N}_1(p)_{A \rightarrow A} \otimes \mathcal{N}_2(q)_{B \rightarrow B} \circ \text{CNOT}_{AB \rightarrow AB} \circ H_{A \rightarrow A} \otimes \text{id}_{B \rightarrow B} \left(\left(U_1(\alpha) |0\rangle\langle 0| U_1^\dagger(\alpha) \right)_A \otimes \left(U_2(\beta) |0\rangle\langle 0| U_2^\dagger(\beta) \right)_B \right). \quad (104)$$

Lemma III.1 provides a key result for evaluating the entanglement fidelity of the teleportation channel $\mathcal{F}(\rho_b) = \mathcal{F}_b(p, q)$ (see Eq. 71) and $\mathcal{F}(\rho_e(\alpha, \beta)) = \mathcal{F}_e(\alpha, \beta, p, q)$ (see Eq. 86). Specifically, the entanglement fidelity can be expressed in a compact form, as shown in the following equation

$$F(\mathcal{F}(\rho_b)) = \text{Tr}[\rho_b \cdot \phi^+], \quad (105)$$

$$F(\mathcal{F}(\rho_e(\alpha, \beta))) = \text{Tr}[\rho_e(\alpha, \beta) \cdot \phi^+]. \quad (106)$$

Drawing upon the insights presented in Lemma I.12, we can obtain a concise expression for the average fidelity of protocol b. This result is fundamental for assessing the efficacy of the noisy teleportation protocol in transmitting quantum states from the sender to the receiver.

Theorem III.2: Performance of Protocol b

The expression for the average fidelity of protocol b, i.e., f_b (see Eq. 73), is given by

$$f_b = \frac{2 \text{Tr}[\rho_b \cdot \phi^+] + 1}{3}, \quad (107)$$

where ρ_b is defined in Eq. 103.

Protocol e can also be evaluated in terms of average fidelity using Lemma I.12, similar to protocol b. However, the calculation of the average fidelity for protocol e is more complex compared to that for protocol b. This is because we need to maximize over all possible values of the pre-processing parameters α and β , which introduces additional computational complexity.

Theorem III.3: Performance of Protocol e

The average fidelity of channel protocol e, i.e., f_e (see Eq. 89), can be calculated using the formula

$$f_e = \frac{2 \left(\max_{\alpha, \beta} \{ \text{Tr}[\rho_e(\alpha, \beta) \cdot \phi^+] \} \right) + 1}{3}. \quad (108)$$

Here, $\rho_e(\alpha, \beta)$ is given by Eq. 104.

Moving on to more complex problems, we will now examine the performance of protocols c, d, and f. Our analysis will begin with protocols c and d, which share the same state of system AB before post-processing (the region highlighted in pink of Fig. 8), namely ρ_b (see Eq. 103). To determine the efficacy of protocols c and d, we can use the lemma that follows, which provides us with a path forward.

Lemma III.4: Connection between Average Fidelity and Entanglement Distillation

When a bipartite quantum state ρ on system AB , with dimension $\dim A = \dim B = d$, undergoes a post-processing $\Theta_{RAB \rightarrow B}^{\text{post}} \in \mathfrak{F}_1(\mathcal{S})$, where \mathcal{S} is a set of allowed operations that can be one of the following $\{\text{LOCC}_1(\text{poly}(d)), \text{LOCC}_k, \text{LOCC}_{\mathbb{N}}, \text{LOCC}, \bar{\text{LOCC}}_{\mathbb{N}}, \text{SEP}, \text{SEPP}, \text{PPT}\}$, then the maximal average fidelity of the resulting channel $\Theta^{\text{post}}(\rho)$, as demonstrated in Fig. 13, is completely characterized by the d -fidelity of \mathcal{S} distillation, which is defined in Def. II.3. In other words, we can determine the maximal average fidelity as

$$\max_{\Theta^{\text{post}} \in \mathfrak{F}_1(\mathcal{S})} f(\Theta^{\text{post}}(\rho)) = \frac{dF_{d,\mathcal{S}}(\rho) + 1}{d + 1}, \quad (109)$$

where $\mathfrak{F}_1(\mathcal{S})$ is defined as the collection of all free channels, as specified in Def. II.1.

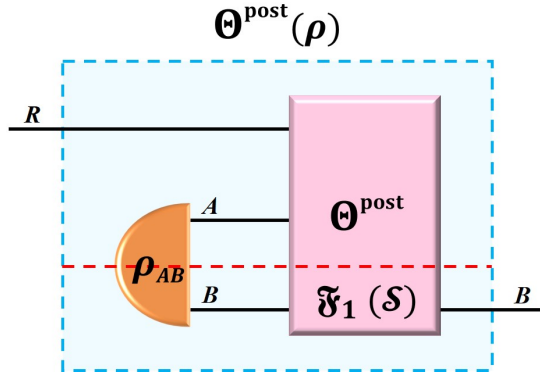


FIG. 13. (Color online) Teleportation channel $\Theta^{\text{post}}(\rho)$, which is created by first preparing an initial state ρ_{AB} , and then subjected to post-processing operations $\Theta_{RAB \rightarrow B}^{\text{post}} \in \mathfrak{F}_1(\mathcal{S})$. The post-processing operation $\Theta_{RAB \rightarrow B}^{\text{post}}$ is designed to transform the static state ρ into a dynamical resource, which can be used to teleport quantum information from message system R to receiver's system B .

Remark III.2. In Eq. 109, $F_{d,\mathcal{S}}(\rho)$, appeared on the right-hand side, is a specific instance of the more general d -fidelity of \mathcal{S} distillation $F_{d,\mathcal{S}}(\mathcal{E})$ (defined in Def. II.3). To develop a more complete understanding of the expression, we unpack the formula for $F_{d,\mathcal{S}}(\rho)$.

$$F_{d,\mathcal{S}}(\rho) := \max_{\Omega \in \mathfrak{F}_1(\mathcal{S})} F_U(\Omega(\rho), \phi_d^+) = \max_{\Omega \in \mathfrak{F}_1(\mathcal{S})} \text{Tr}[\Omega(\rho) \cdot \phi_d^+]. \quad (110)$$

Since the input of $F_{d,\mathcal{S}}$ is a state, the corresponding free morphism simplifies to the case of a superchannel without pre-processing, which is equivalent to a quantum channel.

Proof. The proof will start by showing that the left-hand side is smaller than or equal to the right-hand side. Assuming

that the maximum of the left-hand side is achieved by some quantum channel $\Xi \in \mathfrak{F}_1(\mathcal{S})$, we have

$$\max_{\Theta^{\text{post}} \in \mathfrak{F}_1(\mathcal{S})} f(\Theta^{\text{post}}(\rho)) = f(\Xi(\rho)) = \frac{dF(\Xi(\rho)) + 1}{d+1} = \frac{d \text{Tr}[\Xi(\rho)(\phi_d^+) \cdot \phi_d^+] + 1}{d+1} \leq \frac{dF_{d,\mathcal{S}}(\rho) + 1}{d+1}. \quad (111)$$

The second equation is derived from Lem. I.12, the third equation is based on the definition of entanglement fidelity (see Def. I.4), and the inequality is a direct consequence of Eq. 110. Without loss of generality, we can assume that both ρ and ϕ_d^+ act on the system AB . We can then apply a local operation to transform $\Xi(\rho)(\phi_d^+)$ from system RB to AB . For a visual illustration, see Fig. 14(a). Since local operations (i.e., LO) belong to the set of free morphisms $\mathfrak{F}_1(\mathcal{S})$, the overall operation is still a free channel in $\mathfrak{F}_1(\mathcal{S})$.

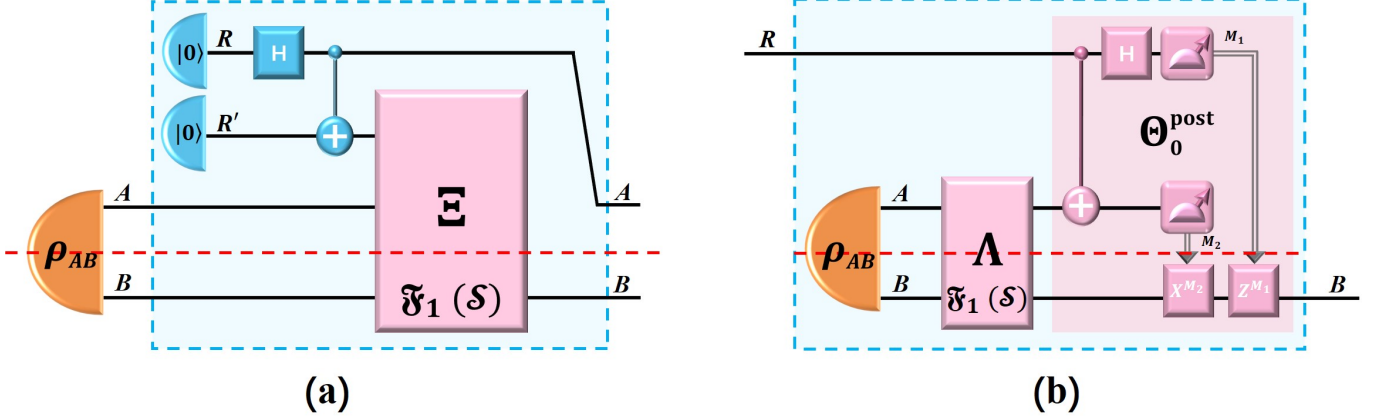


FIG. 14. (Color online) Visual demonstration of the proof of Lem. III.4. Figure (a) illustrates the role of Ξ behind Equation 111, which is a key element of our proof. On the other hand, Figure (b) depicts the construction of a teleportation channel based on Λ (see Eq. 113). In this diagram, the systems located above the dashed red line belong to Alice, while the systems below the dashed line belong to Bob. While we have focused on qubit cases in this figure for the sake of simplicity, it is worth noting that our proof holds for systems of arbitrary finite dimension d .

Next, we will show the inverse direction of the proof by demonstrating that the right-hand side is smaller than or equal to the left-hand side. In this part of the proof, let us assume that the right-hand side value of $F_{d,\mathcal{S}}(\rho)$ is achieved by a particular quantum channel $\Lambda \in \mathfrak{F}_1(\mathcal{S})$. Then, we have

$$F_{d,\mathcal{S}}(\rho) = \text{Tr}[\Lambda(\rho) \cdot \phi_d^+] = F(\mathcal{F}(\Lambda(\rho))) = F(\Theta_0^{\text{post}} \circ \Lambda(\rho)), \quad (112)$$

where Θ_0^{post} is the standard teleportation operation (see the pink box of Fig. 8(a)), this implies

$$\frac{dF_{d,\mathcal{S}}(\rho) + 1}{d+1} = \frac{dF(\Theta_0^{\text{post}} \circ \Lambda(\rho)) + 1}{d+1} = f(\Theta_0^{\text{post}} \circ \Lambda(\rho)) \leq \max_{\Theta^{\text{post}} \in \mathfrak{F}_1(\mathcal{S})} f(\Theta^{\text{post}}(\rho)). \quad (113)$$

Since $\Lambda \in \mathfrak{F}_1(\mathcal{S})$ and $\Theta_0^{\text{post}} \in \text{LOCC}_1(\text{poly}(d)) \subset \mathfrak{F}_1(\mathcal{S})$, we have $\Theta_0^{\text{post}} \circ \Lambda \in \mathfrak{F}_1(\mathcal{S})$. An illustration of the teleportation channel $\Theta_0^{\text{post}} \circ \Lambda(\rho)$ is provided in Fig. 14(b). The second equation of Eq. 112 is obtained using Lem. III.1, which allows us to express the d -fidelity of \mathcal{S} distillation $F_{d,\mathcal{S}}(\rho)$ with respect to the entanglement fidelity of channel $\Theta_0^{\text{post}} \circ \Lambda(\rho)$. Combining Eq. 111 with Eq. 113, we can conclude that the two sides are equal, which completes the proof. \square

Remark III.3. We make two remarks about Lem. III.4. Firstly, it generalizes the main theorem presented in Ref. [19], by extending its scope beyond the LOCC operations considered in that work. Specifically, while LOCC might require an impractically large number of communication rounds, our lemma applies to a broader range of operations, including LOCC_k , making it more practical. Secondly, the proof of our lemma demonstrates that our results are applicable to any set \mathcal{S} that includes $\text{LOCC}_1(\text{poly}(d))$, i.e., $\text{LOCC}_1(\text{poly}(d)) \subset \mathcal{S}$. This means that the inequality in Eq. 109 still holds for a broader range of operations beyond those explicitly considered in the lemma. This observation highlights the generality and versatility of our approach, and its potential applications to various teleportation scenarios.

Equipped with Lem. III.4, we can now express the performance of protocols c and d in a more precise and general way. Specifically, we can apply the inequality in Eq. 109 to obtain the average fidelity of teleportation channel produced by these protocols. This allows us to better understand the effects of noise and imperfections on the entanglement,

and to optimize the protocols for practical applications. First, let's consider the performance of protocol c. Written out explicitly, we have

Theorem III.5: Performance of Protocol c

To calculate the average fidelity of protocol c, denoted by f_c (as defined in Eq. 77), we can use the following expression

$$f_c = \frac{2 \left(\max_{\Omega \in \text{LOCC}(A:B)} \text{Tr}[\Omega(\rho_b) \cdot \phi^+] \right) + 1}{3}, \quad (114)$$

where ρ_b is defined in Eq. 103.

Although Eq. 114 provides a formula for the average fidelity of protocol c, it is still difficult to compute due to the complexity of the mathematical structure of LOCC. This limitation has motivated the development of protocol d, which offers a computable solution to the problem.

Theorem III.6: Performance of Protocol d

To determine the average fidelity of protocol d, which is denoted by f_d as defined in Eq. 81, we can utilize the following expression

$$f_d = \frac{2 \left(\max_{\Omega \in \text{PPT}(A:B)} \text{Tr}[\Omega(\rho_b) \cdot \phi^+] \right) + 1}{3}, \quad (115)$$

where ρ_b is defined in Eq. 103.

Thanks to the mathematical property of positive partial transpose (PPT) operations, the optimization term in the right-hand side of Eq. 115 now takes a tractable semi-definite programming (SDP) form [156, 157]. This enables us to efficiently optimize the fidelity and make performance comparisons between protocol d and other teleportation protocols. Through a deeper examination of the aforementioned optimization, we can simplify it to [22]

$$\begin{aligned} \max_{\Omega \in \text{PPT}(A:B)} \text{Tr}[\Omega(\rho_b) \cdot \phi^+] &= \max \text{Tr}[\rho_b \cdot X_{AB}], \\ \text{s.t. } 0 &\leq X_{AB} \leq \mathbb{1}, \quad -\frac{1}{2}\mathbb{1} \leq X_{AB}^{\mathbf{T}_B} \leq \frac{1}{2}\mathbb{1}, \end{aligned} \quad (116)$$

where \mathbf{T}_B denotes the partial transpose with respect to system B . Writing everything out explicitly, we have

Corollary III.7: Performance of Protocol d Simplified

To determine the average fidelity of protocol d, which is denoted by f_d as defined in Eq. 81, we can utilize the following expression

$$f_d = \frac{2 \max \left\{ \text{Tr}[\rho_b \cdot X_{AB}] \mid 0 \leq X_{AB} \leq \mathbb{1}, -\frac{1}{2}\mathbb{1} \leq X_{AB}^{\mathbf{T}_B} \leq \frac{1}{2}\mathbb{1} \right\} + 1}{3}, \quad (117)$$

where ρ_b is defined in Eq. 103.

The implementation of a quantum superchannel significantly increases the complexity of calculating the average fidelity for protocol f (see Fig. 8(f)). Fortunately, temporal entanglement provides a natural framework for simplifying this calculation. By exploiting the properties of temporal entanglement, we can simplify the calculation of the average fidelity and improve the efficiency of quantum teleportation. Here, we will delve into the details of how temporal entanglement can be leveraged to enhance the performance of quantum teleportation and to achieve higher fidelities. Our starting point will be a generalized version of Lem. III.4.

Lemma III.8: Channel Version of Lem. III.4

Consider a bipartite quantum channel $\mathcal{E}_{A_1 B_1 \rightarrow A_2 B_2}$ with dimensions $\dim A_1 = \dim A_2 = \dim B_1 = \dim B_2 = d$. Let us apply a superchannel $\Theta_{R A_2 B_2 \rightarrow A_1 B_1 B}$ from the set $\mathfrak{F}_2(\mathcal{S})$ to the channel \mathcal{E} , where \mathcal{S} is a set of permissible operations from $\{\text{LOCC}_1(\text{poly}(d)), \text{LOCC}_k, \text{LOCC}_{\mathbb{N}}, \text{LOCC}, \overline{\text{LOCC}}_{\mathbb{N}}, \text{SEP}, \text{SEPP}, \text{PPT}\}$. We can then characterize the maximum achievable average fidelity of the resulting channel $\Theta(\mathcal{E})$ (see Fig. 15) using the d -fidelity of \mathcal{S} distillation, defined in Def. II.3. More precisely, the connection between the maximum achievable average fidelity under free superchannels and the temporal entanglement can be formally characterized by the following equation

$$\max_{\Theta \in \mathfrak{F}_2(\mathcal{S})} f(\Theta(\mathcal{E})) = \frac{dF_{d,\mathcal{S}}(\mathcal{E}) + 1}{d + 1}, \quad (118)$$

where $\mathfrak{F}_2(\mathcal{S})$ is defined as the collection of all free superchannels, as specified in Def. II.1.

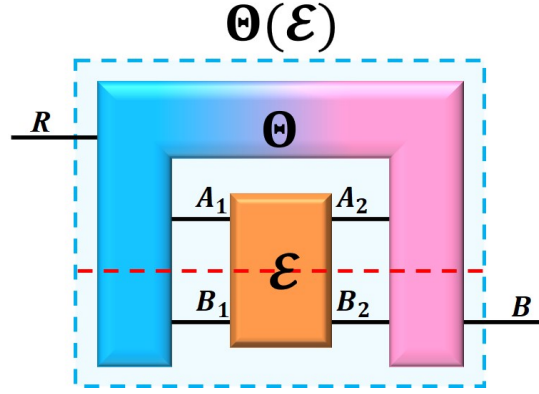


FIG. 15. (Color online) Teleportation channel $\Theta(\mathcal{E})$ used for transmitting quantum information between distant systems. The channel is obtained by applying a superchannel $\Theta \in \mathfrak{F}_2(\mathcal{S})$ to a bipartite channel \mathcal{E} . The bipartite channel plays a crucial role in generating the essential entanglement required for teleportation, while the superchannel applies a series of designed operations between the sender, receiver, and message systems to guarantee the reliable and accurate transmission of quantum states.

Proof. We will prove the equation by establishing an upper bound for the left-hand side and a lower bound for the right-hand side. Firstly, we will show that the left-hand side is bounded above by the right-hand side. Assuming that there exists a quantum superchannel $\Xi \in \mathfrak{F}_2(\mathcal{S})$ that maximizes the left-hand side of Eq. 118, we see that

$$\max_{\Theta \in \mathfrak{F}_2(\mathcal{S})} f(\Theta(\mathcal{E})) = f(\Xi(\mathcal{E})) = \frac{dF(\Xi(\mathcal{E})) + 1}{d + 1} = \frac{d \text{Tr}[\Xi(\mathcal{E})(\phi_d^+ \cdot \phi_d^+)] + 1}{d + 1} \leq \frac{dF_{d,\mathcal{S}}(\mathcal{E}) + 1}{d + 1}. \quad (119)$$

We can derive the second equation of Eq. 119 directly from Lemma I.12. To obtain the third equation of Eq. 119, we use the definition of entanglement fidelity for a quantum channel, as given in Def. I.4. We note that the inequality holds because we can prepare a local ϕ_d^+ state on Alice's side, followed by the free superchannel $\Xi \in \mathfrak{F}_2(\mathcal{S})$. After the interaction, we can apply the local noiseless channel $\text{id}_{R \rightarrow A} \in \text{LO}$. Therefore, we can view the overall effect of $\Xi(\cdot)(\phi_d^+)$ as a superchannel that belongs to $\mathfrak{F}_2(\mathcal{S})$. Fig. 16 provides a visual representation of the action of $\Xi(\cdot)(\phi_d^+)$.

Secondly, we will show that the left-hand side is bounded below by the right-hand side. Assuming that a particular quantum channel $\Lambda \in \mathfrak{F}_2(\mathcal{S})$ achieves the right-hand side value of $F_{d,\mathcal{S}}(\mathcal{E})$, then we can express $F_{d,\mathcal{S}}(\mathcal{E})$ equivalently in the following form

$$F_{d,\mathcal{S}}(\mathcal{E}) = \text{Tr}[\Lambda(\mathcal{E}) \cdot \phi_d^+] = F(\mathcal{F}(\Lambda(\mathcal{E}))) = F(\Theta_0^{\text{post}} \circ \Lambda(\mathcal{E})), \quad (120)$$

where the second equation of Eq. 120 is a direct consequence of Lem. III.1, and the last equation of Eq. 120 comes from Eq. 101, see also Fig. 11 for an illustration. It is worth noting that in this context, $\Lambda(\mathcal{E})$ denotes a quantum state that operates on the composite system AB , while $\Theta_0^{\text{post}} \circ \Lambda(\mathcal{E})$ represents a quantum channel that maps the message system R to Bob's system B . This immediately implies that

$$\frac{dF_{d,\mathcal{S}}(\mathcal{E}) + 1}{d + 1} = \frac{dF(\Theta_0^{\text{post}} \circ \Lambda(\mathcal{E})) + 1}{d + 1} = f(\Theta_0^{\text{post}} \circ \Lambda(\mathcal{E})) \leq \max_{\Theta \in \mathfrak{F}_2(\mathcal{S})} f(\Theta(\mathcal{E})). \quad (121)$$

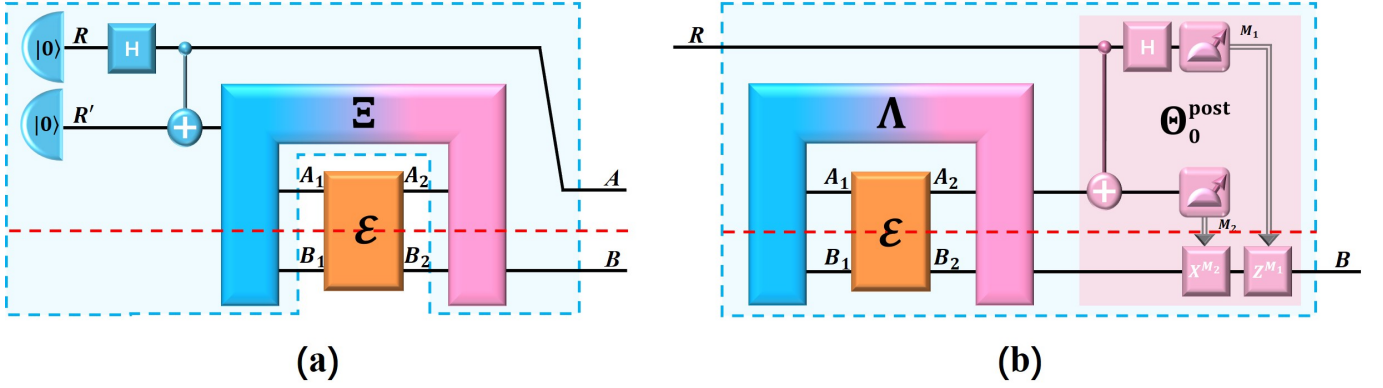


FIG. 16. (Color online) Visual demonstration of the proof of Lem. III.8. Figure (a) shows how the superchannel Ξ supports Eq. 119, which is a crucial part of our proof. Meanwhile, figure (b) illustrates how the teleportation channel is constructed using Λ , as described in Eq. 121. The dashed red line in the diagram serves as a visual separator between the systems belonging to Alice, which are positioned above the line, and the systems belonging to Bob, which are located below the line. Although we have illustrated qubit cases in this figure for simplicity, it is important to emphasize that our proof of Lem. III.8 applies to systems of any finite dimension d .

Since the standard teleportation operation Θ_0^{post} can be realized by using only local operations and one-way classical communication with the communication complexity polynomially dependent on the dimension of the message system, it is an element of the set $\text{LOCC}_1(\text{poly}(d))$. When we compose the superchannel Λ with the channel Θ_0^{post} , the resulting channel still belongs to the set $\mathfrak{F}_2(\mathcal{S})$ for any $\mathcal{S} \in \{\text{LOCC}_1(\text{poly}(d)), \text{LOCC}_k, \text{LOCC}_N, \text{LOCC}, \overline{\text{LOCC}}_N, \text{SEP}, \text{SEPP}, \text{PPT}\}$, which leads to the inequality of Eq. 121. Finally, by combining Eq. 119 with Eq. 121, we have shown that the two sides of Eq. 118 are equal, as required. \square

While entanglement monotones have been extensively studied in the context of bipartite channels, their relevance to other quantum information tasks remains uncertain. To address this open question, we investigate the role of bipartite channel, viewed as a carrier of temporal entanglement, in quantum teleportation and show that it provides unique advantages. Specifically, Lem. III.8 demonstrates that the temporal entanglement of a bipartite channel is crucial for determining the optimal performance of communication protocols that involve encoding, decoding, and quantum memory in quantum teleportation. Furthermore, we find that protocol f consistently outperforms the conventional protocol c when viewed as a function of the quantum channel, and that even stricter protocols exist (see Subsec. III C). Our proof of Lem. III.8 also demonstrates that Eq. 118 applies to any set that includes $\mathfrak{F}_2(\text{LOCC}_1(\text{poly}(d)))$, namely $\text{LOCC}_1(\text{poly}(d)) \subset \mathcal{S}$. One of the key implications of Lem. III.8 is that we can express the average fidelity of protocol f in a different way, by using the entanglement fidelity that corresponds to it. To be more precise, we can obtain

Theorem III.9: Performance of Protocol f

In order to determine the average fidelity of protocol f , which is denoted as f_f and defined in Eq. 93, we can apply the following expression

$$f_f = \frac{2 \left(\max_{\Theta \in \mathfrak{F}_2(\text{LOCC})} \text{Tr}[\Theta(\mathcal{E}(p, q)) \cdot \phi^+] \right) + 1}{3}. \quad (122)$$

In this context, Θ refers to a specific type of LOCC superchannel, i.e., $\mathfrak{F}_2(\text{LOCC})$, that maps the quantum channel $\mathcal{E}(p, q)$ to a bipartite state.

Protocol f (see Fig. 8(f)) is designed to fully exploit the resources of bipartite channel $\mathcal{E}(p, q)$ in quantum communication, taking advantage of the generality of the superchannel formalism for manipulating quantum channels. We can further express the performance of protocol f in terms of entanglement fidelity, as demonstrated in Thm. III.9. However, the evaluation of this performance remains a formidable challenge due to the intricate structure of the LOCC-superchannel $\mathfrak{F}_2(\text{LOCC})$, which is even more complex than that of a LOCC channel. Unfortunately, now we are unable to provide a systematic method for computing it. The exploration of such a method will require the development of new techniques and insights, and we leave it as an open problem for future researches. Although

we are unable to present a quantitative evaluation of the performance of protocol f in this work, we can nonetheless demonstrate a clear advantage of protocol f over the conventional teleportation protocol c (see Fig. 8(c)), which relies solely on post-processing techniques. In the upcoming subsection, we will demonstrate that protocol f achieves a higher entanglement fidelity and, as a result, a higher average fidelity than protocol c for a broad range of noisy models. This superiority underscores the potential of superchannel techniques in expanding the capabilities of quantum communication beyond the confines of conventional teleportation protocols.

C. Numerical Experiments: Dancing with Data

In Subsec. III B, we have simplified the average fidelity of the protocols introduced in Subsec. III A. Building upon these results, we have conducted numerical experiments to compare the performance of two protocols, e and d, shown in Fig. 8(e) and Fig. 8(d), respectively. Protocol e employs LO pre-processing Θ_0^{pre} and LOCC₁(poly(d)) post-processing Θ_0^{post} , while protocol d uses PPT post-processing. Our results show that, in some cases, protocol e outperforms protocol d, with the average fidelity f_e being strictly greater than f_d , which immediately implies that $f_e > f_c$. This demonstrates the necessity of implementing LOCC pre-processing in quantum teleportation. In this subsection, we will provide details of our numerical experiments and discuss the implications of our findings.

Before delving into our analysis, we will introduce a set of noise models that will be considered in this subsection. These noise models are listed in Tab. II and will serve as the foundation for our subsequent discussions. For a more detailed discussion of the noise models we are using in our analysis, please refer to the introduction of protocol b in Subsec. III A. There, we provide a comprehensive overview of the noise models and their associated parameters, which are central to our analysis of the protocol.

Noise Models of $\mathcal{N}_1(p)$ and $\mathcal{N}_2(q)$					
Noise Model (i)	$\mathcal{N}_1 = \mathcal{N}_{AD}(0.43)$ $\mathcal{N}_2 = \mathcal{N}_{BF}(0.04)$	Noise Model (ii)	$\mathcal{N}_1 = \mathcal{N}_{BF}(0.96)$ $\mathcal{N}_2 = \mathcal{N}_{AD}(0.24)$	Noise Model (iii)	$\mathcal{N}_1 = \mathcal{N}_{AD}(0.35)$ $\mathcal{N}_2 = \mathcal{N}_{PF}(0.77)$
Noise Model (iv)	$\mathcal{N}_1 = \mathcal{N}_{PF}(0.28)$ $\mathcal{N}_2 = \mathcal{N}_{AD}(0.59)$	Noise Model (v)	$\mathcal{N}_1 = \mathcal{N}_{AD}(0.23)$ $\mathcal{N}_2 = \mathcal{N}_D(0.91)$	Noise Model (vi)	$\mathcal{N}_1 = \mathcal{N}_D(0.86)$ $\mathcal{N}_2 = \mathcal{N}_{AD}(0.25)$
Noise Model (vii)	$\mathcal{N}_1 = \mathcal{N}_{AD}(0.55)$ $\mathcal{N}_2 = \mathcal{N}_{AD}(0.12)$	Noise Model (viii)	$\mathcal{N}_1 = \mathcal{N}_{AD}(0.18)$ $\mathcal{N}_2 = \text{id}$	Noise Model (ix)	$\mathcal{N}_1 = \text{id}$ $\mathcal{N}_2 = \mathcal{N}_{AD}(0.21)$

TABLE II. List of noise models $\mathcal{N}_1(p)$ and $\mathcal{N}_2(q)$ considered in the bipartite channel $\mathcal{E}(p, q)$ (see Eq. 70). Here, both $\mathcal{N}_1(p)$ and $\mathcal{N}_2(q)$ are noisy channels that are controlled by a single parameter. Abbreviations BF, PF, D, and AD stand for bit flip, phase flip, depolarizing, and amplitude damping channels, which are different types of noise that can affect the transmission of quantum information over the channel. To better understand these noise types, their Kraus are provided in Tab. I.

To better understand the impact of the noisy models on the performance of protocol e, we have defined a fine-grained average fidelity metric $f_e(\alpha, \beta)$ for some fixed p and q ; that is

$$f_e(\alpha, \beta) := f(\mathcal{F}_e(\alpha, \beta, p, q)), \quad (123)$$

where the channel $\mathcal{F}_e(\alpha, \beta, p, q)$ is defined in Eq. 86. The quantity $f_e(\alpha, \beta)$ allows us to measure the average fidelity of the protocol e for each noisy model, providing a more comprehensive understanding of how these models shape the behavior of the protocol. Such insights are essential for optimizing the protocol and ensuring its effectiveness in a variety of conditions. Lastly, it is worth noting that the definition of f_e (see Eq. 89) involves maximizing the fidelity with respect to all parameters α and β . Written in full, that is

$$f_e = \max_{\alpha, \beta} f_e(\alpha, \beta). \quad (124)$$

We present numerical demonstrations of the average fidelity of three different teleportation protocols: f_b (blue), f_d (red), and $f_e(\alpha, \beta)$ (orange), under different noise models (i) - (ix) listed in Tab. II. The fidelity values were obtained by using the theoretical results presented in Subsec. III B. The fidelity f_b represents the performance of noisy teleportation, where the input state is transferred from Alice to Bob via an entangled channel subject to the effects of noise as shown in Fig. 8(b). The fidelity f_d represents the performance of PPT teleportation, where the noisy entangled channel $\mathcal{E}(p, q)$ is followed by PPT operation, as shown in Fig. 8(d). The fidelity $f_e(\alpha, \beta)$ represents

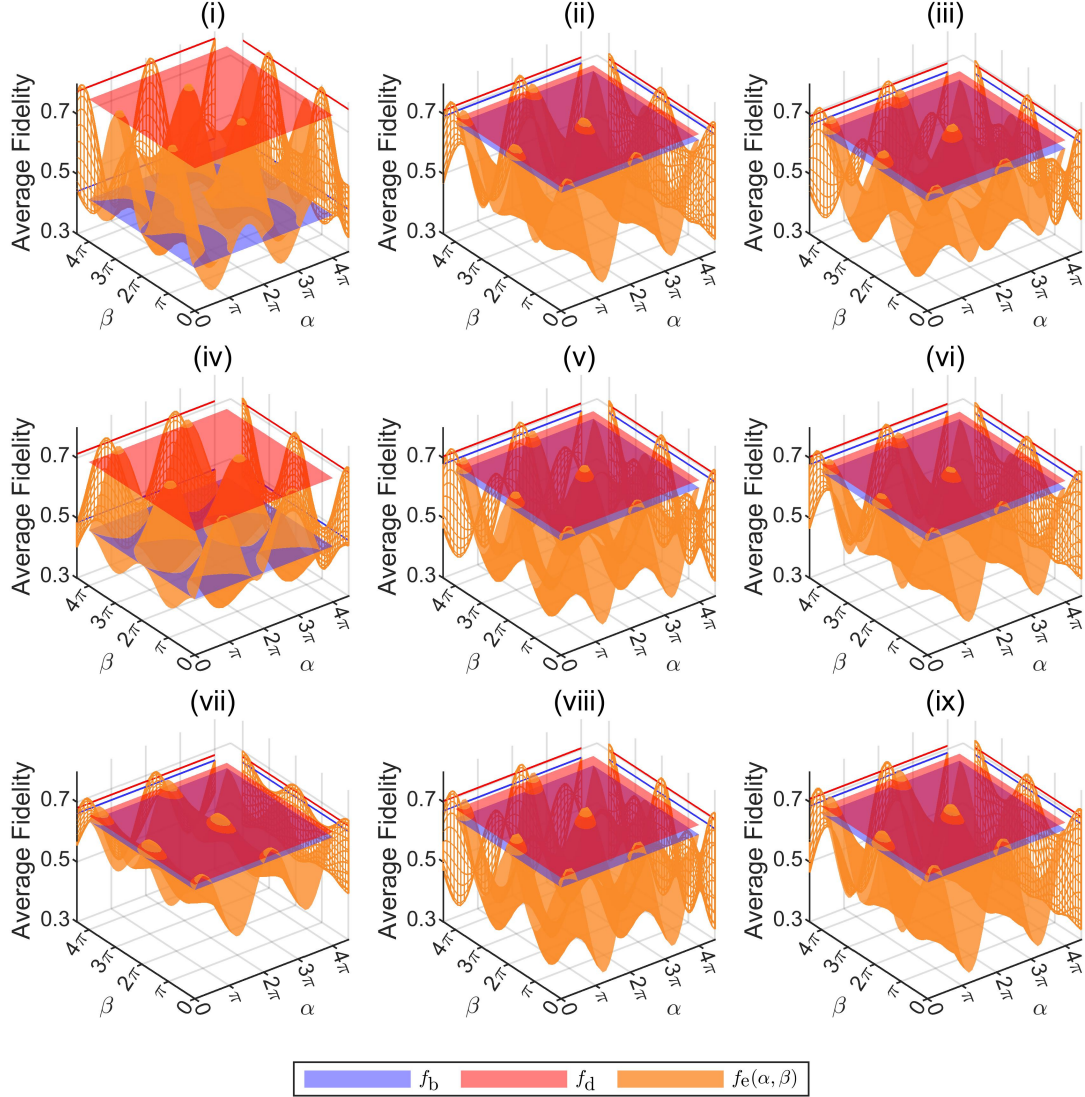


FIG. 17. (Color online) Numerical demonstration of average fidelity f_b (blue), f_d (red) and $f_e(\alpha, \beta)$ (orange) with respect to noise models (i) - (ix) considered in Tab. II. In particular, f_b (see Eq. 73) stands for the performance of noisy teleportation (see Fig. 8(b)), f_d (see Eq. 81) represents the performance of PPT teleportation (see Fig. 8(d)) and $f_e(\alpha, \beta)$ (see Eq. 123) denotes the performance of channel $\mathcal{F}_e(\alpha, \beta, p, q)$ (see Eq. 86) simulated by pre-processing-assisted teleportation (see Fig. 8(e)).

the performance of channel $\mathcal{F}_e(\alpha, \beta, p, q)$, which is simulated by pre-processing-assisted teleportation, as shown in Fig. 8(e). For each noise model, we calculate the average fidelity of these protocols and illustrate the corresponding results in Fig. 17. On the other hand, Fig. 18 provides an alternative comparison between f_b , f_d , and f_e (not $f_e(\alpha, \beta)$), which demonstrates that protocol e outperforms PPT teleportation and hence all other free-post-processing-assisted teleportation protocols.

To assess the advantage of using pre-processing-assisted protocols, we have also calculated the improvement ratio, formally defined as

$$\eta(p, q) := \frac{f_e - f_d}{f_d}. \quad (125)$$

Here, we have not assumed any specific noise model in our calculation of the improvement ratio, which makes the ratio a function of the parameters p and q . We use protocol d as a reference point, as computing the average fidelity for LOCC protocols is generally challenging due to the complex mathematical structure of LOCC. Fig. 19

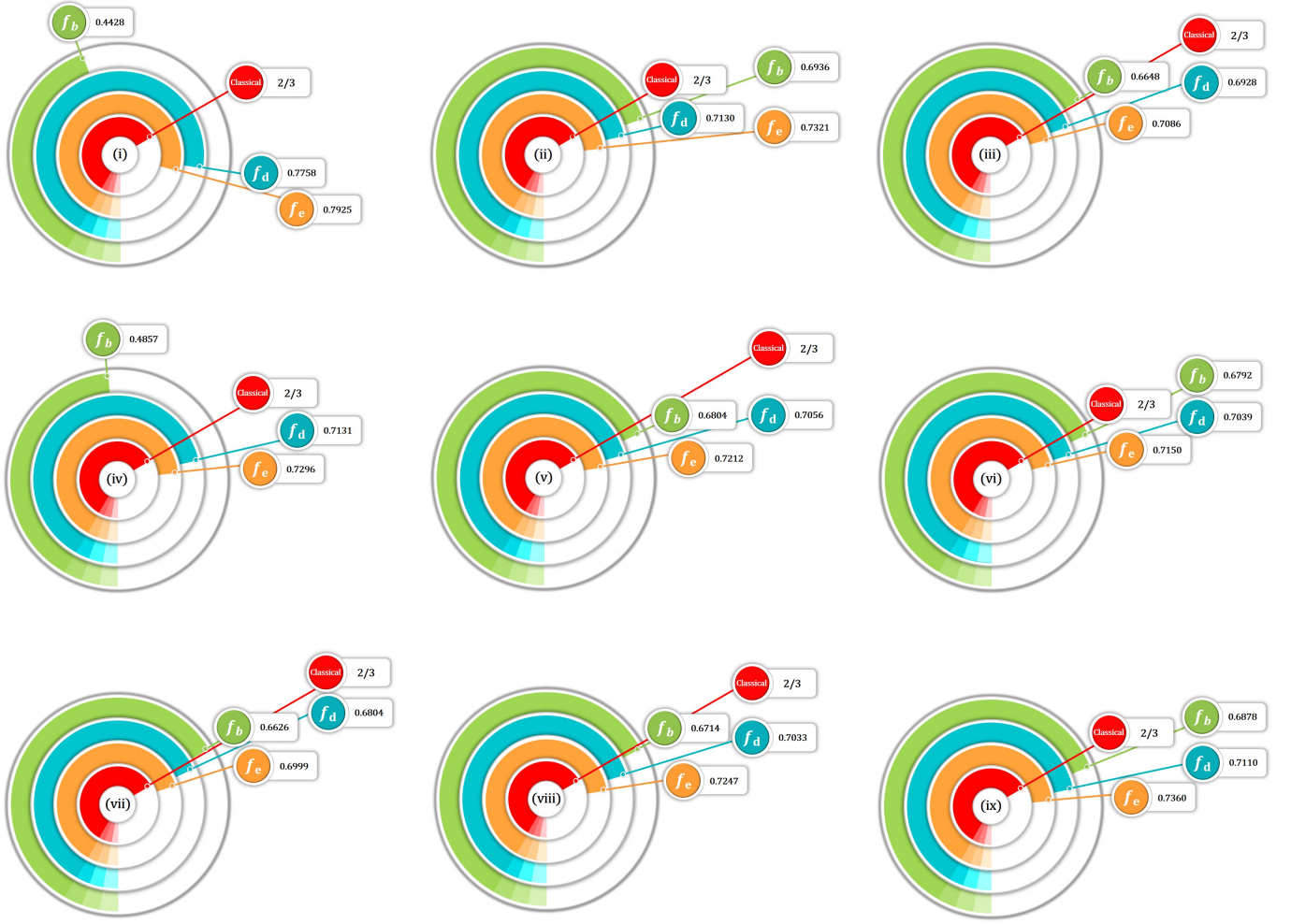


FIG. 18. (Color online) Visual comparison between the average fidelity f_b , f_d , and f_e . Each circle in the diagram contains a lowercase Roman numeral at its center, which represents the specific noise model being considered in Tab. II. The red concentric circles in this diagram represent the classical limit of teleportation, while the orange circles indicate the performance of the pre-processing-assisted quantum teleportation protocol (see Fig. 8(e)). This protocol outperforms both the blue circles of the PPT teleportation (see Fig. 8(d)) and the green circles of noisy teleportation (see Fig. 8(b)).

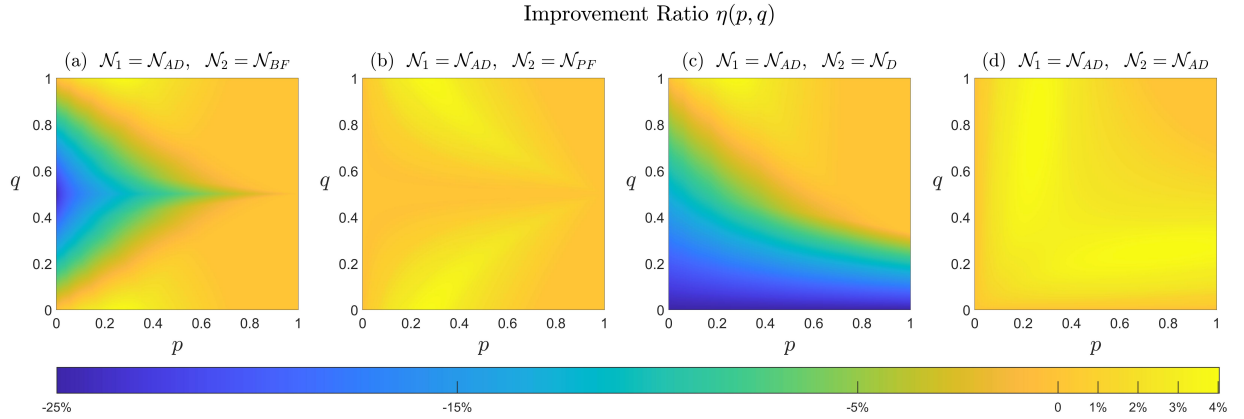


FIG. 19. (Color online) Numerical demonstration of the improvement ratio $\eta(p, q)$, as defined in Eq. 125, across various combinations of noise models. These include the amplitude damping channel \mathcal{N}_{AD} and bit flip channel \mathcal{N}_{BF} , amplitude damping channel \mathcal{N}_{AD} and phase flip channel \mathcal{N}_{PF} , amplitude damping channel \mathcal{N}_{AD} and quantum depolarizing channel \mathcal{N}_D , as well as two amplitude damping channels.

displays the improvement ratio for various combinations of noise channels. Fig. 19 clearly shows that while pre-processing-assisted teleportation protocols are powerful tools for combating noise, they cannot always outperform post-processing-assisted protocols. In fact, these two types of protocols are complementary to each other. However, in some cases, the effect of pre-processing cannot be achieved even with entangling post-processing, such as PPT operations. These numerical observations highlight the importance of considering protocol f, which combining both pre-processing and post-processing techniques, when designing practical quantum communication protocols.

Remark III.4. To better illustrate the benefits of pre-processing (i.e., protocol e) in Fig. 19, we have examined various combinations of noise models. However, to truly observe the advantages of pre-processing, it appears that at least one of the noise channels should be an amplitude damping channel (see Eq. 70 or brown boxes in Fig. 8). This observation is based on numerical data, and we currently lack a theoretical explanation for this behavior. Further investigation is needed to gain a deeper understanding of the underlying principles that govern the effectiveness of pre-processing in mitigating the detrimental effects of noise.

Remark III.5. When evaluating the performance of protocols d and e, it can be observed that the impact of noise $\mathcal{N}_1(p)$ and $\mathcal{N}_2(q)$ is symmetric. Since the SWAP operation is part of both the SEPP and PPT operations (see Eq. 63), the maximum quantity $\max_{\Omega \in \text{PPT}(A:B)} \text{Tr}[\Omega(\rho_b) \cdot \phi^+]$ (see Thm. III.6) and consequently the performance of protocol d remains symmetrical even when there is an exchange of $\mathcal{N}_1(p)$ and $\mathcal{N}_2(q)$, i.e.,

$$\max_{\Omega \in \text{PPT}(A:B)} \text{Tr}[\Omega(\mathcal{N}_1(p)_{A \rightarrow A} \otimes \mathcal{N}_2(q)_{B \rightarrow B} \circ C_{\text{NOT}, AB \rightarrow AB} \circ H_{A \rightarrow A} \otimes id_{B \rightarrow B}(|0\rangle\langle 0|_A \otimes |0\rangle\langle 0|_B)) \cdot \phi^+] \quad (126)$$

$$= \max_{\Omega \in \text{PPT}(A:B)} \text{Tr}[\Omega(\mathcal{N}_2(q)_{A \rightarrow A} \otimes \mathcal{N}_1(p)_{B \rightarrow B} \circ C_{\text{NOT}, AB \rightarrow AB} \circ H_{A \rightarrow A} \otimes id_{B \rightarrow B}(|0\rangle\langle 0|_A \otimes |0\rangle\langle 0|_B)) \cdot \phi^+]. \quad (127)$$

Protocol e exhibits symmetrical behavior in terms of the quantity $\max_{\alpha, \beta} \{\text{Tr}[\rho_e(\alpha, \beta) \cdot \phi^+]\}$ (see Thm. III.3), even if the noise sources $\mathcal{N}_1(p)$ and $\mathcal{N}_2(q)$ are exchanged, as we have maximized over all possible values of α and β , and these parameters exhibit symmetry. Hence, the ratio observed when combining noise sources $\mathcal{N}_1 = \mathcal{N}_{AD}$ and $\mathcal{N}_2 = \mathcal{N}_{BF}$ is symmetric to the ratio observed when switching the noise sources as $\mathcal{N}_2 = \mathcal{N}_{AD}$ and $\mathcal{N}_1 = \mathcal{N}_{BF}$. Therefore, it is unnecessary to gather data for the case where $\mathcal{N}_1 = \mathcal{N}_{BF}$ and $\mathcal{N}_2 = \mathcal{N}_{AD}$, as the figure exhibits symmetry with respect to the line $p = q$. Similar symmetrical results can be obtained for other combinations of noise models. This observation simplifies the data collection processes and highlights the fundamental relationships between the different noise models and their impact on the performance of quantum communication protocols.

Remark III.6. To generate Fig. 19 with a parameter resolution of 0.001, we executed our program on a standard server equipped with a CPU (Intel(R) Xeon(R) Platinum 8280*2, 56 cores, 2.70GHz clock), GPU (NVIDIA Quadro RTX 5000*4, 3072-core, 16GB memory), and RAM (1TB memory). The program was run in 84 concurrent processes, taking approximately 471.54 hours in total. Each sub-figure took 118.18 hours (Fig. 19(a)), 115.99 hours (Fig. 19(b)), 118.32 hours (Fig. 19(c)), and 119.05 hours (Fig. 19(d)), respectively. We calculated the running time using the tic and toc commands in Matlab.

Remark III.7. In recent years, there has been growing interest in exploring the use of catalysts to enhance the performance of quantum information tasks [158–166], including the task of quantum teleportation [163]. While several studies have shown promising results in this area, it's important to note that there are some practical limitations to consider. Specifically, the advantages gained from using catalysts may not always be applicable or feasible in real-world scenarios: (i) Firstly, the catalytic protocols usually utilize an infinite-dimensional catalyst. (ii) Secondly, it should be noted that only the marginal of the system corresponds to the original catalyst. Let's direct our attention to catalytic teleportation to delve into further details. Suppose an initial system at state ρ_{AB} is shared between Alice and Bob, which has been utilized to establish a teleportation channel (see Fig. 13). In order to enhance the efficiency of teleportation, an additional system $\omega_{A'B'}$ shared between Alice and Bob has been introduced, referred to as the catalyst. By applying an LOCC transformation $\Theta^{\text{post}} : ABA'B' \rightarrow ABA'B'$, the final state is obtained, with the marginals σ_{AB} and $\omega_{A'B'}$.

$$\text{Tr}_{A'B'} \Theta^{\text{post}}(\rho \otimes \omega) = \sigma, \quad (128)$$

$$\text{Tr}_{AB} \Theta^{\text{post}}(\rho \otimes \omega) = \omega. \quad (129)$$

Notably, the fidelity of σ_{AB} in teleporting a state is higher compared to the initial state ρ_{AB} . However, the dimension of $\omega_{A'B'}$ is infinite in existing protocols. Importantly, as per Eqs. 128 and 129, tracing out systems $A'B'$ is necessary to obtain σ and achieve better teleportation performance, unless

$$\Theta^{\text{post}}(\rho \otimes \omega) = \sigma \otimes \omega, \quad (130)$$

holds exactly, even if they are arbitrarily close. But, once the catalyst system has been discarded, it is impossible to obtain ω again, preventing its reuse in subsequent protocols and thus rendering it inconsistent with the definition of a catalyst. Unlike catalytic quantum teleportation, our protocol *e* achieves improvements without requiring ancillary systems (see Fig. 8(e)), making it more experimentally feasible.

In summary, teleportation protocols rely on the bipartite channel shared between parties. If we consider only the static state shared between the sender and the receiver as a resource, the use of pre-processing is limited, resulting in the maximal fidelity of f_c achieved by LOCC post-processing. However, viewing the protocol from a channel perspective allows for suitable LOCC pre-processing that can improve teleportation to a fidelity of f_f without consuming additional resources. There are many examples that demonstrate the improvement in performance when pre-processing is implemented in the presence of noises. In comparison to protocols that do not employ pre-processing, these examples, including Figs. 17, 18, and 19, show that pre-processing can enhance the quality of information transmission, reduce the effects of noise and decoherence, and increase the overall fidelity of the teleportation protocol. To achieve a thorough understanding of the capabilities and limitations of quantum teleportation, it is imperative to explore protocols from a channel perspective. By leveraging superchannel-assisted protocols, we can reach the ultimate limits in quantum communication. Thus, gaining a deeper understanding of the underlying dynamical resource, namely the bipartite channel, that enables these protocols can provide valuable insights into the fundamental nature of quantum information and its transmission. Such insights can drive the development of novel quantum communication protocols that exploit the full potential of quantum channels, ultimately leading to significant advances in the field of quantum information processing.

IV. QUANTUM NETWORK

Quantum communication is a rapidly evolving field that holds great promise for secure and efficient information transfer. In our previous Sec. III, we demonstrated the crucial role of entanglement-generating channels in enabling higher fidelity quantum teleportation, compared with the conventional teleportation (protocol *c* of Fig. 8). Building on this foundation, we now extend our framework to the realm of quantum network communication, which requires more complex resource manipulations. In Subsec. IV A, we employ the pre-processing techniques to enhance the performance of quantum repeaters, a key technology for long-distance quantum communication. Our detailed analysis and numerical experiments across various noise models illustrate the practical feasibility and robustness of our approach. Along the way, in Subsec. IV B, we introduce the concept of *adaptive quantum communication protocol* that allows for multiple rounds of quantum operations and possible quantum memory, providing a more general framework for quantum network communication. Additionally, our result shows that the optimal performance of an adaptive quantum communication protocol is directly correlated with the temporal entanglement it possesses. Our findings demonstrate that temporal entanglement, introduced in Sec. II, plays a critical role in transmitting quantum information across a quantum network, underscoring the practical importance of this unique quantum property.

A. Quantum Repeater: Towards a Global Quantum Communication Network

Quantum communication over long distances poses a fundamental challenge [167]: the likelihood of errors increases as the length of the channel connecting the parties grows. This is especially true when using photonic quantum communication over optical fibers, as both photon absorption and depolarization tend to increase exponentially with the length of the fiber. As a result, longer quantum communications experience significant signal quality degradation, leading to increased error rates and reduced efficiency and reliability. Fortunately, there is a solution to this challenge: the use of quantum repeaters [168]. These repeaters can be built with auxiliary particles at intermediate connection points, enabling the transmission of quantum information over longer distances [70, 169–190]. By distributing entangled pairs of particles across the channel, quantum repeaters can help to maintain the integrity of the transmitted information and ensure that the communication remains reliable, efficient, and secure, even over long distances.

One of the key technical tools that enables quantum repeater is entanglement swapping [191–193], which enables long-distance quantum communication. The process involves the transfer of entanglement from two pairs of particles to create a new, entangled pair between two distant locations. This approach allows for the establishment of entanglement across long distances, bypassing the need for direct transmission, which can be subject to significant signal degradation and other sources of interference. By viewing the bipartite channel that generates entanglement between distant locations as a resource, researchers can leverage entanglement swapping as a post-processing step to extract the maximum benefit from this resource. This process is similar to the role of Θ_0^{post} in standard quantum teleportation (see Subsec. III A). In this subsection, we will explore the pre-processing-assisted quantum repeater protocol and its

ability to significantly enhance the fidelity of quantum communication. Compared to traditional quantum repeater protocols, which rely solely on entanglement swapping, the pre-processing-assisted protocol offers an exponential increase in fidelity.

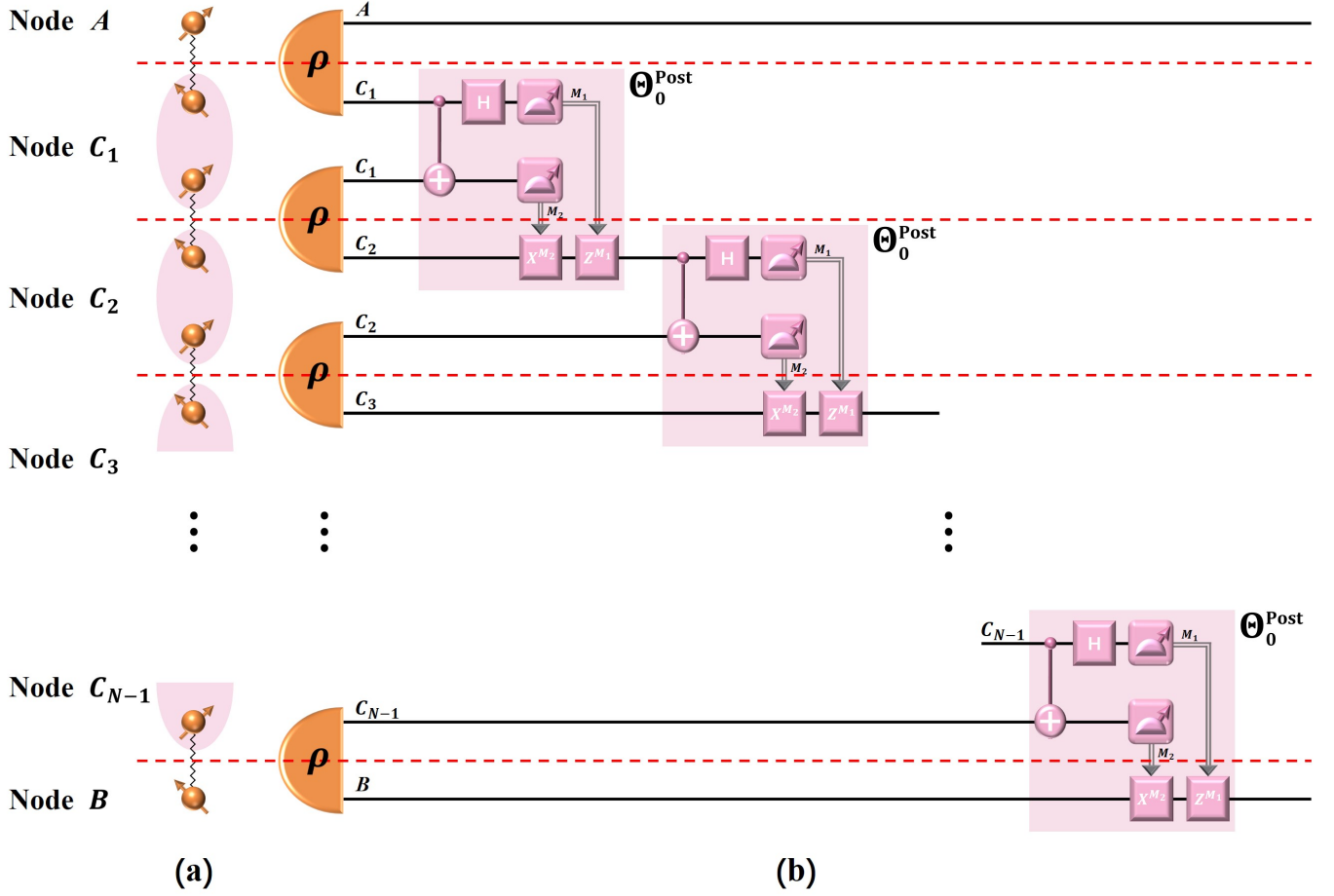


FIG. 20. (Color online) Quantum repeaters: establishing an entangled state between system A and B by connecting a sequence of N bipartite states ρ through $N - 1$ intermediate nodes from C_1 to C_{N-1} . Here, we build the connection using standard entanglement swapping technique, whereby Bell measurements are made within the same intermediate node. Figure (a) depicts a schematic diagram of the quantum repeaters. Meanwhile, Figure (b) shows the circuit diagram of the quantum repeaters.

To establish a secure communication channel between distant nodes A and B , we divide the channel into N segments and create N pairs of qubits, each shared between a connection point and a node. For simplicity, we assume that all N pairs are noisy singlets (see Eq. 33) with the same fidelity F_1 . Using entanglement swapping, we perform Bell measurements on the shared qubits at the intermediate nodes C_1 through C_{N-1} and transmit the measurement outcomes between the nodes to effectively teleport the quantum state of the original qubit from node A to node B , as illustrated in Fig. 20. To be more precise, we can assume that the noisy singlet is expressed in the form of Eq. 33. Therefore, the relationship between the noisy parameter p and the entanglement fidelity F_1 can be characterized by the following formula.

$$F_1 = \frac{p(d^2 - 1) + 1}{d^2}. \quad (131)$$

By connecting N neighboring pairs through entanglement swapping, as demonstrated in Fig. 20, a new pair is obtained with fidelity F_N . The relationship between F_N and F_1 is captured by the following lemma.

Lemma IV.1: Concentrating Noisy Singlets Through Entanglement Swapping

Using entanglement swapping, as demonstrated in Fig. 20, N pairs of noisy singlets (see Eq. 33) with fidelity F_1 can be connected to obtain an entangled state with fidelity F_N . The fidelity of this state can be expressed as follows

$$F_N = \frac{1}{4} + \frac{3}{4} \left(\frac{4F_1 - 1}{3} \right)^N, \quad (132)$$

which provides a quantitative understanding of the relationship between the fidelity of the initial pairs and the resulting fidelity after connecting them.

Remark IV.1. Some readers may consider Eq. 132 to be a special case of Eq. 5 from Ref. [168], where both the elementary pairs and all operations involved in the connection process are perfect. However, this is not the case. Ref. [168] uses the Werner state (see Ref. [194]) as their elementary pair, which is different from the noisy singlet (see Ref. [25]) that we investigate in this work. Furthermore, the proof for Eq. 5 in Ref. [168] is missing, making our Lem. IV.1 a more comprehensive reference for readers interested in quantum repeaters. By providing a detailed proof of Lem. IV.1, we offer a clear and rigorous understanding of the relationship between the fidelity of the initial pairs and the resulting fidelity after they are connected using entanglement swapping.

Proof. We will utilize mathematical induction to demonstrate the validity of this lemma. Given two noisy singlets $\rho = p\phi^+ + (1-p)\mathbb{1} \otimes \mathbb{1}/4$ defined over systems AC_1 and C_1C_2 , both characterized by the same noise parameter $0 \leq p \leq 1$, we can express the resulting overall state as follows

$$\begin{aligned} \rho_{AC_1} \otimes \rho_{C_1C_2} = & p^2 (\phi_{AC_1}^+ \otimes \phi_{C_1C_2}^+) + p(1-p) \left(\phi_{AC_1}^+ \otimes \frac{\mathbb{1}_{C_1}}{2} \otimes \frac{\mathbb{1}_{C_2}}{2} \right) + p(1-p) \left(\frac{\mathbb{1}_A}{2} \otimes \frac{\mathbb{1}_{C_1}}{2} \otimes \phi_{C_1C_2}^+ \right) \\ & + (1-p)^2 \left(\frac{\mathbb{1}_A}{2} \otimes \frac{\mathbb{1}_{C_1}}{2} \otimes \frac{\mathbb{1}_{C_1}}{2} \otimes \frac{\mathbb{1}_{C_2}}{2} \right). \end{aligned} \quad (133)$$

Fig. 20 demonstrates the use of the notation C_1 to represent different systems coexisting at the same node. As the distinction between these systems is clear from the context, there should be no confusion arising from this notation. We can decompose the first term on the right-hand side of Eq. 133 in the following way

$$|\phi^+\rangle_{AC_1} \otimes |\phi^+\rangle_{C_1C_2} = \frac{1}{2\sqrt{2}} \left[|0\rangle_A (|\phi_{00}\rangle_{C_1C_1} + |\phi_{10}\rangle_{C_1C_1}) |0\rangle_{C_2} + |0\rangle_A (|\phi_{01}\rangle_{C_1C_1} + |\phi_{11}\rangle_{C_1C_1}) |1\rangle_{C_2} \right. \quad (134)$$

$$\left. + |1\rangle_A (|\phi_{01}\rangle_{C_1C_1} - |\phi_{11}\rangle_{C_1C_1}) |0\rangle_{C_2} + |1\rangle_A (|\phi_{00}\rangle_{C_1C_1} - |\phi_{10}\rangle_{C_1C_1}) |1\rangle_{C_2} \right], \quad (135)$$

where $|\phi_{ij}\rangle$ stands for the four Bell states, namely $|\phi_{ij}\rangle := \mathbb{1} \otimes X^j Z^i |\phi^+\rangle$, with $i, j \in \{0, 1\}$. After performing a Bell measurement and obtaining the outcomes (i, j) and applying the unitary operation $X^j Z^i$ to the C_2 system, the resulting state of the composite system AC_2 becomes a maximally entangled state $\phi_{AC_2}^+$. Next, we will consider the second component on the right-hand side of Eq. 133, which has the following decomposition

$$\phi_{AC_1}^+ \otimes \frac{\mathbb{1}_{C_1}}{2} \otimes \frac{\mathbb{1}_{C_2}}{2} = \frac{1}{8} \left[\left(|0\rangle_A (|\phi_{00}\rangle_{C_1C_1} + |\phi_{10}\rangle_{C_1C_1}) + |1\rangle_A (|\phi_{01}\rangle_{C_1C_1} - |\phi_{11}\rangle_{C_1C_1}) \right) \right. \quad (136)$$

$$\left. \left(\langle 0|_A (\langle \phi_{00}|_{C_1C_1} + \langle \phi_{10}|_{C_1C_1}) + \langle 1|_A (\langle \phi_{01}|_{C_1C_1} - \langle \phi_{11}|_{C_1C_1}) \right) \right) \right] \quad (137)$$

$$+ \left(|0\rangle_A (|\phi_{01}\rangle_{C_1C_1} + |\phi_{11}\rangle_{C_1C_1}) + |1\rangle_A (|\phi_{00}\rangle_{C_1C_1} - |\phi_{10}\rangle_{C_1C_1}) \right) \quad (138)$$

$$\left. \left(\langle 0|_A (\langle \phi_{01}|_{C_1C_1} + \langle \phi_{11}|_{C_1C_1}) + \langle 1|_A (\langle \phi_{00}|_{C_1C_1} - \langle \phi_{10}|_{C_1C_1}) \right) \right] \otimes \frac{\mathbb{1}_{C_2}}{2}. \quad (139)$$

Regardless of which Bell measurement is performed on node C_1 , the resulting state that acts on system AC_2 is always the same: the maximally mixed state $\mathbb{1}_A \otimes \mathbb{1}_{C_2}/4$. Our attention will now turn to the third component on the

right-hand side of Eq. 133.

$$\frac{\mathbb{1}_A}{2} \otimes \frac{\mathbb{1}_{C_1}}{2} \otimes \phi_{C_1 C_2}^+ = \frac{\mathbb{1}_A}{2} \otimes \frac{1}{8} \left[\left((|\phi_{00}\rangle_{C_1 C_1} + |\phi_{10}\rangle_{C_1 C_1}) |0\rangle_{C_2} + (|\phi_{01}\rangle_{C_1 C_1} + |\phi_{11}\rangle_{C_1 C_1}) |1\rangle_{C_2} \right) \right. \quad (140)$$

$$\left. \left((\langle\phi_{00}|_{C_1 C_1} + \langle\phi_{10}|_{C_1 C_1}) \langle 0|_{C_2} + (\langle\phi_{01}|_{C_1 C_1} + \langle\phi_{11}|_{C_1 C_1}) \langle 1|_{C_2} \right) \right] \quad (141)$$

$$+ \left((|\phi_{01}\rangle_{C_1 C_1} - |\phi_{11}\rangle_{C_1 C_1}) |0\rangle_{C_2} + (|\phi_{00}\rangle_{C_1 C_1} - |\phi_{10}\rangle_{C_1 C_1}) |1\rangle_{C_2} \right) \quad (142)$$

$$\left. \left((\langle\phi_{01}|_{C_1 C_1} - \langle\phi_{11}|_{C_1 C_1}) \langle 0|_{C_2} + (\langle\phi_{00}|_{C_1 C_1} - \langle\phi_{10}|_{C_1 C_1}) \langle 1|_{C_2} \right) \right]. \quad (143)$$

Similarly to the situation with the second component, the resulting state that acts on system AC_2 is always the maximally mixed state, irrespective of which Bell measurement is implemented on node C_1 . Likewise, the last component on the right-hand side of Eq. 133 results in the maximally mixed state, meaning that any Bell measurement performed on this component will yield the same output state on system AC_2 , namely the maximally mixed state.

In conclusion, only the first component on the right-hand side of Eq. 133 can produce a maximally entangled state through entanglement swapping, while all other components will only lead to the maximally mixed state. In full, the resulting state of $\rho_{AC_1} \otimes \rho_{C_1 C_2}$ under entanglement swapping is given by

$$p^2 \phi_{AC_2}^+ + (2p(1-p) + (1-p)^2) \frac{\mathbb{1}_A}{2} \otimes \frac{\mathbb{1}_{C_2}}{2} = p^2 \phi_{AC_2}^+ + (1-p^2) \frac{\mathbb{1}_A}{2} \otimes \frac{\mathbb{1}_{C_2}}{2}. \quad (144)$$

Moving forward, we can analyze the entanglement fidelity of Eq. 144. Writing everything out explicitly, we have

$$F_2 = \text{Tr} \left[\left(p^2 \phi_{AC_2}^+ + (1-p^2) \frac{\mathbb{1}_A}{2} \otimes \frac{\mathbb{1}_{C_2}}{2} \right) \cdot \phi_{AC_2}^+ \right] = \frac{1}{4} + \frac{3}{4} p^2 = \frac{1}{4} + \frac{3}{4} \left(\frac{4F_1 - 1}{3} \right)^2. \quad (145)$$

Here the final equation is obtained directly from Eq. 131, which is a consequence of the relationship between the entanglement fidelity and the noise parameter of the noisy singlet.

To establish a general formula for the resulting state under entanglement swapping, we can perform a mathematical induction. Specifically, let us assume that $N-1$ copies of the noisy singlet will yield a state on system AC_{N-1} in the following form

$$p^{N-1} \phi_{AC_{N-1}}^+ + (1-p^{N-1}) \frac{\mathbb{1}_A}{2} \otimes \frac{\mathbb{1}_{C_{N-1}}}{2}. \quad (146)$$

Under this assumption, the resulting global state over nodes A , C_{N-1} , and B turns out to be

$$\left(p^{N-1} \phi_{AC_{N-1}}^+ + (1-p^{N-1}) \frac{\mathbb{1}_A}{2} \otimes \frac{\mathbb{1}_{C_{N-1}}}{2} \right) \otimes \left(p \phi_{C_{N-1} B}^+ + (1-p) \frac{\mathbb{1}_{C_{N-1}}}{2} \otimes \frac{\mathbb{1}_B}{2} \right) \quad (147)$$

$$= p^N \left(\phi_{AC_{N-1}}^+ \otimes \phi_{C_{N-1} B}^+ \right) + p^{N-1} (1-p) \left(\phi_{AC_{N-1}}^+ \otimes \frac{\mathbb{1}_{C_{N-1}}}{2} \otimes \frac{\mathbb{1}_B}{2} \right) + (1-p^{N-1}) p \left(\frac{\mathbb{1}_A}{2} \otimes \frac{\mathbb{1}_{C_{N-1}}}{2} \otimes \phi_{C_{N-1} B}^+ \right) \quad (148)$$

$$+ (1-p^{N-1}) (1-p) \left(\frac{\mathbb{1}_A}{2} \otimes \frac{\mathbb{1}_{C_{N-1}}}{2} \otimes \frac{\mathbb{1}_{C_{N-1}}}{2} \otimes \frac{\mathbb{1}_B}{2} \right). \quad (149)$$

Based on prior discussions, it is known that entanglement swapping can only generate a single maximally entangled state over system AB from the tensor product of two maximally entangled states, i.e., $\phi_{AC_{N-1}}^+ \otimes \phi_{C_{N-1} B}^+$. Any other states present in Eq. 148 and Eq. 149 would result in maximally mixed states after applying entanglement swapping. Thus, after the entanglement swapping operation, the final state on system AB would be

$$p^N \phi_{AB}^+ + (p^{N-1} (1-p) + (1-p^{N-1}) p + (1-p^{N-1}) (1-p)) \frac{\mathbb{1}_A}{2} \otimes \frac{\mathbb{1}_B}{2} = p^N \phi_{AB}^+ + (1-p^N) \frac{\mathbb{1}_A}{2} \otimes \frac{\mathbb{1}_B}{2}. \quad (150)$$

The process of mathematical induction is now complete. To further our analysis, let us examine the entanglement fidelity of Eq. 150 by expressing the equation in full detail.

$$F_N = \text{Tr} \left[\left(p^N \phi_{AB}^+ + (1-p^N) \frac{\mathbb{1}_A}{2} \otimes \frac{\mathbb{1}_B}{2} \right) \cdot \phi_{AB}^+ \right] = \frac{1}{4} + \frac{3}{4} p^N = \frac{1}{4} + \frac{3}{4} \left(\frac{4F_1 - 1}{3} \right)^N. \quad (151)$$

As previously noted, the final equation is a direct consequence of Eq. 131, which establishes the relationship between the entanglement fidelity and the parameter of noisy singlet. This relationship allows us to derive the expression for the entanglement fidelity presented in the last equation. Having established all necessary arguments and demonstrated the validity of Eq. 132, we conclude that the proof is complete. \square

In the previous Lem. IV.1, we established a general result for quantum repeaters that employ noisy singlets. We will now focus on a specific preparation of noisy singlet and investigate its performance in more detail. As we discussed in Subsec. IB and established through Thm. I.10, the output of the isotropic twirling operator \mathcal{T}_{iso} always results in a noisy singlet. Leveraging this fact, we can now choose the following state as the initial state to be shared between the nodes in Fig. 20.

$$\mu := \mathcal{T}_{\text{iso}}(\rho_b). \quad (152)$$

Here, ρ_b is defined in Eq. 103, which represents the noisy entangled state without implementing any pre-processing. Due to the property that $F(\mathcal{T}_{\text{iso}}(\rho)) = F(\rho)$ holds for any input state ρ , we can conclude that $F(\mu) = F(\rho_b)$. Fig. 21(a) illustrates the process of generating μ .

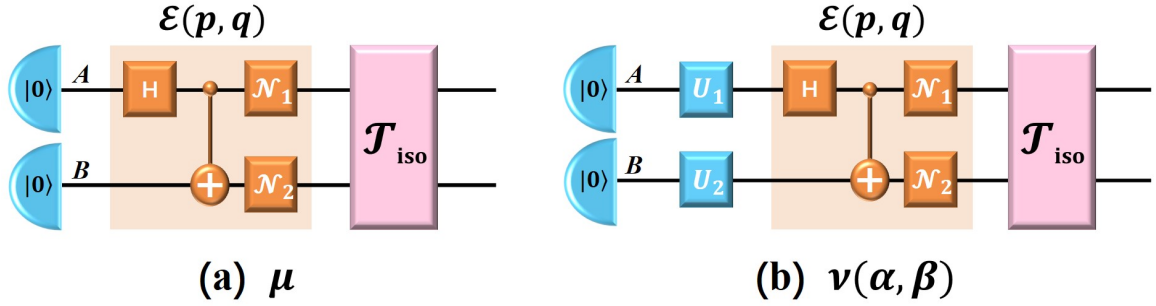


FIG. 21. (Color online) Generations of entangled resources. The first one is denoted by μ (see Eq. 152) and is generated in (a), while the second one is denoted by $\nu(\alpha, \beta)$ (see Eq. 153) and is generated in (b). The entangling gate $\mathcal{E}(p, q)$ and isotropic twirling \mathcal{T}_{iso} are defined in Eq. 70 and Eq. 27 respectively. In (b), the pre-processing step involves two unitary operations, namely U_1 and U_2 , with respective parameters α and β , as defined in Eq. 85.

Moving forward, let's investigate the initial state with pre-processing, as discussed in protocol e of Subsec. III A. Mathematically, we can express the new initial state as $\rho_e(\alpha, \beta)$, which is defined in Eq. 104. After applying the isotropic twirling operation, we obtain

$$\nu(\alpha, \beta) := \mathcal{T}_{\text{iso}}(\rho_e(\alpha, \beta)). \quad (153)$$

The generation of $\nu(\alpha, \beta)$ is depicted in Fig. 21(b). In this context, we are concerned with the scenario where the maximization is performed over all parameters α and β , resulting in the following expression for the entanglement fidelity.

$$F(\nu) := \max_{\alpha, \beta} \text{Tr}[\mathcal{T}_{\text{iso}}(\rho_e(\alpha, \beta)) \cdot \phi^+] = \max_{\alpha, \beta} \text{Tr}[\rho_e(\alpha, \beta) \cdot \phi^+]. \quad (154)$$

The inclusion of pre-processing can affect the output of bipartite channels, resulting in differences between μ and $\nu(\alpha, \beta)$. To determine the effectiveness of pre-processing-assisted protocols, we calculated the improvement ratio $\zeta(p, q)$, which represents the percentage increase in performance achieved by using pre-processing.

$$\zeta(p, q) := \frac{\max_{\alpha, \beta} F(\rho_e(\alpha, \beta)) - F(\rho_b)}{F(\rho_b) - \frac{1}{4}}. \quad (155)$$

The improvement ratio $\zeta(p, q)$ is determined by the characteristics of the noisy entangling channel, namely $\mathcal{E}(p, q)$ (see Eq. 70). As p and q are the parameters that control the behavior of the bipartite channel, the improvement ratio is inherently dependent on these parameters. Tab. III outlines our analysis of four distinct noise models, where we thoroughly examine their individual impact on the improvement ratio $\zeta(p, q)$.

Remark IV.2. To streamline our discussion, we focus on the noisy singlet with a noise parameter $0 < p = \frac{4F_1 - 1}{3} \leq 1$ (see Eq. 131). This implies that F_1 is strictly greater than $1/4$. As a result, the quantity $\zeta(p, q)$ defined in Eq. 155

Noise Models	Entanglement Fidelity $F(\mu)$	Entanglement Fidelity $F(\nu)$	Improvement Ratio $\zeta(p, q)$
$\mathcal{N}_1 = \mathcal{N}_{AD}(p = 0.38), \mathcal{N}_2(q = 1) = \text{id}$	0.6532	0.6860	8.14%
$\mathcal{N}_1 = \mathcal{N}_{AD}(p = 0.40), \mathcal{N}_2(q = 1) = \text{id}$	0.6662	0.6971	7.42%
$\mathcal{N}_1 = \mathcal{N}_{AD}(p = 0.55), \mathcal{N}_2(q = 1) = \text{id}$	0.7583	0.7749	3.27%
$\mathcal{N}_1 = \mathcal{N}_{AD}(p = 0.56), \mathcal{N}_2(q = 1) = \text{id}$	0.7642	0.7798	3.05%

TABLE III. Quantifying the effectiveness of pre-processing techniques: an investigation of improvement ratio $\zeta(p, q)$, defined in Eq. 155, across different noise models. In particular, we analyze the noise models of amplitude damping channel $\mathcal{N}_1(p) = \mathcal{N}_{AD}(p)$ with $p \in \{0.38, 0.40, 0.55, 0.56\}$, while employing the identity channel $\mathcal{N}_2 = \text{id}$ to represent a noiseless evolution of the system (see Fig. 21). We list the corresponding improvement ratios in the final column.

is guaranteed to be non-negative. In this case, the utilization of pre-processing techniques in the quantum repeater protocol presents a clear advantage in the context of the quantity $\zeta(p, q)$. Specifically, Tab. III shows that the use of pre-processing significantly enhances the performance of the protocol compared to the case without pre-processing, which reflects the effectiveness of the pre-processing-assisted protocol in quantum communication over long distances. These findings underscore the importance of incorporating pre-processing techniques into the design of quantum repeater protocols and highlight the potential for further advancements in the field of quantum communication.

Our current objective is to build a quantum network using either μ (see Eq. 152) or $\nu(\alpha, \beta)$ (see Eq. 153) as our entangled resource, and we want to demonstrate the advantages of pre-processing in quantum network communication. To evaluate the performance of these resources, we will measure the fidelity of the resulting state obtained through entanglement swapping, as illustrated in Fig. 20. Afterward, we will compare their effectiveness in quantum network communication by referring to the following theorem.

Theorem IV.2: Performance of Quantum Network with and without Pre-Processing

By connecting N adjacent pairs of μ (as defined in Eq. 152) through entanglement swapping (as depicted in Fig. 20) in quantum network, we can generate a new pair with fidelity

$$\frac{1}{4} + \frac{3}{4} \left(\frac{4F(\mu) - 1}{3} \right)^N. \quad (156)$$

Assuming that the maximization over pre-processing in terms of $U_1(\alpha) \otimes U_2(\beta)$ (as shown in Eq. 85) has been taken into account, the fidelity of the resulting state can be expressed as

$$\frac{1}{4} + \frac{3}{4} \left(\frac{4F(\nu) - 1}{3} \right)^N = \frac{1}{4} + \frac{3}{4} (1 + \zeta(p, q))^N \left(\frac{4F(\mu) - 1}{3} \right)^N. \quad (157)$$

Here, the symbol $\zeta(p, q)$, as defined in Eq. 155, represents the improvement ratio achieved by using pre-processing-assisted protocols (see Fig. 21(b)) compared to standard protocols without pre-processing (see Fig. 21(a)), measured in terms of the entanglement fidelities obtained.

Proof. The expressions in Eq. 156 and the left-hand side of Eq. 157 are direct consequences of Lem. IV.1, which provides a key insight into the performance of the repeater protocol by relating its fidelity to the fidelity of its constituent parts. The proof of the right-hand side of Eq. 157 is a straightforward application of the definition of the improvement ratio $\zeta(p, q)$ and the property of isotropic twirling \mathcal{T}_{iso} . Specifically, we can derive the following result by using the invariant properties of isotropic twirling

$$F(\mu) = F(\rho_b), \quad (158)$$

$$F(\nu) = \max_{\alpha, \beta} F(\rho_e(\alpha, \beta)), \quad (159)$$

where ρ_b and $\rho_e(\alpha, \beta)$ are defined in Eq. 103 and Eq. 104 respectively. These equations, combined with the definition of the improvement ratio $\zeta(p, q)$, immediately yield the right-hand side of Eq. 157. Taken together, these results provide a rigorous mathematical foundation for the performance analysis of the repeater protocol, and demonstrate the power of the improvement ratio concept in characterizing the benefits of using pre-processing-assisted protocols. \square

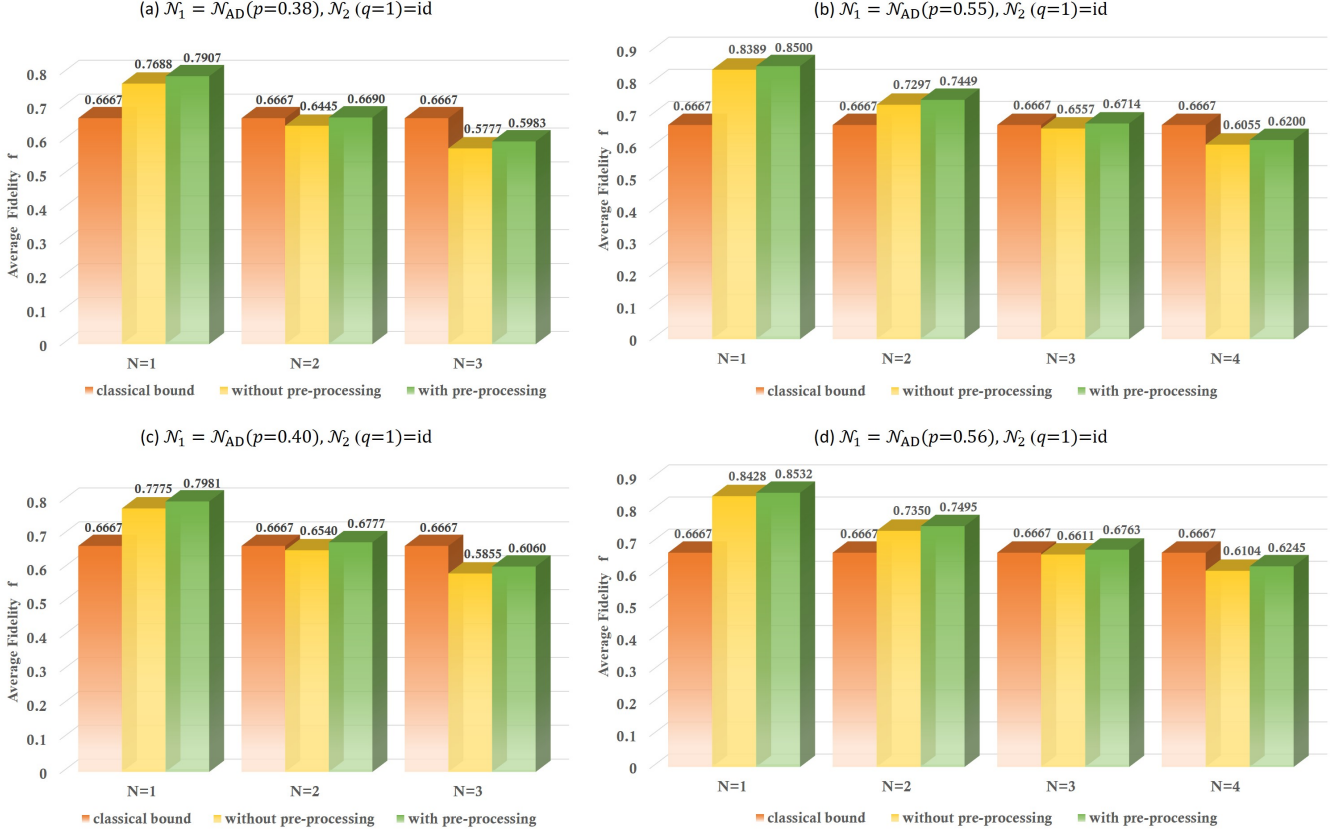


FIG. 22. (Color online) Improving quantum network communication with pre-processing techniques. Here, figures (a) and (c) demonstrate a remarkable doubling effect in the communication distance achieved through the use of pre-processing techniques in quantum repeater protocols, shown in Fig. 20. The comparison between states $\mu = \rho_{\text{iso}}(p)$ (without pre-processing, defined in Eq. 160) and $\nu(\alpha, \beta) = \rho_{\text{iso}}(p, \alpha, \beta)$ (with pre-processing, defined in Eq. 161) highlights the efficacy of pre-processing techniques in improving the performance of quantum communication systems. On the other hand, for different noise parameters, figures (b) and (d) illustrate that the use of pre-processing techniques extends the connective copies of states in quantum network from $N = 2$ copies to $N = 3$ copies. The generations of states $\rho_{\text{iso}}(p)$ and $\rho_{\text{iso}}(p, \alpha, \beta)$ are depicted in Fig. 21.

Remark IV.3. According to the results presented in Thm. IV.2, it is evident that the quantum network with pre-processing, which involves generating $\nu(\alpha, \beta)$ at each step, can perform better than the protocol that uses the initial state μ without pre-processing. Specifically, the resulting entanglement fidelity of the former protocol displays an exponential growth as the number of N increases.

Up to this point, our focus has been on examining the theoretical impact of pre-processing in quantum networks that utilize repeaters. Next, we will transition to conducting numerical experiments to further investigate this topic. In the first experiment, we examine the bipartite channel $\mathcal{E}(p, q)$ (see brown box of Fig. 21), which only contains a single noisy gate. Specifically, we consider $\mathcal{N}_1(p)$ as the amplitude damping channel (see Tab. I), i.e., $\mathcal{N}_1(p) = \mathcal{N}_{AD}(p)$, while at the same time $\mathcal{N}_2(q = 1) = \text{id}$. In this case, let us denote the state shared between parties as

$$\rho_{\text{iso}}(p) := \mathcal{T}_{\text{iso}, AB \rightarrow AB} \circ \mathcal{N}_{AD}(p)_{A \rightarrow A} \otimes \text{id}_{B \rightarrow B} \circ \text{CNOT}_{AB \rightarrow AB} \circ \text{H}_{A \rightarrow A} \otimes \text{id}_{B \rightarrow B} (|0\rangle\langle 0|_A \otimes |0\rangle\langle 0|_B). \quad (160)$$

By applying the pre-processing $U_1(\alpha) \otimes U_2(\beta)$, as defined in Eq. 85, to the systems, the shared state between the parties becomes

$$\rho_{\text{iso}}(p, \alpha, \beta) := \mathcal{T}_{\text{iso}, AB \rightarrow AB} \circ \mathcal{N}_{AD}(p)_{A \rightarrow A} \otimes \text{id}_{B \rightarrow B} \circ \text{CNOT}_{AB \rightarrow AB} \circ \text{H}_{A \rightarrow A} \otimes \text{id}_{B \rightarrow B} \left(\left(U_1(\alpha) |0\rangle\langle 0| U_1^\dagger(\alpha) \right)_A \otimes \left(U_2(\beta) |0\rangle\langle 0| U_2^\dagger(\beta) \right)_B \right). \quad (161)$$

To fully exploit the potential of the pre-processing technique, we aim to optimize all available values of α and β within the state $\rho_{\text{iso}}(p, \alpha, \beta)$.

Fig. 22 presents the results of our first numerical experiment with different parameters p , showcasing how the quantum network performs under varying copies in this scenario. In Fig. 22(a), we focus on the case, where the noise parameter of $\rho_{\text{iso}}(p)$ is $p = 0.38$, and assume that each $\rho_{\text{iso}}(0.38)$ can be used to teleport quantum information with length L . Our results demonstrate that without pre-processing, only one copy of $\rho_{\text{iso}}(0.38)$ can beat the classical limit, resulting in a communication distance of L . However, with pre-processing, even the connection of two copies, with a communication distance of $2L$, can outperform the classical bound of communication. Fig. 23 portrays a schematic diagram of the doubling of communication distance, which highlights the significant potential of pre-processing techniques for global quantum communication. We also observe a similar doubling effect in the case of $p = 0.4$, where the use of pre-processing techniques doubles the communication distance in transmitting quantum information, as shown in Fig. 22(c). This finding is particularly noteworthy as it demonstrates the robustness of pre-processing techniques across different noise regimes. In Fig. 22(b) and Fig. 22(d), we demonstrate that although we cannot double the communication distance, we can extend the connective copies of states in quantum network of Fig. 20 from 2 copies to 3 copies. This extension enables the realization of longer quantum communication channels, which is of critical importance in situations where the initial communication distance of each resource shared between parties is limited.

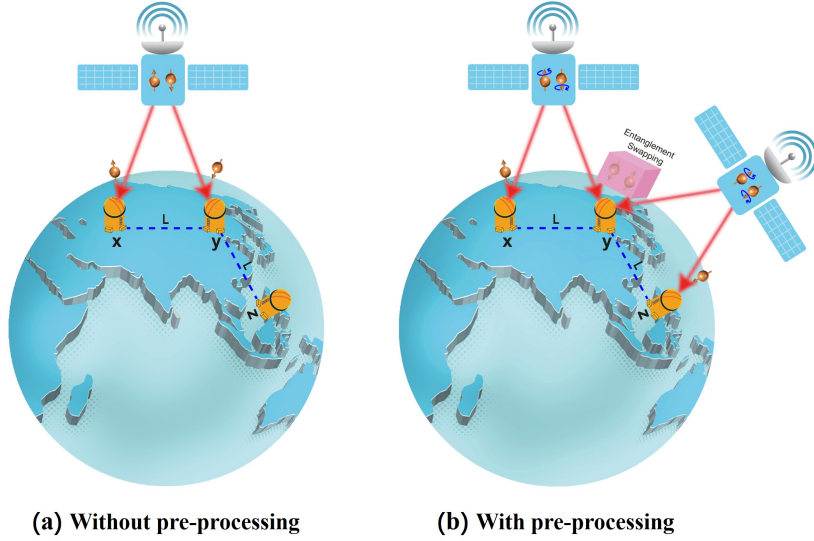


FIG. 23. (Color online) Doubling of communication distance by employing pre-processing techniques: Assuming a satellite distributes an entangled state $\rho_{\text{iso}}(0.38)$, as defined in Eq. 160, to two ground stations, labeled x and y , separated by a distance L , quantum communication with a performance superior to classical protocols can be demonstrated, as shown in (a). However, if an additional ground station z exists, located at the same distance L from y , information transmission from x to z via entanglement swapping at y cannot surpass the classical limit, as $0.6445 < 2/3$ (see Fig. 22(a)). Nevertheless, through the use of pre-processing techniques, it is possible to beat the classical limit without consuming additional resources, i.e., dynamical entanglement, in this protocol, as illustrated in (b). The phenomenon of doubled quantum communication distance is not limited to the entangled state $\rho_{\text{iso}}(0.38)$, as demonstrated by our results for states $\rho_{\text{iso}}(p)$ with $p = 0.4$ (see Fig. 22(c)) and $\rho(p, \alpha, \beta)$ with $p = 0.38$ (see Fig. 25(a)) and $p = 0.4$ (see Fig. 25(c)).

Remark IV.4. Our lemma, denoted as Lem. IV.1, establishes a crucial link between the shared noisy singlet states among communication nodes and the overall performance of quantum repeaters. However, the practical application of the commonly employed noisy bipartite channel $\mathcal{E}(p, q)$, including the generations of state ρ_b in Eq. 103 and state $\rho_e(\alpha, \beta)$ in Eq. 104, to the context of quantum repeater protocols is inherently constrained by its inability to generate the desired noisy singlet states. Consequently, a pivotal gap emerges, demanding a novel approach to bridge it. This void is skillfully filled through the ingenious application of isotropic twirling Def. I.8, a ubiquitous and efficient tool employed in the domain of entanglement theory. By leveraging isotropic twirling, we accomplish the transformation of any input state into a noisy singlet, as eloquently highlighted by our profound theorem, denoted as Theorem I.10. This masterful technique rectifies the previous deficiency while meticulously preserving the delicate degree of entanglement intrinsic to the system. After applying the isotropic twirling \mathcal{T}_{iso} , we transform the states ρ_b and $\rho_e(\alpha, \beta)$ into the forms of $\mu := \mathcal{T}_{\text{iso}}(\rho_b)$ (see Eq. 152) and $\nu(\alpha, \beta) := \mathcal{T}_{\text{iso}}(\rho_e(\alpha, \beta))$ (see Eq. 153), respectively. The undeniable elegance inherent in the twirling channel empowers us to establish a comprehensive framework for quantifying entanglement between any two nodes within quantum repeaters endowed with distributed entanglement. Moreover, our analysis unearths a

profound correlation between entanglement fidelity shared between nodes and the overall performance, enriching our understanding of the intricate interplay between these fundamental concepts.

However, we must confront the formidable challenge posed by the practical implementation of the isotropic twirling \mathcal{T}_{iso} , as articulated by Eq. 27.

$$\mathcal{T}_{\text{iso}}(\cdot) := \int dU U \otimes \bar{U} \cdot U^\dagger \otimes U^{\text{T}}. \quad (162)$$

This formulation necessitates the intricate computation of an integral over the unitary group, rendering the ideal isotropic twirling an arduous feat requiring an infinite number of unitary operations acting upon the input states. These theoretical reflections inevitably propel us towards a critical inquiry: can twirling channels, imbued with such remarkable potential, be effectively harnessed within practical quantum network scenarios? This question assumes paramount importance given the inevitable constraints imposed by the limited repertoire of operations available within real-world quantum networks. In the ensuing analysis, we embark on a numerical exploration of this concern and reveal a remarkable outcome: even with a finite set of randomly generated unitary operations, we can achieve a high-fidelity approximation of the ideal isotropic twirling. To accomplish this, we introduce the following quantum channel for consideration.

$$\mathcal{T}_{\text{iso,app}}(\cdot) := \frac{1}{M} \sum_{i=1}^M U_i \otimes \bar{U}_i \cdot U_i^\dagger \otimes U_i^{\text{T}}. \quad (163)$$

Here M symbolizes the count of randomly generated unitaries taken into account during the analysis. In our numerical analysis, we generate M unitaries using the “RandomUnitary” function available in QETLAB (Quantum Entanglement Theory LABoratory). Notably, when M approaches infinity, the channel $\mathcal{T}_{\text{iso,app}}$ perfectly approximates the ideal isotropic twirling \mathcal{T}_{iso} . To assess the impact of $\mathcal{T}_{\text{iso,app}}$, we employ the Uhlmann fidelity F_U as a metric to quantify the degree of similarity. This is given by

$$F_U(\mathcal{T}_{\text{iso,app}}(\rho), \mathcal{T}_{\text{iso}}(\rho)) = \left(\text{Tr} \left[\sqrt{\sqrt{\mathcal{T}_{\text{iso,app}}(\rho)} \mathcal{T}_{\text{iso}}(\rho) \sqrt{\mathcal{T}_{\text{iso,app}}(\rho)}} \right] \right)^2. \quad (164)$$

In this investigation, we numerically examine two distinct scenarios, namely when ρ corresponds to ρ_b (without pre-processing) or $\rho_e(\alpha, \beta)$ (with pre-processing). Our pivotal query revolves around ascertaining the minimal number of randomly generated unitaries necessary to surpass an exacting performance threshold of 99.5%, namely

$$F_U(\mathcal{T}_{\text{iso,app}}(\rho), \mathcal{T}_{\text{iso}}(\rho)) \geq 0.995. \quad (165)$$

Should it be $M \geq 100$, $M \geq 1000$, or even $M \geq 10000$? In this work, we present compelling evidence that a mere $M \geq 20$ random unitaries, employed within Eq. 163, yield unequivocally satisfactory results for the cases investigated, as illustrated in Fig. 24. Hence, the results of our investigation establish the remarkable efficiency and effectiveness of approximating the isotropic twirling \mathcal{T}_{iso} through the utilization of $\mathcal{T}_{\text{iso,app}}$.

Furthermore, the comprehensive analysis depicted in Fig. 24 unveils a remarkable correlation between the accuracy of the numerical simulations, i.e., $F_U(\mathcal{T}_{\text{iso,app}}(\rho), \mathcal{T}_{\text{iso}}(\rho))$, and the parameter p in the noise models. Notably, as the value of p increases, the simulation accuracy consistently improves, while still allowing for appropriate fluctuations. This observation bears profound significance, as the parameter p directly influences the extent to which the noise channel impacts the entanglement shared between the communication nodes in quantum repeater protocols. By selecting a higher value of p , we effectively enhance the entanglement fidelity of the resulting quantum state. Based on this crucial finding, we put forth a compelling conjecture: the entanglement fidelity of the bipartite state shared between the sender and receiver plays a pivotal role in determining the number of random unitary samples necessary to achieve a desired level of simulation accuracy. Intriguingly, our conjecture suggests an inverse relationship between the entanglement fidelity of the bipartite state shared between the sender and receiver and the computational demands of accurate simulations. In essence, when the bipartite state shared between the sender and receiver exhibits higher entanglement fidelity, fewer random matrix samples are required to attain the desired level of simulation accuracy. Ultimately, these findings contribute to a deeper understanding of entanglement dynamics in the presence of noise.

In our previous discussions, we focused on the cases where the bipartite state shared between parties is subject to an isotropic twirling (colored pink in Fig. 21), as discussed in Thm. IV.2 and our first numerical experiment (see Fig. 22). Although this assumption has simplified our analysis and provided a general formula for N copies in quantum repeater protocols (see Fig. 20), it's important to note that the benefits of using pre-processing are not limited to this scenario. We now move on to investigating a different noise model and exploring the advantages of pre-processing. In

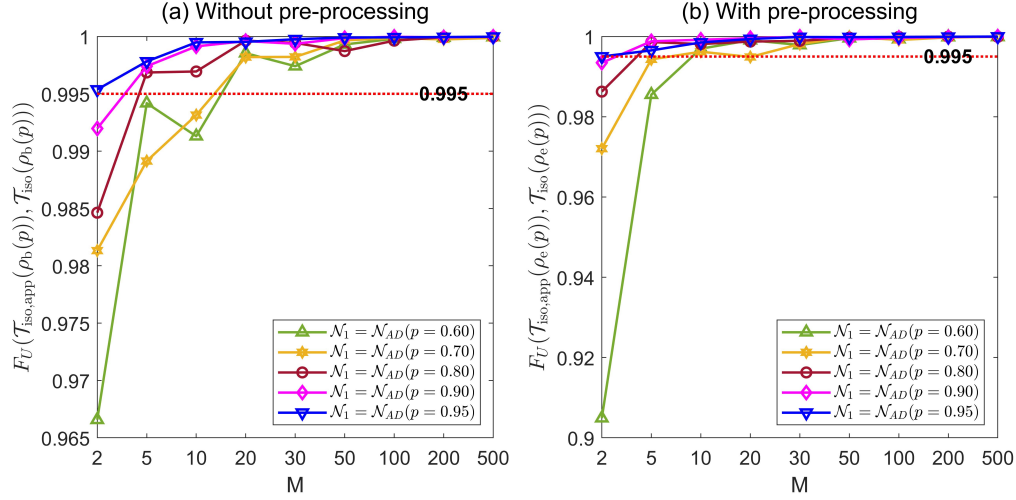


FIG. 24. (Color online) Comparison of $F_U(\mathcal{T}_{\text{iso,app}}(\rho), \mathcal{T}_{\text{iso}}(\rho))$ (see Eq. 164) with respect to varying numbers of random unitaries M (see Eq. 163): Figure (a) illustrates the comparison for different noisy parameter p when considering the case $\rho = \rho_b$. Figure (b) explores the analogous scenario for the case $\rho = \rho_e(\alpha, \beta)$. The amplitude damping channel $\mathcal{N}_1(p) = \mathcal{N}_{\text{AD}}(p)$ (with $p \in \{0.60, 0.70, 0.80, 0.90, 0.95\}$) is employed, while \mathcal{N}_2 is set as the identity channel $\mathcal{N}_2 = \text{id}$ (see Fig. 21).

particular, we direct our attention towards the state acting on the subspace that is spanned by six operators; that are $|00\rangle\langle 00|$, $|00\rangle\langle 11|$, $|11\rangle\langle 00|$, $|11\rangle\langle 11|$, $|01\rangle\langle 01|$, and $|10\rangle\langle 10|$. Our aim is to present a general formula for the entanglement fidelity between two distinct quantum states subjected to this specific noise model. Additionally, we provide numerical evidences that pre-processing techniques confer benefits. To begin with, let us introduce the following lemma.

Lemma IV.3: Concentrating States of Eq. 166 Through Entanglement Swapping

Consider two distinct quantum systems AC and CB and let ρ_{AC} and σ_{CB} be two special quantum states that act on these systems, respectively. In particular, we make the assumption that ρ and σ have the following mathematical form:

$$\rho_{AC} = x_1 |00\rangle\langle 00| + x_2 |00\rangle\langle 11| + x_3 |11\rangle\langle 00| + x_4 |11\rangle\langle 11| + x_5 |01\rangle\langle 01| + x_6 |10\rangle\langle 10|, \quad (166)$$

$$\sigma_{CB} = y_1 |00\rangle\langle 00| + y_2 |00\rangle\langle 11| + y_3 |11\rangle\langle 00| + y_4 |11\rangle\langle 11| + y_5 |01\rangle\langle 01| + y_6 |10\rangle\langle 10|. \quad (167)$$

By performing entanglement swapping (as depicted in Fig. 20) on system C , we can create an entangled state τ between the nodes A and B that is a composite of the two initial states ρ and σ . Denote τ as

$$\tau = z_1 |00\rangle\langle 00| + z_2 |00\rangle\langle 11| + z_3 |11\rangle\langle 00| + z_4 |11\rangle\langle 11| + z_5 |01\rangle\langle 01| + z_6 |10\rangle\langle 10|. \quad (168)$$

Then, the coefficients connecting these three states, i.e., ρ , σ , and τ , can be determined using the following equations

$$z_1 = x_1(y_1 + y_4) + x_5(y_5 + y_6), \quad (169)$$

$$z_2 = x_2(y_2 + y_3), \quad (170)$$

$$z_3 = x_3(y_2 + y_3), \quad (171)$$

$$z_4 = x_4(y_1 + y_4) + x_6(y_5 + y_6), \quad (172)$$

$$z_5 = x_1(y_5 + y_6) + x_5(y_1 + y_4), \quad (173)$$

$$z_6 = x_4(y_5 + y_6) + x_6(y_1 + y_4). \quad (174)$$

In repeater-based communication protocols, the quantum systems A and B typically correspond to the sender and receiver of quantum information, respectively, while the system C represents an intermediate node that serves as a relay for the quantum information.

Proof. Entanglement swapping, a critical technique for achieving long-range quantum communication, involves the transfer of entanglement between two physically separated particles without direct interaction between them. As shown in Fig. 20, the protocol typically comprises two steps: First, a Bell measurement is performed on system C of the joint state $\rho_{AC} \otimes \sigma_{CB}$; Second, a unitary operation is applied to the system B to correct its quantum state, resulting in the creation of an entangled pair τ_{AB} shared by particles A and B .

To describe these steps mathematically, we consider the following decomposition of the initial state $\rho \otimes \sigma$.

$$\rho \otimes \sigma = x_1 \left(y_1 |0000\rangle\langle 0000| + y_2 |0000\rangle\langle 0011| + y_3 |0011\rangle\langle 0000| + y_4 |0011\rangle\langle 0011| + y_5 |0001\rangle\langle 0001| + y_6 |0010\rangle\langle 0010| \right) \quad (175)$$

$$+ x_2 \left(y_1 |0000\rangle\langle 1100| + y_2 |0000\rangle\langle 1111| + y_3 |0011\rangle\langle 1100| + y_4 |0011\rangle\langle 1111| + y_5 |0001\rangle\langle 1101| + y_6 |0010\rangle\langle 1110| \right) \quad (176)$$

$$+ x_3 \left(y_1 |1100\rangle\langle 0000| + y_2 |1100\rangle\langle 0011| + y_3 |1111\rangle\langle 0000| + y_4 |1111\rangle\langle 0011| + y_5 |1101\rangle\langle 0001| + y_6 |1110\rangle\langle 0010| \right) \quad (177)$$

$$+ x_4 \left(y_1 |1100\rangle\langle 1100| + y_2 |1100\rangle\langle 1111| + y_3 |1111\rangle\langle 1100| + y_4 |1111\rangle\langle 1111| + y_5 |1101\rangle\langle 1101| + y_6 |1110\rangle\langle 1110| \right) \quad (178)$$

$$+ x_5 \left(y_1 |0100\rangle\langle 0100| + y_2 |0100\rangle\langle 0111| + y_3 |0111\rangle\langle 0100| + y_4 |0111\rangle\langle 0111| + y_5 |0101\rangle\langle 0101| + y_6 |0110\rangle\langle 0110| \right) \quad (179)$$

$$+ x_6 \left(y_1 |1000\rangle\langle 1000| + y_2 |1000\rangle\langle 1011| + y_3 |1011\rangle\langle 1000| + y_4 |1011\rangle\langle 1011| + y_5 |1001\rangle\langle 1001| + y_6 |1010\rangle\langle 1010| \right). \quad (180)$$

Here, we safely omit the subscripts since they are self-evident from the context. Upon performing a Bell measurement $|\phi_{ij}\rangle := \mathbb{1} \otimes X^j Z^i |\phi^+\rangle$ with $i, j \in \{0, 1\}$, the joint state transforms into

$$\frac{(\mathbb{1}_A \otimes |\phi_{ij}\rangle\langle \phi_{ij}|_{CC} \otimes \mathbb{1}_B) (\rho_{AC} \otimes \sigma_{CB}) (\mathbb{1}_A \otimes |\phi_{ij}\rangle\langle \phi_{ij}|_{CC} \otimes \mathbb{1}_B)}{p_{ij}}. \quad (181)$$

In this expression, $p_{ij} := \text{Tr}[(\mathbb{1}_A \otimes |\phi_{ij}\rangle\langle \phi_{ij}|_{CC} \otimes \mathbb{1}_B) (\rho_{AC} \otimes \sigma_{CB}) (\mathbb{1}_A \otimes |\phi_{ij}\rangle\langle \phi_{ij}|_{CC} \otimes \mathbb{1}_B)]$ represents the probability of obtaining classical outcomes (i, j) . After tracing out system C from the numerator of Eq. 181, we denote the resulting (unnormalized) state as τ_{ij} , giving us

$$\tau_{00} = \frac{1}{2} \left[(x_1 y_1 + x_5 y_6) |00\rangle\langle 00| + x_2 y_2 |00\rangle\langle 11| + x_3 y_3 |11\rangle\langle 00| + (x_4 y_4 + x_6 y_5) |11\rangle\langle 11| + (x_1 y_5 + x_5 y_4) |01\rangle\langle 01| \right. \\ \left. + (x_4 y_6 + x_6 y_1) |10\rangle\langle 10| \right], \quad (182)$$

$$\tau_{01} = \frac{1}{2} \left[(x_1 y_4 + x_5 y_5) |01\rangle\langle 01| + x_2 y_3 |01\rangle\langle 10| + x_3 y_2 |10\rangle\langle 01| + (x_4 y_1 + x_6 y_6) |10\rangle\langle 10| + (x_1 y_6 + x_5 y_1) |00\rangle\langle 00| \right. \\ \left. + (x_4 y_5 + x_6 y_4) |11\rangle\langle 11| \right], \quad (183)$$

$$\tau_{10} = \frac{1}{2} \left[(x_1 y_1 + x_5 y_6) |00\rangle\langle 00| - x_2 y_2 |00\rangle\langle 11| - x_3 y_3 |11\rangle\langle 00| + (x_4 y_4 + x_6 y_5) |11\rangle\langle 11| + (x_1 y_5 + x_5 y_4) |01\rangle\langle 01| \right. \\ \left. + (x_4 y_6 + x_6 y_1) |10\rangle\langle 10| \right], \quad (184)$$

$$\tau_{11} = \frac{1}{2} \left[(x_1 y_4 + x_5 y_5) |01\rangle\langle 01| - x_2 y_3 |01\rangle\langle 10| - x_3 y_2 |10\rangle\langle 01| + (x_4 y_1 + x_6 y_6) |10\rangle\langle 10| + (x_1 y_6 + x_5 y_1) |00\rangle\langle 00| \right. \\ \left. + (x_4 y_5 + x_6 y_4) |11\rangle\langle 11| \right]. \quad (185)$$

Applying the unitary operation $X^j Z^i$ to system B results in the following expression for the entangled state acting on systems A and B .

$$(\mathbb{1} \otimes X^j Z^i) \cdot \frac{\tau_{ij}}{p_{ij}} \cdot (\mathbb{1} \otimes Z^i X^j). \quad (186)$$

Accordingly, the entangled state τ_{AB} obtained by performing entanglement swapping becomes

$$\tau = \sum_{ij} p_{ij} (\mathbb{1} \otimes X^j Z^i) \cdot \frac{\tau_{ij}}{p_{ij}} \cdot (\mathbb{1} \otimes Z^i X^j) \quad (187)$$

$$= \sum_{ij} (\mathbb{1} \otimes X^j Z^i) \cdot \tau_{ij} \cdot (\mathbb{1} \otimes Z^i X^j) \quad (188)$$

$$= (x_1(y_1 + y_4) + x_5(y_5 + y_6)) |00\rangle\langle 00| + (x_4(y_1 + y_4) + x_6(y_5 + y_6)) |11\rangle\langle 11| + x_2(y_2 + y_3) |00\rangle\langle 11| \quad (189)$$

$$+ (x_1(y_5 + y_6) + x_5(y_1 + y_4)) |01\rangle\langle 01| + (x_4(y_5 + y_6) + x_6(y_1 + y_4)) |10\rangle\langle 10| + x_3(y_2 + y_3) |11\rangle\langle 00|, \quad (190)$$

which concludes the proof. \square

We will focus specifically on the case where the resourceful state shared between nodes is represented as ρ_b (that is, in Fig. 20, ρ has been substituted with ρ_b), which is defined in Eq. 103 with $\mathcal{N}_1(p)$ being the amplitude damping channel (i.e., $\mathcal{N}_1(p) = \mathcal{N}_{AD}(p)$), and where we assume that $\mathcal{N}_2(q = 1) = \text{id}$. Namely, we have eliminated the isotropic twirling in μ and $\nu(\alpha, \beta)$ (see Fig. 21). For this scenario, the initial state (see Eq. 160) shared between the nodes is given by

$$\rho(p) := \mathcal{N}_{AD}(p)_{A \rightarrow A} \otimes \text{id}_{B \rightarrow B} \circ \text{CNOT}_{AB \rightarrow AB} \circ \text{H}_{A \rightarrow A} \otimes \text{id}_{B \rightarrow B} (|0\rangle\langle 0|_A \otimes |0\rangle\langle 0|_B) \quad (191)$$

$$= \frac{1}{2} (|00\rangle\langle 00| + \sqrt{p} |00\rangle\langle 11| + \sqrt{p} |11\rangle\langle 00| + p |11\rangle\langle 11| + (1 - p) |01\rangle\langle 01|). \quad (192)$$

For a single-copy of the initial state $\rho(p)$, the relationship between the noisy parameter p and entanglement fidelity F_1 , defined as F (i.e., $F_1 := F$), can be accurately characterized by the following formula.

$$F_1(\rho(p)) := F(\rho(p)) = \frac{1}{4} (1 + \sqrt{p})^2. \quad (193)$$

Our foremost objective is to construct a quantum network that employs $\rho(p)$ considered in Eq. 192 as the entangled resource, with the aim of demonstrating the benefits of pre-processing in quantum network communication. To assess the effectiveness of these resources, we will measure the entanglement fidelity $F_N(\rho(p))$ of the resultant state that arises from concentrating N copies of $\rho(p)$ under entanglement swapping, as shown in Fig. 20. Mathematically, the performance of employing $\rho(p)$ in quantum network communication is characterized by the following theorem.

Theorem IV.4: Performance of Quantum Network with State of Eq. 192

By entanglement swapping N adjacent pairs of quantum states $\rho(p)$ (defined in Eq. 192) in a quantum network (illustrated in Fig. 20), a new pair, denoted by $\rho_N(p)$, can be generated in the form of

$$\rho_N(p) = \frac{1}{4} \left((2 - p + p^N) |00\rangle\langle 00| + 2p^{\frac{N}{2}} |00\rangle\langle 11| + 2p^{\frac{N}{2}} |11\rangle\langle 00| + (p + p^N) |11\rangle\langle 11| + (2 - p - p^N) |01\rangle\langle 01| \right. \\ \left. + (p - p^N) |10\rangle\langle 10| \right), \quad (194)$$

whose performance, as measured by its entanglement fidelity, is determined by

$$F_N(\rho(p)) := F(\rho_N(p)) = \frac{1}{4} (1 + p^{\frac{N}{2}})^2. \quad (195)$$

Utilizing the relationship established in Eq. 193, the expression linking the entanglement fidelity of $\rho_N(p)$ to the initial state $\rho(p)$ shared between parties can be derived as

$$F_N(\rho(p)) = \frac{1}{4} \left(1 + \left(2\sqrt{F_1(\rho(p))} - 1 \right)^N \right)^2. \quad (196)$$

Proof. By taking $\rho = \sigma = \rho(p)$ in Lem. IV.3, we can readily obtain $\rho_2(p)$, which is given by

$$\rho_2(p) = \frac{1}{4} \left((2 - p + p^2) |00\rangle\langle 00| + 2p |00\rangle\langle 11| + 2p |11\rangle\langle 00| + (p + p^2) |11\rangle\langle 11| + (2 - p - p^2) |01\rangle\langle 01| + (p - p^2) |10\rangle\langle 10| \right). \quad (197)$$

The following expression for the entanglement fidelity can be obtained by explicitly writing out its form

$$F_2(\rho(p)) = \frac{1}{4} (1 + p)^2. \quad (198)$$

We will use mathematical induction to prove the validity of the expression for the general case of N . Assuming the validity of Eq. 194 for $N - 1$, which states that

$$\rho_{N-1}(p) = \frac{1}{4} \left((2 - p + p^{N-1}) |00\rangle\langle 00| + 2p^{\frac{N-1}{2}} |00\rangle\langle 11| + 2p^{\frac{N-1}{2}} |11\rangle\langle 00| + (p + p^{N-1}) |11\rangle\langle 11| + (2 - p - p^{N-1}) |01\rangle\langle 01| + (p - p^{N-1}) |10\rangle\langle 10| \right). \quad (199)$$

Applying Lem. IV.3 once again by setting $\rho = \rho_{N-1}(p)$ and $\sigma = \rho(p)$, we can derive the general form of $\rho_N(p)$

$$\rho_N(p) = z_1 |00\rangle\langle 00| + z_2 |00\rangle\langle 11| + z_3 |11\rangle\langle 00| + z_4 |11\rangle\langle 11| + z_5 |01\rangle\langle 01| + z_6 |10\rangle\langle 10| \quad (200)$$

with the following coefficients

$$z_1 = \frac{1}{4} (2 - p + p^{N-1}), \quad z_2 = \frac{1}{2} p^{\frac{N-1}{2}}, \quad z_3 = \frac{1}{2} p^{\frac{N-1}{2}}, \quad (201)$$

$$z_4 = \frac{1}{4} (p + p^{N-1}), \quad z_5 = \frac{1}{4} (2 - p - p^{N-1}), \quad z_6 = \frac{1}{4} (p - p^{N-1}), \quad (202)$$

as required. The expressions in Eq. 195 and Eq. 196 follow straightforwardly from Eq. 194, thus concluding the proof. \square

Turning to the examination of pre-processing effects, it is crucial to emphasize that our objective is not to provide an analytic formula for pre-processing in general. In other words, we are not going to demonstrate the all-encompassing formula of F_N for the state $\rho(p, \alpha, \beta)$ obtained by applying $U_1(\alpha) \otimes U_2(\beta)$, as defined in Eq. 85.

$$\rho(p, \alpha, \beta) := \mathcal{N}_{\text{AD}}(p)_{A \rightarrow A} \otimes \text{id}_{B \rightarrow B} \circ \text{CNOT}_{AB \rightarrow AB} \circ \text{H}_{A \rightarrow A} \otimes \text{id}_{B \rightarrow B} \left(\left(U_1(\alpha) |0\rangle\langle 0| U_1^\dagger(\alpha) \right)_A \otimes \left(U_2(\beta) |0\rangle\langle 0| U_2^\dagger(\beta) \right)_B \right). \quad (203)$$

Rather, we center our attention on a particular form of $U_1(\alpha) \otimes U_2(\beta)$ with $\beta = 0$, namely $U_1(\alpha) \otimes \mathbb{1}$, that produces relatively straightforward outcomes. This approach proves sufficient for observing the influence of pre-processing and deriving critical insights. In this case, the bipartite state that is shared between the parties is given by

$$\rho(p, \alpha) := \rho(p, \alpha, 0) = \frac{1}{2} \left(a^2 |00\rangle\langle 00| + ab\sqrt{p} |00\rangle\langle 11| + ab\sqrt{p} |11\rangle\langle 00| + b^2 p |11\rangle\langle 11| + b^2 (1 - p) |01\rangle\langle 01| \right). \quad (204)$$

Here, the parameters a and b within the coefficients take on the following forms:

$$a := \cos \frac{\alpha}{2} + \sin \frac{\alpha}{2}, \quad (205)$$

$$b := \cos \frac{\alpha}{2} - \sin \frac{\alpha}{2}. \quad (206)$$

The entanglement fidelity $F_N(\rho(p, \alpha))$ of the resulting state that emerges from concentrating N copies of $\rho(p, \alpha)$ (see Eq. 204) via entanglement swapping, depicted in Fig. 20, is determined by the following theorem.

Theorem IV.5: Performance of Quantum Network with State of Eq. 204

Through the process of entanglement swapping, N neighboring pairs of states $\rho(p, \alpha)$ (as defined in Eq.204) within a quantum network (depicted in Fig. 20) can produce a new pair, denoted as $\rho_N(p, \alpha)$, in the following form

$$\rho_N(p, \alpha) = \frac{1}{2^N} \left(w_{N,1} |00\rangle\langle 00| + w_{N,2} |00\rangle\langle 11| + w_{N,3} |11\rangle\langle 00| + w_{N,4} |11\rangle\langle 11| + w_{N,5} |01\rangle\langle 01| + w_{N,6} |10\rangle\langle 10| \right), \quad (207)$$

where the coefficients $w_{N,i}$ ($N \geq 2, i \in \{1, \dots, 6\}$) are described by the following recursive formula

$$w_{N,1} := (a^2 + b^2 p) w_{N-1,1} + b^2 (1-p) w_{N-1,5}, \quad (208)$$

$$w_{N,2} := (2ab\sqrt{p}) w_{N-1,2}, \quad (209)$$

$$w_{N,3} := (2ab\sqrt{p}) w_{N-1,3}, \quad (210)$$

$$w_{N,4} := (a^2 + b^2 p) w_{N-1,4} + b^2 (1-p) w_{N-1,6}, \quad (211)$$

$$w_{N,5} := b^2 (1-p) w_{N-1,1} + (a^2 + b^2 p) w_{N-1,5}, \quad (212)$$

$$w_{N,6} := b^2 (1-p) w_{N-1,4} + (a^2 + b^2 p) w_{N-1,6}. \quad (213)$$

In the case where $N = 1$, we have

$$w_{1,1} = a^2, \quad (214)$$

$$w_{1,2} = ab\sqrt{p}, \quad (215)$$

$$w_{1,3} = ab\sqrt{p}, \quad (216)$$

$$w_{1,4} = b^2 p, \quad (217)$$

$$w_{1,5} = b^2 (1-p), \quad (218)$$

$$w_{1,6} = 0, \quad (219)$$

which denote the coefficients (up to $1/2$) of $\rho_N(p, \alpha)$. The performance of $\rho_N(p, \alpha)$ in quantum network communication, as evaluated by its entanglement fidelity, is determined using the following equation

$$F_N(\rho(p, \alpha)) := F(\rho_N(p, \alpha)) = \frac{1}{2^{N+1}} (w_{N,1} + w_{N,2} + w_{N,3} + w_{N,4}). \quad (220)$$

Remark IV.5. Given that the proof of the aforementioned Theorem IV.5 is an immediate consequence of Lemma IV.3, a detailed proof is omitted here. The entanglement fidelity F_N of the state $\rho(p, \alpha)$ for $N = 1, 2, 3$ is expressed by the following formulas.

$$F_1(\rho(p, \alpha)) := F(\rho(p, \alpha)) = \frac{1}{4} (a + b\sqrt{p})^2, \quad (221)$$

$$F_2(\rho(p, \alpha)) := F(\rho_2(p, \alpha)) = \frac{1}{8} (a^4 + b^4 + (6a^2b^2 - 2b^4)p + 2b^4p^2), \quad (222)$$

$$F_3(\rho(p, \alpha)) := F(\rho_3(p, \alpha)) = \frac{1}{16} (a^6 + 3a^2b^4 + (3a^4b^2 - 6a^2b^4 + 3b^6)p + 8a^3b^3p\sqrt{p} + (6a^2b^4 - 6b^6)p^2 + 4b^6p^3). \quad (223)$$

These formulas can be used to plot the yellow, currant, and green lines in Fig. 26.

Remark IV.6. Even for bipartite qubit systems, calculating the entanglement fidelity F_N of the state obtained by entanglement swapping N adjacent pairs of an arbitrary state ρ in a quantum network, as depicted in Fig. 20, presents a challenging problem that goes beyond the scope of this work. This calculation requires some techniques and a deep understanding of the underlying structures, and as such, it remains an open problem that warrants further investigation in future researchs.

In addition to theoretical developments, we turn our attention to numerical experiments related to the state $\rho(p, \alpha, \beta)$ (defined in Eq. 203) in the context of quantum network communication. Specifically, we perform numerical experiments by scanning over all possible values of α and β in the pre-processing of form $U_1(\alpha) \otimes U_2(\beta)$. In Fig. 25(a) and Fig. 25(c),

we demonstrate how our pre-processing techniques can double the communication distance when transmitting quantum information, similar to the data investigated in Fig. 22. However, in Fig. 25(b) and Fig. 25(d), we show that doubling the communication distance is not always feasible. Nevertheless, the pre-processing techniques can still increase the number of connective copies of states in the quantum network of Fig. 20 from 2 to 3.

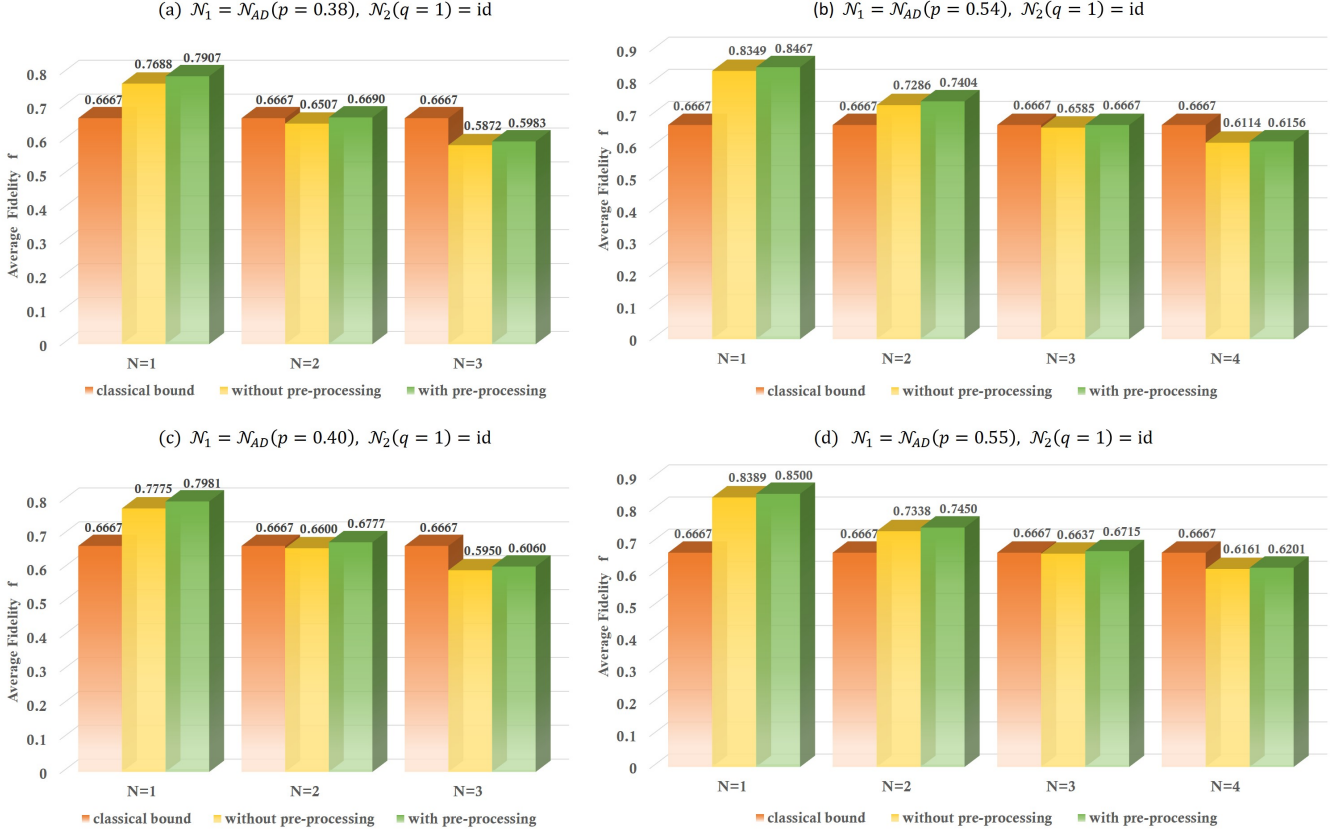


FIG. 25. (Color online) Enhancing the efficiency of quantum network communication by employing pre-processing techniques. Specifically, figures (a) and (c) show a doubling effect in the communication distance achieved with pre-processing compared to without pre-processing, as evidenced by the comparison between states $\rho(p)$ (defined in Eq. 192) and $\rho(p, \alpha, \beta)$ (defined in Eq. 203). Moreover, our numerical experiments indicate that pre-processing techniques enable the extension of connective copies of states in quantum networks from $N = 2$ to $N = 3$, as illustrated in figures (b) and (d) for different noise parameters.

Through these numerical experiments (see Fig. 22 and Fig. 25), our findings have exhibited the capability of pre-processing-assisted quantum network communication to increase the number of connective copies of states, thereby enhancing the distance of communication. Building on this, we now move on to proposing a comprehensive investigation of the efficacy of pre-processing techniques. Specifically, we will explore the impact of various parametric values of pre-processing, namely α and β , on the performance of quantum network communication for the noise model considered in Fig. 25(c) – $\mathcal{N}_1 = \mathcal{N}_{AD}(p = 0.4)$ and $\mathcal{N}_2 = \text{id}$. Fig. 26 showcases a detailed comparison between various parametric values of $U_1(\alpha) \otimes U_2(\beta)$ in pre-processing, shedding light on their respective impacts on the performance of the system.

The quantum network communication model considered in Lem. IV.1 tells us that higher entanglement fidelity of the initial state shared between parties, denoted by F_1 , leads to better performance in network communication when connecting N copies. Mathematically, it is equivalent to say that if we have two noisy singlets ρ and σ satisfying

$$F_1(\rho) := F(\rho) \geq F_1(\sigma) := F(\sigma), \quad (224)$$

then the entanglement fidelities obtained by connecting N copies of ρ and σ through entanglement swapping (see Fig. 20) meet the following inequality

$$F_N(\rho) := F(\rho_N) \geq F_N(\sigma) := F(\sigma_N), \quad (225)$$

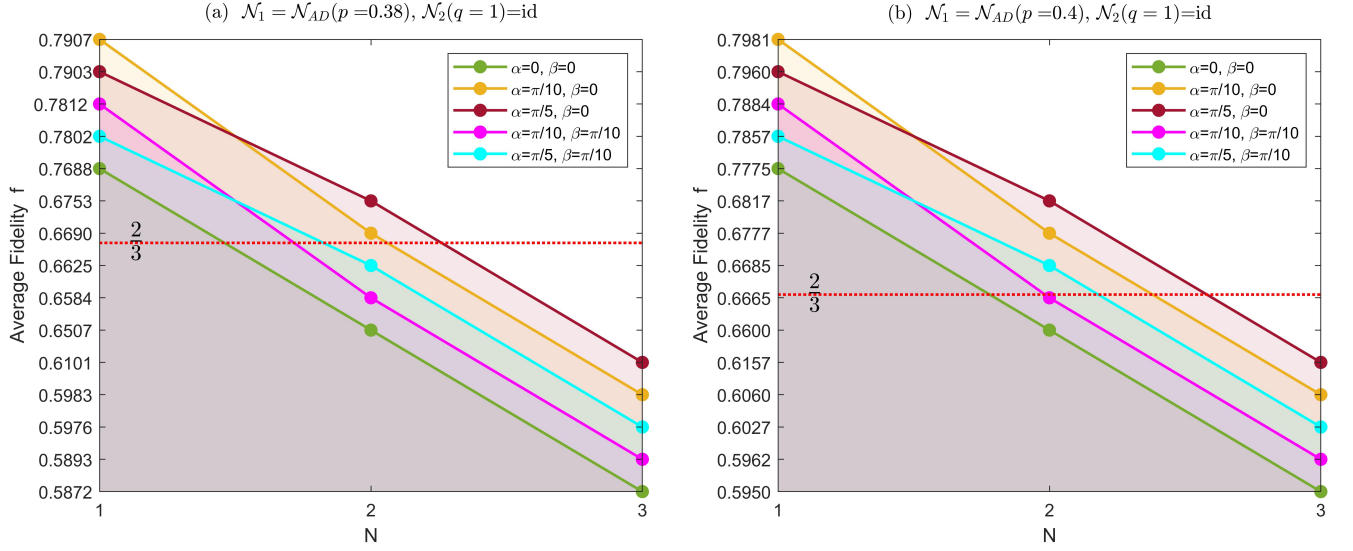


FIG. 26. (Color online) Comparison of the average fidelities f_N obtained by connecting N copies of $\rho(p, \alpha, \beta)$, defined in Eq. 203, through entanglement swapping with $\mathcal{N}_1 = \mathcal{N}_{AD}(p)$ and $\mathcal{N}_2 = \text{id}$. Specifically, figure (a) demonstrates the obtained results for $p = 0.38$, while figure (b) illustrates the case of $p = 0.40$.

due to the result of Eq. 132. Here, ρ_N denotes the entangled state resulting from the tensor product of N identical copies of ρ , followed by entanglement swapping. A similar definition holds for σ_N . Subsec. IIIB clarifies that the entangled states ρ_N and σ_N can be employed to construct teleportation channels, namely $\mathcal{F}(\rho_N)$ and $\mathcal{F}(\sigma_N)$. The process of constructing these channels is depicted in Figure 11, and their mathematical definition is given by Equation 101. Thanks to Lem. I.12 and Lem. III.1, we have

$$f_N(\rho) := f(\mathcal{F}(\rho_N)) = \frac{dF_N(\rho) + 1}{d + 1}, \quad (226)$$

where $f_N(\rho)$ denotes the average fidelity of teleportation channel $\mathcal{F}(\rho_N)$ obtained by connecting N copies of bipartite state ρ through entanglement swapping and implementing Θ_0^{post} on the message, sender, and receiver system. Then the monotonicity property of F_N suggests that there is a direct correlation between the quality of the shared entanglement and the efficiency of quantum communication. Expressing the results in terms of average fidelity, Eq. 225 indicates that

$$f_N(\rho) \geq f_N(\sigma). \quad (227)$$

It is natural to inquire whether the monotonicity property of entanglement fidelity holds for general quantum states beyond the noisy singlet? In other words, can we expect that higher entanglement fidelity of the initial state shared between parties always leads to better performance in quantum network communication when connecting multiple copies, regardless of the specific structure of quantum state in question? This question is of great interest and importance for the field of quantum communication, as it has significant implications for the development and optimization of repeater-based quantum network communication protocols. Based on the data presented in Fig. 26, we can confidently conclude that the answer to the aforementioned question is simply negative! For state $\rho(p, \alpha, \beta)$ (see Eq. 203) with $\mathcal{N}_1 = \mathcal{N}_{AD}(p = 0.38)$ and $\mathcal{N}_2 = \text{id}$, we have

$$f_1(\rho(0.38, \frac{\pi}{10}, 0)) \approx 0.7907 > f_1(\rho(0.38, \frac{\pi}{5}, 0)) \approx 0.7903. \quad (228)$$

Upon connecting two copies of the quantum states, we observe a reverse direction of Eq. 228. Specifically, we find that the entanglement fidelity of the resulting state after connecting two copies in one case can be lower than the entanglement fidelity of the other case, even though the opposite was true for the initial states; that is

$$f_2(\rho(0.38, \frac{\pi}{10}, 0)) \approx 0.6690 < f_2(\rho(0.38, \frac{\pi}{5}, 0)) \approx 0.6753. \quad (229)$$

In Fig. 26, the data related to states with $(\alpha, \beta) = (\frac{\pi}{10}, 0)$ and $(\alpha, \beta) = (\frac{\pi}{5}, 0)$ are represented by yellow and currant lines, respectively. The comparison of Eq. 228 and Eq. 229 reveals that the relationship between a single copy and the

multiple copies of quantum states in quantum network communication is complex and non-monotonic, which poses a significant challenge to the development of quantum communication technologies. This observation underscores the urgent need for further theoretical investigations to establish a comprehensive understanding of the underlying principles governing quantum communication networks. Such efforts will enable the design of more efficient and robust quantum communication protocols and pave the way for the realization of a global quantum network.

In concluding this subsection, we shall undertake a more comprehensive comparison of the datasets presented in Fig. 22 and Fig. 25 by tabulating their respective attributes in Tab. IV. It is worth mentioning that our analysis extends beyond the noise model discussed in Fig. 22 and Fig. 25, as evidenced by the additional data presented in Tab. IV. With the addition of this expanded dataset, we can conduct a more thorough and in-depth analysis of the quantum network's performance, offering a more nuanced understanding of its capabilities and limitations under a broader range of noise conditions.

		Average Fidelity							
		without pre-processing				with pre-processing			
		N=1	N=2	N=3	N=4	N=1	N=2	N=3	N=4
with isotropic twirling	$\mathcal{N}_1 = \mathcal{N}_{AD}(p = 0.38), \mathcal{N}_2(q = 1) = \text{id}$	0.768814	0.644522	0.577699	0.541773	0.790689	0.669000	0.598253	0.557122
	$\mathcal{N}_1 = \mathcal{N}_{AD}(p = 0.40), \mathcal{N}_2(q = 1) = \text{id}$	0.777485	0.653996	0.585463	0.547430	0.798069	0.677690	0.605928	0.563147
	$\mathcal{N}_1 = \mathcal{N}_{AD}(p = 0.42), \mathcal{N}_2(q = 1) = \text{id}$	0.786025	0.663620	0.593599	0.553543	0.805323	0.686445	0.613852	0.569523
	$\mathcal{N}_1 = \mathcal{N}_{AD}(p = 0.54), \mathcal{N}_2(q = 1) = \text{id}$	0.834949	0.724382	0.650313	0.600694	0.846652	0.740335	0.666625	0.615522
	$\mathcal{N}_1 = \mathcal{N}_{AD}(p = 0.55), \mathcal{N}_2(q = 1) = \text{id}$	0.838873	0.729670	0.655658	0.605497	0.849950	0.744931	0.671427	0.619982
	$\mathcal{N}_1 = \mathcal{N}_{AD}(p = 0.56), \mathcal{N}_2(q = 1) = \text{id}$	0.842777	0.734992	0.661100	0.610443	0.853230	0.749543	0.676292	0.624543
without isotropic twirling	$\mathcal{N}_1 = \mathcal{N}_{AD}(p = 0.38), \mathcal{N}_2(q = 1) = \text{id}$	0.768814	0.650733	0.587228	0.551609	0.790689	0.669024	0.598294	0.557170
	$\mathcal{N}_1 = \mathcal{N}_{AD}(p = 0.40), \mathcal{N}_2(q = 1) = \text{id}$	0.777485	0.660000	0.594994	0.557600	0.798069	0.677719	0.605979	0.563208
	$\mathcal{N}_1 = \mathcal{N}_{AD}(p = 0.42), \mathcal{N}_2(q = 1) = \text{id}$	0.786025	0.669400	0.603078	0.563986	0.805323	0.686477	0.613911	0.569596
	$\mathcal{N}_1 = \mathcal{N}_{AD}(p = 0.54), \mathcal{N}_2(q = 1) = \text{id}$	0.834949	0.728600	0.658516	0.611372	0.846652	0.740366	0.666689	0.615611
	$\mathcal{N}_1 = \mathcal{N}_{AD}(p = 0.55), \mathcal{N}_2(q = 1) = \text{id}$	0.838873	0.733750	0.663693	0.616084	0.849950	0.744960	0.671489	0.620068
	$\mathcal{N}_1 = \mathcal{N}_{AD}(p = 0.56), \mathcal{N}_2(q = 1) = \text{id}$	0.842777	0.738933	0.668958	0.620924	0.853230	0.749570	0.676350	0.624625

TABLE IV. Investigating the effectiveness of pre-processing techniques: analyzing the average fidelity f_N of a state obtained through entanglement swapping (see Fig. 20) under various noise models, with and without pre-processing. More precisely, we analyze the noise models of amplitude damping channel $\mathcal{N}_1(p) = \mathcal{N}_{AD}(p)$ with $p \in \{0.38, 0.40, 0.42, 0.54, 0.55, 0.56\}$, while employing the identity channel $\mathcal{N}_2 = \text{id}$ to represent a noiseless evolution of the system (see Fig. 21). Here, we use dark blue shading to indicate that the corresponding average fidelity exceeds the classical limit of $2/3$. Conversely, light blue shading denotes cases where the performance falls below this limit.

Notably, the primary variance between the two figures (namely Fig. 22 and Fig. 25) pertains to the adoption of isotropic twirling, which involves randomly applying a set of unitary operations to a quantum state, in a way that preserves the overall symmetry of the system. As explained in Subsec. IB, isotropic twirling \mathcal{T}_{iso} does not affect the entanglement fidelity of a state. Therefore, if we have a state ρ , its performance and that of $\mathcal{T}_{\text{iso}}(\rho)$ in teleportation remains unchanged, since for a single copy of resource shared between the sender and the receiver, we have

$$f_1(\rho) := f(\rho) = f_1(\mathcal{T}_{\text{iso}}(\rho)) := f(\mathcal{T}_{\text{iso}}(\rho)). \quad (230)$$

However, when multiple copies of bipartite states are connected through entanglement swapping, isotropic twirling might decrease the fidelity of the resulting entangled state. This is in contrast to the case where single bipartite states are considered. The data listed in Tab. IV supports the following inequality,

$$f_N(\rho) \geq f_N(\mathcal{T}_{\text{iso}}(\rho)), \quad (231)$$

demonstrating that the average fidelity of quantum network communication generally decreases as a result of isotropic twirling. Here $f_N(\rho)$ stands for the average fidelity of a state obtained by connecting N copies of a given bipartite state ρ through entanglement swapping (as illustrated in Fig. 20). Moreover, Tab. IV reveals an intriguing trend in the performance of quantum network communication. Despite a noticeable decrease in average fidelity, a striking result emerges – pre-processing-assisted network communication exhibits remarkable noise resilience against isotropic twirling. Quite remarkable, the performance remains almost unaffected whether the bipartite channel is subjected to isotropic twirling or not. Although our numerical investigations provide important insights into the robustness of pre-processing-assisted network communication under isotropic twirling, the generality of these results beyond the specific models considered in our work remains an open question. Further exploration of this issue is necessary to establish the extent to which our findings hold more generally. However, this is a challenging and multi-faceted problem that extends beyond the scope of our present work, and will be the subject of future research.

B. All-In-One Communication Framework: That's all you need

The quantum repeater is a promising approach for building a quantum network that allows for the reliable transfer of unknown quantum states over long distances, as explained in Subsec. IV A. However, the assumption of identical Bell measurements on independent and identically distributed (i.i.d.) quantum states in each protocol round, commonly used in this approach, cannot be justified a priori despite its analytical convenience. In reality, error rates in quantum network communication can fluctuate due to variations in nodes or environmental factors, thus necessitating the introduction of an adaptive communication protocol that can dynamically adjust its behavior in response to such changes. Imperfect devices and transmission channels also introduce noise into quantum networks, making continuous monitoring and adjustment of the network critical for reliable and efficient quantum communication. As in classical wireless communication, adaptive communication protocols [195–197] optimize communication parameters for successful transmission by accounting for variations in network conditions such as distance, obstacles, and interference. In this subsection, we will introduce the most general framework of adaptive quantum communication protocols, analyse their performance, determine their limitations in terms of average fidelities, and explore the relationship between their communication capability and inherent temporal entanglement (see Sec. II).

Assuming, without loss of generality, that the adaptive quantum communication protocol is designed to transmit information from the sender, Alice, to the receiver, Bob, denoted by systems A and B , respectively, we consider a communication channel with $N - 1$ intermediate nodes. These nodes, denoted by C_i with $i \in \{1, \dots, N - 1\}$, are controlled by agents 1 to $N - 1$. The agents serve as intermediaries between the sender and receiver, enabling the transfer of information in a quantum network. Traditional quantum communication protocols have focused on the quantum channel between Alice, Bob, and agents in a single round. However, our approach goes beyond this limitation and considers the use of multiple rounds of quantum channels shared between them. This enables the creation of an adaptive quantum communication protocol that can more effectively transmit quantum information. Key to our approach is the assumption that the sender, receiver, and agents have access to a quantum memory that connects the different quantum channels together. By utilizing this quantum memory, we can optimize the transmission of quantum information, resulting in a more reliable and efficient communication protocol.

Before elucidating the mathematical underpinnings of adaptive quantum communication protocols, we focus on a specific instance illustrated in Fig. 27 to develop a more intuitive grasp. This protocol consists of two resourceful bipartite operations, denoted as \mathcal{E}_1 and \mathcal{E}_2 , each comprising a learning machine implemented through a joint POVM on multiple systems, and a retrieving device realized using a quantum channel. These operations are linked by a quantum memory, which enables their communication to be dynamically adjusted based on changing conditions of the channel. Here, the ability to adaptively optimize the communication in this way arises from the use of a memory-assisted quantum feedback control scheme. While this special scheme does not account for intermediate nodes between sender and receiver, such nodes can greatly enhance long-distance quantum communication.

From a resource-theoretical perspective, the bipartite superchannel \mathcal{E} (refer to the orange dashed box in Fig. 27) shared between the sender and receiver is a critical resource for the transmission of quantum information. To fully leverage its power, we employ a free morphism $\Theta \in \mathfrak{F}_3(\mathcal{S})$ (as detailed in Subsec. ID and Sec. II), where \mathcal{S} is a set of permissible operations from $\{\text{LOCC}_1(\text{poly}(d)), \text{LOCC}_k, \text{LOCC}_{\mathbb{N}}, \text{LOCC}, \overline{\text{LOCC}}_{\mathbb{N}}, \text{SEP}, \text{SEPP}, \text{PPT}\}$. By applying this free morphism, we transform \mathcal{E} into a quantum channel $\Theta(\mathcal{E})_{R \rightarrow B_5}$ between the message system R and the receiver system B_5 .

As a fundamental building block of quantum communication technologies, quantum teleportation relies on the creation (represented by the brown box of Fig. 8(f)) and manipulation (identified by the gradient superchannel in Fig. 8(f)) of entangled states between distant parties. In particular, the success of the protocol is determined by the quality of the bipartite channel, which carries the resources of temporal entanglement. Moving beyond teleportation to quantum network communication, the challenge becomes more complex due to the involvement of multiple parties

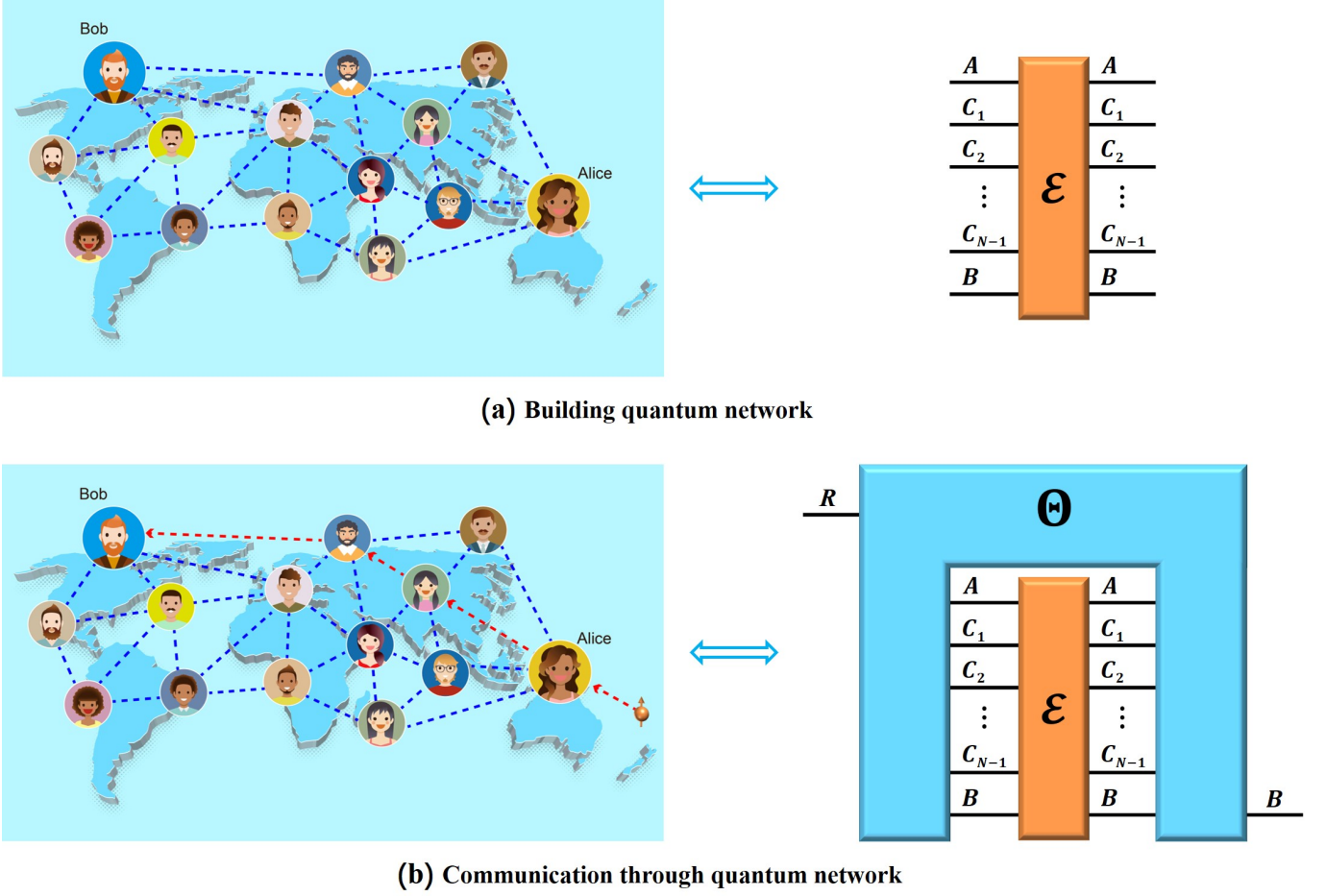


FIG. 28. (Color online) A schematic diagram of single-round communication through a quantum network: In order to establish a reliable and secure physical quantum network between the sender Alice, receiver Bob, and third-party agents, we employ a multi-input and multi-output quantum channel denoted as \mathcal{E} , as described in the orange box of (a). However, to fully exploit the capabilities of multipartite quantum channel \mathcal{E} in quantum network communications, it is crucial to integrate free operations like $\text{LOCC}_1(\text{poly}(d))$ (see Subsec. II A), and utilize local memory to construct a quantum superchannel Θ , highlighted in the blue “2-comb” of (b). By utilizing this quantum superchannel, we can transform the quantum network into a direct point-to-point channel between the message system R and the receiver’s system B , thereby providing a secure communication pathway.

dashed box highlighted in Fig. 29) that adapts to dynamic network conditions? To address this question, we propose a novel approach based on the use of a high-level free morphism $\Theta \in \mathfrak{F}_{k+1}(\mathcal{S})$ (examine the blue “comb” highlighted in Fig. 29) with \mathcal{S} being a set of permissible operations from

$$\{\text{LOCC}_1(\text{poly}(d)), \text{LOCC}_k, \text{LOCC}_N, \text{LOCC}, \overline{\text{LOCC}_N}, \text{SEP}, \text{SEPP}, \text{PPT}\}, \quad (235)$$

which acts as a transformative tool to convert the dynamical resource \mathcal{E} into a functional channel $\Theta(\mathcal{E})_{R \rightarrow B_{2k+1}}$ for transmitting message encoded by ψ on system R (see Subsec. I D and Sec. II). As \mathcal{E} lacks any direct input port for ψ (see also the role of $\mathcal{E}(p, q)$ in quantum teleportation), the use of Θ is essential to enable the information transmission. Here both R and A -related systems are under the control of the sender.

From a quantum communication perspective, the success of quantum communication relies on the ability to preserve and transmit quantum states accurately and reliably. In this context, the performance of a quantum channel, denoted by $\Theta(\mathcal{E})$, is characterized by the maximal average fidelity $f(\Theta(\mathcal{E}))$ (see Def. I.3), which measures the degree of similarity between the transmitted quantum state and the received one. The goal of quantum network communication is to maximize this fidelity under all possible free morphisms $\Theta \in \mathfrak{F}_{k+1}(\mathcal{S})$, which captures different physical restrictions in the laboratory. From an entanglement-theoretic perspective, especially in the single-shot setting, where the transmission of a single copy of adaptive quantum communication protocol \mathcal{E} is considered, the quality of the channel is captured by the d -fidelity of \mathcal{S} distillation, denoted by $F_{d,\mathcal{S}}(\mathcal{E})$ (see Def. II.3). This fidelity measures the ability to extract the maximum amount of entanglement from the initial adaptive quantum communication protocol \mathcal{S} . In what

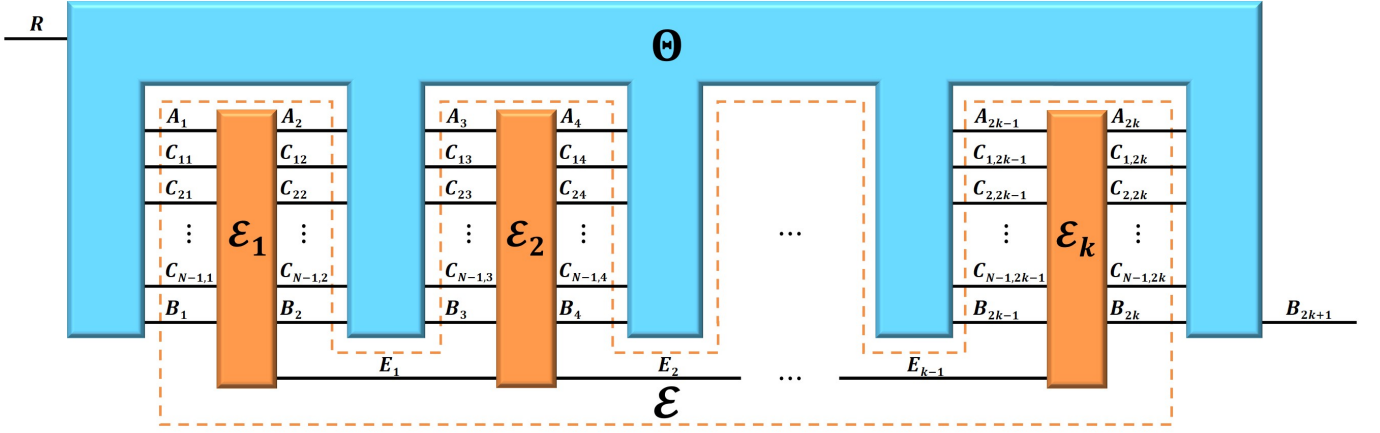


FIG. 29. (Color online) The architecture of general adaptive quantum communication protocol \mathcal{E} , utilizing non-Markovian quantum feedback to ensure secure transmission of quantum information encoded by state ψ on system R . The orange dashed box represents the protocol \mathcal{E} itself, while the blue “comb” represents a free morphism $\Theta \in \mathfrak{F}_{k+1}(\mathcal{S})$ (see Subsec. I D and Sec. II) that transforms \mathcal{E} into a quantum channel from the message system, denoted as R , to the receiver’s system, denoted as B_{2k+1} . The construction of \mathcal{E} (see Eq. 234) involves k rounds of multipartite quantum operations denoted as \mathcal{E}_i , with $1 \leq i \leq k$. These operations are shared among the sender, intermediary agents, and the receiver, and are used to manipulate quantum systems. This manipulation includes processes such as learning and retrieving information. Here, the sender holds the message system R and the quantum systems related to A , while the intermediary agents hold those related to C , and the receiver holds those related to B . To connect the quantum operations together, quantum memory systems denoted as E_i , with $1 \leq i \leq k-1$, are employed. These memory systems are used to store the quantum state of the system at the end of each round, preserving the information for use in the subsequent rounds.

follows, we will show that the temporal entanglement associated with the adaptive quantum communication protocol \mathcal{E} under free morphisms $\mathfrak{F}_{k+1}(\mathcal{S})$ determines its capability of communication in a quantum network. Specifically, the higher the d -fidelity of \mathcal{S} distillation, the better the performance of the resulting channel, as it implies a higher degree of entanglement between the sender and receiver. This result highlights the importance of understanding the underlying temporal entanglement properties of quantum communication protocols and the role of free morphisms in shaping their performance.

Theorem IV.6: Temporal Entanglement Determines Quantum Network Communications

Given an adaptive quantum communication protocol \mathcal{E} (see Eq. 234), a free morphism $\Theta \in \mathfrak{F}_{k+1}(\mathcal{S})$ will transform the protocol \mathcal{E} into a point-to-point channel $\Theta(\mathcal{E})$, as illustrated in Fig. 29. Under all free morphisms, the resulting channel’s highest efficacy is determined by the equation provided below

$$\max_{\Theta \in \mathfrak{F}_{k+1}(\mathcal{S})} f(\Theta(\mathcal{E})) = \frac{dF_{d,\mathcal{S}}(\mathcal{E}) + 1}{d + 1}, \quad (236)$$

Here, we use f to denote the average fidelity, as defined in Def. I.3, and $F_{d,\mathcal{S}}$ to represent the d -fidelity of \mathcal{S} distillation, as defined in Def. II.3. The set \mathcal{S} encompasses permissible operations, including $\text{LOCC}_1(\text{poly}(d))$, LOCC_k , $\text{LOCC}_{\mathbb{N}}$, LOCC , $\overline{\text{LOCC}}_{\mathbb{N}}$, SEP , SEPP , and PPT . For ease of exposition, we assume that all systems have the same dimension d .

Proof. To establish the validity of Eq. 236, we first demonstrate that the left-hand side is upper-bounded by the right-hand side. Let us suppose that there exists a free morphism $\Xi \in \mathfrak{F}_{k+1}(\mathcal{S})$ which attains the maximal performance of adaptive quantum communication protocol \mathcal{E} in terms of average fidelity f . Then we have

$$\max_{\Theta \in \mathfrak{F}_{k+1}(\mathcal{S})} f(\Theta(\mathcal{E})) = f(\Xi(\mathcal{E})) = \frac{dF(\Xi(\mathcal{E})) + 1}{d + 1} = \frac{d \text{Tr}[\Xi(\mathcal{E})(\phi_d^+ \cdot \phi_d^+)] + 1}{d + 1} \leq \frac{dF_{d,\mathcal{S}}(\mathcal{E}) + 1}{d + 1}. \quad (237)$$

The second equation of Eq. 237 follows directly from Lem. I.12. The third equation of Eq. 237 is based on the standard definition of entanglement fidelity, defined in Def. I.4. Without loss of generality, we can assume that ϕ_d^+ acts on the bipartite system $A_{2k+1}B_{2k+1}$. To prove the inequality of Eq. 237, we apply a local operation $\text{id}_{R \rightarrow A_{2k+1}}$ to $\Xi(\mathcal{E})(\phi_d^+)$ that maps the subsystem R to A_{2k+1} and leaves the subsystem B_{2k+1} unchanged, as illustrated in Fig. 30(a). The

transformation $\text{id}_{R \rightarrow A_{2k+1}}$ corresponds to a local operation, given that the sender controls the message system R and all systems related to A . Consequently, the overall operation $\text{id}_{R \rightarrow A_{2k+1}} \circ \Xi(\phi_{d,RR'}^+)$ constitutes a free morphism in $\mathfrak{F}_{k+1}(\mathcal{S})$, leading to the conversion of the adaptive quantum communication protocol \mathcal{E} into a state acting on system $A_{2k+1}B_{2k+1}$.

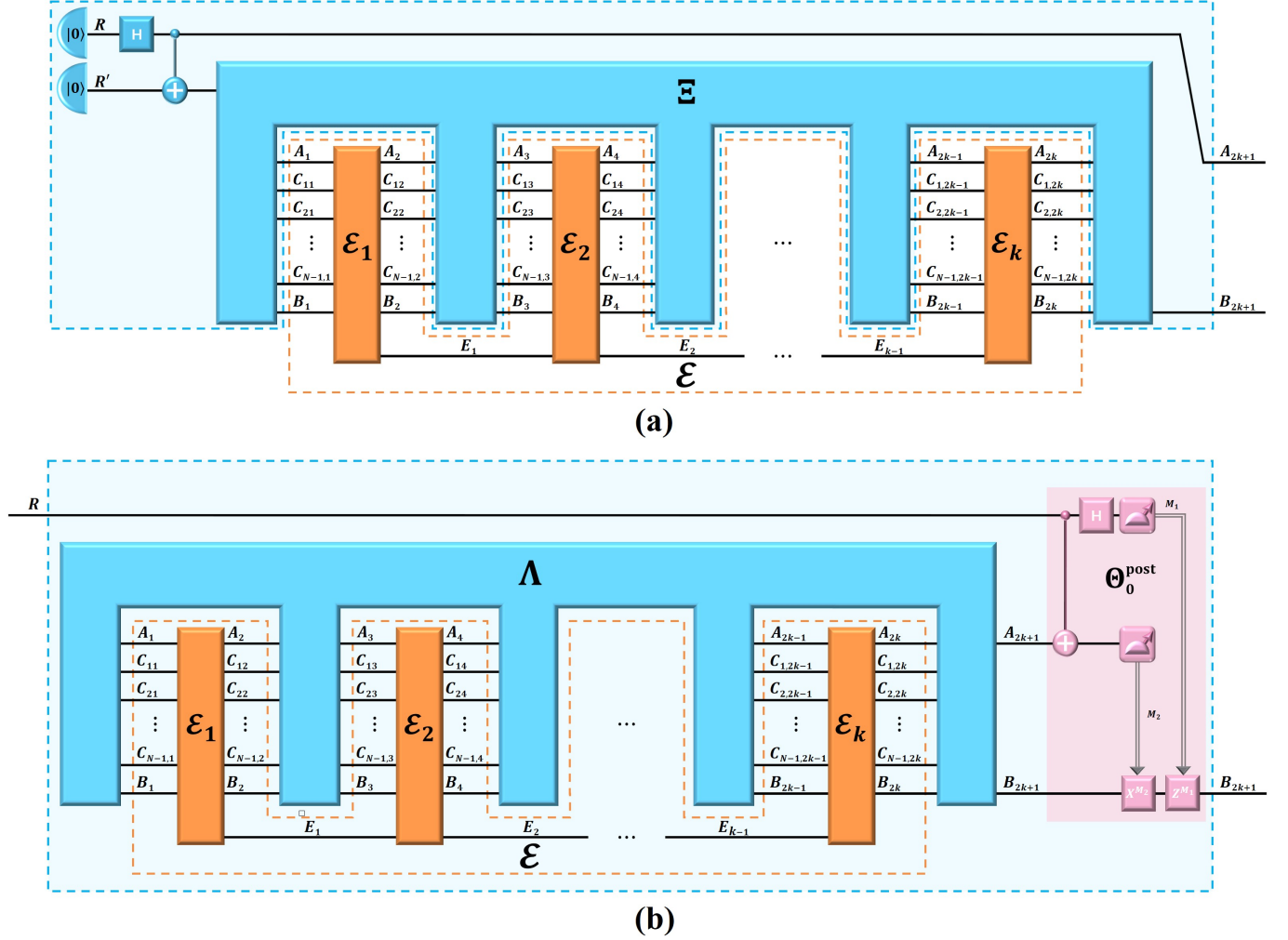


FIG. 30. (Color online) Graphical representation of the proof of Thm. IV.6, showcasing the fundamental mechanisms underlying Eq. 236. In figure (a), we illustrate how the free morphism $\Xi \in \mathfrak{F}_{k+1}(\mathcal{S})$ supports Eq. 237, a key component of our proof. Figure (b) shows the construction of the network communication channel using Λ and Θ_0^{post} , as described in Eq. 239. The dashed orange box represents the adaptive quantum communication protocol \mathcal{E} . While we have presented qubit cases for simplicity, it is important to emphasize that our proof for Thm. IV.6 is applicable to quantum systems of any finite dimension d .

We now proceed to prove the converse direction by demonstrating that the right-hand side is smaller than or equal to the left-hand side of Eq. 236. To this end, we assume that the right-hand side value of $F_{d,\mathcal{S}}(\mathcal{E})$ is attained by a free morphism $\Lambda \in \mathfrak{F}_{k+1}(\mathcal{S})$, namely

$$F_{d,\mathcal{S}}(\mathcal{E}) = \text{Tr}[\Lambda(\mathcal{E}) \cdot \phi_d^+] = F(\mathcal{F}(\Lambda(\mathcal{E}))) = F(\Theta_0^{\text{post}} \circ \Lambda(\mathcal{E})), \quad (238)$$

where \mathcal{F} stands for the teleportation channel created by consuming resourceful state $\Lambda(\mathcal{E})$ (see Fig. 11), and Θ_0^{post} is the standard teleportation operation (see the pink box of Fig. 8(a)). The second equation in Eq. 238 directly follows from Lem. III.1, while the last equation is obtained by using the definition of \mathcal{F} (See Eq. 101). It is important to note that in this context, the quantum state $\Lambda(\mathcal{E})$ operates on the composite system $A_{2k+1}B_{2k+1}$, whereas the quantum

channel $\Theta_0^{\text{post}} \circ \Lambda(\mathcal{E})$ maps the message system to receiver's system. With this defined, we see that

$$\frac{dF_{d,\mathcal{S}}(\mathcal{E}) + 1}{d + 1} = \frac{dF(\Theta_0^{\text{post}} \circ \Lambda(\mathcal{E})) + 1}{d + 1} = f(\Theta_0^{\text{post}} \circ \Lambda(\mathcal{E})) \leq \max_{\Theta \in \mathfrak{F}_{k+1}(\mathcal{S})} f(\Theta(\mathcal{E})). \quad (239)$$

The standard teleportation operation Θ_0^{post} is protocol that can be implemented using only local operations and one-way classical communication with the communication complexity polynomially dependent on the dimension of the message system. As such, it is an element of the set $\text{LOCC}_1(\text{poly}(d))$. When we compose the free morphism Λ with the standard teleportation operation Θ_0^{post} , the resulting quantum circuit fragment $\Theta_0^{\text{post}} \circ \Lambda$ still belongs to the set $\mathfrak{F}_{k+1}(\mathcal{S})$ for any $\mathcal{S} \in \{\text{LOCC}_1(\text{poly}(d)), \text{LOCC}_k, \text{LOCC}_{\mathbb{N}}, \text{LOCC}, \overline{\text{LOCC}_{\mathbb{N}}}, \text{SEP}, \text{SEPP}, \text{PPT}\}$. This implies the inequality shown in Eq. 239. Combining Eq. 237 with Eq. 239, we have demonstrated that the two sides of Eq. 236 are equal, as required by the theorem. \square

The advent of the worldwide network has revolutionized the way we live our lives, connecting people and information in ways that were once unimaginable. The potential of a global quantum network is even more profound, promising to usher in a new era of communication by enabling quantum information exchange between any two points on Earth. By harnessing the power of quantum mechanics, a quantum network has the potential to achieve unparalleled capabilities that are provably impossible with classical information processing alone, when combined with the classical network we have today. Quantum information comes in various forms within a quantum network, such as the polarization state of a photon, the spin of an electron, or the excitation state of an atom. While numerous technologies have been developed to teleport these states, optimizing the performance of quantum communication remains a challenge. Despite the availability of sequential resourceful operations and quantum memory, which form an adaptive quantum communication protocol (highlighted in the orange dashed box of Fig. 29), the fundamental limitation (in terms of average fidelity) associated with this resource remains unknown.

Here, we have successfully addressed the question of optimal quantum communication performance by establishing a connection with the concept of temporal entanglement (introduced in Sec. II), as demonstrated by our Thm. IV.6. This achievement paves the way for the future development of a global quantum network and brings us closer to realizing the full potential of this revolutionary technology. Despite such a progress in the field of quantum network communications, there are still several questions that remain unanswered. For instance, given an adaptive quantum communication protocol \mathcal{E} , how can we efficiently compute its d -fidelity of \mathcal{S} distillation, i.e., $F_{d,\mathcal{S}}(\mathcal{E})$ defined in Def. II.3, which involves determining the fidelity of a set of permissible operations from $\{\text{LOCC}_1(\text{poly}(d)), \text{LOCC}_k, \text{LOCC}_{\mathbb{N}}, \text{LOCC}, \overline{\text{LOCC}_{\mathbb{N}}}, \text{SEP}, \text{SEPP}, \text{PPT}\}$? As a free morphism (see the blue “comb” of Fig. 29) can involve multiple rounds of quantum channels, and quantum memory may exist between them, finding an exact solution is extremely challenging. Therefore, one possible approach is to relax the free morphisms considered in this work and develop upper bounds for the performance of the adaptive quantum communication protocol \mathcal{E} . This strategy can help us gain a better understanding of the capabilities and limitations of quantum network communication protocols and guide the development of future protocols with enhanced performance. Readers who are interested in exploring the relaxation of free morphisms are encouraged to refer to Ref. [198–202] and references therein, which offer in-depth investigations on the relaxation of free morphisms in the context of quantum channels, a special case of quantum circuit fragment (see Subsec. ID) considered here.

-
- [1] A. Jamiolkowski, Linear transformations which preserve trace and positive semidefiniteness of operators, Reports on Mathematical Physics **3**, 275 (1972).
 - [2] M.-D. Choi, Completely positive linear maps on complex matrices, Linear Algebra and its Applications **10**, 285 (1975).
 - [3] M. A. Nielsen and I. L. Chuang, *Quantum Computation and Quantum Information: 10th Anniversary Edition* (Cambridge University Press, 2010).
 - [4] M. M. Wilde, *Quantum Information Theory* (Cambridge University Press, 2013).
 - [5] J. Watrous, *The Theory of Quantum Information* (Cambridge University Press, 2018).
 - [6] F. Verstraete, V. Murg, and J. Cirac, Matrix product states, projected entangled pair states, and variational renormalization group methods for quantum spin systems, Advances in Physics **57**, 143 (2008), <https://doi.org/10.1080/14789940801912366>.
 - [7] R. Orús, A practical introduction to tensor networks: Matrix product states and projected entangled pair states, Annals of Physics **349**, 117 (2014).
 - [8] J. C. Bridgeman and C. T. Chubb, Hand-waving and interpretive dance: an introductory course on tensor networks, Journal of Physics A: Mathematical and Theoretical **50**, 223001 (2017).
 - [9] J. I. Cirac, D. Pérez-García, N. Schuch, and F. Verstraete, Matrix product states and projected entangled pair states: Concepts, symmetries, theorems, Rev. Mod. Phys. **93**, 045003 (2021).

- [10] B. Coecke and R. Duncan, Interacting quantum observables, in *Automata, Languages and Programming*, edited by L. Aceto, I. Damgård, L. A. Goldberg, M. M. Halldórsson, A. Ingólfssdóttir, and I. Walukiewicz (Springer Berlin Heidelberg, Berlin, Heidelberg, 2008) pp. 298–310.
- [11] B. Coecke and R. Duncan, Interacting quantum observables: categorical algebra and diagrammatics, *New Journal of Physics* **13**, 043016 (2011).
- [12] B. Coecke and A. Kissinger, *Picturing Quantum Processes: A First Course in Quantum Theory and Diagrammatic Reasoning* (Cambridge University Press, 2017).
- [13] J. van de Wetering, ZX-calculus for the working quantum computer scientist, arXiv preprint arXiv:2012.13966 (2020).
- [14] B. Coecke, Basic ZX-calculus for students and professionals, arXiv preprint arXiv:2303.03163 (2023).
- [15] G. Chiribella, G. M. D’Ariano, and P. Perinotti, Theoretical framework for quantum networks, *Phys. Rev. A* **80**, 022339 (2009).
- [16] G. Chiribella, G. M. D’Ariano, and P. Perinotti, Quantum circuit architecture, *Phys. Rev. Lett.* **101**, 060401 (2008).
- [17] G. Chiribella, G. M. D’Ariano, and P. Perinotti, Informational derivation of quantum theory, *Phys. Rev. A* **84**, 012311 (2011).
- [18] G. Chiribella and D. Ebler, Optimal quantum networks and one-shot entropies, *New Journal of Physics* **18**, 093053 (2016).
- [19] M. Horodecki, P. Horodecki, and R. Horodecki, General teleportation channel, singlet fraction, and quasidistillation, *Phys. Rev. A* **60**, 1888 (1999).
- [20] A. Uhlmann, The “transition probability” in the state space of a $*$ -algebra, *Reports on Mathematical Physics* **9**, 273 (1976).
- [21] R. Jozsa, Fidelity for mixed quantum states, *Journal of Modern Optics* **41**, 2315 (1994), <https://doi.org/10.1080/09500349414552171>.
- [22] E. Rains, A semidefinite program for distillable entanglement, *IEEE Transactions on Information Theory* **47**, 2921 (2001).
- [23] M. R. Geller and Z. Zhou, Efficient error models for fault-tolerant architectures and the pauli twirling approximation, *Phys. Rev. A* **88**, 012314 (2013).
- [24] Z. Cai and S. C. Benjamin, Constructing smaller pauli twirling sets for arbitrary error channels, *Scientific reports* **9**, 11281 (2019).
- [25] M. Horodecki and P. Horodecki, Reduction criterion of separability and limits for a class of distillation protocols, *Phys. Rev. A* **59**, 4206 (1999).
- [26] M. A. Nielsen, A simple formula for the average gate fidelity of a quantum dynamical operation, *Physics Letters A* **303**, 249 (2002).
- [27] G. Chiribella, G. M. D’Ariano, and P. Perinotti, Transforming quantum operations: Quantum supermaps, *EPL (Europhysics Letters)* **83**, 30004 (2008).
- [28] G. Gour, Comparison of quantum channels by superchannels, *IEEE Transactions on Information Theory* **65**, 5880 (2019).
- [29] B. Regula and R. Takagi, Fundamental limitations on distillation of quantum channel resources, *Nature Communications* **12**, 4411 (2021).
- [30] B. Regula and R. Takagi, One-shot manipulation of dynamical quantum resources, *Phys. Rev. Lett.* **127**, 060402 (2021).
- [31] C. Simon, V. Bužek, and N. Gisin, No-signaling condition and quantum dynamics, *Phys. Rev. Lett.* **87**, 170405 (2001).
- [32] A. Peres and D. R. Terno, Quantum information and relativity theory, *Rev. Mod. Phys.* **76**, 93 (2004).
- [33] P. Horodecki and R. Ramanathan, The relativistic causality versus no-signaling paradigm for multi-party correlations, *Nature Communications* **10**, 1701 (2019).
- [34] D. Leung and W. Matthews, On the power of ppt-preserving and non-signalling codes, *IEEE Transactions on Information Theory* **61**, 4486 (2015).
- [35] S. Popescu and D. Rohrlich, Causality and nonlocality as axioms for quantum mechanics, in *Causality and Locality in Modern Physics*, edited by G. Hunter, S. Jeffers, and J.-P. Vigiér (Springer Netherlands, Dordrecht, 1998) pp. 383–389.
- [36] D. Beckman, D. Gottesman, M. A. Nielsen, and J. Preskill, Causal and localizable quantum operations, *Phys. Rev. A* **64**, 052309 (2001).
- [37] T. Eggeling, D. Schlingemann, and R. F. Werner, Semicausal operations are semilocalizable, *Europhysics Letters* **57**, 782 (2002).
- [38] M. Piani, M. Horodecki, P. Horodecki, and R. Horodecki, Properties of quantum nonsignaling boxes, *Phys. Rev. A* **74**, 012305 (2006).
- [39] R. Van Meter and S. J. Devitt, The path to scalable distributed quantum computing, *Computer* **49**, 31 (2016).
- [40] M. Caleffi, A. S. Cacciapuoti, and G. Bianchi, Quantum internet: From communication to distributed computing!, in *Proceedings of the 5th ACM International Conference on Nanoscale Computing and Communication*, NANOCOM ’18 (Association for Computing Machinery, New York, NY, USA, 2018).
- [41] A. S. Cacciapuoti, M. Caleffi, F. Tafuri, F. S. Cataliotti, S. Gherardini, and G. Bianchi, Quantum internet: Networking challenges in distributed quantum computing, *IEEE Network* **34**, 137 (2020).
- [42] S. J. Devitt, Performing quantum computing experiments in the cloud, *Phys. Rev. A* **94**, 032329 (2016).
- [43] H.-Y. Ku, N. Lambert, F.-J. Chan, C. Emary, Y.-N. Chen, and F. Nori, Experimental test of non-macrorealistic cat states in the cloud, *npj Quantum Information* **6**, 98 (2020).
- [44] Z.-P. Yang, H.-Y. Ku, A. Baishya, Y.-R. Zhang, A. F. Kockum, Y.-N. Chen, F.-L. Li, J.-S. Tsai, and F. Nori, Deterministic one-way logic gates on a cloud quantum computer, *Phys. Rev. A* **105**, 042610 (2022).
- [45] Y. Ma, E. Kashefi, M. Arapinis, K. Chakraborty, and M. Kaplan, Qenclave - a practical solution for secure quantum cloud computing, *npj Quantum Information* **8**, 128 (2022).
- [46] H. J. Kimble, The quantum internet, *Nature* **453**, 1023 (2008).

- [47] S. Pirandola and S. L. Braunstein, Physics: Unite to build a quantum internet, *Nature* **532**, 169 (2016).
- [48] C. Simon, Towards a global quantum network, *Nature Photonics* **11**, 678 (2017).
- [49] S. Wehner, D. Elkouss, and R. Hanson, Quantum internet: A vision for the road ahead, *Science* **362**, eaam9288 (2018), <https://www.science.org/doi/pdf/10.1126/science.aam9288>.
- [50] M. Pant, H. Krovi, D. Towsley, L. Tassioulas, L. Jiang, P. Basu, D. Englund, and S. Guha, Routing entanglement in the quantum internet, *npj Quantum Information* **5**, 25 (2019).
- [51] R. Valivarthi, S. I. Davis, C. Peña, S. Xie, N. Lauk, L. Narváez, J. P. Allmaras, A. D. Beyer, Y. Gim, M. Hussein, G. Iskander, H. L. Kim, B. Korzh, A. Mueller, M. Rominsky, M. Shaw, D. Tang, E. E. Wollman, C. Simon, P. Spentzouris, D. Oblak, N. Sinclair, and M. Spiropulu, Teleportation systems toward a quantum internet, *PRX Quantum* **1**, 020317 (2020).
- [52] D. Awschalom, K. K. Berggren, H. Bernien, S. Bhawe, L. D. Carr, P. Davids, S. E. Economou, D. Englund, A. Faraon, M. Fejer, S. Guha, M. V. Gustafsson, E. Hu, L. Jiang, J. Kim, B. Korzh, P. Kumar, P. G. Kwiat, M. Lončar, M. D. Lukin, D. A. Miller, C. Monroe, S. W. Nam, P. Narang, J. S. Orcutt, M. G. Raymer, A. H. Safavi-Naeini, M. Spiropulu, K. Srinivasan, S. Sun, J. Vučković, E. Waks, R. Walsworth, A. M. Weiner, and Z. Zhang, Development of quantum interconnects (quics) for next-generation information technologies, *PRX Quantum* **2**, 017002 (2021).
- [53] S. L. N. Hermans, M. Pompili, H. K. C. Beukers, S. Baier, J. Borregaard, and R. Hanson, Qubit teleportation between non-neighbouring nodes in a quantum network, *Nature* **605**, 663 (2022).
- [54] S. F. Bush, W. A. Challenger, and G. Mantelet, A perspective on industrial quantum networks, *AVS Quantum Science* **3**, 030501 (2021), <https://doi.org/10.1116/5.0051881>.
- [55] W. J. Munro, N. L. Piparo, J. Dias, M. Hanks, and K. Nemoto, Designing tomorrow's quantum internet, *AVS Quantum Science* **4**, 020503 (2022), <https://doi.org/10.1116/5.0092069>.
- [56] A. Forbes, Progress in quantum networks, *AVS Quantum Science* **4**, 030401 (2022), <https://doi.org/10.1116/5.0118569>.
- [57] K. Fang, J. Zhao, X. Li, Y. Li, and R. Duan, Quantum network: from theory to practice (2022), arXiv:2212.01226 [quant-ph].
- [58] K. Azuma, S. E. Economou, D. Elkouss, P. Hilaire, L. Jiang, H.-K. Lo, and I. Tzitrin, Quantum repeaters: From quantum networks to the quantum internet (2022), arXiv:2212.10820 [quant-ph].
- [59] M. Gu, K. Wiesner, E. Rieper, and V. Vedral, Quantum mechanics can reduce the complexity of classical models, *Nature Communications* **3**, 762 (2012).
- [60] J. Thompson, A. J. P. Garner, V. Vedral, and M. Gu, Using quantum theory to simplify input-output processes, *npj Quantum Information* **3**, 6 (2017).
- [61] T. J. Elliott, M. Gu, A. J. P. Garner, and J. Thompson, Quantum adaptive agents with efficient long-term memories, *Phys. Rev. X* **12**, 011007 (2022).
- [62] K.-D. Wu, C. Yang, R.-D. He, M. Gu, G.-Y. Xiang, C.-F. Li, G.-C. Guo, and T. J. Elliott, Implementing quantum dimensionality reduction for non-markovian stochastic simulation, *Nature Communications* **14**, 2624 (2023).
- [63] Y. Yang, Memory effects in quantum metrology, *Phys. Rev. Lett.* **123**, 110501 (2019).
- [64] A. Altherr and Y. Yang, Quantum metrology for non-markovian processes, *Phys. Rev. Lett.* **127**, 060501 (2021).
- [65] Q. Liu, Z. Hu, H. Yuan, and Y. Yang, Optimal strategies of quantum metrology with a strict hierarchy, *Phys. Rev. Lett.* **130**, 070803 (2023).
- [66] F. A. Pollock, C. Rodríguez-Rosario, T. Frauenheim, M. Paternostro, and K. Modi, Non-Markovian quantum processes: Complete framework and efficient characterization, *Phys. Rev. A* **97**, 012127 (2018).
- [67] P. Taranto, F. A. Pollock, S. Milz, M. Tomamichel, and K. Modi, Quantum markov order, *Phys. Rev. Lett.* **122**, 140401 (2019).
- [68] S. Milz and K. Modi, Quantum stochastic processes and quantum non-markovian phenomena, *PRX Quantum* **2**, 030201 (2021).
- [69] P. Kómár, E. M. Kessler, M. Bishof, L. Jiang, A. S. Sørensen, J. Ye, and M. D. Lukin, A quantum network of clocks, *Nature Physics* **10**, 582 (2014).
- [70] X. Liu, J. Hu, Z.-F. Li, X. Li, P.-Y. Li, P.-J. Liang, Z.-Q. Zhou, C.-F. Li, and G.-C. Guo, Heralded entanglement distribution between two absorptive quantum memories, *Nature* **594**, 41 (2021).
- [71] L.-Z. Liu, Y.-Z. Zhang, Z.-D. Li, R. Zhang, X.-F. Yin, Y.-Y. Fei, L. Li, N.-L. Liu, F. Xu, Y.-A. Chen, and J.-W. Pan, Distributed quantum phase estimation with entangled photons, *Nature Photonics* **15**, 137 (2021).
- [72] K. Beloy, M. I. Bodine, T. Bothwell, S. M. Brewer, S. L. Bromley, J.-S. Chen, J.-D. Deschênes, S. A. Diddams, R. J. Fasano, T. M. Fortier, Y. S. Hassan, D. B. Hume, D. Kedar, C. J. Kennedy, I. Khader, A. Koepke, D. R. Leibbrandt, H. Leopardi, A. D. Ludlow, W. F. McGrew, W. R. Milner, N. R. Newbury, D. Nicolodi, E. Oelker, T. E. Parker, J. M. Robinson, S. Romisch, S. A. Schäffer, J. A. Sherman, L. C. Sinclair, L. Sonderhouse, W. C. Swann, J. Yao, J. Ye, X. Zhang, and B. A. C. O. N. B. Collaboration*, Frequency ratio measurements at 18-digit accuracy using an optical clock network, *Nature* **591**, 564 (2021).
- [73] B. K. Malia, Y. Wu, J. Martínez-Rincón, and M. A. Kasevich, Distributed quantum sensing with mode-entangled spin-squeezed atomic states, *Nature* **612**, 661 (2022).
- [74] N. Lambert, Y.-N. Chen, Y.-C. Cheng, C.-M. Li, G.-Y. Chen, and F. Nori, Quantum biology, *Nature Physics* **9**, 10 (2013).
- [75] K. Ried, M. Agnew, L. Vermeyden, D. Janzing, R. W. Spekkens, and K. J. Resch, A quantum advantage for inferring causal structure, *Nature Physics* **11**, 414 (2015).
- [76] J.-P. W. MacLean, K. Ried, R. W. Spekkens, and K. J. Resch, Quantum-coherent mixtures of causal relations, *Nature Communications* **8**, 15149 (2017).
- [77] Y. Xiao, Y. Yang, X. Wang, Q. Liu, and M. Gu, Quantum uncertainty principles for measurements with interventions

- (2023), arXiv:2305.07914 [quant-ph].
- [78] L. Mazzola, C. A. Rodríguez-Rosario, K. Modi, and M. Paternostro, Dynamical role of system-environment correlations in non-markovian dynamics, *Phys. Rev. A* **86**, 010102 (2012).
 - [79] M. Ringbauer, C. J. Wood, K. Modi, A. Gilchrist, A. G. White, and A. Fedrizzi, Characterizing quantum dynamics with initial system-environment correlations, *Phys. Rev. Lett.* **114**, 090402 (2015).
 - [80] F. A. Pollock, C. Rodríguez-Rosario, T. Frauenheim, M. Paternostro, and K. Modi, Operational markov condition for quantum processes, *Phys. Rev. Lett.* **120**, 040405 (2018).
 - [81] L. Li, M. J. Hall, and H. M. Wiseman, Concepts of quantum non-markovianity: A hierarchy, *Physics Reports* **759**, 1 (2018).
 - [82] G. A. L. White, C. D. Hill, F. A. Pollock, L. C. L. Hollenberg, and K. Modi, Demonstration of non-markovian process characterisation and control on a quantum processor, *Nature Communications* **11**, 6301 (2020).
 - [83] R. Horodecki, P. Horodecki, M. Horodecki, and K. Horodecki, Quantum entanglement, *Rev. Mod. Phys.* **81**, 865 (2009).
 - [84] Z. Zhao, Y.-A. Chen, A.-N. Zhang, T. Yang, H. J. Briegel, and J.-W. Pan, Experimental demonstration of five-photon entanglement and open-destination teleportation, *Nature* **430**, 54 (2004).
 - [85] X.-M. Jin, J.-G. Ren, B. Yang, Z.-H. Yi, F. Zhou, X.-F. Xu, S.-K. Wang, D. Yang, Y.-F. Hu, S. Jiang, T. Yang, H. Yin, K. Chen, C.-Z. Peng, and J.-W. Pan, Experimental free-space quantum teleportation, *Nature Photonics* **4**, 376 (2010).
 - [86] X.-S. Ma, T. Herbst, T. Scheidl, D. Wang, S. Kropatschek, W. Naylor, B. Wittmann, A. Mech, J. Kofler, E. Anisimova, V. Makarov, T. Jennewein, R. Ursin, and A. Zeilinger, Quantum teleportation over 143 kilometres using active feed-forward, *Nature* **489**, 269 (2012).
 - [87] S. Takeda, T. Mizuta, M. Fuwa, P. van Loock, and A. Furusawa, Deterministic quantum teleportation of photonic quantum bits by a hybrid technique, *Nature* **500**, 315 (2013).
 - [88] S. Pirandola, J. Eisert, C. Weedbrook, A. Furusawa, and S. L. Braunstein, Advances in quantum teleportation, *Nature Photonics* **9**, 641 (2015).
 - [89] Q.-C. Sun, Y.-L. Mao, S.-J. Chen, W. Zhang, Y.-F. Jiang, Y.-B. Zhang, W.-J. Zhang, S. Miki, T. Yamashita, H. Terai, X. Jiang, T.-Y. Chen, L.-X. You, X.-F. Chen, Z. Wang, J.-Y. Fan, Q. Zhang, and J.-W. Pan, Quantum teleportation with independent sources and prior entanglement distribution over a network, *Nature Photonics* **10**, 671 (2016).
 - [90] A. K. Ekert, Quantum cryptography based on bell's theorem, *Phys. Rev. Lett.* **67**, 661 (1991).
 - [91] A. K. Ekert, Quantum cryptography and Bell's theorem, in *Quantum Measurements in Optics*, edited by P. Tombesi and D. F. Walls (Springer US, Boston, MA, 1992) pp. 413–418.
 - [92] D. Deutsch, A. Ekert, R. Jozsa, C. Macchiavello, S. Popescu, and A. Sanpera, Quantum privacy amplification and the security of quantum cryptography over noisy channels, *Phys. Rev. Lett.* **77**, 2818 (1996).
 - [93] R. Raussendorf and H. J. Briegel, A one-way quantum computer, *Phys. Rev. Lett.* **86**, 5188 (2001).
 - [94] R. Raussendorf and H. J. Briegel, Computational model underlying the one-way quantum computer, *Quantum Info. Comput.* **2**, 443–486 (2002).
 - [95] R. Raussendorf, D. E. Browne, and H. J. Briegel, Measurement-based quantum computation on cluster states, *Phys. Rev. A* **68**, 022312 (2003).
 - [96] H. J. Briegel, D. E. Browne, W. Dür, R. Raussendorf, and M. Van den Nest, Measurement-based quantum computation, *Nature Physics* **5**, 19 (2009).
 - [97] J. D. Biamonte, M. E. S. Morales, and D. E. Koh, Entanglement scaling in quantum advantage benchmarks, *Phys. Rev. A* **101**, 012349 (2020).
 - [98] C. H. Bennett, G. Brassard, S. Popescu, B. Schumacher, J. A. Smolin, and W. K. Wootters, Purification of noisy entanglement and faithful teleportation via noisy channels, *Phys. Rev. Lett.* **76**, 722 (1996).
 - [99] F. Buscemi and N. Datta, Distilling entanglement from arbitrary resources, *Journal of Mathematical Physics* **51**, 10.1063/1.3483717 (2010), 102201, https://pubs.aip.org/aip/jmp/article-pdf/doi/10.1063/1.3483717/15605799/102201_1_online.pdf.
 - [100] F. Buscemi and N. Datta, Entanglement cost in practical scenarios, *Phys. Rev. Lett.* **106**, 130503 (2011).
 - [101] F. Buscemi and N. Datta, General theory of environment-assisted entanglement distillation, *IEEE Transactions on Information Theory* **59**, 1940 (2013).
 - [102] X. Wang and R. Duan, Irreversibility of asymptotic entanglement manipulation under quantum operations completely preserving positivity of partial transpose, *Phys. Rev. Lett.* **119**, 180506 (2017).
 - [103] M. Berta, F. G. S. L. Brandão, M. Christandl, and S. Wehner, Entanglement cost of quantum channels, *IEEE Transactions on Information Theory* **59**, 6779 (2013).
 - [104] X. Wang and M. M. Wilde, Cost of quantum entanglement simplified, *Phys. Rev. Lett.* **125**, 040502 (2020).
 - [105] X. Wang and M. M. Wilde, Exact entanglement cost of quantum states and channels under positive-partial-transpose-preserving operations, *Phys. Rev. A* **107**, 012429 (2023).
 - [106] G. Gour and C. M. Scandolo, Dynamical entanglement, *Phys. Rev. Lett.* **125**, 180505 (2020).
 - [107] G. Gour and C. M. Scandolo, Entanglement of a bipartite channel, *Phys. Rev. A* **103**, 062422 (2021).
 - [108] C. Brukner, S. Taylor, S. Cheung, and V. Vedral, Quantum entanglement in time (2004), arXiv:quant-ph/0402127 [quant-ph].
 - [109] S. Milz, F. A. Pollock, T. P. Le, G. Chiribella, and K. Modi, Entanglement, non-markovianity, and causal non-separability, *New Journal of Physics* **20**, 033033 (2018).
 - [110] F. Costa, M. Ringbauer, M. E. Goggin, A. G. White, and A. Fedrizzi, Unifying framework for spatial and temporal quantum correlations, *Phys. Rev. A* **98**, 012328 (2018).
 - [111] M. Zych, F. Costa, I. Pikovski, and C. Brukner, Bell's theorem for temporal order, *Nature Communications* **10**, 3772

- (2019).
- [112] S. Milz, D. Jurkschat, F. A. Pollock, and K. Modi, Delayed-choice causal order and nonclassical correlations, *Phys. Rev. Res.* **3**, 023028 (2021).
 - [113] S. Milz, C. Spee, Z.-P. Xu, F. A. Pollock, K. Modi, and O. Gühne, Genuine multipartite entanglement in time, *SciPost Phys.* **10**, 141 (2021).
 - [114] G. Giudice, G. Giudici, M. Sonner, J. Thoeniss, A. Lerose, D. A. Abanin, and L. Piroli, Temporal entanglement, quasiparticles, and the role of interactions, *Phys. Rev. Lett.* **128**, 220401 (2022).
 - [115] B. Coecke, T. Fritz, and R. W. Spekkens, A mathematical theory of resources, *Information and Computation* **250**, 59 (2016), quantum Physics and Logic.
 - [116] E. Chitambar and G. Gour, Quantum resource theories, *Rev. Mod. Phys.* **91**, 025001 (2019).
 - [117] M. Piani and J. Watrous, All entangled states are useful for channel discrimination, *Phys. Rev. Lett.* **102**, 250501 (2009).
 - [118] M. Piani, M. Cianciaruso, T. R. Bromley, C. Napoli, N. Johnston, and G. Adesso, Robustness of asymmetry and coherence of quantum states, *Phys. Rev. A* **93**, 042107 (2016).
 - [119] C. Napoli, T. R. Bromley, M. Cianciaruso, M. Piani, N. Johnston, and G. Adesso, Robustness of coherence: An operational and observable measure of quantum coherence, *Phys. Rev. Lett.* **116**, 150502 (2016).
 - [120] W. Zheng, Z. Ma, H. Wang, S.-M. Fei, and X. Peng, Experimental demonstration of observability and operability of robustness of coherence, *Phys. Rev. Lett.* **120**, 230504 (2018).
 - [121] R. Takagi, B. Regula, K. Bu, Z.-W. Liu, and G. Adesso, Operational advantage of quantum resources in subchannel discrimination, *Phys. Rev. Lett.* **122**, 140402 (2019).
 - [122] A. F. Ducuara and P. Skrzypczyk, Operational interpretation of weight-based resource quantifiers in convex quantum resource theories, *Phys. Rev. Lett.* **125**, 110401 (2020).
 - [123] R. Uola, T. Bullock, T. Kraft, J.-P. Pellonpää, and N. Brunner, All quantum resources provide an advantage in exclusion tasks, *Phys. Rev. Lett.* **125**, 110402 (2020).
 - [124] A. Streltsov, G. Adesso, and M. B. Plenio, Colloquium: Quantum coherence as a resource, *Rev. Mod. Phys.* **89**, 041003 (2017).
 - [125] S. Mac Lane, *Categories for the working mathematician*, Vol. 5 (Springer Science & Business Media, 2013).
 - [126] E. Chitambar, D. Leung, L. Mančinska, M. Ozols, and A. Winter, Everything you always wanted to know about locc (but were afraid to ask), *Communications in Mathematical Physics* **328**, 303 (2014).
 - [127] D. Sauerwein, N. R. Wallach, G. Gour, and B. Kraus, Transformations among pure multipartite entangled states via local operations are almost never possible, *Phys. Rev. X* **8**, 031020 (2018).
 - [128] M. Grassl, M. Rötteler, and T. Beth, Computing local invariants of quantum-bit systems, *Phys. Rev. A* **58**, 1833 (1998).
 - [129] B. Kraus, Local unitary equivalence of multipartite pure states, *Phys. Rev. Lett.* **104**, 020504 (2010).
 - [130] B. Kraus, Local unitary equivalence and entanglement of multipartite pure states, *Phys. Rev. A* **82**, 032121 (2010).
 - [131] V. Gheorghiu and R. B. Griffiths, Separable operations on pure states, *Phys. Rev. A* **78**, 020304 (2008).
 - [132] E. Chitambar and R. Duan, Nonlocal entanglement transformations achievable by separable operations, *Phys. Rev. Lett.* **103**, 110502 (2009).
 - [133] F. G. S. L. Brandão and M. B. Plenio, Entanglement theory and the second law of thermodynamics, *Nature Physics* **4**, 873 (2008).
 - [134] F. G. S. L. Brandão and M. B. Plenio, A generalization of quantum stein's lemma, *Communications in Mathematical Physics* **295**, 791 (2010).
 - [135] M. Berta, F. G. S. L. Brandão, G. Gour, L. Lami, M. B. Plenio, B. Regula, and M. Tomamichel, On a gap in the proof of the generalised quantum stein's lemma and its consequences for the reversibility of quantum resources (2022), arXiv:2205.02813 [quant-ph].
 - [136] L. Lami and B. Regula, No second law of entanglement manipulation after all, *Nature Physics* **19**, 184 (2023).
 - [137] E. M. Rains, Bound on distillable entanglement, *Phys. Rev. A* **60**, 179 (1999).
 - [138] E. M. Rains, Erratum: Bound on distillable entanglement [phys. rev. a 60, 179 (1999)], *Phys. Rev. A* **63**, 019902 (2000).
 - [139] K. Audenaert, M. B. Plenio, and J. Eisert, Entanglement cost under positive-partial-transpose-preserving operations, *Phys. Rev. Lett.* **90**, 027901 (2003).
 - [140] I. Georgescu, 25 years of experimental quantum teleportation, *Nature Reviews Physics* **4**, 695 (2022).
 - [141] C. H. Bennett and S. J. Wiesner, Communication via one- and two-particle operators on einstein-podolsky-rosen states, *Phys. Rev. Lett.* **69**, 2881 (1992).
 - [142] C. H. Bennett, G. Brassard, C. Crépeau, R. Jozsa, A. Peres, and W. K. Wootters, Teleporting an unknown quantum state via dual classical and Einstein-podolsky-rosen channels, *Phys. Rev. Lett.* **70**, 1895 (1993).
 - [143] C. H. Bennett, D. P. DiVincenzo, J. A. Smolin, and W. K. Wootters, Mixed-state entanglement and quantum error correction, *Phys. Rev. A* **54**, 3824 (1996).
 - [144] D. Bouwmeester, J.-W. Pan, K. Mattle, M. Eibl, H. Weinfurter, and A. Zeilinger, Experimental quantum teleportation, *Nature* **390**, 575 (1997).
 - [145] D. Boschi, S. Branca, F. De Martini, L. Hardy, and S. Popescu, Experimental realization of teleporting an unknown pure quantum state via dual classical and einstein-podolsky-rosen channels, *Phys. Rev. Lett.* **80**, 1121 (1998).
 - [146] J.-G. Ren, P. Xu, H.-L. Yong, L. Zhang, S.-K. Liao, J. Yin, W.-Y. Liu, W.-Q. Cai, M. Yang, L. Li, K.-X. Yang, X. Han, Y.-Q. Yao, J. Li, H.-Y. Wu, S. Wan, L. Liu, D.-Q. Liu, Y.-W. Kuang, Z.-P. He, P. Shang, C. Guo, R.-H. Zheng, K. Tian, Z.-C. Zhu, N.-L. Liu, C.-Y. Lu, R. Shu, Y.-A. Chen, C.-Z. Peng, J.-Y. Wang, and J.-W. Pan, Ground-to-satellite quantum teleportation, *Nature* **549**, 70 (2017).
 - [147] E. Diamanti, Quantum signals could soon span the globe, *Nature* **549**, 41 (2017).

- [148] X.-X. Xia, Q.-C. Sun, Q. Zhang, and J.-W. Pan, Long distance quantum teleportation, *Quantum Science and Technology* **3**, 014012 (2017).
- [149] H. Dai, Q. Shen, C.-Z. Wang, S.-L. Li, W.-Y. Liu, W.-Q. Cai, S.-K. Liao, J.-G. Ren, J. Yin, Y.-A. Chen, Q. Zhang, F. Xu, C.-Z. Peng, and J.-W. Pan, Towards satellite-based quantum-secure time transfer, *Nature Physics* **16**, 848 (2020).
- [150] B. Li, Y. Cao, Y.-H. Li, W.-Q. Cai, W.-Y. Liu, J.-G. Ren, S.-K. Liao, H.-N. Wu, S.-L. Li, L. Li, N.-L. Liu, C.-Y. Lu, J. Yin, Y.-A. Chen, C.-Z. Peng, and J.-W. Pan, Quantum state transfer over 1200 km assisted by prior distributed entanglement, *Phys. Rev. Lett.* **128**, 170501 (2022).
- [151] C.-Y. Lu, Y. Cao, C.-Z. Peng, and J.-W. Pan, Micius quantum experiments in space, *Rev. Mod. Phys.* **94**, 035001 (2022).
- [152] I. Marcikic, H. de Riedmatten, W. Tittel, H. Zbinden, and N. Gisin, Long-distance teleportation of qubits at telecommunication wavelengths, *Nature* **421**, 509 (2003).
- [153] O. Landry, J. A. W. van Houwelingen, A. Beveratos, H. Zbinden, and N. Gisin, Quantum teleportation over the swisscom telecommunication network, *J. Opt. Soc. Am. B* **24**, 398 (2007).
- [154] R. Valivarthi, M. I. G. Puigibert, Q. Zhou, G. H. Aguilar, V. B. Verma, F. Marsili, M. D. Shaw, S. W. Nam, D. Oblak, and W. Tittel, Quantum teleportation across a metropolitan fibre network, *Nature Photonics* **10**, 676 (2016).
- [155] F. Grosshans, Teleportation becomes streetwise, *Nature Photonics* **10**, 623 (2016).
- [156] L. Vandenberghe and S. Boyd, Semidefinite programming, *SIAM Review* **38**, 49 (1996), <https://doi.org/10.1137/1038003>.
- [157] S. Boyd and L. Vandenberghe, *Convex Optimization* (Cambridge University Press, 2004).
- [158] D. Jonathan and M. B. Plenio, Entanglement-assisted local manipulation of pure quantum states, *Phys. Rev. Lett.* **83**, 3566 (1999).
- [159] R. Duan, Y. Feng, X. Li, and M. Ying, Multiple-copy entanglement transformation and entanglement catalysis, *Phys. Rev. A* **71**, 042319 (2005).
- [160] F. Ding, X. Hu, and H. Fan, Amplifying asymmetry with correlating catalysts, *Phys. Rev. A* **103**, 022403 (2021).
- [161] P. Lipka-Bartosik and P. Skrzypczyk, All states are universal catalysts in quantum thermodynamics, *Phys. Rev. X* **11**, 011061 (2021).
- [162] N. Shiraishi and T. Sagawa, Quantum thermodynamics of correlated-catalytic state conversion at small scale, *Phys. Rev. Lett.* **126**, 150502 (2021).
- [163] P. Lipka-Bartosik and P. Skrzypczyk, Catalytic quantum teleportation, *Phys. Rev. Lett.* **127**, 080502 (2021).
- [164] T. V. Kondra, C. Datta, and A. Streltsov, Catalytic transformations of pure entangled states, *Phys. Rev. Lett.* **127**, 150503 (2021).
- [165] R. Takagi and N. Shiraishi, Correlation in catalysts enables arbitrary manipulation of quantum coherence, *Phys. Rev. Lett.* **128**, 240501 (2022).
- [166] R. Rubboli and M. Tomamichel, Fundamental limits on correlated catalytic state transformations, *Phys. Rev. Lett.* **129**, 120506 (2022).
- [167] W. Tittel, J. Brendel, H. Zbinden, and N. Gisin, Violation of bell inequalities by photons more than 10 km apart, *Phys. Rev. Lett.* **81**, 3563 (1998).
- [168] H.-J. Briegel, W. Dür, J. I. Cirac, and P. Zoller, Quantum repeaters: The role of imperfect local operations in quantum communication, *Phys. Rev. Lett.* **81**, 5932 (1998).
- [169] L. M. Duan, M. D. Lukin, J. I. Cirac, and P. Zoller, Long-distance quantum communication with atomic ensembles and linear optics, *Nature* **414**, 413 (2001).
- [170] Z.-S. Yuan, Y.-A. Chen, B. Zhao, S. Chen, J. Schmiedmayer, and J.-W. Pan, Experimental demonstration of a bdcz quantum repeater node, *Nature* **454**, 1098 (2008).
- [171] L. Jiang, J. M. Taylor, K. Nemoto, W. J. Munro, R. Van Meter, and M. D. Lukin, Quantum repeater with encoding, *Phys. Rev. A* **79**, 032325 (2009).
- [172] A. G. Fowler, D. S. Wang, C. D. Hill, T. D. Ladd, R. Van Meter, and L. C. L. Hollenberg, Surface code quantum communication, *Phys. Rev. Lett.* **104**, 180503 (2010).
- [173] N. Sangouard, C. Simon, H. de Riedmatten, and N. Gisin, Quantum repeaters based on atomic ensembles and linear optics, *Rev. Mod. Phys.* **83**, 33 (2011).
- [174] W. J. Munro, A. M. Stephens, S. J. Devitt, K. A. Harrison, and K. Nemoto, Quantum communication without the necessity of quantum memories, *Nature Photonics* **6**, 777 (2012).
- [175] S. Muralidharan, J. Kim, N. Lütkenhaus, M. D. Lukin, and L. Jiang, Ultrafast and fault-tolerant quantum communication across long distances, *Phys. Rev. Lett.* **112**, 250501 (2014).
- [176] W. J. Munro, K. Azuma, K. Tamaki, and K. Nemoto, Inside quantum repeaters, *IEEE Journal of Selected Topics in Quantum Electronics* **21**, 78 (2015).
- [177] K. Azuma, K. Tamaki, and H.-K. Lo, All-photonic quantum repeaters, *Nature Communications* **6**, 6787 (2015).
- [178] F. Ewert, M. Bergmann, and P. van Loock, Ultrafast long-distance quantum communication with static linear optics, *Phys. Rev. Lett.* **117**, 210501 (2016).
- [179] S. Pirandola, R. Laurenza, C. Ottaviani, and L. Banchi, Fundamental limits of repeaterless quantum communications, *Nature Communications* **8**, 15043 (2017).
- [180] M. Zwerger, A. Pirker, V. Dunjko, H. J. Briegel, and W. Dür, Long-range big quantum-data transmission, *Phys. Rev. Lett.* **120**, 030503 (2018).
- [181] M. K. Bhaskar, R. Riedinger, B. Machielse, D. S. Levonian, C. T. Nguyen, E. N. Knall, H. Park, D. Englund, M. Lončar, D. D. Sukachev, and M. D. Lukin, Experimental demonstration of memory-enhanced quantum communication, *Nature* **580**, 60 (2020).
- [182] J. Borregaard, H. Pichler, T. Schröder, M. D. Lukin, P. Lodahl, and A. S. Sørensen, One-way quantum repeater based

- on near-deterministic photon-emitter interfaces, *Phys. Rev. X* **10**, 021071 (2020).
- [183] J. Walln fer, A. A. Melnikov, W. D r, and H. J. Briegel, Machine learning for long-distance quantum communication, *PRX Quantum* **1**, 010301 (2020).
 - [184] Y.-F. Pu, S. Zhang, Y.-K. Wu, N. Jiang, W. Chang, C. Li, and L.-M. Duan, Experimental demonstration of memory-enhanced scaling for entanglement connection of quantum repeater segments, *Nature Photonics* **15**, 374 (2021).
 - [185] C. Liorni, H. Kampermann, and D. Bru , Quantum repeaters in space, *New Journal of Physics* **23**, 053021 (2021).
 - [186] F. Rozp dek, K. Noh, Q. Xu, S. Guha, and L. Jiang, Quantum repeaters based on concatenated bosonic and discrete-variable quantum codes, *npj Quantum Information* **7**, 102 (2021).
 - [187] K. Sharman, F. Kimiaee Asadi, S. C. Wein, and C. Simon, Quantum repeaters based on individual electron spins and nuclear-spin-ensemble memories in quantum dots, *Quantum* **5**, 570 (2021).
 - [188] M. F. Askarani, A. Das, J. H. Davidson, G. C. Amaral, N. Sinclair, J. A. Slater, S. Marzban, C. W. Thiel, R. L. Cone, D. Oblak, and W. Tittel, Long-lived solid-state optical memory for high-rate quantum repeaters, *Phys. Rev. Lett.* **127**, 220502 (2021).
 - [189] H. Wang, M. E. Trusheim, L. Kim, H. Raniwala, and D. R. Englund, Field programmable spin arrays for scalable quantum repeaters, *Nature Communications* **14**, 704 (2023).
 - [190] K. Ito, T. Kondo, K. Mannami, K. Niizeki, D. Yoshida, K. Minaguchi, M. Zheng, X. Xie, F.-L. Hong, and T. Horikiri, Frequency-multiplexed storage and distribution of narrowband telecom photon pairs over a 10-km fiber link with long-term system stability, *Phys. Rev. Appl.* **19**, 024070 (2023).
 - [191] M.  ukowski, A. Zeilinger, M. A. Horne, and A. K. Ekert, “event-ready-detectors” Bell experiment via entanglement swapping, *Phys. Rev. Lett.* **71**, 4287 (1993).
 - [192] A. Zeilinger, M. A. Horne, H. Weinfurter, and M.  ukowski, Three-particle entanglements from two entangled pairs, *Phys. Rev. Lett.* **78**, 3031 (1997).
 - [193] J.-W. Pan, D. Bouwmeester, H. Weinfurter, and A. Zeilinger, Experimental entanglement swapping: Entangling photons that never interacted, *Phys. Rev. Lett.* **80**, 3891 (1998).
 - [194] R. F. Werner, Quantum states with Einstein-Podolsky-Rosen correlations admitting a hidden-variable model, *Phys. Rev. A* **40**, 4277 (1989).
 - [195] W. R. Heinzelman, J. Kulik, and H. Balakrishnan, Adaptive protocols for information dissemination in wireless sensor networks, in *Proceedings of the 5th Annual ACM/IEEE International Conference on Mobile Computing and Networking*, MobiCom ’99 (Association for Computing Machinery, New York, NY, USA, 1999) p. 174–185.
 - [196] A. Dunkels, F.  sterlind, and Z. He, An adaptive communication architecture for wireless sensor networks, in *Proceedings of the 5th International Conference on Embedded Networked Sensor Systems*, SenSys ’07 (Association for Computing Machinery, New York, NY, USA, 2007) p. 335–349.
 - [197] P. Padhy, R. K. Dash, K. Martinez, and N. R. Jennings, A utility-based adaptive sensing and multihop communication protocol for wireless sensor networks, *ACM Trans. Sen. Netw.* **6**, 10.1145/1754414.1754423 (2010).
 - [198] E. Kaur, S. Das, M. M. Wilde, and A. Winter, Extendibility limits the performance of quantum processors, *Phys. Rev. Lett.* **123**, 070502 (2019).
 - [199] E. Kaur, S. Das, M. M. Wilde, and A. Winter, Resource theory of unextendibility and nonasymptotic quantum capacity, *Phys. Rev. A* **104**, 022401 (2021).
 - [200] M. Berta, F. Borderi, O. Fawzi, and V. B. Scholz, Semidefinite programming hierarchies for constrained bilinear optimization, *Mathematical Programming* **194**, 781 (2022).
 - [201] T. Holdsworth, V. Singh, and M. M. Wilde, Quantifying the performance of approximate teleportation and quantum error correction via symmetric 2-ppt-extendible channels, *Phys. Rev. A* **107**, 012428 (2023).
 - [202] A. U. Siddiqui and M. M. Wilde, The swap imposter: Bidirectional quantum teleportation and its performance, *AVS Quantum Science* **5**, 011407 (2023), <https://doi.org/10.1116/5.0135467>.